THE UNIVERSITY OF QUEENSLAND

DEPARTMENT OF CIVIL ENGINEERING

REPORT CH55/05

APPLICATIONS OF THE SAINT-VENANT EQUATIONS AND METHOD OF CHARACTERISTICS TO THE DAM BREAK WAVE PROBLEM

AUTHOR: H. CHANSON

HYDRAULIC MODEL REPORTS

This report is published by the Department of Civil Engineering at the University of Queensland. Requests for copies of any of the Hydraulic Model Reports should be addressed to the Departmental Secretary.

The interpretation and opinions expressed herein are solely those of the author(s). Considerable care has been taken to ensure accuracy of the material presented. Nevertheless, responsibility for the use of this material rests with the user.

Department of Civil Engineering
The University of Queensland
Brisbane QLD 4072
AUSTRALIA

Telephone: (61 7) 3365 4163
Fax: (61 7) 3365 4599

URL: www.uq.edu.au/civeng

First published in 2005 by
Hubert CHANSON *
Department of Civil Engineering
The University of Queensland, Brisbane QLD 4072, Australia

ISBN No. 1864997966

The University of Queensland, St Lucia

APPLICATIONS OF THE SAINT-VENANT EQUATIONS AND METHOD OF CHARACTERISTICS TO THE DAM BREAK WAVE PROBLEM

by

Hubert CHANSON
Dept of Civil Engineering, The University of Queensland, Brisbane QLD 4072, Australia
Email: h.chanson@uq.edu.au
Url : http://www.uq.edu.au/~e2hchans/

REPORT No. CH 55/05
ISBN 1864997966
Department of Civil Engineering, The University of Queensland
May, 2005

Photograph of the Malpasset dam taken in 1981 (Accident on 2 December 1959) - View from the reservoir looking downstream at the right abutment with the writer's car on the bottom righ for scale

ABSTRACT

Surge waves resulting from dam breaks have been responsible for numerous losses. Modern predictions of dam break wave rely too often on numerical predictions, validated with limited data sets. Despite a few studies, there has been a lack of basic theoretical and physical studies for the past 40 years. Current knowledge of dam break wave surging down rough surfaces remains rudimentary, while there is still some arguments of the flow fundamentals.

The present work is focused on simple solutions of the dam break wave problem using the Saint-Venant equations and the method of characteristics. Analytical solutions are developed for an instantaneous dam break with a semi-infinite reservoir in a wide rectangular channel. After a review of well-known solutions, further ideal-fluid flow solutions are detailed. These include ideal dam break wave flow on horizontal and sloping channels, with or without initial flow motion. The effect of the presence of water in the downstream channel is discussed. New analytical solutions of dam break wave of real fluids are developed for turbulent flow (Section 4.) and laminar flow motion (Section 5.). These simple theoretical developments include the break wave in horizontal channels with bed friction, dam break wave with initial flow motion, and dam break waves on flat slope channels with bed friction and initial flow motion. The analytical results were validated by successful comparisons between theoretical results and several experimental data sets obtained in large-size facilities. Later the analytical results are applied to three different turbulent flow situations: a dam break, the swash zone, and a tsunami runup.

The advantages of the present developments are five-fold. First the theoretical results yield simple explicit analytical expressions of the dam break wave with flow resistance. The theoretical results compare well with experimental data and with more advanced theoretical solutions. They include both laminar and turbulent flow motion. Second the developments are simple, and they yield nice pedagogical applications of the Saint-Venant equations and method of characteristics that are well-suited to undergraduate teaching of hydraulic engineering. Third the analytical solutions may be used to validate numerical solutions of the method of characteristics applied to the dam break wave problem. Fourth the development is applied to a wide range of flow conditions, including the effects of bed slope and initial flow motion. This yields a wide range of practical applications. Fifth the simplicity of the equations may allow the extension of the method to more complex fluids (e.g. non-Newtonian fluids).

It is however acknowledged that the present approach is limited to semi-infinite reservoir, rectangular channel and quasi-instantaneous dam break.

Keywords : Dam break wave, Analytical solutions, Saint-Venant equation, Method of characteristics, Wave runup, Tsunami runup.

TABLE OF CONTENTS

NOTATION

The following symbols are used in this report :

A	flow cross-section area (m^2);
a	wave amplitude (m) (paragraph 6.4);
B	free-surface width (m);
C	1- celerity (m/s) of a small disturbance for an observer travelling with the flow; 2- wave celerity (m/s) (paragraph 6.4);
C_g	wave group celerity (m/s) (paragraph 6.4);
C_o	initial celerity (m/s) of a small disturbance in the reservoir with initial reservoir depth d_o;
D_H	hydraulic diameter : $D_H = 4*A/P_W$;
d	flow depth (m) measured normal to the invert;
d_s	dam break wave front thickness (m);
d_o	initial reservoir height (m) measured normal to the chute invert;
d_1	flow depth (m) at the upstream end of the wave tip region;
d_2	flow depth (m) immediately behind the positive surge (paragraph 3.2);
d_3	initial flow depth (m) in the downstream channel (paragraph 3.2);
E	wave energy spectral density (J/m^2) (paragraph 6.4);
F_1	dimensionless function (paragraph 2.3.3);
F_2	dimensionless function (paragraph 2.3.3);
Fr	1- flow Froude number : $Fr = V/\sqrt{g*d}$; 2- surge Froude number: $Fr = (U \pm V)/\sqrt{g*d}$;
Fr_o	initial reservoir flow Froude number;
f	Darcy-Weisbach friction factor;
g	gravity constant (m/s^2); $g = 9.8\ m/s^2$;
H_{dam}	vertical reservoir height (m) at the gate;
H_{max}	maximum wave height (m) at breaking measured above the still water level (paragraph 5.4);
h	roughness element height (m);
L	channel length (m);
L_{res}	reservoir length (m);
l	1- longitudinal spacing (m) between roughness elements; 2- wave length (m) (paragraph 5.4);
M	mass of fluid (kg/m) per unit width in the wave tip region;
P_W	wetted perimeter (m);
Q	volume flow rate (m^3/s);
q	volume flow rate per unit width (m^2/s);
S_f	friction slope;
S_o	bed slope : $S_o = \sin\theta$;
T	dimensionless time (paragraph 2.3);
t	time (s) from dam removal;
U	wave front celerity (m/s);
V	flow velocity (m/s);
V_H	uniform equilibrium flow velocity (m/s) for a water depth H_{dam};
V_o	initial reservoir velocity (m/s) positive downstream;
V_1	flow velocity (m/s) at the upstream end of the wave tip region;
V_2	flow velocity (m/s) immediately behind the positive surge (paragraph 3.2);
V_3	initial velocity (m/s) in the downstream channel (paragraph 3.2), positive upstream;
W	1- channel width (m); 2- Average energy flux (J/m/s) (paragraph 6.4);
X	1- dimensionless distance (paragraph 2.3);

	2- dimensionless depth (paragraph 3.2);
x	longitudinal distance (m) measured from the dam;
x_S	wave front position (m);
x'	dimensionless variable;
$(x_S)_{max}$	maximum runup distance (m) for a dam break wave on an upward slope;
x_1	location (m) at the upstream end of the wave tip region;
y	distance (m) normal to the bed; vertical distance (m) for a horizontal channel;
z	vertical elevation (m);
$(z)_{max}$	maximum runup elevation (m) for a dam break wave on an upward slope;

Greek symbols

α	laminar flow resitance correction coefficient;
Φ	momentum per unit width in the wave tip region (kg/s);
ϕ	momentum per unit area (Pa.s) (paragraph 6.4);
ϕ_F	average momentum flux (N/s) (paragraph 6.4);
μ	dynamic viscosity (Pa.s);
ν	kinematic viscosity (m^2/s) : $\nu = \mu/\rho$;
π	$\pi = 3.14159265358979323846264 3$;
θ	bed slope angle;
ρ	fluid density (kg/m^3);
ΣForces	resultant of the forces applied to the wave tip region per unit width (N/m);
τ_o	boundary shear stress (Pa);

Subscript

dw	deep water flow conditions (paragraph 6.4);
o	initial flow conditions in the reservoir;
1	flow conditions at the upstream end of the wave tip region;
2	flow conditions immediately behind the positive surge (paragraph 3.2)
3	initial flow conditions in the downstream channel (paragraph 3.2);

Abbreviations

D/S (or d/s)	downstream;
U/S (or u/s)	upstream;

Notation

$\frac{D}{Dt}$	absolute differential;
$\frac{\partial}{\partial y}$	partial differentiation with respect to y;
$\dot{x}$	first derivative;
$\ddot{x}$	second derivative.

ABOUT THE CONTRIBUTOR

HUBERT CHANSON

Hubert CHANSON is a Reader in environmental fluid mechanics and water engineering at the University of Queensland, Brisbane, Australia. His research interests include design of hydraulic structures, experimental investigations of two-phase flows, coastal hydrodynamics, water quality modelling, environmental management and natural resources. He is the author of six books : "Hydraulic Design of Stepped Cascades, Channels, Weirs and Spillways" (*Pergamon*, 1995), "Air Bubble Entrainment in Free-Surface Turbulent Shear Flows" (*Academic Press*, 1997), "The Hydraulics of Open Channel Flows : An Introduction" (*Butterworth-Heinemann*, 1999 & 2004), "The Hydraulics of Stepped Chutes and Spillways" (*Balkema*, 2001) and "Environmental Hydraulics of Open Channel Flows" (*Elsevier*, 2004). He co-authored the book "Fluid Mechanics for Ecologists" (*IPC Press*, 2002). His textbook "The Hydraulics of Open Channel Flows : An Introduction" has already been translated into Chinese (*Hydrology Bureau of Yellow River Conservancy Committee*) and Spanish (*McGraw Hill Interamericana*), and it was re-edited in 2004. His publication record includes over 300 international refereed papers and his work was cited over 1,200 times since 1990.

The International Association for Hydraulic engineering and Research (IAHR) presented Hubert Chanson the 13th Arthur Ippen award in 2003 for outstanding achievements in hydraulic engineering. This award is regarded as the highest achievement in hydraulic research. The American Society of Civil Engineers, Environmental and Water Resources Institute (ASCE-EWRI) presented Hubert CHANSON with the 2004 award for the best practice paper in the Journal of Irrigation and Drainage Engineering ([1]). In 1999 he was awarded a Doctor of Engineering from the University of Queensland for outstanding research achievements in gas-liquid bubbly flows.

He has been awarded six fellowships from the Australian Academy of Science. In 1995 he was a Visiting Associate Professor at National Cheng Kung University (Taiwan R.O.C.). He was a Visiting Research Fellow at Toyohashi University of Technology (Japan) in 1999 and 2001. In 2004, he was a Visiting Professorial Fellow at Université de Bretagne Occidentale (France), and a Visiting Senior Research Fellow at Laboratoire Central des Ponts et Chaussées (France) and at McGill University (Canada). Hubert Chanson was invited to deliver numerous keynote lectures. He lectured several short courses in Australia and overseas (e.g. Taiwan, Japan, Italy).

His Internet home page is {http://www.uq.edu.au/~e2hchans}. He also developed a gallery of photographs website {http://www.uq.edu.au/~e2hchans/photo.html} that received more than 110,000 hits since inception.

[1]CHANSON, H., and TOOMBES, L. (2002). "Energy Dissipation and Air Entrainment in a Stepped Storm Waterway: an Experimental Study." *Jl of Irrigation and Drainage Engrg.*, ASCE, Vol. 128, No. 5, pp. 305-315 (ISSN 0733-9437).

1. INTRODUCTION

1.1 PRESENTATION

Surge waves resulting from dam breaks have been responsible for numerous losses of life (Fig. 1-1). Figure 1A shows ruins of the St Francis dam break in 1928. More than 450 people were killed in the catastrophe. Figure 1B presents the Möhne dam break inflicted by RAF bombers on 17 May 1943 during the dam buster campaign. Figure 1C shows what is left from the Lake Ha!Ha! dam overtopped in July 1996. Related situations include flash floods, flood runoff in ephemeral streams, debris flow surges, surging waves in the swash zone, rising tides in dry estuaries and tsunami runup on dry land. Appendix A lists major tsunami events, including the 26 December 2004 catastrophe. Applications of dam break wave theory to tsunami surges are discussed specifically in paragraph 6.4.

In all cases, the surge front is a shock characterised by a sudden discontinuity and extremely rapid variations of flow depth and velocity. Hydraulic researchers studied initially surging flows in laboratory facilities. In recent years, numerical studies have been plenty. For example, for the period 2003-2004 alone, the international database Science Citation Index ™, The Web of Science™, lists 40 journal articles on dam break, including 34 numerical studies, 4 experimental studies and only one theoretical development.

Fig. 1-1 - Photographs of dam break catastrophes
(A) St Francis dam break, USA (12 March 1928) (Courtesy of Santa Clarita Valley Historical Society) - Looking upstream - Note onlookers standing in the foreground, in front of a 65 m high remnant part of the dam - The remnant monolith was blasted on 23 May 1929

(B) Möhne dam break (Germany, 17 May 1943), after RAF bomber attack - View from right bank (Courtesy of Ruhrverband, Essen, Germany) - More than 1,300 people died in the catastrophe, mostly inmates of a POW camp located downstream of the dam

(C) Lake Ha!Ha! Québec, Canada, 18-21 July 1996 - Looking upstream at the breached dam (Courtesy of Natural Resources Canada)

Modern predictions of dam break wave rely too often on numerical predictions, validated with limited data sets. Albeit major research funding and "concerted actions", there has been a lack of basic theoretical and physical studies for the past 40 years. Despite a few studies (DRESSLER 1954, ESCANDE et al. 1961, CHANSON 2004c,d), current knowledge of dam break wave surging down rough surfaces remains rudimentary. Further there is still some arguments of the flow fundamentals. Some basic findings have been sometimes contradictory. For example, some measurements highlighted a boundary layer region in the surging wave leading edge (e.g. MANO 1984, DAVIES 1988, FUJIMA and SHUTO 1990, CHANSON 2004d), while others indicated quasi-uniform vertical velocity distributions (ESTRADE 1967, WANG 2002, JENSEN et al. 2003, WOOD et al. 2003).

1.2 BASIC EQUATIONS

A dam break wave is the flow resulting from a sudden release of a mass of fluid in a channel. In this section, the basic equations for unsteady open channel flow are first described.

In unsteady open channel flows, the velocities and water depths change with time and longitudinal position. For one-dimensional applications, the continuity and momentum equations yield the Saint-Venant equations. They are named after the French engineer Adhémar Jean Claude BARRÉ de SAINT-VENANT (BARRÉ de SAINT-VENANT 1871a,b). The application of the Saint-Venant equations is limited by some basic assumptions : (1) the flow is one dimensional; (2) the streamline curvature is very small and the pressure distributions are hydrostatic; (3) the flow resistance are the same as for a steady uniform flow for the same depth and velocity; (4) the bed slope is small enough to satisfy : $\cos\theta \approx 1$ and $\sin\theta \approx \tan\theta \approx \theta$; (5) the water density is a constant; and (6) the channel has fixed boundaries, and air entrainment and sediment motion are neglected.

With these hypotheses, the unsteady flow can be characterised at any point and any time by two variables: e.g., V and d where V is the flow velocity and d is the water depth (e.g. LIGGETT 1994, MONTES 1998, CHANSON 2004a,b). The unsteady flow properties are described by a system of two partial differential equations :

$$\frac{\partial d}{\partial t} + \frac{A}{B} * \frac{\partial V}{\partial x} + V * \frac{\partial d}{\partial x} + \frac{V}{B} * \left(\frac{\partial A}{\partial x}\right)_{d=constant} = 0 \qquad (1\text{-}1)$$

$$\frac{\partial V}{\partial t} + V * \frac{\partial V}{\partial x} + g * \frac{\partial d}{\partial x} + g * (S_f - S_o) = 0 \qquad (1\text{-}2)$$

where t is the time, x is the streamwise co-ordinate, A is the cross-section area, B is the free-surface width, S_o is the bed slope ($S_o = \sin\theta$), θ is the angle between the bed and the horizontal, with $\theta > 0$ for a downward slope, and S_f is the friction slope. The friction slope is defined as : $S_f = f/2*V^2/(g*D_H)$ where D_H is the hydraulic diameter and the Darcy friction factor f is a non-linear function of both relative roughness and flow Reynolds number. Equation (1-1) is the continuity equation and Equation (1-2) is the dynamic equation.

The Saint-Venant equations cannot be solved analytically usually because of non-linear terms and complicated functions. Examples of non-linear terms include the friction slope S_f while complicated functions include the flow cross-section A(d) and free-surface width B(d) of natural channels. A mathematical technique to solve the system of partial differential equations formed by the Saint-Venant equations is the method of characteristics. It yields a characteristic system of equations :

$$\frac{D}{Dt}(V + 2 * C) = - g * (S_f - S_o) \qquad \text{forward characteristic} \quad (1\text{-}3a)$$

$$\frac{D}{Dt}(V - 2 * C) = - g * (S_f - S_o) \qquad \text{backward characteristic} \quad (1\text{-}3b)$$

along :

$$\frac{dx}{dt} = V + C \qquad \text{forward characteristic C1 (1-4a)}$$

$$\frac{dx}{dt} = V - C \qquad \text{backward characteristic C2 (1-4b)}$$

where C is the celerity of a small disturbance for an observer travelling with the flow : $C = \sqrt{g*A/B}$. For an observer travelling along the forward characteristic, Equation (1-3a) is valid at any point. For an observer travelling on the backward characteristic, Equation (1-3b) is satisfied everywhere. The system of four equations formed by Equations (1-3) and (1-4) represents the characteristic system of equations that replaces the differential form of the Saint-Venant equations.

1.3 STRUCTURE OF THE REPORT

This report describes a series of theoretical analyses of dam break wave. It is based upon the developments of simple analytical solutions for instantaneous dam break wave of the Saint-Venant equations and method of characteristics. In the next section, well-known analytical solutions are presented. In section 3, ideal-fluid flow solutions of the dam break wave problem are developed. Section 4 introduces new simple analytical solutions for dry horizontal and sloping channels with turbulent flow motion. These are applied in Section 6 and the results are compared with ideal fluid flow solutions. Section 5 presents new analytical solutions of laminar dam break wave motion.

It is the aim of this work to provide simple explicit solutions of dam break wave problems for turbulent and laminar flows that are easily understood by students, young researchers and professionals. Such simple solutions may also provide simple expressions to validate the development and use of numerical models.

2. A BIBLIOGRAPHIC REVIEW

2.1 PRESENTATION

Major dam break catastrophes include the failures of the Puentes dam (Spain, 1802), Dale Dyke dam (UK, 1864), Habra dam (Algeria, 1881), South Fork (Johnstown) dam (USA, 1889), Bouzey dam (France, 1895), St Francis dam (USA 1928) and Malpasset dam (France, 1959) (Fig. 2-1). Figure 2-1 shows the remains of the Malpasset dam in 2004. The photograph may be compared with the cover page photograph (page i) taken in 1981. Both show that little changed in the valley since the aftermath of the event. These dam failures motivated basic studies on the dam break wave, including the milestone contribution by RITTER (1892).

In this section, three well-known analytical solutions of instantaneous dam break waves are presented : RITTER' (1892) solution for an ideal fluid flow on a horizontal channel with a semi-infinite reservoir, WHITHAM's (1955) development for a real-fluid flow on a horizontal channel with a semi-infinite reservoir, and HUNT's (1982,1984) solution for a real-fluid flow down a sloping channel. Note that all analytical solutions assume an instantaneous dam break. Such an approximation is often reasonable for concrete dam failures (e.g. Fig. 2-1).

Fig. 2-1 - Photograph of the Malpasset dam (Failure on 2 December 1959) in September 2004 (Courtesy of Sylvia BRIECHLE) - View from the left abutment of the dam wall ruins - More than 300 people died in the catastrophe

2.2 DAM BREAK ON A DRY, HORIZONTAL, FRICTIONLESS CHANNEL : RITTER'S (1892) SOLUTION

Considering an ideal dam break surging over a dry river bed, the method of characteristics may be applied to solve completely the wave profile as first proposed by RITTER in 1892 (e.g. HENDERSON 1966, MONTES 1998). RITTER's (1892) work was initiated by the South Fork dam's (Johnstown) catastrophe. LEVIN (1952) argued that BARRÉ de SAINT-VENANT (1871a,b) solved this problem. This is not strictly correct, but the extension of the reasoning of BARRÉ de SAINT-VENANT (1871a) yields indeed Ritter's solution for an instantaneous dam break wave in a dry channel.

The dam break may be idealised by a vertical wall that is suddenly removed (Fig. 2-2). After removal of the wall, a negative wave propagates upstream and a dam break wave moves downstream. In the reservoir, upstream of the negative wave leading edge, the water depth is constant $d = d_o$ and the velocity is zero. Although there is considerable vertical acceleration during the initial instants of fluid motion, such acceleration is not taken into account by the method of characteristics and the pressure distributions are assumed hydrostatic.

For an ideal dam break over a dry horizontal two-dimensional channel with a semi-infinite reservoir, the basic equations are :

$$\frac{D}{Dt}(V + 2 * C) = 0 \qquad \text{forward characteristic (2-1a)}$$

$$\frac{D}{Dt}(V - 2 * C) = 0 \qquad \text{backward characteristic (2-1b)}$$

along :

$$\frac{d\,x}{dt} = V + C \qquad \text{forward characteristic C1 (2-2a)}$$

$$\frac{d\,x}{dt} = V - C \qquad \text{backward characteristic C2 (2-2b)}$$

Equations (2-1) and (2-2) mean that (V+2*C) is a constant along a forward characteristic whose trajectory is given by Equation (2-2a). Along a backward characteristic (trajectory given by Eq. (2-2b)), (V-2*C) is a constant. The characteristic curves are often drawn in the (x,t) plane as shown in Figure 2-2, where the horizontal axis is the longitudinal distance x from the dam and the vertical axis is the time t from dam break.

The instantaneous dam break creates a negative wave propagating upstream into a fluid at rest with known water depth. In the (x, t) plane, the initial negative wave characteristic has a slope $dt/dx = -1/C_o$ where $C_o = \sqrt{g*d_o}$ for a rectangular channel (Fig. 2-2). On the initial backward characteristic, $V = 0$ and $C = C_o$ everywhere. Hence, on any forward characteristic issuing from the initial backward characteristic for $t > 0$, $V + 2*C = 2*C_o$. In the {x, t} plane (Fig. 2-2 bottom), the slope of the forward characteristic is :

$$\frac{d\,t}{dx} = \frac{1}{2 * C_o - \sqrt{g * d}}$$

Along each forward characteristic, the water depth decreases with increasing distance x: i.e., $\partial d/\partial x < 0$. The forward characteristic is a concave curve and its slope tends to $dt/dx = 1/(2*C_o)$ ([1]) (Fig. 2-2). The forward characteristic issuing from the origin (x = 0, t = 0) propagates downstream while

---

[1]The equation of the forward charactersitics issuing from the initial backwavard characteristic for $t_{E1} > 0$ is (HOGG, A.J. (2005), *Person. Comm.*):

$$\frac{x}{d_o} = 2 * \sqrt{\frac{g}{d_o}} * t - 3 * \sqrt{\frac{g}{d_o}} * t_{E1}^{2/3} * t^{1/3}$$

satisfying :

$$V + 2 * C = 2 * C_o$$

and d = 0 (hence C = 0) at the leading edge of the dam break wave front. The propagation speed of the dam break wave front equals :

$$U = 2 * \sqrt{g * d_o} \qquad (2\text{-}3)$$

The forward characteristic issuing from (x = 0, t = 0) is basically a straight line as sketched in Figure 2-2 ([2]). Considering any backward characteristic issuing from the dam break wave front (Fig. 2-2, trajectory F1-G1), the C2 characteristics are straight lines because the initial backward characteristic is a straight line (HENDERSON 1966). The inverse slope of each backward characteristic is a constant :

$$\frac{dx}{dt} = V - C = 2 * C_o - 3 * C$$

The integration of the inverse slope gives the water surface profile at the intersection of the C2 characteristics with a horizontal line t = constant (Fig. 2-1, point G1). That is, at a given time, the free-surface profile between the leading edge of the negative wave and the wave front is a parabola:

$$\frac{x}{t * \sqrt{g * d_o}} = 2 - 3 * \sqrt{\frac{d}{d_o}} \qquad \text{for } -1 \leq \frac{x}{t * \sqrt{g * d_o}} \leq +2 \quad (2\text{-}4)$$

At the origin (x = 0), Equation (2-4) predicts a constant water depth :

$$\frac{d(x=0)}{d_o} = \frac{4}{9} \qquad (2\text{-}5)$$

Similarly the velocity at the origin is deduced as :

$$\frac{V(x=0)}{\sqrt{g * d_o}} = \frac{2}{3} \qquad (2\text{-}6)$$

After dam break, the flow depth and velocity at the origin are both constants, and the water discharge per unit width at x = 0 equals :

$$\frac{q(x=0)}{\sqrt{g * d_o^3}} = \frac{8}{27} \qquad (2\text{-}7)$$

Basically critical flow conditions occur at x = 0 for t > 0.

Note that BARRÉ de SAINT-VENANT (1871a) proposed first the parabolic free-surface profile (Eq. (2-4)) for a frictionless surge in a horizontal channel. Although he assumed an initial water depth, his reasoning is valid for both initially-dry and initial-water depth situations as discussed in section 3.2.

Remarks

The parabolic free-surface profile (Eq. (2-4)) may be sometimes rewritten as in terms of the celerity of small disturbance C and of the water depth d :

$$\frac{C}{C_o} = \frac{1}{3} * \left(2 - \frac{x}{t * \sqrt{g * d_o}}\right) \qquad \text{for } -1 \leq \frac{x}{t * \sqrt{g * d_o}} \leq +2 \quad (2\text{-}8)$$

$$\frac{d}{d_o} = \frac{1}{9} * \left(2 - \frac{x}{t * \sqrt{g * d_o}}\right)^2 \qquad \text{for } -1 \leq \frac{x}{t * \sqrt{g * d_o}} \leq +2 \quad (2\text{-}9)$$

Along the parabolic free-surface profile, the flow velocity V equals :

[2]The straight line issuing from the origin (x = 0, t = 0) is a singularity line.

$$\frac{V}{\sqrt{g * d_o}} = \frac{2}{3} * \left(1 + \frac{x}{t * \sqrt{g * d_o}}\right) \qquad \text{for } -1 \leq \frac{x}{t * \sqrt{g * d_o}} \leq +2 \quad (2\text{-}10)$$

Fig. 2-2 - Sketch of a dam break wave in a dry horizontal channel with zero initial velocity

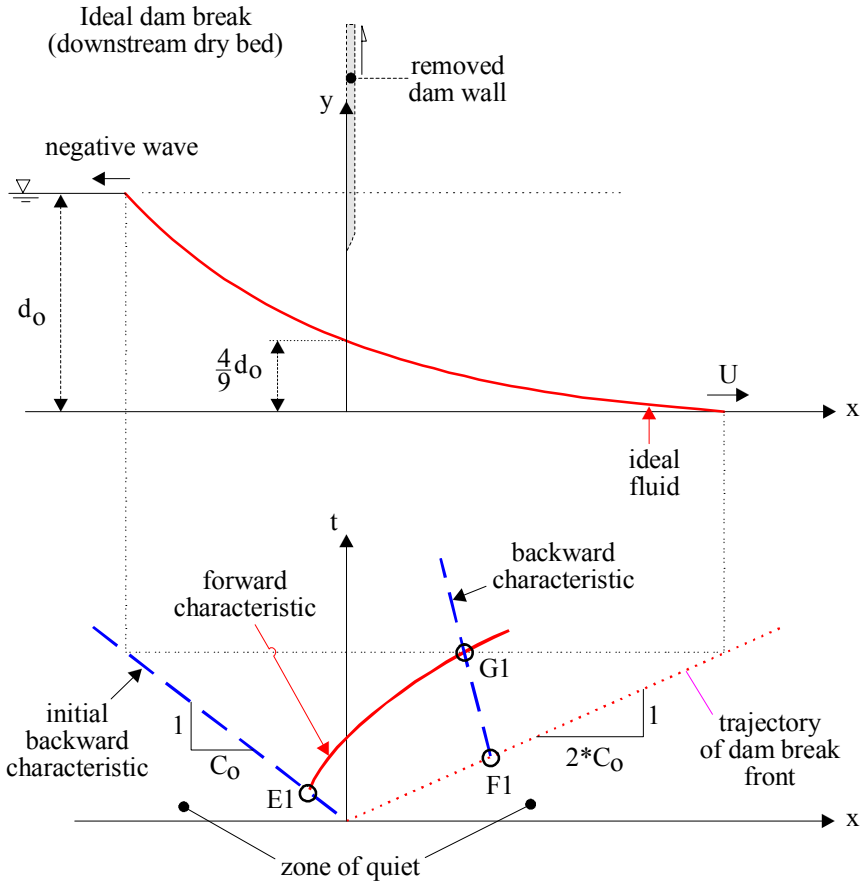

2.3 DAM BREAK IN A DRY HORIZONTAL CHANNEL WITH BED FRICTION: WHITHAM'S (1955) SOLUTION

2.3.1 Basic equations

Experimental observations showed that the flow properties were well approximated by RITTER's theory between the most upstream extent of the initial backward characteristic and a flow region immediately upstream of the dam break wave leading tip (DRESSLER 1952,1954, WHITHAM 1955, ESTRADE 1967). WHITHAM (1955) developed an analytical solution of dam break wave with bed friction in a horizontal, prismatic, wide rectangular channel with a semi-infinite reservoir. WHITHAM considered the dam break wave as an ideal fluid flow for $x \leq x_1$ and a "boundary layer" region in the wave tip (Fig. 2-3). He analysed the wave tip region using an integral method ([3]). The transition between the ideal dam break wave profile and the wave tip is denoted point F2 and shown in Figure 2-3. Point F2 is located at $x = x_1$ where the flow depth is d_1 and the velocity is V_1.

[3]WHITHAM (1955) suggested that his method was based upon the Pohlhausen technique. The method developed by POHLHAUSEN in 1921 is based upon an integral treatment of the boundary layer, and the approximation of the velocity distribution by a polynomial of degree 4 (SCHLICHTING 1979, pp. 201-214; COMOLET 1976, pp. 177-182). In WHITHAM's development, the velocity distribution is assumed uniform and constant in the wave tip region. WHITHAM (1955) considered the wave tip as a "boundary layer", but the analogy is limited !

Dam removal takes place at t = 0 and the dam wall is located at x = 0. The dam break is idealised by a vertical wall that is suddenly removed (Fig. 2-3). In the reservoir, upstream of the leading edge of the negative wave, the water depth is constant and the velocity is zero.
For $x \leq x_1$, the mathematical treatment is identical to that developed in paragraph 2.2. In the wave tip region ($x_1 \leq x \leq x_S$), the continuity equation yields :

$$\frac{dM}{dt} = \rho * d_1 * \left(V_1 - \frac{dx_1}{dt}\right) \qquad \text{Wave tip region (2-11)}$$

where M is the mass of water in the wave tip region per unit width, ρ is the fluid density, and d_1, V_1 and x_1 are respectively the flow depth, velocity and location of the point F2 (Fig. 2-3).
The momentum principles gives :

$$\frac{d\Phi}{dt} = \rho * V_1 * d_1 * \left(V_1 - \frac{dx_1}{dt}\right) + \Sigma Forces \qquad \text{Wave tip region (2-12)}$$

where Φ is the total momentum in the wave tip region per unit width and ΣForces is the resultant of the forces applied to the control volume (i.e. wave tip region) in the horizontal direction per unit width. The latter includes the pressure force at $x = x_1$ and the bottom flow resistance (Fig. 2-3) :

$$\Sigma Forces = \frac{1}{2} * \rho * g * d_1^2 - \int_{x_1}^{x_S} \frac{f}{8} * \rho * V^2 * dx \qquad (2\text{-}13)$$

where f is the Darcy-Weisbach friction factor.
At point F2 ($x = x_1$), the water depth must satisfy the ideal fluid flow solution that is valid between the upstream extent of the initial backward characteristics and the point F2 :

$$\frac{\sqrt{g * d_1}}{\sqrt{g * d_o}} = \frac{1}{3} * \left(2 - \frac{x_1}{t * \sqrt{g * d_o}}\right) \qquad (2\text{-}8)$$

$$\frac{V_1}{\sqrt{g * d_o}} = \frac{2}{3} * \left(1 + \frac{x_1}{t * \sqrt{g * d_o}}\right) \qquad (2\text{-}10)$$

These two equations may be transformed to express d_1 and x_1 as functions of V_1:

$$\frac{d_1}{d_o} = \left(1 - \frac{1}{2} * \frac{V_1}{\sqrt{g * d_o}}\right)^2 \qquad (2\text{-}14)$$

$$\frac{x_1}{t * \sqrt{g * d_o}} = \left(\frac{3}{2} * \frac{V_1}{\sqrt{g * d_o}} - 1\right) \qquad (2\text{-}15)$$

The integral form of the continuity equation for the wave tip region may then be integrated between t = 0 when M = 0 and a time t. It yields :

$$M = \rho * \sqrt{g * d_o^3} * \left(1 - \frac{V_1}{2 * \sqrt{g * d_o}}\right)^3 * t \qquad \text{Mass of fluid in wave tip (2-16)}$$

Importantly, the mass of fluid in the wave tip region (i.e. $x_1 \leq x \leq x_S$) equals the mass of fluid for ($x_1 \leq x \leq 2*\sqrt{g*d_o}*t$) in the ideal fluid flow profile. That is, it satisfies :

$$M = \int_{x_1}^{2*\sqrt{g*d_o}*t} \frac{1}{9 * g} * \left(2 * \sqrt{g * d_o} - \frac{x}{t}\right)^2 * dx \qquad (2\text{-}17)$$

Fig. 2-3 - Sketch of a dam break wave in a horizontal dry channel with bottom friction (Whitham's solution)

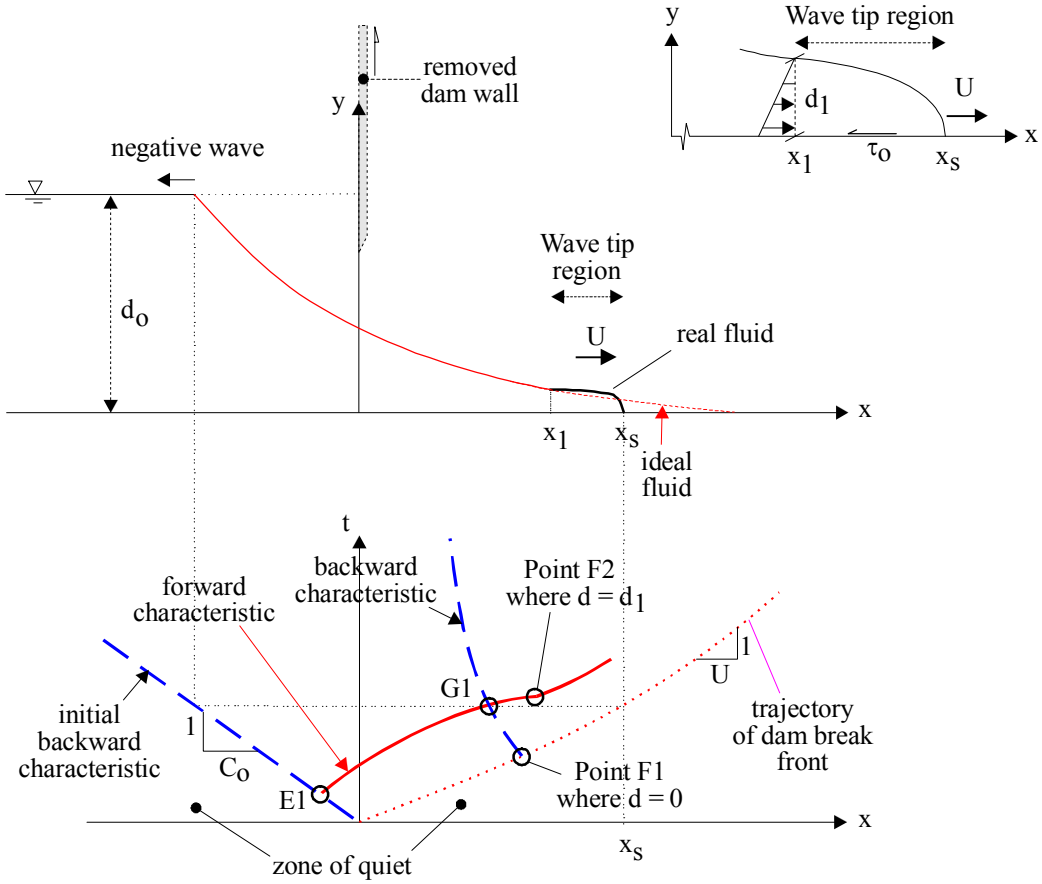

2.3.2 Analytical solution

Up to this stage, WHITHAM's (1955) development makes no assumption on the velocity field in the wave tip region nor on the boundary friction distribution. In the following, the velocity in the wave tip region is assumed to be the shock wave celerity U (i.e. $U = V_1$) while the Darcy friction factor is assumed constant in the wave tip region.

Since the velocity is constant in the wave tip region, the momentum in the wave tip region equals : $\Phi = M*U$ and the variations with time of the momentum Φ equals :

$$\frac{d\,\Phi}{dt} = M * \frac{d\,U}{dt} + U * \frac{d\,M}{dt} \qquad (2\text{-}18)$$

Combining with the continuity equation, it yields :

$$U * \frac{d\,M}{dt} = \frac{1}{2} * \rho * g * d_1^2 - \int_{x_1}^{x_S} \frac{f}{8} * \rho * U^2 * dx \qquad \text{Wave tip region} \quad (2\text{-}19)$$

Assuming a constant Darcy friction factor in the wave tip region, the momentum equation can be simplified as :

$$U * \frac{d\,M}{dt} = \frac{1}{2} * \rho * g * d_1^2 - \frac{f}{8} * \rho * U^2 * (x_S - x_1) \qquad \text{Wave tip region} \quad (2\text{-}20)$$

Replacing x_1, d_1, M by their expression in terms of the wave front celerity (i.e. Eq. (2-15), (2-14) and (2-16) respectively), the momentum equation yields:

$$\left(1 - \frac{1}{2} * \frac{U}{\sqrt{g*d_o}}\right)^3 * t * \frac{\frac{dU}{dt}}{\sqrt{g * d_o}} = \frac{1}{2} * \left(1 - \frac{1}{2} * \frac{U}{\sqrt{g*d_o}}\right)^4 - \frac{f}{8} * \left(\frac{U}{\sqrt{g*d_o}}\right)^2 * \left(\frac{x_S}{d_o} - \sqrt{\frac{g}{d_o}} * t * \left(\frac{3}{2} * \frac{U}{\sqrt{g*d_o}} - 1\right)\right) \quad (2\text{-}21)$$

Noting that $U = dx_S/dt$, the momentum equation may be rewritten as a differential equation in terms of the wave front location x_S using the dot notation for derivatives ([4]):

$$\left(1 - \frac{1}{2} * \frac{\dot{x}_S}{\sqrt{g*d_o}}\right)^3 * t * \frac{\ddot{x}_S}{\sqrt{g * d_o}} = \frac{1}{2} * \left(1 - \frac{1}{2} * \frac{\dot{x}_S}{\sqrt{g*d_o}}\right)^4 - \frac{f}{8} * \left(\frac{\dot{x}_S}{\sqrt{g*d_o}}\right)^2 * \left(\frac{x_S}{d_o} - \sqrt{\frac{g}{d_o}} * t * \left(\frac{3}{2} * \frac{\dot{x}_S}{\sqrt{g*d_o}} - 1\right)\right) \quad (2\text{-}22)$$

Two new dimensionless variables X and T are then introduced:

$$X = \frac{f}{8} * \left(2 * \sqrt{\frac{g}{d_o}} * t - \frac{x_S}{d_o}\right) \quad (2\text{-}23)$$

$$T = \frac{f}{8} * \sqrt{\frac{g}{d_o}} * t \quad (2\text{-}24)$$

X is proportional to the dimensionless distance that the wave front lags behind the ideal fluid flow solution, and T is a dimensionless time. Denoting $\dot{X} = dX/dT$ and $\ddot{X} = dX^2/dT^2$, the derivatives of X equal :

$$\dot{X} = 2 * \left(1 - \frac{1}{2} * \frac{\dot{x}_S}{\sqrt{g*d_o}}\right) \quad (2\text{-}25)$$

$$\ddot{X} = -\frac{8}{g * f} * \ddot{x}_S \quad (2\text{-}26)$$

since :

$$\dot{X} = \frac{dX}{dt} * \frac{dt}{dT}$$

$$\frac{dt}{dT} = \frac{8}{f} * \sqrt{\frac{d_o}{g}}$$

and where $\dot{x}_S = dx_S/dt$ and $\ddot{x}_S = dx_S^2/dt^2$.

The momentum equation may be transformed in terms of X and T :

$$-\frac{\dot{X}^3}{8} * T * \ddot{X} = \frac{\dot{X}^4}{32} - (2 - \dot{X})^2 * \left(\frac{3}{2} * T * \dot{X} - X\right) \quad (2\text{-}27)$$

WHITHAM (1955) solved this differential equation using a Taylor expansion. The first seven terms are:

$$T = 0.02431 * (\dot{X})^3 + 0.02163 * (\dot{X})^4 + 0.01496 * (\dot{X})^5 + 0.00941 * (\dot{X})^6$$

[4]Note a typographic error in WHITHAM's (1955) Equation (17). In the present development, the first term in the right handside of the equation starts with 1/2.

$$+ 0.00563 * (\dot{X})^7 + 0.00327 * (\dot{X})^8 + 0.00186 * (\dot{X})^9 + \ldots \quad (2\text{-}28)$$

where $\dot{X} = dX/dT$:

$$\dot{X} = 2 * \left(1 - \frac{1}{2} * \frac{\dot{x}_S}{\sqrt{g * d_o}} \right)$$

Fig. 2-4 - Dimensionless free-surface profile at $t*\sqrt{g/d_o} = 6.44$ assuming f = 0.03 - Comparison between the theories of DRESSLER (1952) and WHITHAM (1955)

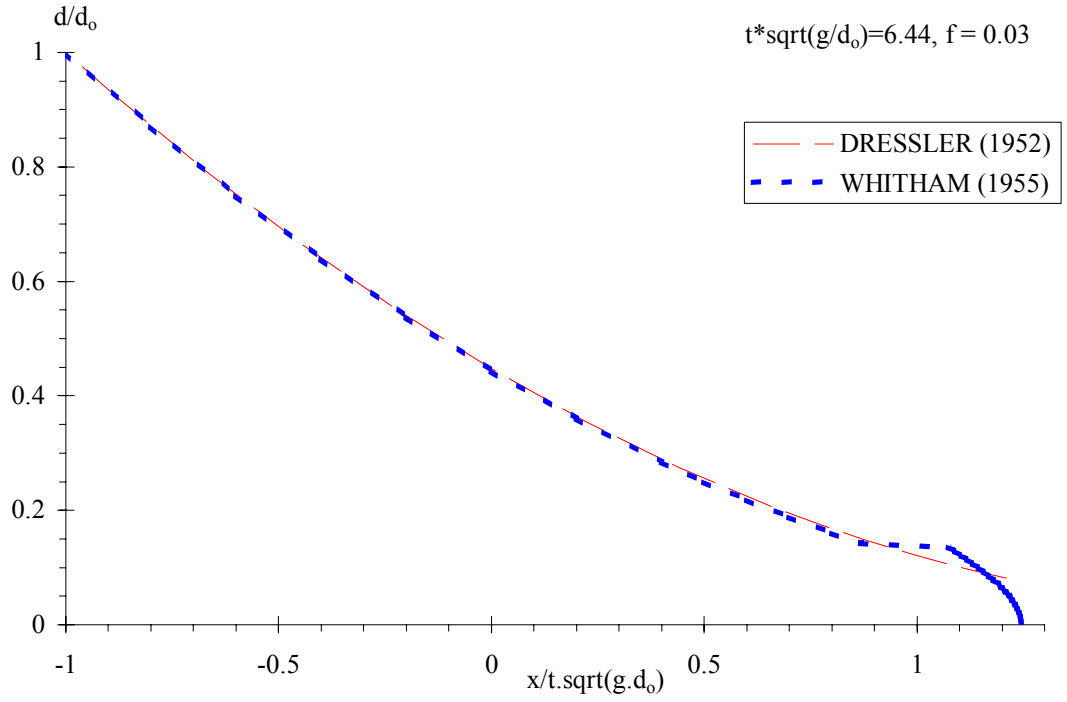

Remarks

In the wave tip region ($x_1 < x < x_S$), the free-surface profile may be deduced from the dynamic wave equation :

$$\frac{\partial U}{\partial t} + g * \frac{\partial d}{\partial x} + \frac{f}{8} * \frac{U^2}{d} = 0 \qquad \text{Dynamic wave equation}$$

since $\partial V/\partial x = 0$ in the wave tip region where V = U. Note that $U = \dot{x}_S = dx_S/dt$ and $dU/dt = \ddot{x}_S = dx_S^2/dt^2$.

At a given time t, U and dU/dt are known constants independent of x. The integration of the dynamic wave equation with respect to x yields a first approximation of the instantaneous free-surface profile :

$$\frac{x_S - x}{d_o} = -\frac{f}{8} * \frac{U^2}{g * d_o} * \left(\frac{g}{\frac{\partial U}{\partial t}} \right)^2 * \left(\mathrm{Ln}\left(1 + \frac{8}{f} * \frac{\frac{d}{d_o}}{\frac{U^2}{g * d_o}} * \frac{\frac{\partial U}{\partial t}}{g} \right) - \frac{8}{f} * \frac{\frac{d}{d_o}}{\frac{U^2}{g * d_o}} * \frac{\frac{\partial U}{\partial t}}{g} \right)$$

Wave front profile (2-29)

An application of Equation (2-29) is shown on Figure 2-4 where the results are compared with the analytical results of DRESSLER (1952) for the same flow resistance and at the same dimensionless

time (see below).

2.3.3 Discussion : comparison with DRESSLER's (1952) theory

DRESSLER (1952) presented another solution for the dam break wave on a dry, two-dimensional, horizontal channel with a semi-infinite reservoir. His development is based upon the complete Saint-Venant equations :

$$\frac{\partial d}{\partial t} + d * \frac{\partial V}{\partial x} + V * \frac{\partial d}{\partial x} = 0 \quad (2\text{-}30)$$

$$\frac{\partial V}{\partial t} + V * \frac{\partial V}{\partial x} + g * \frac{\partial d}{\partial x} + g * S_f = 0 \quad (2\text{-}31)$$

where the friction slope S_f is :

$$S_f = \frac{f}{8} * \frac{V^2}{g * d}$$

for a wide rectangular channel and f is the Darcy friction factor.

DRESSLER (1952) used a perturbation method to solve Equations (2-30) and (2-31) assuming a constant friction factor f. His first order correction for the flow resistance gives the velocity and celerity at any position :

$$\frac{V}{\sqrt{g * d_o}} = \frac{2}{3} * \left(1 + \frac{x}{t * \sqrt{g * d_o}}\right) + F_1 * \frac{f}{8} * \sqrt{\frac{g}{d_o}} * t \quad (2\text{-}32)$$

$$\frac{C}{\sqrt{g * d_o}} = \frac{1}{3} * \left(2 - \frac{x}{t * \sqrt{g * d_o}}\right) + F_2 * \frac{f}{8} * \sqrt{\frac{g}{d_o}} * t \quad (2\text{-}33)$$

where f is the Darcy friction factor. The functions F_1 and F_2 are respectively :

$$F_1 = - \frac{108}{7 * \left(2 - \frac{x}{t * \sqrt{g * d_o}}\right)^2} + \frac{12}{2 - \frac{x}{t * \sqrt{g * d_o}}} - \frac{8}{3} + \frac{8 * \sqrt{3}}{189} * \left(2 - \frac{x}{t * \sqrt{g * d_o}}\right)^{3/2} \quad (2\text{-}34)$$

$$F_2 = \frac{6}{5 * \left(2 - \frac{x}{t * \sqrt{g * d_o}}\right)} - \frac{2}{3} + \frac{4 * \sqrt{3}}{135} * \left(2 - \frac{x}{t * \sqrt{g * d_o}}\right)^{3/2} \quad (2\text{-}35)$$

At a given time t, Equation (2-32) predicts an increasing velocity V with increasing distance x towards the wave front and a maximum next to the wave front. DRESSLER (1952) assumed the location of maximum velocity as the locus of the wave front.

Both theories of DRESSLER (1952) and WHITHAM (1955) were compared successfully with the experimental data of SCHOKLITSCH (1917), DRESSLER (1954) and ESTRADE (1967). Figure 2-5 shows some comparison. The results demonstrate very close agreement between the theories of DRESSLER (1952) and WHITHAM (1955) despite different approaches. Figure 2-5 shows also close agreement with experimental observations. But WHITHAM and DRESSLER both highlighted the limitation of their respective theories when the wave tip region becomes large. Further the Darcy friction factor must be deduced from the best data fit for optimum correlation. The most accurate estimate of the Darcy friction factor is based upon the best data fit of instantaneous free-surface profiles. Lesser accurate predictions for the friction factor may be deduced from best fit of wave front celerity and location data.

Recently, HOGG and PRITCHARD (2004) used WHITHAM's approach to conduct an asymptotic expansion for the velocity and water depth. They also included a momentum correction coefficient

and investigated its effect of the dam break wave properties.
For completeness, note a best fit of WHITHAM's (1955) solution :

$$\frac{U}{\sqrt{g*d_o}} = \frac{2}{1 + 2.90724 * \left(\frac{f}{8} * \sqrt{\frac{g * t^2}{d_o}}\right)^{0.4255}} \qquad (2\text{-}36)$$

Fig. 2-5 - Dimensionless free-surface profile : comparison between an experiment of SCHOKLITSCH (1917, Fig. 14), the theories of RITTER (1892), DRESSLER (1952) and WHITHAM (1955) for $t*\sqrt{g/d_o} = 108$

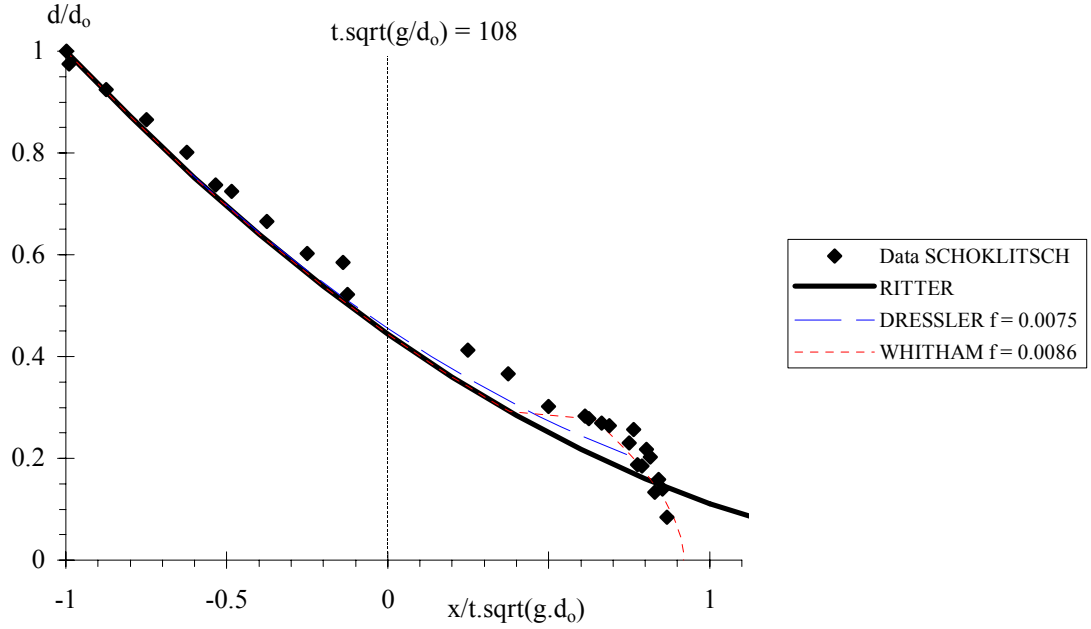

2.4 DAM BREAK ON A DRY SLOPING CHANNEL WITH BED FRICTION: HUNT'S (1982,1984) SOLUTION

2.4.1 Basic equations

HUNT (1982,1984) developed a complete kinematic wave solution of the turbulent dam break wave down a sloping, prismatic, two-dimensional channel (Fig. 2-6). HUNT (1994) extended the development to laminar dam break wave. In unsteady flows, the dynamic equation (Eq. (1-2)) may be simplified when one or more terms become negligible. In a kinematic wave model, the acceleration and inertial terms are neglected in the dynamic wave equation, and the free-surface is assumed parallel to the channel bottom (e.g. CHANSON 2004a,b). The differential form of the Saint-Venant equations is simplified as :

$$\frac{\partial d}{\partial t} + \frac{\partial (V * d)}{\partial x} = 0 \qquad \text{Continuity equation (2-37)}$$

$$S_f = S_o \qquad \text{Kinematic wave equation (2-38)}$$

The kinematic wave equation may be rewritten as :

$$V = \sqrt{\frac{8 * g}{f}} * \sqrt{\frac{D_H}{4}} * \sqrt{S_o} \qquad (2\text{-}38b)$$

where f is the Darcy-Weisbach friction factor, and D_H is the hydraulic diameter ([5]). Equation (2-38)

[5]For a wide rectangular channel, the hydraulic diameter or equivalent pipe diameter equals : D_H =

expresses an unique relationship between the velocity V and the water depth d, hence the cross-section area at a given location x .

Fig. 2-6 - Dam break wave down a sloping channel

(A) Definition sketch

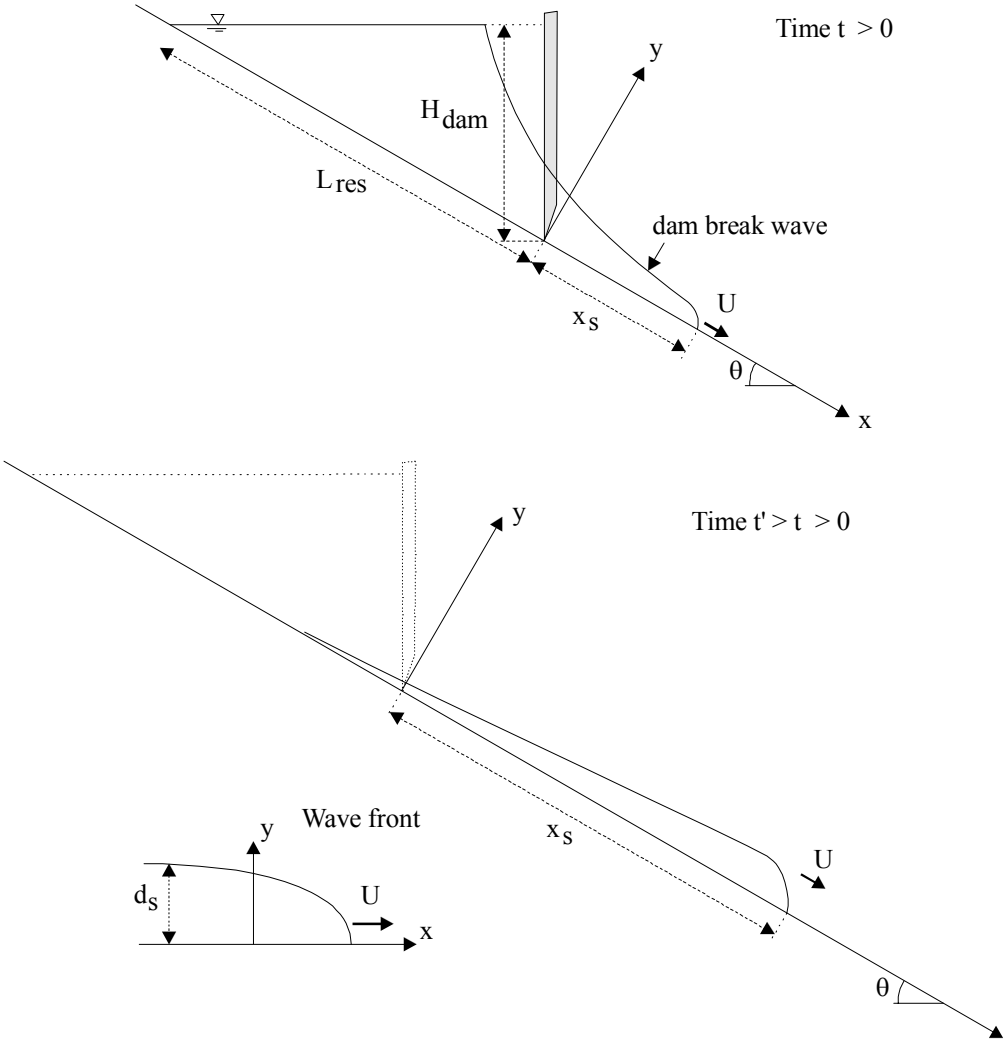

(B) Characteristics and dam break wave front path in the (x, t) plane

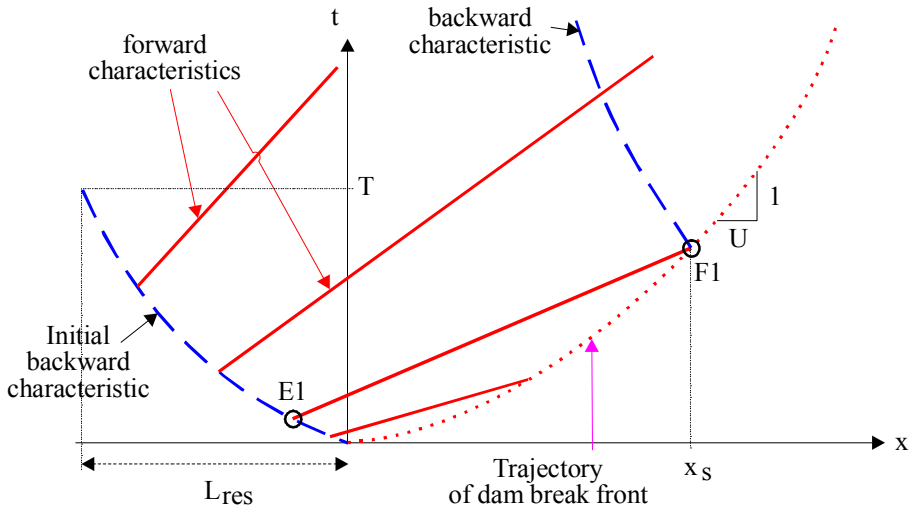

4*d where d is the flow depth.

For a wide rectangular channel, the combination of the continuity and momentum equations yields :

$$\frac{\partial d}{\partial t} + \frac{3}{2} * \sqrt{\frac{8 * g}{f} * S_o * d} * \frac{\partial d}{\partial x} = 0 \qquad (2\text{-}39)$$

Equation (2-39) maybe rewritten as :

$$\frac{D d}{Dt} = 0 \qquad (2\text{-}41)$$

along the characteristic trajectory :

$$\frac{d x}{dt} = \frac{3}{2} * \sqrt{\frac{8 * g}{f} * S_o * d} \qquad \text{Characteristic trajectory} \quad (2\text{-}42)$$

where D/Dt characterises the absolute differentiation operator.
For a turbulent flow assuming a constant Darcy friction factor, the integration of Equations (2-41) and (2-42) gives :

$$d = \text{constant} \qquad (2\text{-}43)$$

along

$$x = \frac{3}{2} * \sqrt{\frac{8 * g}{f} * S_o} * \sqrt{d} * t + \text{constant} \qquad (2\text{-}44)$$

Equation (2-44) shows that the forward characteristics are straight lines since d and f are constants, as sketched in Figure 2-6B.
The boundary conditions include the conservation of mass :

$$\int_{x=-L_{res}}^{x_S} d * dx = \frac{1}{2} * H_{dam} * L_{res} * \cos\theta = \frac{1}{2} * d_o * L_{res} \qquad (2\text{-}45)$$

where L_{res} is the reservoir length, H_{dam} is the dam height, d_o is the initial reservoir height measured normal to the chute invert and x_S is the wave front position (Fig. 2-6). Considering the forward characteristic d = constant issued from the initial backward characteristic, its trajectory is :

$$x = \frac{3}{2} * \sqrt{\frac{8 * g}{f} * S_o} * \sqrt{d} * t \qquad (2\text{-}46)$$

Combining Equations (2-45) and (2-46), it yields the location x_S of the shock (i.e. dam break wave front) and its celerity U as sketched in Figure 2-6B.

2.4.2 Complete solution for turbulent flows

HUNT's analysis yields a system of three equations :

$$\frac{V_H * t}{L_{res}} = \frac{1 - \left(\frac{d_S}{H_{dam}}\right)^2}{\left(\frac{d_S}{H_{dam}}\right)^{3/2}} \qquad (2\text{-}47)$$

$$\frac{x_S}{L_{res}} = \frac{\frac{3}{2}}{\frac{d_S}{H_{dam}}} - \frac{1}{2} * \frac{d_S}{H_{dam}} - 1 \qquad (2\text{-}48)$$

$$\frac{U}{V_H} = -\frac{3}{4} * \frac{V_H * t}{L_{res}} + \sqrt{\frac{x_S + L_{res}}{L_{res}} + \left(\frac{3}{4} * \frac{V_H * t}{L_{res}}\right)^2} \qquad (2\text{-}49)$$

where t is the time with t = 0 at dam break, d_S is the dam break wave front thickness, x_S is the dam break wave front position measured from the dam site, C_S is the wave front celerity, H_{dam} is the reservoir height at dam site, L is the reservoir length, and S_o is the bed slope, $S_o = H_{dam}/L_{res}$ (Fig. 2-6). The velocity V_H is the uniform equilibrium flow velocity for a water depth H_{dam} :

$$V_H = \sqrt{\frac{8*g}{f} * H_{dam} * S_o} \qquad (2\text{-}50)$$

where f is the Darcy friction factor which is assumed constant. Equations (2-47), (2-48) and (2-49) are valid for $S_o = S_f$ where S_f is the friction slope, and when the free-surface is parallel to the bottom of the sloping channel. Equation (2-48) may be transformed :

$$\frac{d_S}{H_{dam}} = \frac{3}{2} * \frac{L_{res}}{x_S - L_{res}} \qquad \text{for } x_S/L_{res} > 4 \quad (2\text{-}48b)$$

HUNT (1984,1988) developed an analytical expression of the shock front shape :

$$\frac{x - x_S}{L_{res}} = \frac{d_S}{H_{dam}} * \left(\frac{d}{d_S} + Ln\left(1 - \frac{d}{d_S}\right) + \frac{1}{2}\right) \qquad (2\text{-}51)$$

where d is the depth (or thickness) measured normal to the bottom, and d_S and x_S may be calculated using Equations (2-47) and (2-48) respectively. Note that Equation (2-51) applies only to the rounded nose of the shock.

2.4.3 Discussion

The above development is valid for turbulent dam break waves. HUNT (1982) showed that the assumption is valid after the wave front travelled approximately four reservoir lengths downstream of the gate : i.e., $x_S/L_{res} > 4$. The assumption is not valid in the initial instants after dam break nor until the free-surface becomes parallel to the chute invert. HUNT (1984) commented however that his approach could be adapted for $x_S/L_{res} < 4$: "*it is possible that an approach similar [...] could be used to route the flood downstream and that the result might be valid even for relatively small distance downstream*". The dynamic wave equation is simplified by neglecting acceleration and inertial terms, and the free-surface is assumed parallel to the channel bottom ($S_o \approx S_f$). The kinematic wave approximation gives the relationship between the velocity and the water depth :

$$V = V_H * \sqrt{\frac{d}{H_{dam}}} \qquad (2\text{-}52)$$

Once the flood wave has travelled approximately four lengths of reservoir downstream of the dam site, the free-surface profile of the dam break wave follows :

$$\frac{x + L_{res}}{L_{res}} = \frac{d}{H_{dam}} + \frac{3}{2} * \frac{V_H * t}{L_{res}} * \sqrt{\frac{d}{H_{dam}}} \qquad \text{for } x \le x_S \text{ and } x_S/L > 4 \quad (2\text{-}53)$$

The elegant development of HUNT (1982, 1984) was verified by several series of experiments (e.g. HUNT 1984, NSOM et al. 2000). Importantly, it was found to be robust and applicable to a wide range of flow situations including turbulent flow motion on smooth and very-rough inverts (HUNT 1984, CHANSON 2004c,d), laminar flow motion (HUNT 1994, DEBIANE 2000), and even non-Newtonian thixotropic fluid flows with some extension (CHANSON et al. 2004).

3. IDEAL-FLUID FLOW SOLUTIONS OF THE DAM BREAK PROBLEM

3.1 PRESENTATION

An understanding of one-dimensional and two-dimensional flow of ideal fluid provides the engineer with a broader approach to real-fluid flow situations. Although no ideal fluid actually exists, many real fluids have small viscosity and the effects of compressibility may be small. Practical applications include the motion of a dam break wave (Fig. 3-1) surging down an horizontal plane (RITTER's solution) for which an ideal fluid flow solution is directly applicable, but for the initial instants and in the leading edge of the surging waters.

For an ideal fluid flow, the Saint-Venant equations may be simplified since the flow resistance, hence the friction slope, are zero :

$$\frac{\partial d}{\partial t} + \frac{A}{B} * \frac{\partial V}{\partial x} + V * \frac{\partial d}{\partial x} + \frac{V}{B} * \left(\frac{\partial A}{\partial x}\right)_{d=constant} = 0 \qquad \text{Continuity equation (3-1)}$$

$$\frac{\partial V}{\partial t} + V * \frac{\partial V}{\partial x} + g * \frac{\partial d}{\partial x} - g * S_o = 0 \qquad \text{Dynamic equation (3-2)}$$

where S_o is the bed slope ($S_o = \sin\theta$), θ is the angle between the bed and the horizontal, with $\theta > 0$ for a downward slope. It yields a characteristic system of equations :

$$\frac{D}{Dt}(V + 2 * C) = g * S_o \qquad \text{forward characteristic (3-3a)}$$

$$\frac{D}{Dt}(V - 2 * C) = g * S_o \qquad \text{backward characteristic (3-3b)}$$

along :

$$\frac{dx}{dt} = V + C \qquad \text{forward characteristic C1 (3-4a)}$$

$$\frac{dx}{dt} = V - C \qquad \text{backward characteristic C2 (3-4b)}$$

Basically ($V + 2*C - g*S_o*t$) is constant along a forward characteristic while ($V - 2*C - g*S_o*t$) is a constant on each backward characteristic for a constant slope channel.

Simple wave theory

Simple solutions of the Saint-Venant equations may be developed for a "simple wave". A simple wave is defined as a wave for which ($S_o = S_f = 0$) with initially constant water depth and flow velocity. An example is the dam break wave on a horizontal, friction channel (RITTER's solution). The characteristic system of equations for a simple wave is :

$$\frac{D}{Dt}(V + 2 * C) = 0 \qquad \text{forward characteristic (3-5a)}$$

$$\frac{D}{Dt}(V - 2 * C) = 0 \qquad \text{backward characteristic (3-5b)}$$

along :

$$\frac{dx}{dt} = V + C \qquad \text{forward characteristic C1 (3-6a)}$$

$$\frac{dx}{dt} = V - C \qquad \text{backward characteristic C2 (3-6b)}$$

In simple terms, (V+2*C) is a constant along the forward characteristic. For an observer moving at the absolute velocity (V + C), the term (V + 2*C) is constant. Similarly (V - 2*C) is constant along the backward characteristic. When the characteristic trajectories can be plotted in the (x, t) plane,

they represent the path of the observers travelling on the forward and backward characteristics. On each forward characteristic, the slope of the trajectory is 1/(V+C) and (V+2*C) is a constant along the characteristic trajectory. Altogether the characteristic trajectories form contour lines of (V+2*C) and (V-2*C).
In a simple wave problem ($S_o = S_f = 0$), a family of characteristic trajectories is a series of straight lines if any one curve of the family (i.e. C1 or C2) is a straight line (HENDERSON 1966). For the dam break wave on a horizontal, frictionless channel, the initial backward characteristic is a straight line (section 2.2). Hence all backward characteristics are straight lines.
Note that the locations of the dam break wave front form a singularity line, which might be considered as a forward characteristic trajectory in RITTER's solution.

Fig. 3-1 - Photograph of the Möhne dam break (17 May 1943) - View from the left bank

3.2 DAM BREAK IN A FRICTIONLESS HORIZONTAL CHANNEL INITIALLY FILLED WITH WATER WITH NON-ZERO INITIAL VELOCITIES

3.3.1 Presentation

Although many developments consider an initially dry channel, some practical applications comprise situations where some fluid is at rest or in motion in the downstream channel. It is however a different situation from an initially dry channel bed because the dam break wave is led by a positive surge (Fig. 3-2). In other words, a dam break wave on a dry bed is not comparable to a dam break wave propagating over some water, and the shock front is a totally different process (see Applications in Section 5.). This problem was solved by BARRÉ de SAINT-VENANT (1871b) for a rising tide in a channel with initial water depth.
Considering the propagation of a dam break wave over a layer water, the initial downstream depth d_3 satisfies $d_3 > 0$ and the initial velocity is V_3 (Fig. 3-2). Further the flow velocity behind the dam is V_o for $t < 0$ and the dam wall advances at a translation speed V_o prior to dam removal. Dam removal takes place at $t = 0$ when the dam is located at $x = 0$. The dam break is idealised by a vertical wall that is suddenly removed (Fig. 3-2).
The basic flow equations are the characteristic system of equations, and the continuity and momentum equations across the positive surge front. That is :

$$\frac{D}{Dt}(V + 2 * C) = 0 \qquad \text{along } \frac{dx}{dt} = V + C \text{ (forward characteristic)} \quad (3\text{-}5a)$$

$$\frac{D}{Dt}(V - 2 * C) = 0 \qquad \text{along } \frac{dx}{dt} = V - C \text{ (backward characteristic)} \quad (3\text{-}5b)$$

$$d_1 * (U + V_3) = d_2 * (U - V_2) \qquad \text{Continuity equation} \quad (3\text{-}7)$$

$$d_2 * (U - V_2)^2 - d_3 * (U + V_3)^2 = \frac{1}{2} * g * d_3^2 - \frac{1}{2} * g * d_2^2$$

Momentum equation (3-8)

where U is the positive surge celerity for an observer fixed on the channel bank, and the subscripts 3 and 2 refer respectively to the flow conditions upstream and downstream of the positive surge front: i.e., initial flow conditions and new flow conditions behind the surge front (Fig. 3-2). Note that V_3 is positive upstream while V_o, V_2 and U are positive in the downstream direction (Fig. 3-2).

Fig. 3-2 - Sketch of a dam break wave in a horizontal channel initially filled with water

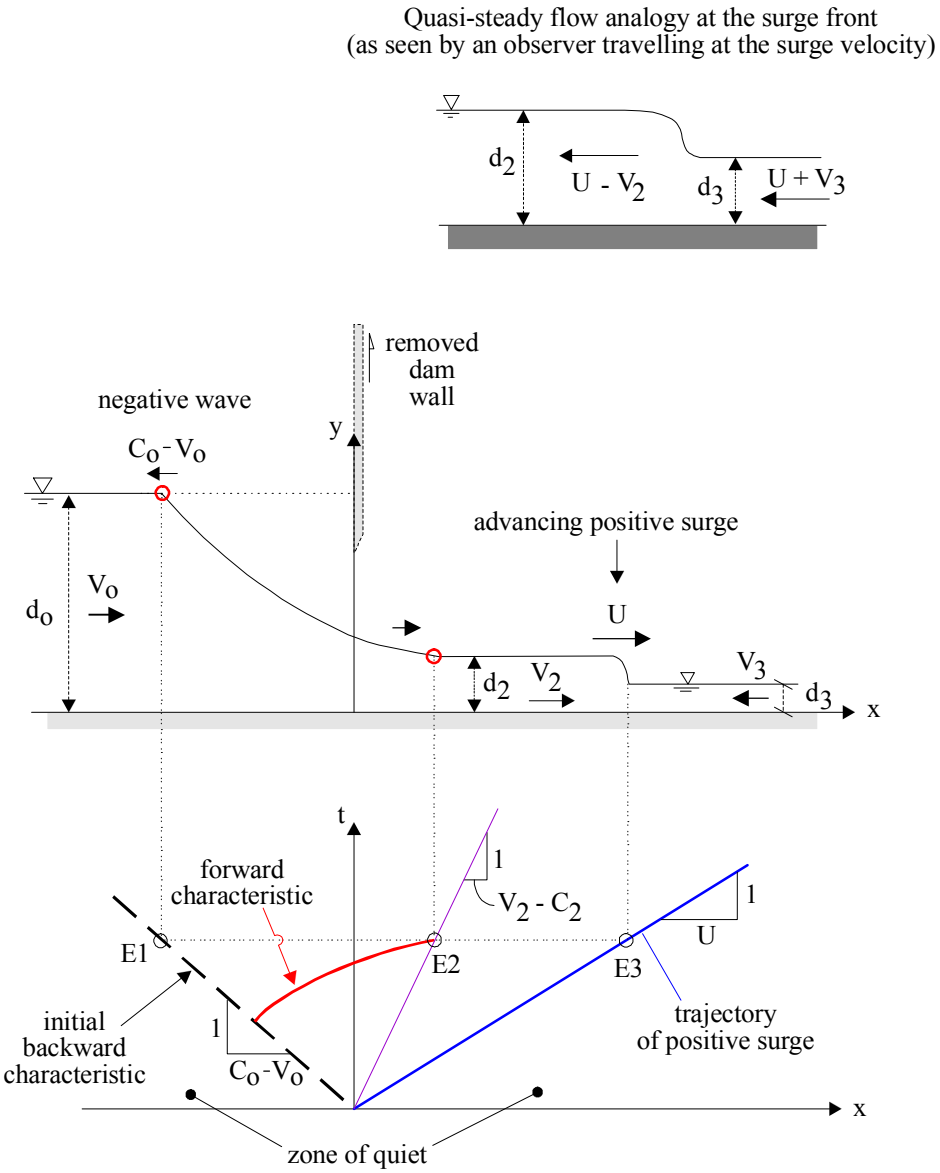

For the positive surge, the continuity and momentum equations yield :

$$\frac{d_2}{d_3} = \frac{1}{2} * \left(\sqrt{1 + 8 * Fr_3^2} - 1\right) \quad (3\text{-}9)$$

$$Fr_2 = \frac{2^{3/2} * Fr_3}{\left(\sqrt{1 + 8 * Fr_3^2} - 1\right)^{3/2}} \quad (3\text{-}10)$$

where the surge Froude numbers Fr_1 and Fr_2 are defined as :

$$Fr_1 = \frac{U + V_3}{\sqrt{g * d_3}} \qquad \text{upstream surge Froude number}$$

$$Fr_2 = \frac{U - V_2}{\sqrt{g * d_2}} \qquad \text{downstream surge Froude number}$$

Immediately after the dam break, a negative surge propagates into the reservoir with known water depth d_o and velocity V_o. In the (x, t) plane, the initial negative wave characteristic has a slope $dt/dx = -1/(C_o - V_o)$ where $C_o = \sqrt{g*d_o}$ assuming a rectangular channel (Fig. 3-2). The initial backward characteristic is a straight line, hence all the C2 characteristics are straight lines.
For $t > 0$, the forward characteristics issuing from the initial backward characteristics cannot intersect the downstream water level ($d = d_3$) because it would involve a discontinuity in velocity. The velocity in the downstream channel is a constant ($V = V_3$) but, on the forward characteristics, it satisfies :

$$V + 2 * C = V_o + 2 * C_o \quad (3\text{-}11)$$

Such a discontinuity in flow velocity and depth can only take place as a positive surge which is sketched in Figure 3-2.

3.2.2 Detailed solution

Considering a horizontal, rectangular channel, the water surface is horizontal and the water depth equals d_o upstream of the leading edge of the negative wave (Fig. 3-2, left of point E1). Between the leading edge of the negative wave (point E1) and the point E2, the free-surface profile is a parabola:

$$\frac{x}{t} = V_o + 2 * \sqrt{g * d_o} - 3 * \sqrt{g * d} \qquad x_{E1} \le x \le x_{E2} \quad (3\text{-}12)$$

and the location of the point E1 is given by :

$$x_{E1} = (V_o - C_o) * t \quad (3\text{-}13)$$

Between the point E2 and the positive surge (point E3), the free-surface profile is horizontal. The flow depth d_2 and velocity V_2 must satisfy the continuity and momentum equations across the positive surge front, as well as the condition along the C1 forward characteristics issuing from the initial negative characteristic and reaching point E2 :

$$V_2 + 2 * \sqrt{g * d_2} = V_o + 2 * \sqrt{g * d_o} \qquad \text{Forward characteristics} \quad (3\text{-}14)$$

The combination of Equation (3-14) and of the continuity and momentum equations across the surge front (Eq. (3-7) and (3-8)) forms a system of three equations with three unknowns V_2, d_2 and U. The system of equations may be solved graphically.
Once the positive surge forms (Fig. 3-2), the locations of the points E2 and E3 satisfy respectively:

$$x_{E2} = (V_2 - C_2) * t \quad (3\text{-}15)$$

$$x_{E3} = U * t \quad (3\text{-}16)$$

where $C_2 = \sqrt{g*d_2}$ for a rectangular channel. It can be shown that the surge front (point E3)

advances faster than the point E2.
The surge celerity U satisfies :

$$\sqrt{\frac{d_o}{d_3}} * \left(1 + \frac{1}{2} * \frac{V_o}{\sqrt{g*d_o}}\right) = \frac{1}{2} * \frac{U}{\sqrt{g * d_3}} * \left(1 - \frac{1}{X}\right) - \frac{1}{2} * \frac{V_3}{\sqrt{g * d_3}} * \frac{1}{X} + \sqrt{X} \quad (3\text{-}17)$$

where

$$X = \frac{1}{2} * \left(\sqrt{1 + 8 * \frac{(U + V_3)^2}{g * d_3}} - 1\right) \quad (3\text{-}18)$$

Note that $X = d_2/d_3$ and that the flow conditions behind the surge front (d_2, V_2) are deduced from the quasi-steady flow analogy (Eq. (3-7) to (3-10)).
The above result shows that the dimensionless surge velocity $U/\sqrt{g*d_3}$ is a function of the ratio d_o/d_3 and of the initial flow Froude numbers $V_o/\sqrt{g*d_o}$ and $V_3/\sqrt{g*d_3}$. For $V_o > 0$ and $V_3 = 0$, the above result shows a faster surge celerity for a given ratio d_o/d_3 than for $V_o = V_3 = 0$. The latter solution is commonly treated in textbooks (e.g. HENDERSON 1966, MONTES 1998, CHANSON 2004a,b).

Fig. 3-3 - Graphical solution of the flow conditions for a dam break wave in a horizontal channel initially filled with water and with zero initial velocity ($V_o = V_3 = 0$) (after CHANSON 2004b)

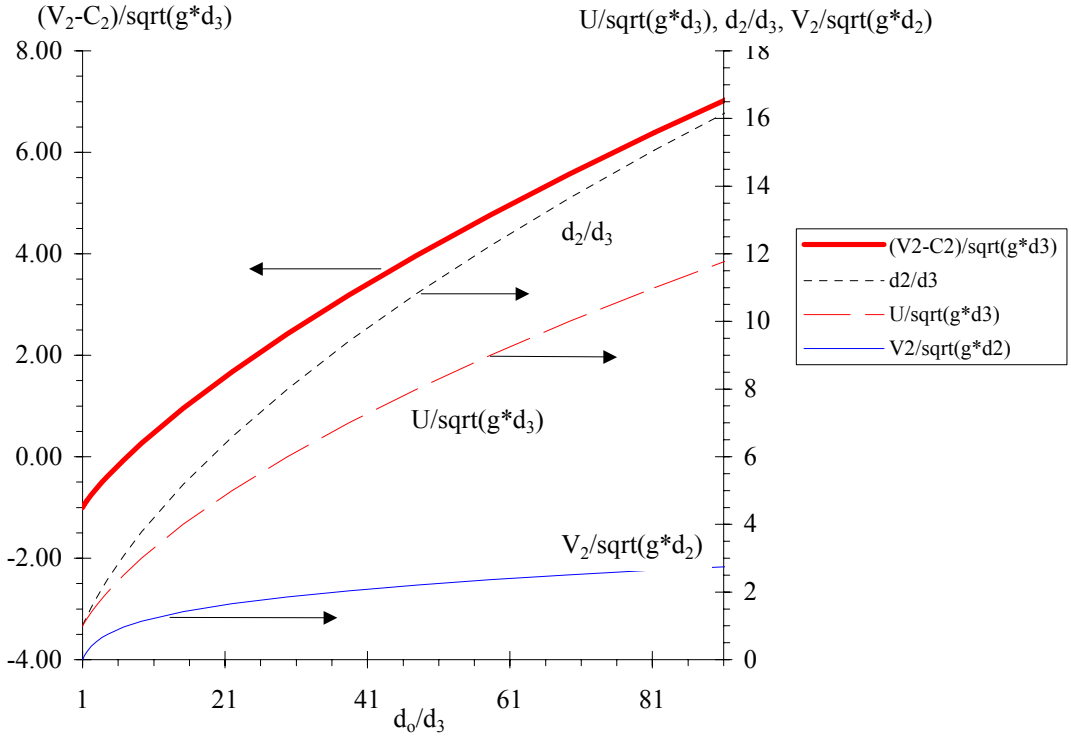

3.3 Discussion

Experimental observations compared well with the above development, and they showed that bottom friction is negligible. Experimental evidences included BAZIN (1865b, pp. 536-553) (see also DARCY and BAZIN 1865), SCHOKLITSCH (1917), CAVAILLE (1965) ([6]), ESTRADE (1967) and more recently CHANSON et al. (2002). Interestingly, BAZIN (1865b) repeated experiments in a large canal with different initial conditions.

[6]CAVAILLE (1965) repeated identical experiments on smooth and rough inverts for three initial water depth to reservoir height ratios.

For the simple case of a channel initially filled with still water ($V_3 = 0$) and with zero initial reservoir translation ($V_o = 0$), a graphical solution of the basic equations is presented in Figure 3-3. Figure 3-3 shows $U/\sqrt{g*d_3}$, d_2/d_3 and $V_2/\sqrt{g*d_2}$ (Right axis), and $(V_2-C_2)/\sqrt{g*d_3}$ (Left axis) as functions of the ratio d_o/d_3, where $C_2 = \sqrt{g*d_2}$.

3.3 DAM BREAK IN A DRY FRICTIONLESS HORIZONTAL CHANNEL WITH AN INITIAL VELOCITY

Considering an ideal dam break surging over a dry frictionless horizontal bed, the initial flow velocity behind the dam is V_o (i.e. for $t < 0$) and the dam advances at a translation speed V_o prior to dam removal. Dam removal takes place at $t = 0$ when the dam is at $x = 0$. The dam break is idealised by a vertical wall that is suddenly removed (Fig. 3-4). After removal of the wall, a negative wave propagates upstream (for $V_o < C_o$) and a dam break wave moves downstream.

The basic equations are those of the simple wave. The instantaneous dam break creates a negative wave propagating upstream into a fluid with known water depth d_o and velocity V_o. In the (x, t) plane, the initial negative wave characteristic has a slope $dt/dx = -1/(C_o-V_o)$ where $C_o = \sqrt{g*d_o}$ assuming a rectangular channel (Fig. 3-4). The initial backward characteristic is a straight line.

Forward characteristics can be drawn issuing from the initial backward characteristic for $t > 0$ (Fig. 3-4, trajectory E1-G1). On each forward characteristic, the flow conditions satisfy :

$$V + 2 * C = V_o + 2 * C_o \qquad (3\text{-}19)$$

because $V = V_o$ and $C = C_o = \sqrt{g*d_o}$ everywhere in the reservoir (Fig. 3-4, point E1).

The forward characteristic issuing from the origin ($x = 0$, $t = 0$) propagates downstream while satisfying :

$$V + 2 * C = V_o + 2 * C_o$$

and $d = 0$ (hence $C = 0$) at the leading edge of the wave front. The propagation speed of the dam break wave front equals :

$$\frac{U}{\sqrt{g * d_o}} = 2 + \frac{V_o}{\sqrt{g * d_o}} \qquad (3\text{-}20)$$

Considering any backward characteristic issuing from the dam break wave front (Fig. 3-4, trajectory F1-G1), the C2 characteristic is a straight line because the initial backward characteristic is a straight line. The inverse slope of the backward characteristic is a constant :

$$\frac{d\,x}{dt} = V - C = V_o + 2 * C_o - 3 * C \qquad (3\text{-}21)$$

The integration of the inverse slope gives the water surface profile at the intersection of the C2 characteristic with a horizontal line t = constant (Fig. 3-4, point G1). That is, at a given time, the free-surface profile between the leading edge of the negative wave and the wave front is a parabola:

$$\frac{x}{t * \sqrt{g * d_o}} = 2 + \frac{V_o}{\sqrt{g * d_o}} - 3 * \sqrt{\frac{d}{d_o}}$$

$$\text{for } \frac{V_o}{\sqrt{g*d_o}} - 1 \le \frac{x}{t * \sqrt{g * d_o}} \le 2 + \frac{V_o}{\sqrt{g*d_o}} \qquad (3\text{-}22)$$

At the location ($x = V_o*t$), the above equation predicts a constant water depth during the dam break wave $d(x=V_o*t) = 4/9*d_o$.

Note that the reasoning is valid for $V_o < 0$ or $V_o > 0$, including for $V_o > C_o$. It is a simple extension of RITTER's solution (paragraph 2.2). It may be compared with the solution for an initial non-zero downstream water depth (paragraph 3.2) with $d_3 > 0$.

Fig. 3-4 - Sketch of a dam break wave in a dry frictionless horizontal channel with non-zero initial velocity

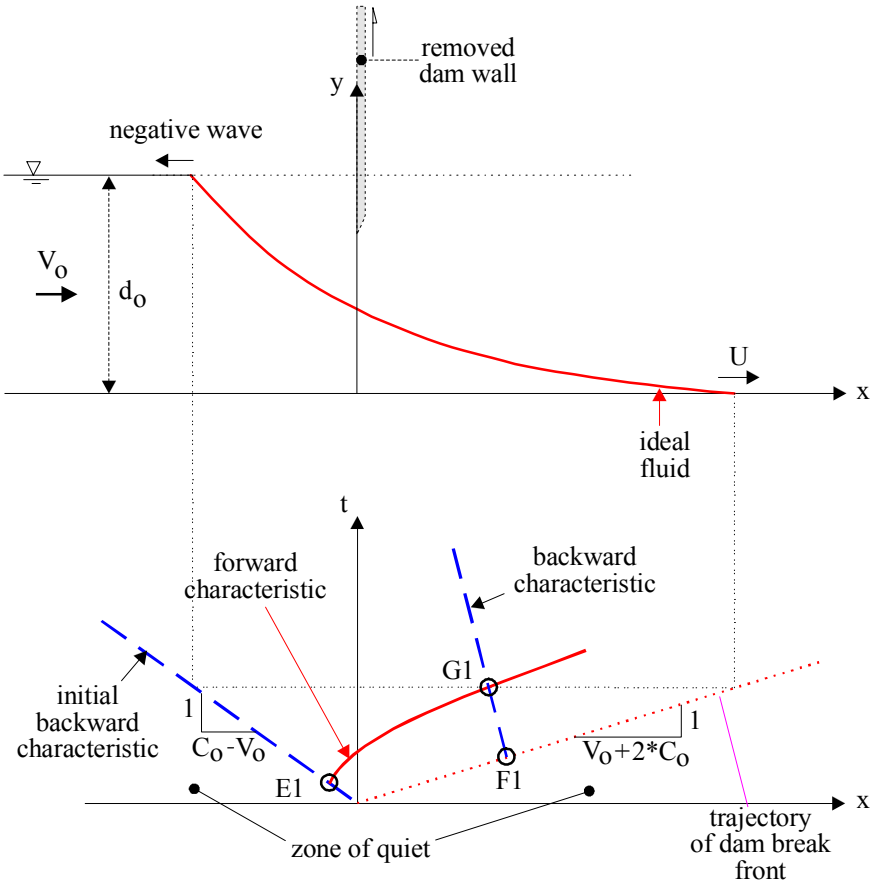

3.4 DAM BREAK WAVE ON A DRY FRICTIONLESS SLOPING UPWARD CHANNEL

3.4.1 Basic equations

For a dam break wave in a dry, sloping upward channel with zero initial velocity, in a prismatic, wide rectangular channel, the method of characteristics may be applied :

$$\frac{D}{Dt}(V + 2 * C) = g * S_o \qquad \text{forward characteristic} \quad (3\text{-}3a)$$

$$\frac{D}{Dt}(V - 2 * C) = g * S_o \qquad \text{backward characteristic} \quad (3\text{-}3b)$$

along :

$$\frac{dx}{dt} = V + C \qquad \text{forward characteristic C1} \quad (3\text{-}4a)$$

$$\frac{dx}{dt} = V - C \qquad \text{backward characteristic C2} \quad (3\text{-}4b)$$

That is, $(V + 2*C - g*S_o*t)$ is a constant along a forward characteristic and $(V - 2*C - g*S_o*t)$ is constant on a backward characteristic for a constant slope channel.

The dam break with zero initial velocity may be idealised by a vertical wall that is suddenly removed (Fig. 3-5). The instantaneous dam break creates a negative wave propagating upstream into a fluid at rest with known water depth (i.e. d_o at the gate). In the (x, t) plane, the initial

negative wave characteristic has a slope dt/dx = -1/C with $C = C_o$ for t = 0 (Fig. 3-5) ([7]).
Forward characteristics can be drawn issuing from the initial backward characteristic for t > 0 (Fig. 3-5). On the forward characteristic issuing from the origin (x = 0, t = 0), the flow conditions must satisfy :

$$V_{F1} + 2 * C_{F1} - g * S_o * t_{F1} = V_O + 2 * C_O - g * S_o * t_O$$
$$= 2 * C_o - g * S_o * t_{E1} \quad (3\text{-}23)$$

since V = 0 at the origin (Fig. 3-5). At the leading edge of the dam break wave front, the water depth is zero, hence $C_{F1} = 0$, and the propagation speed of the dam break wave front equals :

$$U = 2 * C_o + g * S_o * t_{F1} \quad (3\text{-}24)$$

Fig. 3-5 - Sketch of a dam break wave in a dry, frictionless, sloping upward, rectangular channel with zero initial velocity

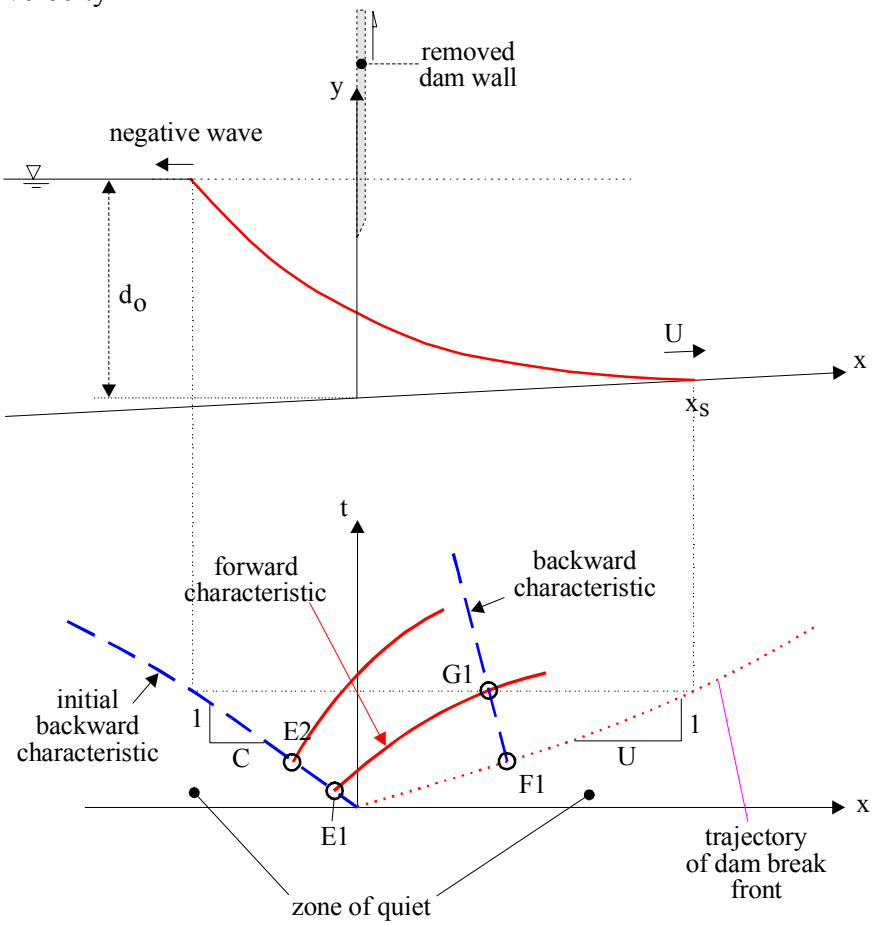

In dimensionless form, an estimate of the dam break wave celerity for a flat slope is :

$$\frac{U}{\sqrt{g * d_o}} = 2 + S_o \sqrt{\frac{g}{d_o}} * t \quad (3\text{-}25)$$

where S_o is negative for an inclined upward slope as sketched in Figure 3-5. Since $U = dx_S/dt$, the location x_S of the wave front is :

$$\frac{x_S}{t * \sqrt{g * d_o}} = 2 + \frac{1}{2} * S_o * \sqrt{\frac{g}{d_o}} * t \quad (3\text{-}26)$$

---

[7]For a flat slope, the initial backward characteristic propagates upstream with a celerity $C_o = \sqrt{g*d_o}$ in first approximation.

Note that the dam break wave celerity becomes zero (U = 0) when :

$$\sqrt{\frac{g}{d_o}} * t = -\frac{2}{S_o} \qquad U = 0 \quad (3\text{-}26)$$

corresponding to

$$\frac{(x_s)_{max}}{d_o} = -\frac{2}{S_o} \qquad U = 0 \quad (3\text{-}27)$$

For an upward slope, the maximum elevation reached by the wave front runup is $z_{max} = 2*d_o$. The result is independent of the bed slope. However, this reasoning is based upon equations derived for the initial stage of the dam break wave on a flat slope.

3.4.2 Free-surface profile

Considering any backward characteristic issuing from the dam break wave front (Fig. 3-5, trajectory F1-G1), the inverse slope of the backward characteristics is :

$$\frac{dx}{dt} = V - C$$

Considering the point G1 at the intersection of the C2 characteristics with a forward characteristic issued from the initial backward characteristic (Fig. 3-5, trajectory E1-G1), the characteristic equations yield :

$$V + 2 * C - g * S_o * t = 2 * C_{E1} - g * S_o * t_{E1} \qquad (3\text{-}28)$$

Hence the inverse slope of the backward characteristics is :

$$\frac{dx}{dt} = 2 * C_{E1} - 3 * C + g * S_o * (t - t_{E1}) \qquad (3\text{-}29)$$

Assuming that $t_{E1} << t$ and $C_{E1} \approx C_o$ ([8]), the integration of the inverse slope gives the water surface profile at the intersection of the C2 characteristics with a horizontal line t = constant (Fig. 3-5, point G1). At a given time t, the free-surface profile between the leading edge of the negative wave and the wave front is :

$$\frac{x}{t * \sqrt{g * d_o}} = 2 - 3 * \sqrt{\frac{d}{d_o}} + \frac{1}{2} * S_o * \sqrt{\frac{g}{d_o}} * t$$

$$\text{for } -1 \le \frac{x}{t * \sqrt{g * d_o}} \le 2 + \frac{1}{2} * S_o * \sqrt{\frac{g}{d_o}} * t \quad (3\text{-}30)$$

The free-surface profile may be sometimes rewritten in terms of the celerity of small disturbance C and of the water depth d:

$$\frac{C}{\sqrt{g * d_o}} = \frac{1}{3} * \left(2 + \frac{1}{2} * S_o * \sqrt{\frac{g}{d_o}} * t - \frac{x}{t * \sqrt{g * d_o}} \right)$$

$$\text{for } -1 \le \frac{x}{t * \sqrt{g * d_o}} \le 2 + \frac{1}{2} * S_o * \sqrt{\frac{g}{d_o}} * t \quad (3\text{-}31)$$

$$\frac{d}{d_o} = \frac{1}{9} * \left(2 + \frac{1}{2} * \sqrt{\frac{g}{d_o}} * S_o * t - \frac{x}{t} \right)^2$$

$$\text{for } -1 \le \frac{x}{t * \sqrt{g * d_o}} \le 2 + \frac{1}{2} * S_o * \sqrt{\frac{g}{d_o}} * t \quad (3\text{-}32)$$

[8] That is, the negative characteristics are straight lines.

Along the free-surface profile, the flow velocity V equals :

$$\frac{V}{\sqrt{g * d_o}} = \frac{2}{3} * \left(1 + S_o * \sqrt{\frac{g}{d_o}} * t + \frac{x}{t * \sqrt{g * d_o}} \right)$$

$$\text{for } -1 \leq \frac{x}{t * \sqrt{g*d_o}} \leq 2 + \frac{1}{2} * S_o * \sqrt{\frac{g}{d_o}} * t \quad (3\text{-}33)$$

At the dam location (x = 0), the water depth and flow velocity become functions of time. For an inclined upward plane, the flow rate at the dam site decreases with time :

$$\frac{q(x=0)}{\sqrt{g * d_o^3}} = \frac{8}{27} * \left(1 + \frac{1}{4} * \sqrt{\frac{g}{d_o}} * S_o * t \right)^2 * \left(1 + \sqrt{\frac{g}{d_o}} * S_o * t \right) \quad (3\text{-}34)$$

For a horizontal channel ($S_o = 0$), the results yield RITTER's solution (paragraph 2.2).
It must be emphasised again that the development is limited to the initial stages of the dam break wave on a flat slope (paragraph 3.4.1).

3.5 DAM BREAK WAVE ON A DRY FRICTIONLESS SLOPING UPWARD CHANNEL WITH SOME INITIAL VELOCITY

3.5.1 Basic equations

For a dam break wave in a dry, sloping upward channel with some initial velocity V_o, in a prismatic, wide rectangular channel, the method of characteristics may be applied. The dam break is idealised by a vertical wall that is suddenly removed at t = 0 when the dam wall is at x = 0.
The instantaneous dam break creates a negative wave propagating upstream into a fluid with known water depth and flow velocity. During the initial stages of a dam break wave on a flat slope, it is reasonable to assume that the initial negative wave characteristic has a slope $dt/dx \approx -1/(C_o - V_o)$ where $C_o = \sqrt{g*d_o}$. Forward characteristics can be drawn issuing from the initial backward characteristic for t > 0. Considering the initial forward characteristic issuing from the origin (Fig. 3-6, trajectory O-F1), the flow conditions satisfy :

$$V_o + 2 * C_o = V_{F1} + 2 * C_{F1} - g * S_o * t_{F1} \quad (3\text{-}35)$$

where $C_o = \sqrt{g*d_o}$.
At the leading edge of the dam break wave front, the water depth is zero (i.e. $C_{F1} = 0$), and the propagation speed of the dam break wave front equals :

$$U = 2 * C_o + V_o + g * S_o * t_{F1} \quad (3\text{-}36)$$

In the initial stages of the dam break wave on a flat slope, the dimensionless expression of the dam break wave celerity is :

$$\frac{U}{\sqrt{g * d_o}} = 2 + \frac{V_o}{\sqrt{g * d_o}} + S_o \sqrt{\frac{g}{d_o}} * t \quad (3\text{-}37)$$

where S_o is negative for an inclined upward slope as sketched in Figure 3-6. Since $U = dx_S/dt$, the location x_S of the wave front is :

$$\frac{x_S}{t * \sqrt{g * d_o}} = 2 + \frac{V_o}{\sqrt{g * d_o}} + \frac{1}{2} * S_o * \sqrt{\frac{g}{d_o}} * t \quad (3\text{-}38)$$

For an upward sloping channel, the dam break wave celerity becomes zero (U = 0) when :

$$\sqrt{\frac{g}{d_o}} * t = - \frac{2 + \frac{V_o}{\sqrt{g * d_o}}}{S_o} \qquad U = 0 \quad (3\text{-}39)$$

corresponding to

$$\frac{(x_s)_{max}}{d_o} = -\frac{2}{S_o} * \left(1 + \frac{1}{2} * \frac{V_o}{\sqrt{g * d_o}}\right)^2 \qquad U = 0 \quad (3\text{-}40)$$

The maximum elevation reached by the wave front runup is : $z_{max}/d_o = 2 + V_o/\sqrt{g*d_o}$. The result is independent of the bed slope, but the reasoning is based upon equations derived for the initial stages of the dam break wave on a flat slope.

Remarks
PEREGRINE and WILLIAMS (2001) proposed a complete solution of the problem using a slightly different approach.

Fig. 3-6 - Sketch of a dam break wave in a dry, frictionless, sloping upward, rectangular channel with some initial velocity

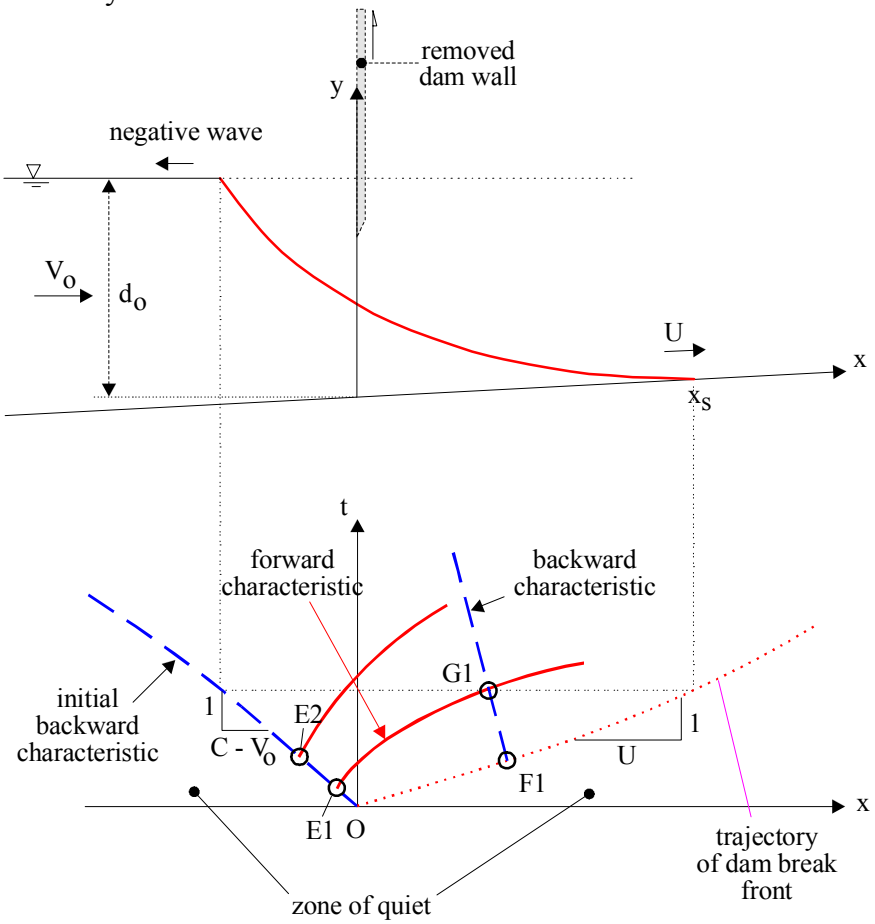

3.5.2 Free-surface profile

Considering any backward characteristic issuing from the dam break wave front (Fig. 3-6, trajectory F1-G1), the inverse slope of the backward characteristics is :

$$\frac{dx}{dt} = V - C$$

Considering the point G1 at the intersection of the C2 characteristics with a forward characteristic issued from the initial backward characteristic (Fig. 3-6, trajectory E1-G1), the characteristic equations yield :

$$V + 2 * C - g * S_o * t = V_o + 2 * C_o - g * S_o * t_{E1} \qquad (3\text{-}41)$$

Hence the inverse slope of the backward characteristics is :

$$\frac{d\,x}{dt} = V_o + 2 * C_o - 3 * C + g * S_o *(t - t_{E1}) \qquad (3\text{-}42)$$

Assuming that $t_{E1} << t$ and that the negative characteristics are straight lines, the integration of the inverse slope gives the water surface profile at the intersection of the C2 characteristics with a horizontal line t = constant (Fig. 3-6, point G1). At a given time t, the free-surface profile between the leading edge of the negative wave and the wave front is :

$$\frac{x}{t * \sqrt{g * d_o}} = 2 + \frac{V_o}{\sqrt{g * d_o}} - 3 * \sqrt{\frac{d}{d_o}} + \frac{1}{2} * S_o * \sqrt{\frac{g}{d_o}} * t$$

$$\text{for } \frac{V_o}{\sqrt{g * d_o}} - 1 \le \frac{x}{t * \sqrt{g*d_o}} \le 2 + \frac{V_o}{\sqrt{g * d_o}} + \frac{1}{2} * S_o * \sqrt{\frac{g}{d_o}} * t \qquad (3\text{-}43)$$

The free-surface profile may be sometimes as in terms of the celerity of small disturbance C and of the water depth d:

$$\frac{C}{\sqrt{g * d_o}} = \frac{1}{3} * \left(2 + \frac{V_o}{\sqrt{g * d_o}} + \frac{1}{2} * S_o * \sqrt{\frac{g}{d_o}} * t - \frac{x}{t * \sqrt{g * d_o}} \right)$$

$$\text{for } \frac{V_o}{\sqrt{g * d_o}} - 1 \le \frac{x}{t * \sqrt{g*d_o}} \le 2 + \frac{V_o}{\sqrt{g * d_o}} + \frac{1}{2} * S_o * \sqrt{\frac{g}{d_o}} * t \qquad (3\text{-}44)$$

$$\frac{d}{d_o} = \frac{1}{9} * \left(2 + \frac{V_o}{\sqrt{g * d_o}} + \frac{1}{2} * \sqrt{\frac{g}{d_o}} * S_o * t - \frac{x}{t} \right)^2$$

$$\text{for } \frac{V_o}{\sqrt{g * d_o}} - 1 \le \frac{x}{t * \sqrt{g*d_o}} \le 2 + \frac{V_o}{\sqrt{g * d_o}} + \frac{1}{2} * S_o * \sqrt{\frac{g}{d_o}} * t \qquad (3\text{-}45)$$

Along the free-surface profile, the flow velocity V equals :

$$\frac{V}{\sqrt{g * d_o}} = \frac{2}{3} * \left(1 + \frac{1}{2} * \frac{V_o}{\sqrt{g * d_o}} + S_o * \sqrt{\frac{g}{d_o}} * t + \frac{x}{t * \sqrt{g * d_o}} \right)$$

$$\text{for } \frac{V_o}{\sqrt{g * d_o}} - 1 \le \frac{x}{t * \sqrt{g*d_o}} \le 2 + \frac{V_o}{\sqrt{g * d_o}} + \frac{1}{2} * S_o * \sqrt{\frac{g}{d_o}} * t \qquad (3\text{-}46)$$

For a horizontal channel, the results yield the solutions developed in paragraph 2.2 and 3.3 for $V_o = 0$ and $V_o > 0$ respectively.

It must be emphasised again that the development is limited to the initial stages of the dam break wave on a flat slope (paragraph 3.5.1).

4. REAL-FLUID FLOW SOLUTIONS OF THE DAM BREAK PROBLEM (TURBULENT FLOW MOTION)

4.1 PRESENTATION

Experimental observations showed that the dam break front propagates at a slower pace than the ideal fluid flow predictions. Further the leading edge of the shock has a rounded shape. These findings were confirmed by a few prototype data : e.g., for the Malpasset dam break (FAURE and NAHAS 1965). Both results have direct implications for the predictions of real dam break waves (e.g. Fig. 4-1).

In this section, flow resistance is taken into account. Simple solutions are developed for turbulent flow motion in horizontal and flat-slope channels. The results are compared with experimental observations (App. B), and practical applications are developed in Section 6. Laminar flow solutions are developed in Section 5.

Fig. 4-1 - Photograph of the Dale Dyke dam break (11 March 1864) (Courtesy of Michael ARMITAGE) - Looking upstream at the ruptured dam - More than 150 people died in the catastrophe

4.2 DAM BREAK IN A DRY HORIZONTAL CHANNEL WITH BED FRICTION AND ZERO INITIAL VELOCITY (DIFFUSIVE WAVE MODEL)

4.2.1 Presentation

For a dam break wave in a dry horizontal channel with a semi-infinite reservoir, experiments showed that RITTER's theory is not valid to predict the flow properties at the leading tip of the wave front. Let us consider a dam break wave fed by a semi-infinite reservoir into a horizontal, prismatic, wide rectangular channel. The dam break is idealised by a vertical wall located at $x = 0$ that is suddenly removed at $t = 0$ (Fig. 4-2).

Experimental measurements (App. B) demonstrated that the wave front has a rounded shape and its celerity U is less than $2*C_O$. These observations demonstrated further that the flow properties were well approximated by RITTER's theory between the most upstream extent of the initial backward characteristic and a flow region immediately upstream of the dam break wave leading tip. Herein the dam break flow is analysed as an ideal-fluid flow region behind a flow resistance-dominated tip zone. The transition between the ideal dam break wave profile and the wave tip region is denoted

F2 as shown in Figure 4-2. Point F2 is located at $x = x_1$ where the flow depth is d_1 and the velocity is V_1.

In the wave tip region ($x_1 \leq x \leq x_S$), flow resistance is dominant, and the acceleration and inertial terms are small. The flow velocity does not vary rapidly in the forward tip zone and experimental data showed that it is about the wave front celerity U (DRESSLER 1952,1954, ESTRADE 1967, LAUBER 1997). The dynamic wave equation may be reduced into a diffusive wave equation :

$$\frac{\partial d}{\partial x} + \frac{f}{8} * \frac{U^2}{g*d} = 0 \qquad \text{Wave tip region (4-1)}$$

Next to the leading edge of the wave, the slope of the free-surface becomes important to counterbalance the flow resistance. The integration of the diffusive wave equation (Eq. (4-1)) yields the shape of the wave front

$$d = \sqrt{\frac{f}{4 * g} * U^2 * (x_S - x)} \qquad \text{Wave front profile (4-2)}$$

assuming a constant Darcy friction factor f in the wave tip region and where x_S is the wave front location. Equation (4-2) would be suitable to turbulent flow motion, but another result is obtained for laminar flow motion (Section 5).

The above equations are not strictly correct. In the wave tip region, the free-surface curvature is not negligible and the flow resistance is very significant. As a result, the Saint-Venant equations are not valid. But Equations (4-1) and (4-2) provide a simple, yet relatively realistic estimate of the wave tip shape (see below).

Fig. 4-2 - Sketch of dam break wave in a horizontal dry channel with bottom friction

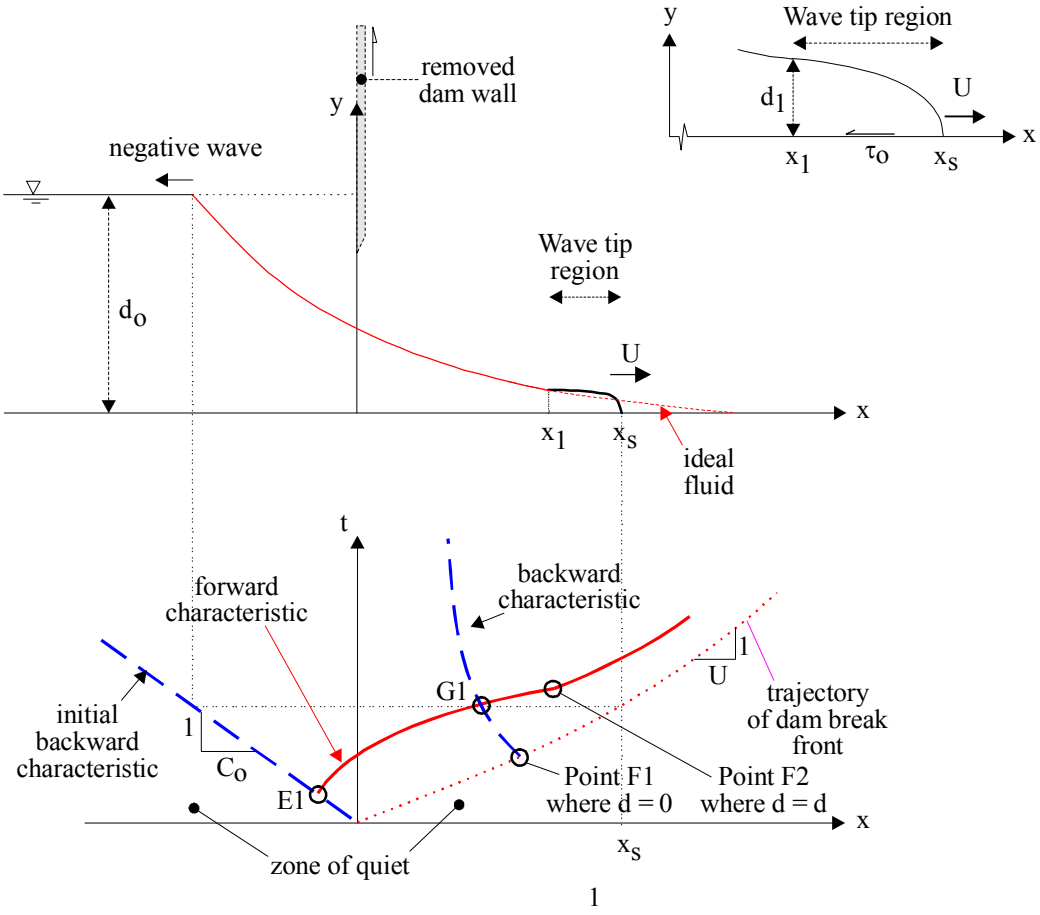

1

4.2.2 Detailed solution

The instantaneous dam break creates a negative wave propagating upstream into a still fluid with known water depth d_o. In the (x, t) plane, the initial negative wave characteristic has a slope dt/dx = $-1/C_o$ where $C_o = \sqrt{g*d_o}$. Note that the initial backward characteristic is a straight line, but the other backward characteristics are not ([1]). Forward characteristics can be drawn issuing from the initial backward characteristic for t > 0 (Fig. 4-2). Between the points E1 and F2, the flow properties satisfy the ideal dam break wave properties :

$$\sqrt{\frac{d}{d_o}} = \frac{1}{3} * \left(2 - \frac{x}{t * \sqrt{g * d_o}}\right) \qquad -1 \le \frac{x}{t * \sqrt{g * d_o}} \le \frac{x_1}{t * \sqrt{g * d_o}} \quad (4\text{-}3)$$

$$\frac{V}{\sqrt{g * d_o}} = \frac{2}{3} * \left(1 + \frac{x}{t * \sqrt{g * d_o}}\right) \qquad -1 \le \frac{x}{t * \sqrt{g * d_o}} \le \frac{x_1}{t * \sqrt{g * d_o}} \quad (4\text{-}4)$$

where d and V are the flow depth and velocity respectively at a distance x from the dam, and t is the time from the instantaneous dam removal.

For $x_1 \le x \le x_S$ (i.e. wave tip region), it is assumed that the velocity of water does not vary rapidly and that it equals the wave front celerity U. The flow properties in the wave tip region may be estimated using the diffusion wave equation taking into account flow resistance (Eq. (4-1)) assuming V = U. The integration of the diffusive wave equation yields the wave front profile:

$$\frac{d}{d_o} = \sqrt{\frac{f}{4} * \frac{U^2}{g * d_o} * \frac{x_S - x}{d_o}} \qquad \frac{x_1}{t * \sqrt{g * d_o}} \le \frac{x}{t * \sqrt{g * d_o}} \le \frac{x_S}{t * \sqrt{g * d_o}} \quad (4\text{-}5)$$

assuming a constant Darcy friction factor for $x_1 \le x \le x_S$.

Since the free-surface and velocity must be continue at the point F2, its flow properties (x_1, V_1, d_1) must satisfy :

$$\sqrt{\frac{d_1}{d_o}} = \frac{1}{3} * \left(2 - \frac{x_1}{\sqrt{g * d_o} * t}\right) \quad (4\text{-}6)$$

$$\frac{V_1}{\sqrt{g*d_o}} = \frac{2}{3} * \left(1 + \frac{x_1}{\sqrt{g * d_o} * t}\right) \quad (4\text{-}7)$$

$$\frac{U}{\sqrt{g * d_o}} = \frac{V_1}{\sqrt{g * d_o}} \quad (4\text{-}8)$$

$$\frac{d_1}{d_o} = \sqrt{\frac{f}{4} * \frac{U^2}{g * d_o} * \frac{x_S - x_1}{d_o}} \quad (4\text{-}9)$$

The conservation of mass must be further satisfied. Specifically the mass of fluid in the wave tip region (i.e. $x_1 \le x \le x_S$) must equal the mass of fluid in the ideal fluid flow profile for $x_1 \le x \le 2*\sqrt{g*d_o}*t$. It yields :

$$\int_{x_1}^{x_S} \sqrt{\frac{f}{4 * g} * U^2 * (x_S - x)} * dx = \int_{x_1}^{2*\sqrt{g*d_o}*t} \frac{1}{9 * g} * \left(2 * \sqrt{g * d_o} - \frac{x}{t}\right)^2 * dx \quad (4\text{-}10)$$

Note that the continuity equation becomes a differential equation in terms of the wave front location x_S and celerity $U = dx_S/dt$. It must be stressed that the development is limited. The Saint-Venant

[1]Because the problem is not a simple wave since $S_f > 0$.

equations, hence the diffusive wave equation, are not valid near the wave leading edge where the free-surface curvature is not small and where the flow resistance becomes very significant.
The above equations may be transformed to express d_1 and x_1 as functions of U:

$$\frac{d_1}{d_o} = \left(1 - \frac{1}{2} * \frac{U}{\sqrt{g * d_o}}\right)^2 \quad (4\text{-}11)$$

$$\frac{x_1}{\sqrt{g * d_o} * t} = \left(\frac{3}{2} * \frac{U}{\sqrt{g * d_o}} - 1\right) \quad (4\text{-}12)$$

The continuity equation (Eq. (4-10)) yields a polynomial equation in terms of the wave front location x_S, wave celerity $U = dx_S/dt$ and location x_1 of the point F2 :

$$\frac{2}{3} * \sqrt{\frac{f}{4} * \frac{U^2}{g * d_o}} * \left(\frac{x_S - x_1}{\sqrt{g * d_o} * t}\right)^{3/2} = \frac{1}{27} * \sqrt[4]{\frac{d_o}{g}} * \frac{1}{\sqrt{t}} * \left(2 - \frac{x_1}{\sqrt{g * d_o} * t}\right)^3 \quad (4\text{-}13)$$

Since the wave tip region has a parabolic free-surface profile, the water depth at point F2 satisfies:

$$\frac{d_1}{d_o} = \sqrt{\frac{f}{4} * \frac{U^2}{g * d_o} * \frac{x_S - x_1}{d_o}} \quad (4\text{-}9)$$

and hence the wave tip region length is:

$$\frac{x_S - x_1}{d_o} = \frac{4}{f} * \frac{g * d_o}{U^2} * \left(1 - \frac{1}{2} * \frac{U}{\sqrt{g*d_o}}\right)^4 \quad (4\text{-}14)$$

By replacing into the continuity equation, the exact solution in terms of the wave front celerity is :

$$\frac{8}{3} * \frac{1}{f} * \frac{\left(1 - \frac{1}{2} * \frac{U}{\sqrt{g * d_o}}\right)^3}{\frac{U^2}{g*d_o}} = \sqrt{\frac{g}{d_o}} * t \quad (4\text{-}15)$$

while the wave front location equals:

$$\frac{x_S}{d_o} = \left(\frac{3}{2} * \frac{U}{\sqrt{g * d_o}} - 1\right) * \sqrt{\frac{g}{d_o}} * t + \frac{4}{f * \frac{U^2}{g*d_o}} * \left(1 - \frac{1}{2} * \frac{U}{\sqrt{g*d_o}}\right)^4 \quad (4\text{-}16)$$

and the free-surface profile satisfies :

$$\frac{d}{d_o} = 1 \qquad \frac{x}{d_o} \le -\sqrt{\frac{g}{d_o}} * t \quad (4\text{-}17a)$$

$$\frac{d}{d_o} = \frac{1}{9} * \left(2 - \frac{x}{t * \sqrt{g * d_o}}\right)^2$$

$$-\sqrt{\frac{g}{d_o}} * t \le \frac{x}{d_o} \le \left(\frac{3}{2} * \frac{U}{\sqrt{g * d_o}} - 1\right) * \sqrt{\frac{g}{d_o}} * t \quad (4\text{-}17b)$$

$$\frac{d}{d_o} = \sqrt{\frac{f}{4} * \frac{U^2}{g * d_o} * \frac{x_S - x}{d_o}} \qquad \left(\frac{3}{2} * \frac{U}{\sqrt{g * d_o}} - 1\right) * \sqrt{\frac{g}{d_o}} * t \le \frac{x}{d_o} \le \frac{x_S}{d_o} \quad (4\text{-}17c)$$

$$\frac{d}{d_o} = 0 \qquad \frac{x_s}{d_o} \leq \frac{x}{d_o} \quad (4\text{-}17d)$$

The location of point F2 is given by :

$$\frac{x_1}{\sqrt{g * d_o} * t} = \left(\frac{3}{2} * \frac{U}{\sqrt{g * d_o}} - 1\right) \quad (4\text{-}18)$$

Typical analytical results are summarised in Figure 4-3 for several values of the Darcy friction factor f and they are compared with experimental observations of wave front properties and free-surface profile.

Fig. 4-3 - Dimensionless wave front location, celerity and free-surface profile solutions as functions of the Darcy friction factor

(A) Dimensionless wave front location - Comparison with experimental data (DRESSLER 1954, LAUBER 1997)

Reference :	DRESSLER Smooth	DRESSLER Sand paper	DRESSLER Slats	LAUBER
Roughness :	Painted timber	Sand paper	Strips: 6.3 mm high, 22.4 m apart	PVC invert

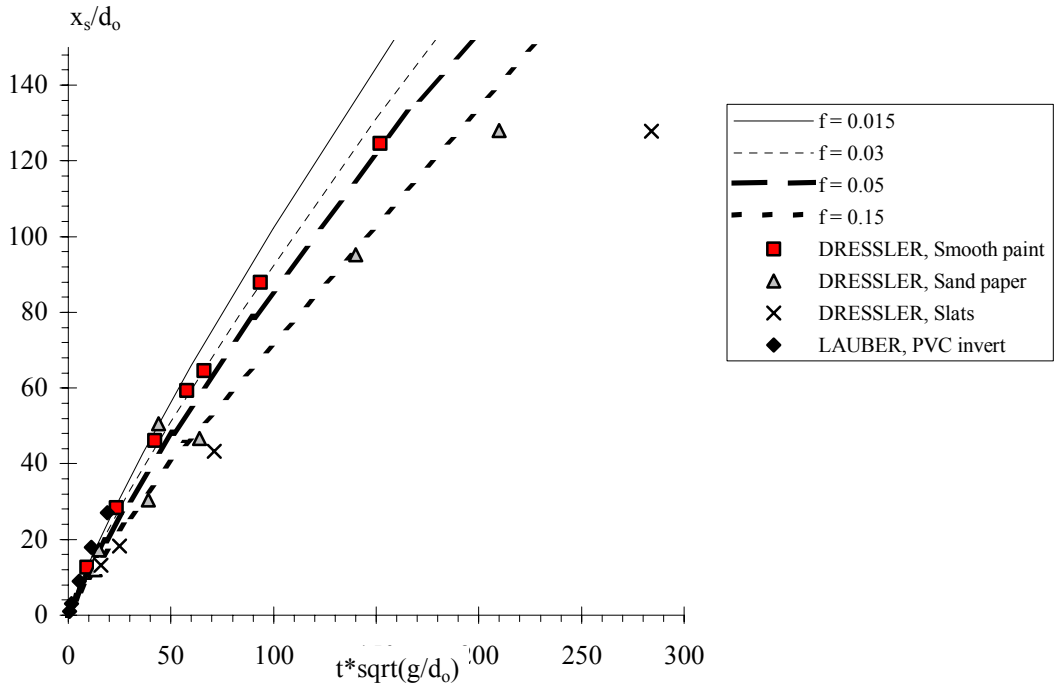

(B) Dimensionless wave front celerity - Comparison with the theoretical results of WHITHAM (1955) and the semi-empirical model of LAUBER (1997) for f = 0.03

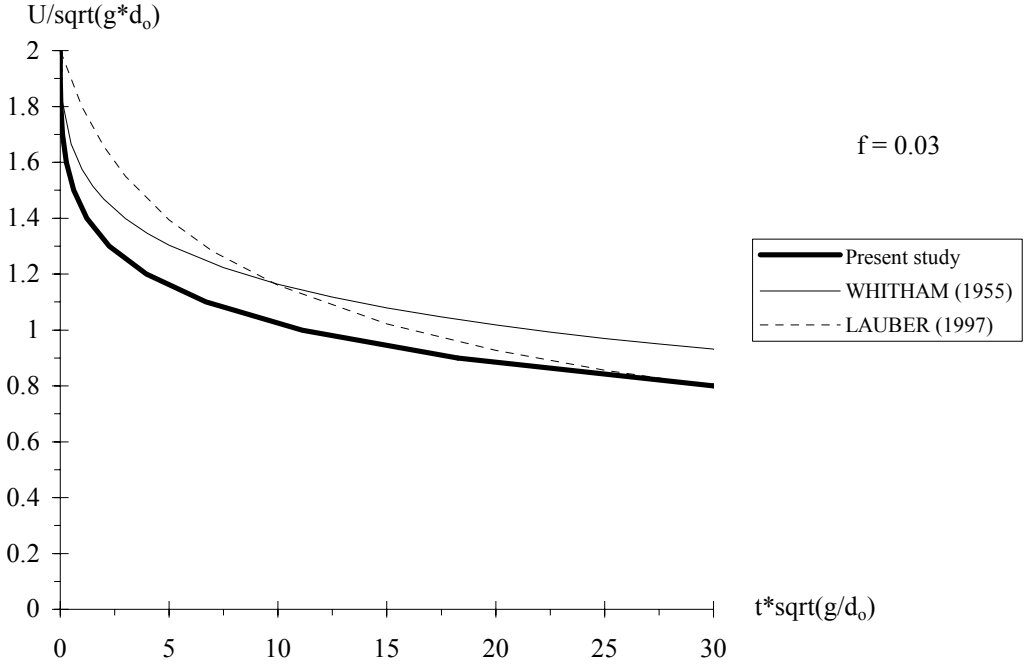

(C) Dimensionless free-surface profiles - Comparison with experimental data

(C1) Comparison with SCHOKLITSCH's (1917) data

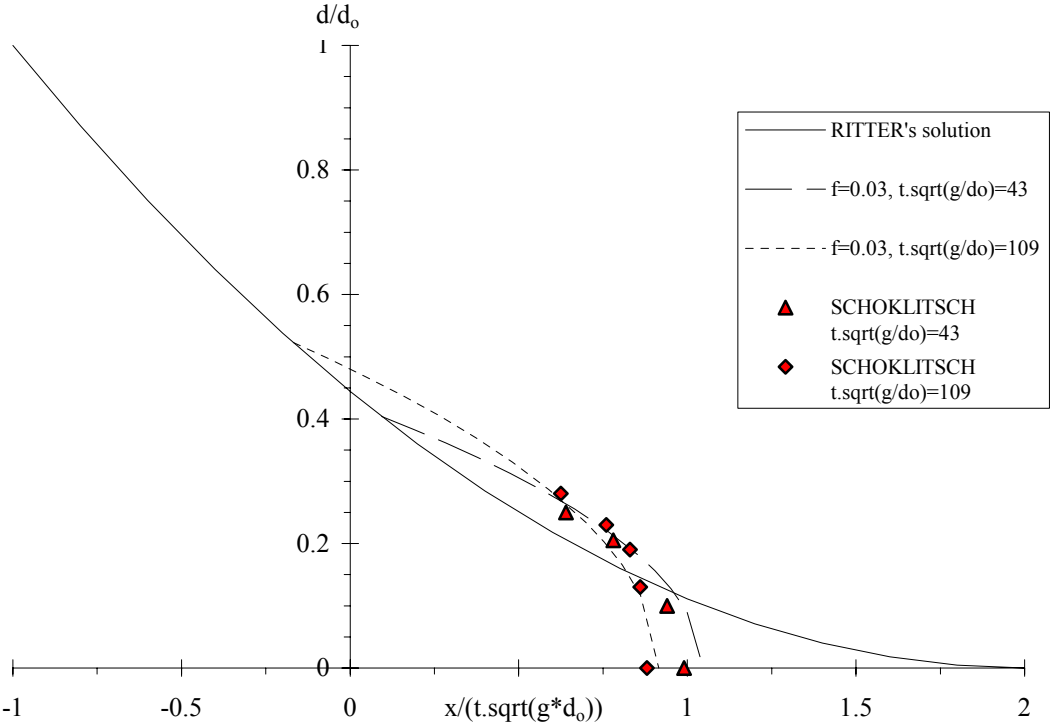

(C2) Comparison with DRESSLER's (1954) data on sand paper invert

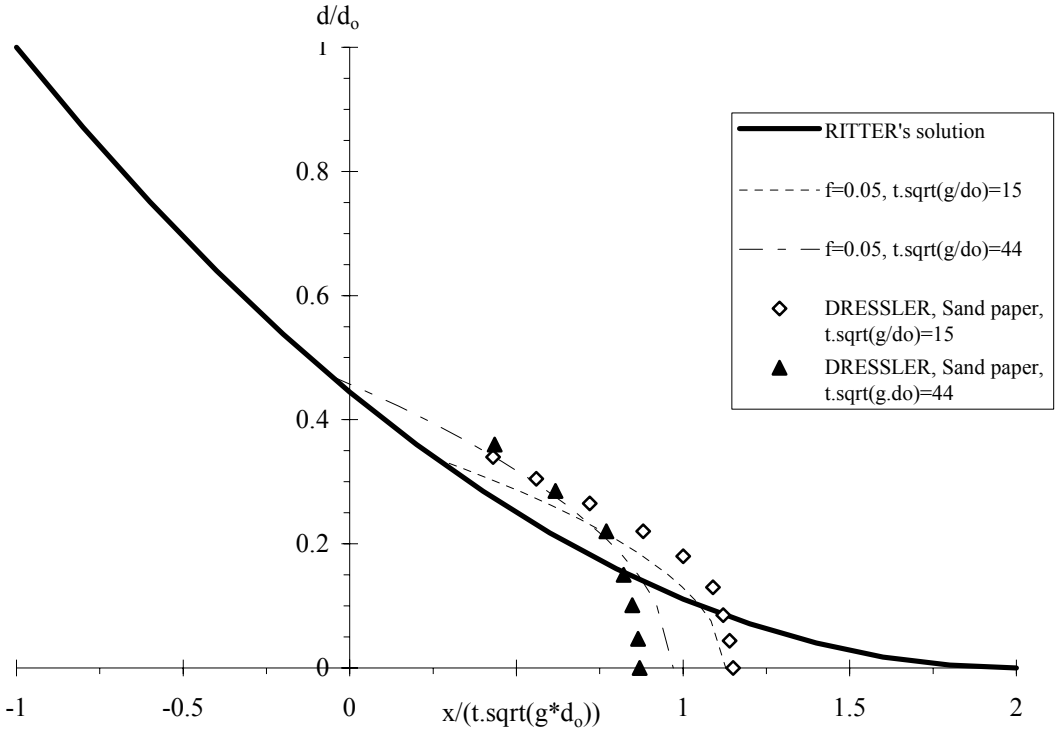

(C3) Comparison with DRESSLER's (1954) data on slats (strip roughness)

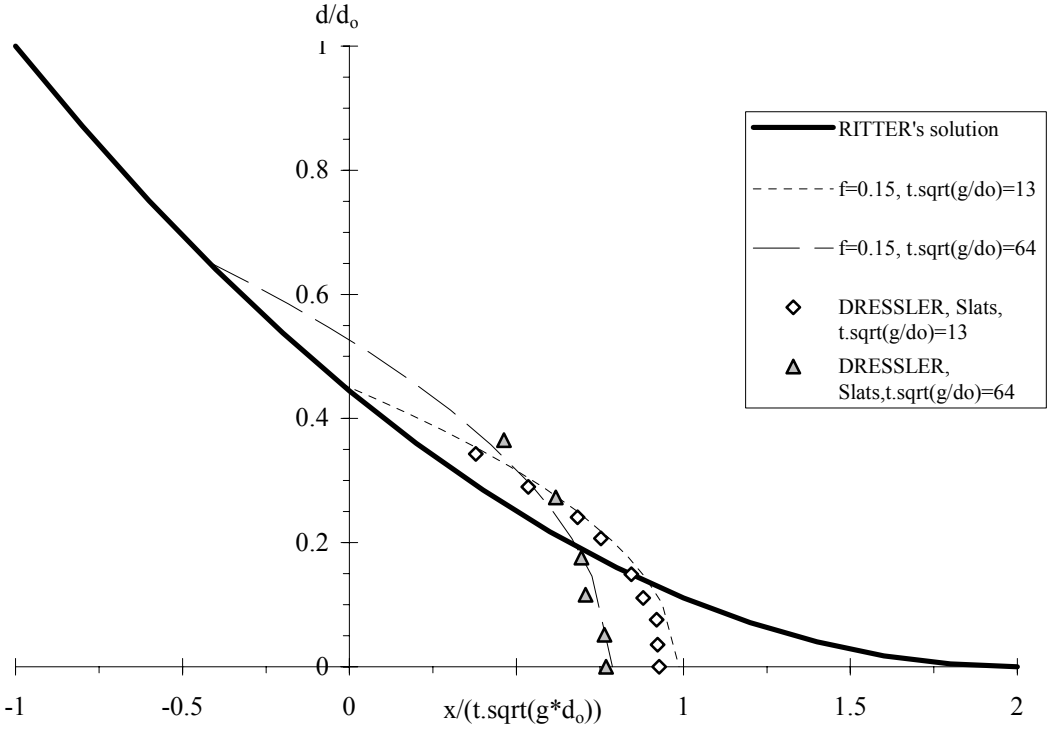

(C4) Comparison with CAVAILLE's (1965) data on smooth invert

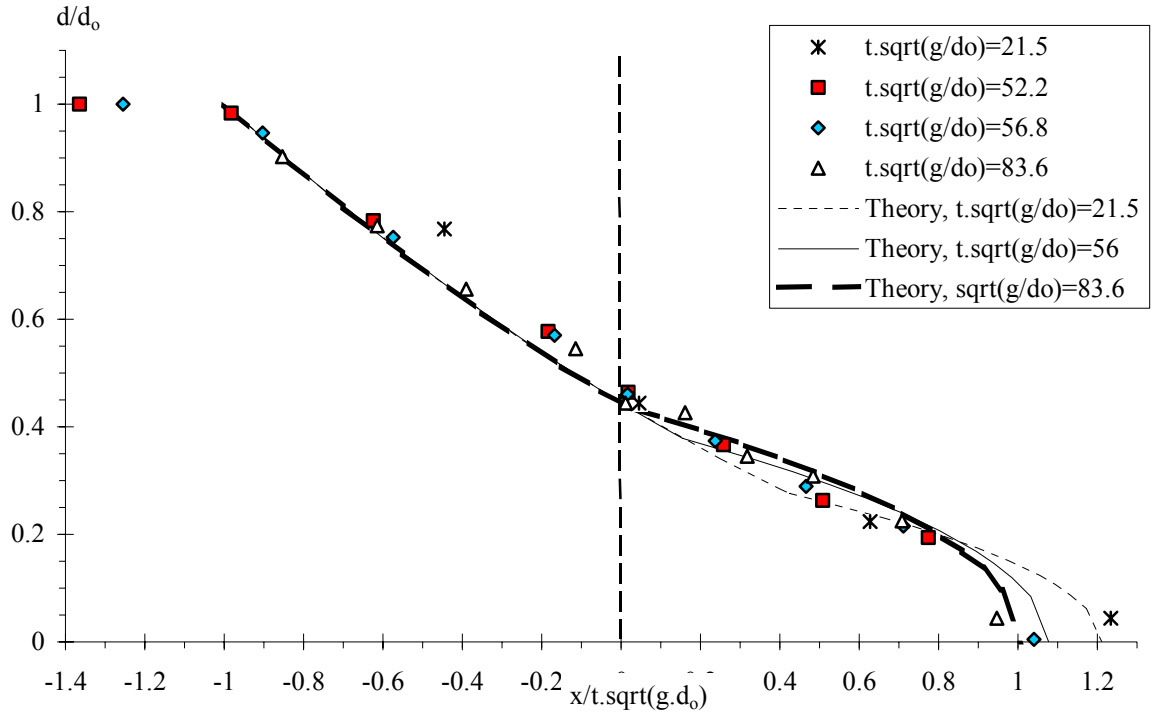

4.2.3 Comparison with experimental data

The present solution was compared with the analytical solutions of DRESSLER (1952) and WHITHAM (1955), and a semi-empirical model by LAUBER (1997) ([2]). Asymptotic approximations for small and large times t are summarised in Table 4-1, while the wave front celerity expression is listed in Table 4-2. These are compared with well-known solutions.

The present development was successfully compared with experimental data in turbulent flows by SCHOKLITSCH (1917), DRESSLER (1954), FAURE and NAHAS (1961), CAVAILLE (1965), ESTRADE (1967) and LAUBER (1997). Some examples are presented in Figure 4-3. The theory is compared qualitatively with viscous flow solutions in Section 5. Note that the above development makes no assumption on the type of flow motion. It is applicable provided that the Darcy friction factor may be assumed constant. Such an approximation is usually valid in turbulent flows.

Great care must be taken in the selection of the Darcy friction factor. Since the water depth along the dam break wave ranges from zero at the wave front to the reservoir depth at the upstream end, friction factor estimates must be calibrated and validated with experimental data. Typical results are summarised in Table 4-3. For the data sets listed in Table 4-3, the friction factor was found to be almost independent of time and experimental flow conditions for a given type of roughness. The results were further consistent between independent data sets (Table 4-3). Note that accurate calibrations of the flow resistance must be performed using instantaneous free-surface profiles. These provide a Lagrangian description on the flow. Alternate techniques based upon wave front location and celerity, or fixed point measurements, are less accurate and they might provide only some order of magnitude.

In the present study, the flow resistance is assumed to be a step function with a constant friction coefficient in the wave tip region and zero flow resistance in the flow behind. A typical longitudinal distribution of boundary shear stress is presented in Figure 4-4. The results are compared with the theoretical result of DRESSLER (1952) for the same friction factor and dimensionless time. On the same graph, the theoretical free-surface profiles are plotted also. Basically both approaches (DRESSLER, Present study) yield very close free-surface profiles although they assume different

[2]All these solutions were developed for turbulent flow motion.

longitudinal boundary shear stress distributions (Fig. 4-4). Lastly note that all methods (DRESSLER 1952, WHITHAM 1955, Present study) assume a constant Darcy friction factor f. The physics of such an assumption is questionable.

Table 4-1 - Asymptotic solutions of dam break wave on dry horizontal channel with boundary friction

Reference (1)	Asymptotic solution (2)	Remarks (3)
Small time t		
DRESSLER (1952)	$\frac{U}{\sqrt{g*d_o}} = 2 - 3.59 * \frac{f}{8} * \sqrt{\frac{g}{d_o}} * t$	
WHITHAM (1953)	$\frac{U}{\sqrt{g*d_o}} = 2 - 4.58 * \frac{f}{8} * \sqrt{\frac{g}{d_o}} * t$	in DRESSLER (1954).
WHITHAM (1955)	$\frac{U}{\sqrt{g*d_o}} = 2 - 3.452 * \frac{f}{8} * \sqrt{\frac{g}{d_o}} * t$	
Present study (diffusive wave model)	$\frac{U}{\sqrt{g*d_o}} = 2 - \sqrt[3]{12*f*\sqrt{\frac{g}{d_o}} * t}$	$\frac{U}{\sqrt{g*d_o}} > 1.2$ to 1.5
Large time t		
Present study (diffusive wave model)	$\frac{U}{\sqrt{g*d_o}} = \sqrt{\frac{8}{3} * \frac{1}{f * \sqrt{\frac{g}{d_o}} * t}}$	$\frac{U}{\sqrt{g*d_o}} < 0.3$ to 0.4

Table 4-2 - Dimensionless expression of the dam break wave celerity for dam break on dry horizontal channel with boundary friction

Reference (1)	Dam break wave celerity (2)	Remarks (3)
WHITHAM (1955)	$\frac{U}{\sqrt{g*d_o}} = \frac{2}{1 + 2.90724 * \left(\frac{f}{8} * \sqrt{\frac{g * t^2}{d_o}}\right)^{0.4255}}$	Best fit of exact solution.
LAUBER (1997)	$\frac{U}{\sqrt{g*d_o}} = \frac{4 * 0.06}{f * t * \sqrt{\frac{g}{d_o}}} * \left(\sqrt{1 + \frac{f}{0.06} * t * \sqrt{\frac{g}{d_o}}} - 1\right)$	Semi-empirical development assuming a wave tip height of $0.06*d_o$.
Present study (diffusive wave model)	$\frac{8}{3} * \frac{1}{f} * \frac{\left(1 - \frac{1}{2} * \frac{U}{\sqrt{g * d_o}}\right)^3}{\frac{U^2}{g*d_o}} = \sqrt{\frac{g}{d_o}} * t$	Exact analytical solution.

Table 4-3 - Typical flow resistance estimate for best data fit by the diffusive wave model (Present analysis)

Data set (1)	Type of invert (2)	f (1) (3)	Remarks (4)
SCHOKLITSCH (1917)	Smooth	0.03	Based upon instantaneous free-surface profiles. $40 \leq t^*\sqrt{g/d_o} \leq 110$
DRESSLER (1954)			Based upon instantaneous free-surface profiles.
	Smooth paint	0.03	$40 \leq t^*\sqrt{g/d_o} \leq 70$
	Sand paper	0.05	$15 \leq t^*\sqrt{g/d_o} \leq 50$
	2D strip (Slats) h = 0.00635 m l = 0.0254 m	0.15	$10 \leq t^*\sqrt{g/d_o} \leq 65$
CAVAILLE (1965)			Based upon instantaneous free-surface profiles.
	Smooth	0.02	$21 \leq t^*\sqrt{g/d_o} \leq 84$
	Rough (cylindrical elements ∅ = 20 mm in zigzag, l = 28 mm, h= 8 mm)	0.3	$32 \leq t^*\sqrt{g/d_o} \leq 137$
LAUBER (1997)	PVC	0.015	Based upon wave front location and celerity. $0 \leq t^*\sqrt{g/d_o} \leq 20$

Notes : h : roughness element height; l : longitudinal spacing between roughness element; (1) : value for the best data fit by the diffusive wave model.

4.2.4 Discussion

The present method yields an explicit expression of the wave front celerity, wave front location and wave tip region characteristics for turbulent flow motion. Equation (4-15) provides a direct relationship between the dimensionless wave front celerity $U/\sqrt{g^*d_o}$ and dimensionless time $t^*\sqrt{g/d_o}$. Equation (4-16) yields the dimensionless wave front location x_S/d_o as a function of the dimensionless wave front celerity $U/\sqrt{g^*d_o}$. Equations (4-18) and (4-19) give the entire dimensionless free-surface profile $d/d_o = F(x/(t^*\sqrt{g^*d_o}))$. This simple system of linear equations provides a means to assess easily the effect of the flow resistance on the dam break wave propagation of real fluids.

The main advantages of the present development are three-fold. It is a simple explicit method that compares well with experimental data and theoretical solutions. Further it a simple pedagogical application linking together the simple wave equations, yielding RITTER's solution, with a diffusive wave equation for the wave tip region. More this explicit solution may be used to validate simple numerical solutions of the method of characteristics applied to the dam break wave problem.

Limitations of the diffusive wave model

The comparisons show that the diffusive wave approximation (paragraph 4.2.2) is reasonable for relatively small times after dam break (Fig. 4-3). It might become less valuable when the wave tip region becomes large. It is also limited to a semi-infinite reservoir, and it assumes a constant Darcy-Weisbach friction factor in the wave tip region.

A further limitation of the diffusive wave model is the use of the Saint-Venant equations and their underlying assumptions (paragraph 1.2). For example, the Saint-Venant equations are not valid

during the initial instants following dam break : i.e., $t^*\sqrt{g/d_o} < 3$ (LAUBER 1997). Some researchers studied specifically the initial instants of the dam break and the effects of its duration. For example, POHLE (1952), DRESSLER (1954), ESTRADE and MARTINOT-LAGARDE (1964), MARTINOT-LAGARDE and ESTRADE (1966), LAUBER (1997), STANSBY et al. (1998) for the initial stages of dam break flow; ESTRADE (1967) and LAUBER (1997) on the effects of gate opening duration. Experimental observations suggested further that the celerity of the initial backward characteristics is initially about $-\sqrt{2}*\sqrt{g*d_o}$ (LAUBER 1997, LEAL et al. 2001). It was proposed that the difference was caused by streamline curvature effects at the leading edge of the negative wave.

Fig. 4-4 - Dimensionless boundary shear stress distributions and free-surface profiles - Comparison between present study and DRESSLER's (1952) theoretical results for f = 0.03 and $t^*\sqrt{g/d_o} = 6.43$

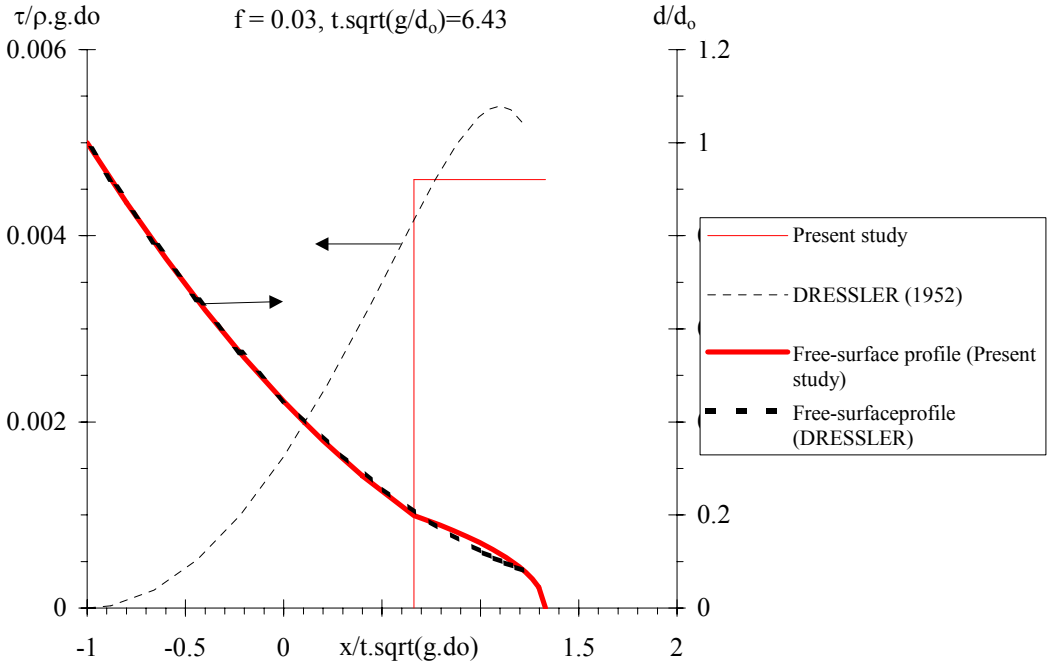

4.3 DAM BREAK IN A DRY HORIZONTAL CHANNEL WITH BED FRICTION AND WITH NON-ZERO INITIAL VELOCITY (DIFFUSIVE WAVE MODEL)

The above problem (dam break wave in a horizontal channel with flow resistance) may be extended if the flow velocity behind the dam is V_o for $t < 0$ as sketched in Figure 4-5. It is assumed that the translation of both dam and reservoir at the speed V_o is frictionless prior to dam removal, and that the translation of the undisturbed reservoir remains frictionless for $t \geq 0$. The latter assumption is consistent with the diffusive wave model in which the flow behind the wave tip region is assumed frictionless. The dam break is idealised by a vertical wall that is suddenly removed. Dam removal takes place instantaneously at $t = 0$ when the dam is at $x = 0$.

The instantaneous dam break creates a negative wave propagating upstream ([3]) into the reservoir with a known water depth d_o. In the (x, t) plane, the initial negative wave characteristic has a slope $dt/dx = -1/(C_o-V_o)$ where $C_o = \sqrt{g*d_o}$ assuming a rectangular channel. Note that the initial backward characteristic is a straight line.

[3]The negative wave propagates upstream if $V_o < C_o$. For $V_o > C_o$, the leading edge of the initial negative characteristic may propagate downstream.

Forward characteristics can be drawn issuing from the initial backward characteristic for t > 0. Between the points E1 and F2 (Fig. 4-5), the flow properties satisfy the ideal dam break wave properties :

$$\sqrt{\frac{d}{d_o}} = \frac{1}{3} * \left(2 + \frac{V_o}{\sqrt{g * d_o}} - \frac{x}{t * \sqrt{g * d_o}} \right)$$

$$\text{for } -1 + \frac{V_o}{\sqrt{g * d_o}} \leq \frac{x}{t * \sqrt{g * d_o}} \leq \frac{x_1}{t * \sqrt{g * d_o}} \quad (4\text{-}19)$$

$$\frac{V}{\sqrt{g * d_o}} = \frac{2}{3} * \left(1 + \frac{1}{2} * \frac{V_o}{\sqrt{g * d_o}} + \frac{x}{t * \sqrt{g * d_o}} \right)$$

$$\text{for } -1 + \frac{V_o}{\sqrt{g * d_o}} \leq \frac{x}{t * \sqrt{g * d_o}} \leq \frac{x_1}{t * \sqrt{g * d_o}} \quad (4\text{-}20)$$

Fig. 4-5 - Sketch of a dam break wave in a horizontal dry channel with bottom friction with initial reservoir motion

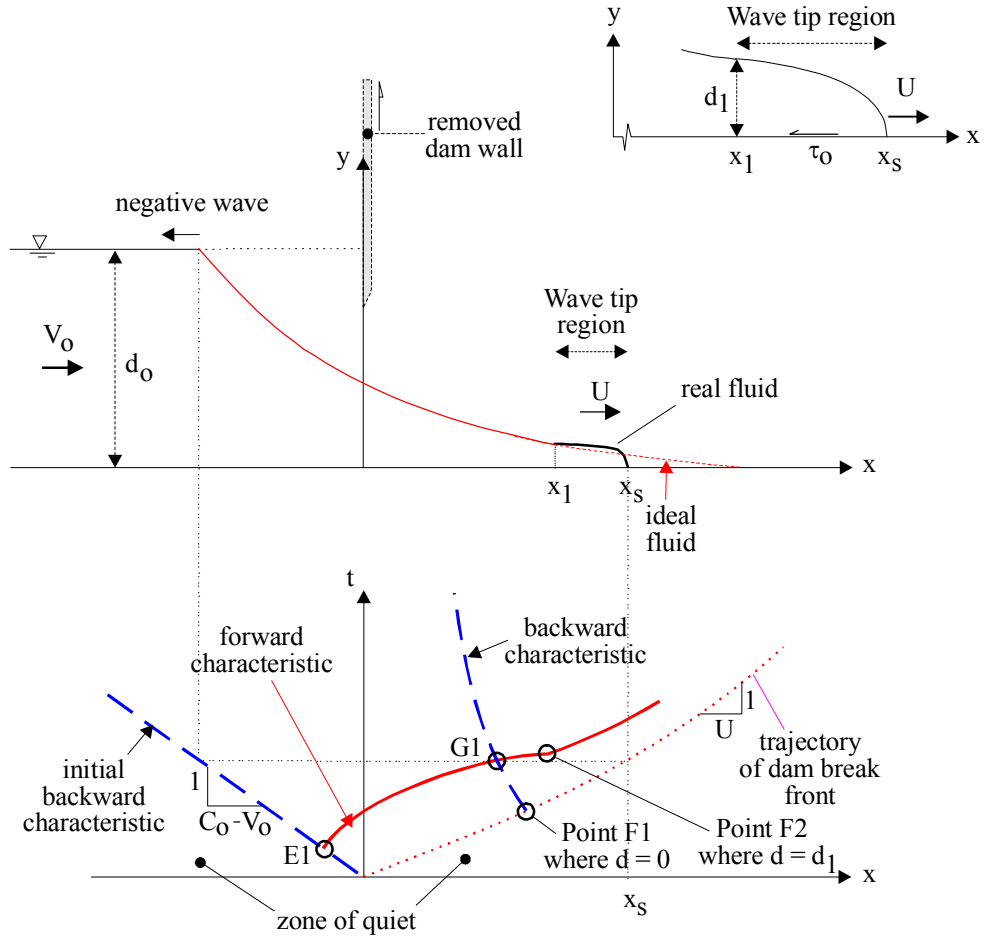

For $x_1 \leq x \leq x_S$, the flow properties are calculated using the diffusion wave equation taking into account flow resistance (Eq. (4-1)). Since the flow depth and velocity must be continue at the point F2, the flow properties at point F2 (x_1, V_1, d_1) and at wave front (x_S, U) are deduced from :

$$\sqrt{\frac{d_1}{d_o}} = \frac{1}{3} * \left(2 + \frac{V_o}{\sqrt{g * d_o}} - \frac{x_1}{\sqrt{g * d_o} * t} \right) \quad (4\text{-}21)$$

$$\frac{V_1}{\sqrt{g*d_o}} = \frac{2}{3} * \left(1 + \frac{1}{2} * \frac{V_o}{\sqrt{g * d_o}} + \frac{x_1}{\sqrt{g * d_o} * t} \right) \quad (4\text{-}22)$$

$$\frac{U}{\sqrt{g * d_o}} = \frac{V_1}{\sqrt{g * d_o}} \quad (4\text{-}23)$$

$$\frac{d_1}{d_o} = \sqrt{\frac{f}{4} * \frac{U^2}{g * d_o} * \frac{x_S - x_1}{d_o}} \quad (4\text{-}24)$$

The conservation of mass must be further satisfied. The mass of fluid in the wave tip region (i.e. $x_1 \le x \le x_S$) equals the mass of fluid in the ideal fluid flow profile for $x_1 \le x \le (2*\sqrt{g*d_o}+V_o)*t$:

$$\int_{x_1}^{x_S} \sqrt{\frac{f}{4 * g} * U^2 * (x_S - x)} * dx = \int_{x_1}^{(2*\sqrt{g*d_o}+V_o)*t} \frac{1}{9 * g} * \left(V_o + 2 * \sqrt{g * d_o} - \frac{x}{t} \right)^2 * dx \quad (4\text{-}25)$$

The above equations may be transformed to express d_1 and x_1 as functions of U:

$$\frac{d_1}{d_o} = \left(1 + \frac{1}{2} * \frac{V_o}{\sqrt{g * d_o}} - \frac{1}{2} * \frac{U}{\sqrt{g * d_o}} \right)^2 \quad (4\text{-}26)$$

$$\frac{x_1}{\sqrt{g * d_o} * t} = \frac{3}{2} * \frac{U}{\sqrt{g * d_o}} - \frac{1}{2} * \frac{V_o}{\sqrt{g * d_o}} - 1 \quad (4\text{-}27)$$

The continuity equation becomes an equation in terms of the wave front location x_S and celerity U:

$$\frac{2}{3} * \sqrt{\frac{f}{4} * \frac{U^2}{g * d_o}} * \left(\frac{x_S - x_1}{\sqrt{g * d_o} * t} \right)^{3/2} = \frac{1}{27} * \sqrt[4]{\frac{d_o}{g}} * \frac{1}{\sqrt{t}} * \left(2 + \frac{V_o}{\sqrt{g * d_o}} - \frac{x_1}{\sqrt{g * d_o} * t} \right)^3 \quad (4\text{-}28)$$

The wave tip region has a parabolic free-surface profile (Eq. (4-2)). The water depth at point F2 satisfies:

$$\frac{d_1}{d_o} = \sqrt{\frac{f}{4} * \frac{U^2}{g * d_o} * \frac{x_S - x_1}{d_o}} \quad (4\text{-}29)$$

and the wave tip region length is:

$$\frac{x_S - x_1}{d_o} = \frac{4}{f} * \frac{g * d_o}{U^2} * \left(1 + \frac{1}{2} * \frac{V_o}{\sqrt{g * d_o}} - \frac{1}{2} * \frac{U}{\sqrt{g*d_o}} \right)^4 \quad (4\text{-}30)$$

The exact solution in terms of the wave front celerity is :

$$\frac{8}{3} * \frac{1}{f} * \frac{\left(1 + \frac{1}{2} * \frac{V_o}{\sqrt{g * d_o}} - \frac{1}{2} * \frac{U}{\sqrt{g * d_o}} \right)^3}{\frac{U^2}{g*d_o}} = \sqrt{\frac{g}{d_o}} * t \quad (4\text{-}31)$$

while the wave front location equals:

$$\frac{x_S}{d_o} = \left(\frac{3}{2} * \frac{U}{\sqrt{g * d_o}} - \frac{1}{2} * \frac{V_o}{\sqrt{g * d_o}} - 1\right) * \sqrt{\frac{g}{d_o}} * t + \frac{4}{f * \frac{U^2}{g * d_o}} * \left(1 + \frac{1}{2} * \frac{V_o}{\sqrt{g * d_o}} - \frac{1}{2} * \frac{U}{\sqrt{g * d_o}}\right)^4 \quad (4\text{-}32)$$

and the free-surface profile satisfies :

$$\frac{d}{d_o} = 1 \qquad \text{for } \frac{x}{d_o} \le \frac{V_o - \sqrt{g * d_o}}{d_o} * t \quad (4\text{-}33a)$$

$$\frac{d}{d_o} = \frac{1}{9} * \left(2 + \frac{V_o}{\sqrt{g * d_o}} - \frac{x}{t * \sqrt{g * d_o}}\right)^2$$

$$\text{for } \frac{V_o - \sqrt{g * d_o}}{d_o} * t \le \frac{x}{d_o} \le \left(\frac{3}{2} * \frac{U}{\sqrt{g * d_o}} - \frac{1}{2} * \frac{V_o}{\sqrt{g * d_o}} - 1\right) * \sqrt{\frac{g}{d_o}} * t \quad (4\text{-}33b)$$

$$\frac{d}{d_o} = \sqrt{\frac{f}{4} * \frac{U^2}{g * d_o} * \frac{x_S - x}{d_o}}$$

$$\text{for } \left(\frac{3}{2} * \frac{U}{\sqrt{g * d_o}} - \frac{1}{2} * \frac{V_o}{\sqrt{g * d_o}} - 1\right) * \sqrt{\frac{g}{d_o}} * t \le \frac{x}{d_o} \le \frac{x_S}{d_o} \quad (4\text{-}33c)$$

$$\frac{d}{d_o} = 0 \qquad \text{for } \frac{x_S}{d_o} \le \frac{x}{d_o} \quad (4\text{-}33d)$$

Fig. 4-6 - Dimensionless wave front location and celerity for a dam break wave on a dry horizontal bed for different initial flow conditions ($Fr_o = V_o/\sqrt{g*d_o}$)
(A) Dimensionless wave front location for f = 0.03

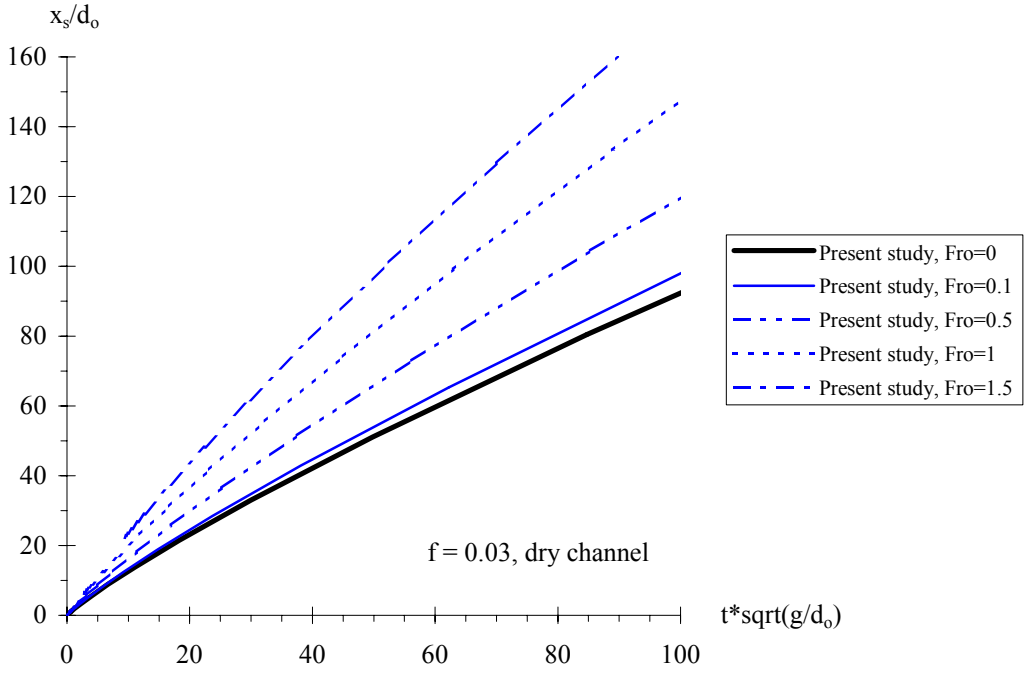

(B) Dimensionless wave front celerity for f = 0.03

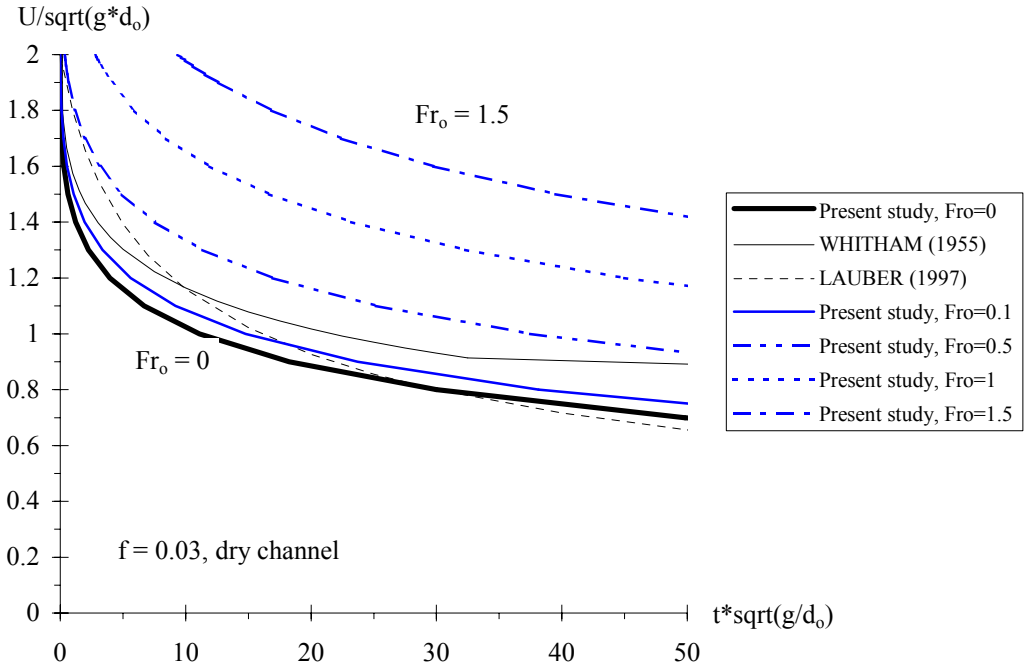

The location x_1 of point F2 is deduced from Equations (4-30) and (4-32). Typical results are presented in Figure 4-6 for several initial flow Froude numbers $Fr_o = V_o/\sqrt{g*d_o} = V_o/C_o$ and one value of the Darcy friction factor. Note that the results yield the results obtained in paragraph 4.2 for $V_o = 0$ (i.e. $Fr_o = 0$).

4.4 DAM BREAK IN A DRY, UPWARD SLOPING CHANNEL WITH BED FRICTION

4.4.1 Basic equations

Considering an ideal dam break surging over a dry river bed with some boundary friction, the method of characteristics may be applied. For a dam break over a dry channel, the basic equations are :

$$\frac{D}{Dt}(V + 2 * C) = - g * \left(\frac{f}{8} * \frac{V^2}{g*d} - S_o\right) \qquad \text{forward characteristic (4-34a)}$$

$$\frac{D}{Dt}(V - 2 * C) = - g * \left(\frac{f}{8} * \frac{V^2}{g*d} - S_o\right) \qquad \text{backward characteristic (4-34b)}$$

along :

$$\frac{d\,x}{dt} = V + C \qquad \text{forward characteristic C1 (4-35a)}$$

$$\frac{d\,x}{dt} = V - C \qquad \text{backward characteristic C2 (4-35b)}$$

where S_o is negative for an inclined upward plane as sketched in Figure 4-7.

In the following development, the flow is assumed to be an ideal fluid region behind a friction dominated wave tip region. In the wave tip region, flow resistance is dominant, and the acceleration and inertial terms are small. The dynamic wave equation may be reduced into a diffusive wave equation (paragraphs 4.2 & 4.3) :

$$\frac{\partial d}{\partial x} + \frac{f}{8} * \frac{U^2}{g*d} - S_o = 0 \qquad \text{Wave front (4-36)}$$

Next to the leading edge of the wave, the slope of the free-surface becomes important to counterbalance the flow resistance and bed slope. The integration of the diffusive wave equation yields the shape of the wave front

$$\frac{x_S - x}{d_o} = -\frac{f}{8 * S_o^2} * \frac{U^2}{g * d_o} * \left(Ln\left(1 - \frac{8 * S_o}{f} * \frac{g * d_o}{U^2} * \frac{d}{d_o}\right) + \frac{8 * S_o}{f} * \frac{g * d_o}{U^2} * \frac{d}{d_o} \right)$$

Wave front (4-37)

assuming a constant Darcy friction factor and where x_S is the wave front location. Figure 4-8 illustrates some results in terms of the dimensionless water depth d/d_o.

Fig. 4-7 - Sketch of a dam break wave in a dry, sloping upward, rectangular channel with boundary friction

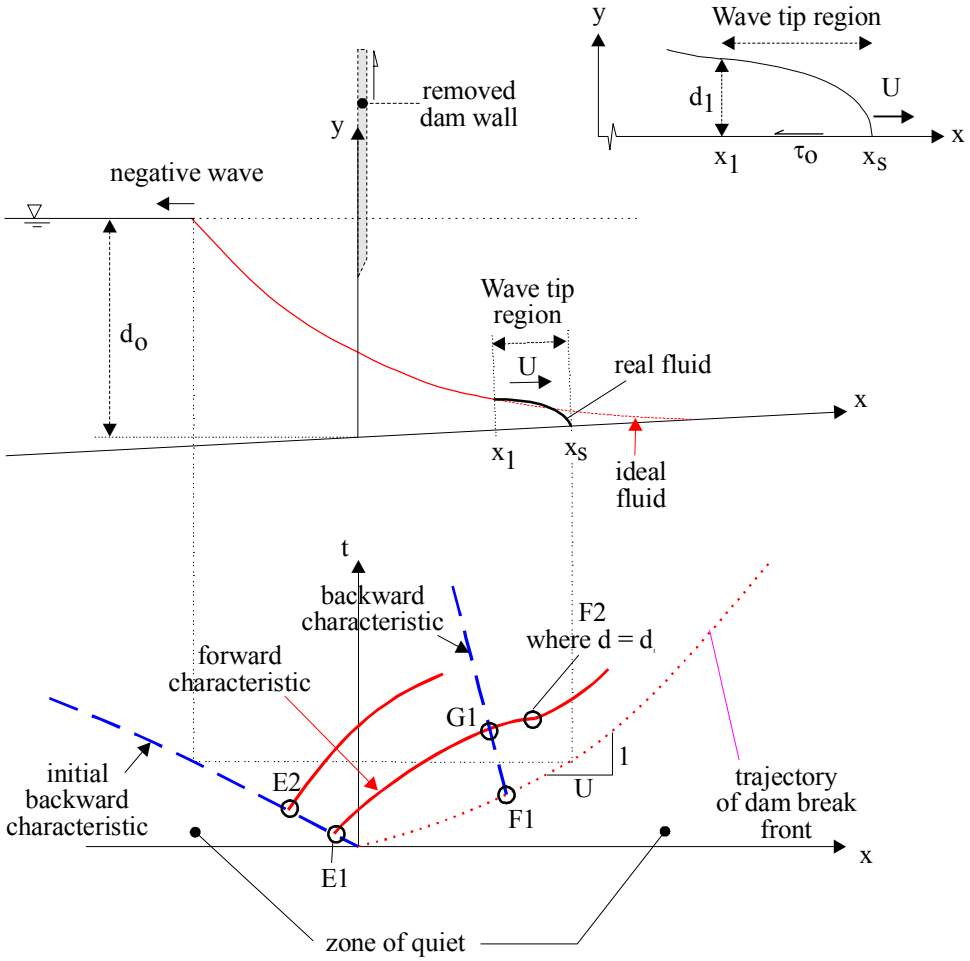

Discussion

Very close to the wave front ($(x_S-x)/d_o << 1$), the shape of the free-surface profile may be approximated using a truncated Taylor series for the logarithm of $1 + x'$:

$$Ln(1 + x') = x' - \frac{x'^2}{2} + \frac{x'^3}{3} - \ldots \qquad (4\text{-}38)$$

Using the first two terms of the development, Equation (4-37) may be approximated by a parabolic relationship which was derived for a horizontal channel (paragraph 4.2):

$$\frac{x_S - x}{d_o} \approx \frac{4}{f} * \frac{g * d_o}{U^2} * \left(\frac{d}{d_o}\right)^2$$

Wave front for $(x_S-x)/d_o << 1$ (4-2b)

Using the first three terms of the Taylor development, the shape of the free-surface profile may be approximated by:

$$\frac{x_S - x}{d_o} \approx \frac{4}{f} * \frac{g * d_o}{U^2} * \left(\frac{d}{d_o}\right)^2 * \left(1 - \frac{9}{2} * \frac{g * d_o}{U^2} * S_o * \frac{d}{d_o}\right)$$

Wave front for $(x_S-x)/d_o << 1$ (4-39)

Very close to the leading edge of the wave, the flow resistance effect is most significant and both equations (4-2b) and (4-38) are reasonable approximations.

Fig. 4-8 - Instantaneous free-surface profile of the wave front (Eq. (4-37)) for a dam break wave in a dry, sloping upward channel (diffusive wave solution) - f = 0.03, $U/\sqrt{g*d_o} = 1$

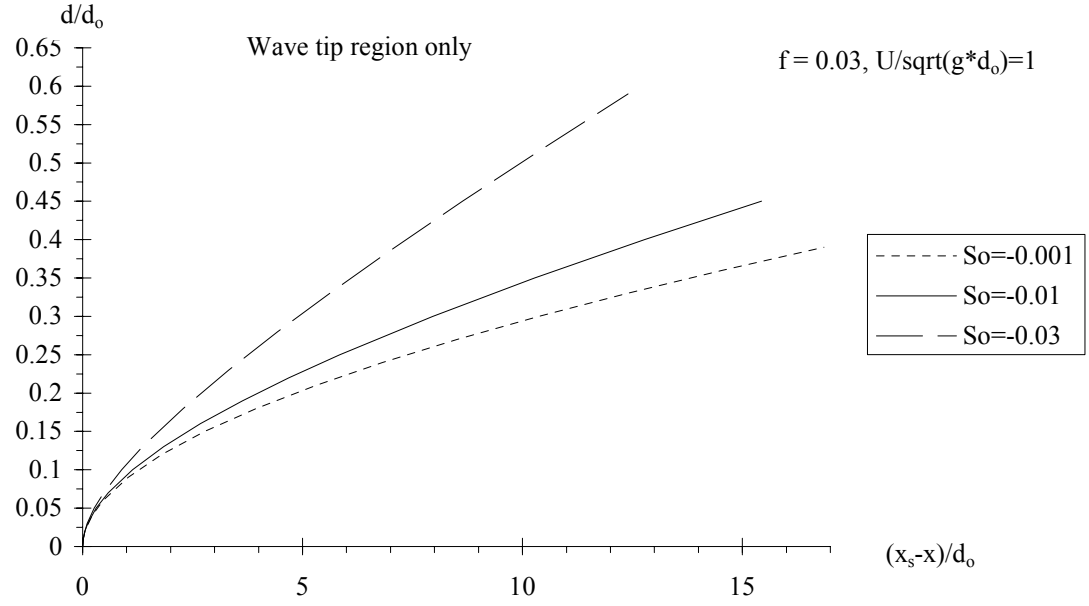

4.4.2 Complete solution

Considering a dam break wave in a sloping upward, prismatic, wide rectangular channel with some flow resistance and a semi-infinite reservoir, dam removal takes place at t = 0 and the dam is located at x = 0 (Fig. 4-7). The dam break wave is approximated by an ideal fluid flow solution (paragraph 3.4) for $x \le x_1$ and a diffusive wave model for $x_1 \le x \le x_S$. The transition between the ideal dam break wave profile and the wave tip is denoted F2 as shown in Figure 4-7. Point F2 is located at $x = x_1$ where the flow depth is d_1 and the velocity is V_1.

The instantaneous dam break creates a negative wave propagating upstream into a fluid at rest with known water depth. In the (x, t) plane, the initial negative wave characteristic has a slope dt/dx = -1/C with $C = C_o$ for t = 0 (Fig. 4-7). (For a flat slope, the initial backward characteristic propagates with a celerity $C_o = \sqrt{g*d_o}$ in first approximation.)

Forward characteristics can be drawn issuing from the initial backward characteristic for t > 0. Between the points E1 and F2 (Fig. 4-7), the flow properties satisfy the ideal dam break wave properties (paragraph 3.4) :

$$\sqrt{\frac{d}{d_o}} = \frac{1}{3} * \left(2 + \frac{1}{2} * \sqrt{\frac{g}{d_o}} * S_o * t - \frac{x}{t * \sqrt{g * d_o}}\right)$$

$$\text{for } -1 \le \frac{x}{t * \sqrt{g*d_o}} \le \frac{x_1}{t * \sqrt{g*d_o}} \quad (4\text{-}40)$$

$$\frac{V}{\sqrt{g * d_o}} = \frac{2}{3} * \left(1 + \sqrt{\frac{g}{d_o}} * S_o * t + \frac{x}{t * \sqrt{g * d_o}}\right)$$

$$\text{for } -1 \le \frac{x}{t * \sqrt{g*d_o}} \le \frac{x_1}{t * \sqrt{g*d_o}} \quad (4\text{-}41)$$

For $x_1 \le x \le x_S$ (i.e. wave tip region), it is assumed that the velocity of water does not vary rapidly and equals the wave front celerity U. The flow properties in the wave tip region may be estimated using the diffusion wave equation taking into account flow resistance and bed slope :

$$\frac{\partial d}{\partial x} + \frac{f}{8} * \frac{U^2}{g*d} - S_o = 0 \qquad \text{Wave tip region} \quad (4\text{-}36)$$

assuming V = U.

The free-surface profile and velocity must be continue at point F2. Hence the flow properties at the point F2 (x_1, V_1, d_1) must satisfy :

$$\sqrt{\frac{d_1}{d_o}} = \frac{1}{3} * \left(2 + \frac{1}{2} * \sqrt{\frac{g}{d_o}} * S_o * t - \frac{x_1}{t * \sqrt{g * d_o}}\right) \quad (4\text{-}42)$$

$$\frac{V_1}{\sqrt{g * d_o}} = \frac{2}{3} * \left(1 + \sqrt{\frac{g}{d_o}} * S_o * t + \frac{x_1}{t * \sqrt{g * d_o}}\right) \quad (4\text{-}43)$$

$$U = V_1 \quad (4\text{-}44)$$

$$\frac{x_S - x_1}{d_o} = -\frac{f}{8 * S_o^2} * \frac{U^2}{g * d_o} * \left(\text{Ln}\left(1 - \frac{8 * S_o}{f} * \frac{g * d_o}{U^2} * \frac{d_1}{d_o}\right) + \frac{8 * S_o}{f} * \frac{g * d_o}{U^2} * \frac{d_1}{d_o}\right) \quad (4\text{-}45)$$

The conservation of mass must be further satisfied. That is, the mass of fluid in the wave tip region (i.e. $x_1 \le x \le x_S$) equals the mass of fluid for $x_1 \le x$ in the ideal fluid flow profile:

$$\int_{x_1}^{x_S} d * dx = \int_{x_1}^{2*(\sqrt{g*d_o} + g*S_o/4*t)*t} \frac{1}{9 * g} * \left(2 * \sqrt{g * d_o} + \frac{1}{2} * g * S_o * t - \frac{x}{t}\right)^2 * dx \quad (4\text{-}46)$$

where the real-fluid flow depth d (left handside term) satisfies :

$$\frac{x_S - x}{d_o} = -\frac{f}{8 * S_o^2} * \frac{U^2}{g * d_o} * \left(\text{Ln}\left(1 - \frac{8 * S_o}{f} * \frac{g * d_o}{U^2} * \frac{d}{d_o}\right) + \frac{8 * S_o}{f} * \frac{g * d_o}{U^2} * \frac{d}{d_o}\right) \quad (4\text{-}37)$$

At a time t, the above equations (Eq. (4-37), (4-42), (4-43), (4-44) & (4-45)) constitute a system of 5 equations with 5 unknowns : i.e., the wave front celerity and location, and the flow properties at the point F2.

The complete free-surface profile is :

$$\frac{d}{d_o} = \frac{1}{9} * \left(2 + \frac{1}{2} * \sqrt{\frac{g}{d_o}} * S_o * t - \frac{x}{t * \sqrt{g * d_o}}\right)^2$$

$$\text{for } -1 \le \frac{x}{t * \sqrt{g * d_o}} \le \frac{x_1}{t * \sqrt{g * d_o}} \quad (4\text{-}47)$$

$$\frac{x_S - x}{d_o} = -\frac{f}{8 * S_o^2} * \frac{U^2}{g * d_o} * \left(Ln\left(1 - \frac{8 * S_o}{f} * \frac{g * d_o}{U^2} * \frac{d}{d_o}\right) + \frac{8 * S_o}{f} * \frac{g * d_o}{U^2} * \frac{d}{d_o}\right)$$

$$\text{for } \frac{x_1}{t * \sqrt{g * d_o}} \le \frac{x}{t * \sqrt{g * d_o}} \le \frac{x_S}{t * \sqrt{g * d_o}} \quad (4\text{-}37)$$

4.4.3 Simplified solution

The problem may be solved analytically by approximating the free-surface profile in the wave tip region. For $x_1 \le x \le x_S$ (i.e. wave tip region), the velocity of water is assumed to equal the wave front celerity U, and the flow properties may be estimated using a diffusion wave :

$$\frac{\partial d}{\partial x} + \frac{f}{8} * \frac{U^2}{g*d} + S_o = 0 \qquad \text{Wave front} \quad (4\text{-}36)$$

assuming V = U. The above equation was solved analytically in paragraph 4.4.1. A truncated Taylor series of the solution was

$$d \approx \sqrt{\frac{f}{4 * g} * U^2 * (x_S - x)} \qquad \text{Wave front} \quad (4\text{-}38)$$

assuming a constant Darcy friction factor, neglecting the effect of the bed slope and where x_S is the wave front location.

Within this approximation, the water depth and velocity must be continue at point F2,. That is, they must satisfy :

$$\sqrt{\frac{d_1}{d_o}} = \frac{1}{3} * \left(2 + \frac{1}{2} * \sqrt{\frac{g}{d_o}} * S_o * t - \frac{x_1}{t * \sqrt{g * d_o}}\right) \quad (4\text{-}42)$$

$$\frac{V_1}{\sqrt{g * d_o}} = \frac{2}{3} * \left(1 + \sqrt{\frac{g}{d_o}} * S_o * t + \frac{x_1}{t * \sqrt{g * d_o}}\right) \quad (4\text{-}43)$$

$$U = V_1 \quad (4\text{-}44)$$

$$\frac{d_1}{d_o} = \sqrt{\frac{f}{4} * \frac{U^2}{g * d_o} * \frac{x_S - x_1}{d_o}} \quad (4\text{-}48)$$

The conservation of mass must be satisfied. The mass of fluid in the wave tip region (i.e. $x_1 \le x \le x_S$) must be equal the mass of fluid in the wave tip of the ideal fluid flow profile (i.e. for $x_1 \le x \le (2*(\sqrt{g*d_o}+g*S_o/4*t)*t)$) :

$$\int_{x_1}^{x_S} \sqrt{\frac{f}{4 * g} * U^2 * (x_S - x)} * dx =$$

$$\int_{x_1}^{2*(\sqrt{g*d_o} + g*S_o/4*t)*t} \frac{1}{9 * g} * \left(2 * \sqrt{g * d_o} + \frac{1}{2} * g * S_o * t - \frac{x}{t}\right)^2 * dx \quad (4\text{-}49)$$

The continuity equation is a polynomial equation in terms of the wave front location x_S, wave front celerity $U = dx_S/dt$ and location x_1 of the point F2 :

$$\frac{2}{3} * \sqrt{\frac{f}{4 * g} * U^2} * (x_S - x_1)^{3/2} = \frac{t}{27 * g} * \left(2 * \sqrt{g * d_o} + \frac{1}{2} * g * S_o * t - \frac{x_1}{t}\right)^3 \quad (4\text{-}50)$$

Since the wave tip region has a parabolic free-surface profile (Eq. (4-38)), the water depth at point F2 satisfies:

$$\frac{d_1}{d_o} = \sqrt{\frac{f}{4} * \frac{U^2}{g * d_o} * \frac{x_S - x_1}{d_o}} \quad (4\text{-}51)$$

and the dimensionless length of the wave tip region is :

$$\frac{x_S - x_1}{d_o} = \frac{4}{f} * \frac{1}{\frac{U^2}{g * d_o}} * \left(1 + \frac{1}{2} * \sqrt{\frac{g}{d_o}} * S_o * t - \frac{1}{2} * \frac{U}{\sqrt{g * d_o}}\right)^4 \quad (4\text{-}52)$$

Since Equation (4-43) may be rewritten :

$$\frac{x_1}{\sqrt{g * d_o} * t} = \frac{3}{2} * \frac{U}{\sqrt{g * d_o}} - \sqrt{\frac{g}{d_o}} * S_o * t - 1 \quad (4\text{-}43b)$$

and by replacing into the continuity equation, the exact solution of the dam break wave in terms of the wave front celerity is :

$$\frac{8}{3} * \frac{1}{f} * \frac{\left(1 + \frac{1}{2} * \sqrt{\frac{g}{d_o}} * S_o * t - \frac{1}{2} * \frac{U}{\sqrt{g * d_o}}\right)^3}{\frac{U^2}{g * d_o}} = \sqrt{\frac{g}{d_o}} * t \quad (4\text{-}53)$$

while the wave front location equals:

$$\frac{x_S}{d_o} = \left(\frac{3}{2} * \frac{U}{\sqrt{g * d_o}} - \sqrt{\frac{g}{d_o}} * S_o * t - 1\right) * \sqrt{\frac{g}{d_o}} * t + \frac{4}{f} * \frac{1}{\frac{U^2}{g * d_o}} * \left(1 + \frac{1}{2} * \sqrt{\frac{g}{d_o}} * S_o * t - \frac{1}{2} * \frac{U}{\sqrt{g * d_o}}\right)^4 \quad (4\text{-}54)$$

and the free-surface profile is :

$$\frac{d}{d_o} = 1 \qquad \text{for } \frac{x}{d_o} \le -\sqrt{\frac{g}{d_o}} * t \quad (4\text{-}55a)$$

$$\frac{d}{d_o} = \frac{1}{9} * \left(2 + \frac{1}{2} * \sqrt{\frac{g}{d_o}} * S_o * t - \frac{x}{\sqrt{g * d_o} * t}\right)^2$$

$$\text{for } -\sqrt{\frac{g}{d_o}} * t \le \frac{x}{d_o} \le \left(\frac{3}{2} * \frac{U}{\sqrt{g * d_o}} - \sqrt{\frac{g}{d_o}} * S_o * t - 1\right) * \sqrt{\frac{g}{d_o}} * t \quad (4\text{-}55b)$$

$$\frac{d}{d_o} = \sqrt{\frac{f}{4 * g} * U^2 * (x_S - x)}$$

$$\text{for } \left(\frac{3}{2} * \frac{U}{\sqrt{g * d_o}} - \sqrt{\frac{g}{d_o}} * S_o * t - 1\right) * \sqrt{\frac{g}{d_o}} * t \leq \frac{x_S}{d_o} \leq \frac{x_S}{d_o} \quad (4\text{-}55c)$$

$$\frac{d}{d_o} = 0 \qquad \text{for } \frac{x_S}{d_o} \leq \frac{x_S}{d_o} \quad (4\text{-}55d)$$

The location of point F2 is given from Equation (4-43b).
Equation (4-53) provides an explicit relationship between the dimensionless wave front celerity $U/\sqrt{g*d_o}$ and dimensionless time $t*\sqrt{g/d_o}$. Note that the solution in terms of the wave front celerity is non-linear with the dimensionless time being present on both sides of Equation (4-53). Equation (4-54) yields the dimensionless wave front location x_S/d_o as a function of the dimensionless wave front celerity $U/\sqrt{g*d_o}$ and dimensionless time $t*\sqrt{g/d_o}$. Equations (4-55) and (4-43b) give the entire dimensionless free-surface profile $d/d_o = F(x/(t*\sqrt{g*d_o}))$. This simple system of equations provides a means to assess the effect of the flow resistance on the dam break wave propagation on a flat-slope invert. Typical analytical results are summarised in Figure 4-9 for several bed slopes. Figure 4-9A presents the dimensionless wave front location for three bed slopes, while Figure 4-9B shows the dimensionless wave front celerity. Figure 4-9C illustrates the wave front shape at a given time for three bed slopes.

Discussion
For small dimensionless times $\sqrt{g/d_o}*t$, the effect of bed slope is small and the solution tends to the exact solution obtained for a horizontal channel. The asymptotic development for small dimensionless times is :

$$\frac{U}{\sqrt{g * d_o}} = 2 - \sqrt[3]{12 * f * \sqrt{\frac{g}{d_o}} * t} \qquad \sqrt{g/d_o} * t << 1 \quad (4\text{-}56)$$

For a sloping upward channel, the wave front celerity tends to zero with increasing time.
For sloping downward channels, Equation (4-53) has two solutions in terms of the front celerity for small times $\sqrt{g/d_o}*t$, but only one is physically meaningful. There is further a limiting time for which there is only one solution in terms of the wave front celerity. For larger times, the wave reaches some form of uniform equilibrium between gravity effects and flow resistance which corresponds to a singularity of the differential form of the Saint-Venant equations. Indeed steady uniform equilibrium flow conditions are a singularity for both differential forms of Saint-Venant equations and backwater equation.

Limitations
The results are based upon a series of crude approximations. In particular, it is assumed that the wave tip region is primarily affected by bed friction while the ideal-fluid flow motion behind is mostly affected by inertial effects and the gravity force component. Further the development assumes relatively small times t and a flat bed slope. In particular, it implies $C = C_o$ anywhere on the initial backward characteristic, and straight backward characteristics in the ideal fluid flow region.
Note that the present development is valid for turbulent flow motion assuming that of a constant Darcy friction factor.

Fig. 4-9 - Flow properties for a dam break wave in a dry, sloping upward, rectangular channel with boundary friction and with zero initial velocity (diffusive wave solution) assuming f = 0.03
(A) Dimensionless wave front location

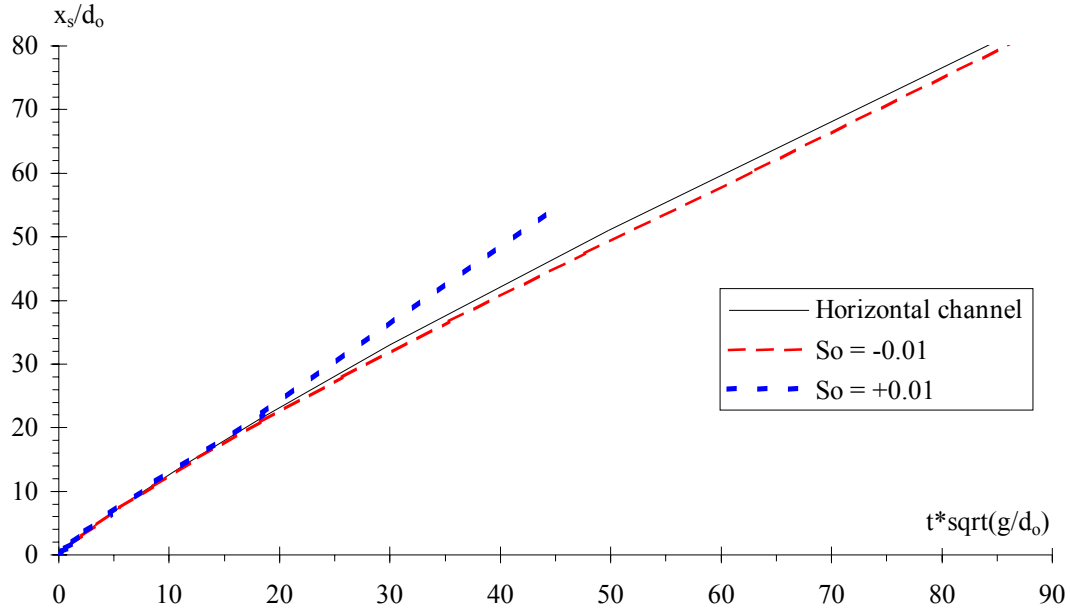

(B) Dimensionless wave front celerity

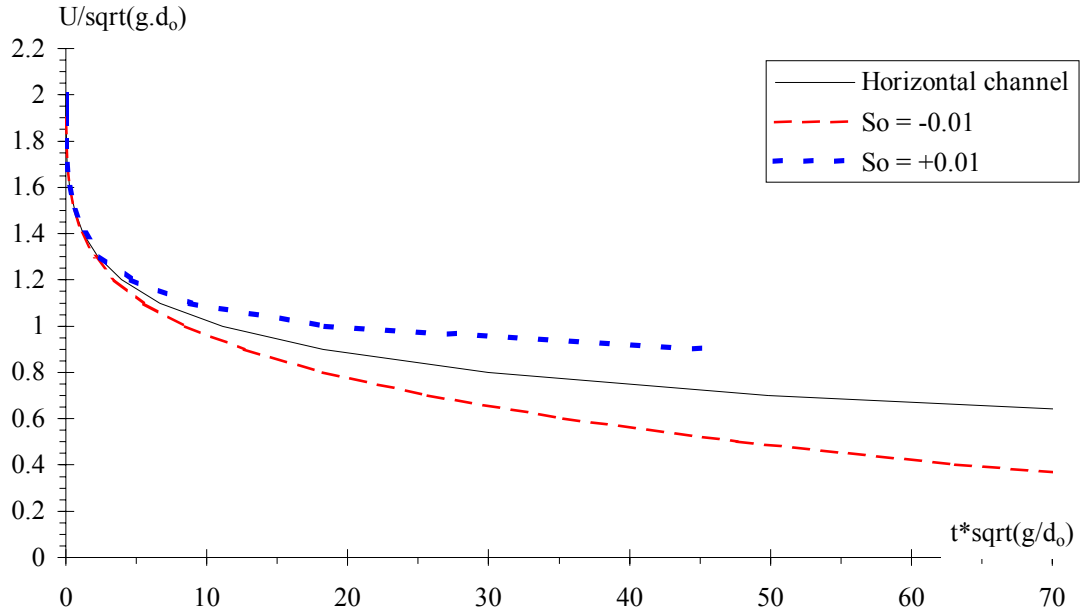

(C) Free-surface profile for $t^*\sqrt{g/d_o} = 2.25$ - Detail of the wave tip region

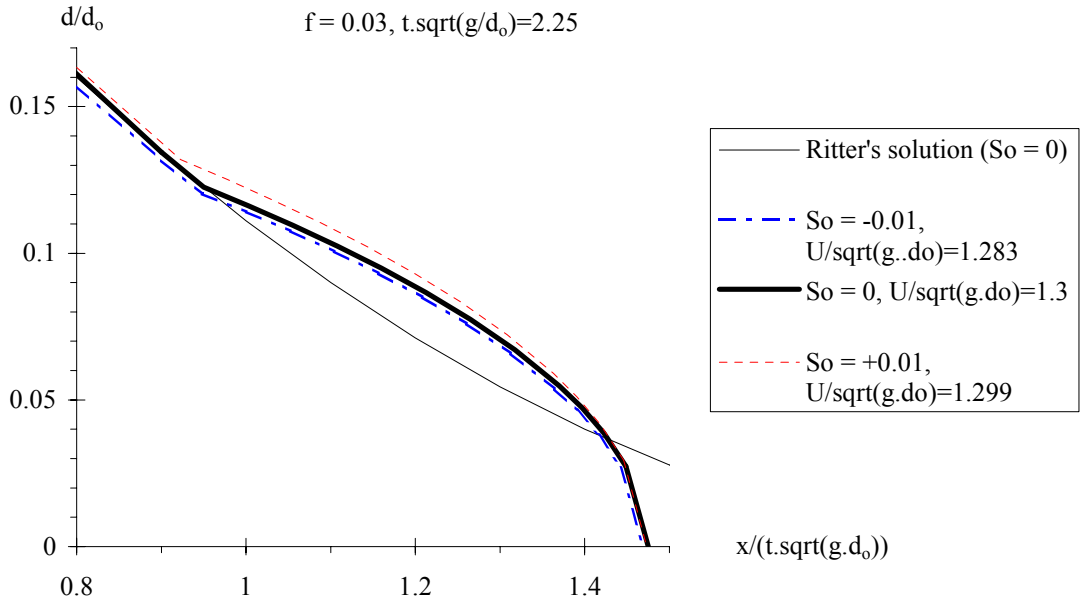

Fig. 4-10 - Sketch of a dam break wave in a dry, sloping upward, rectangular channel with boundary friction and with initial flow motion

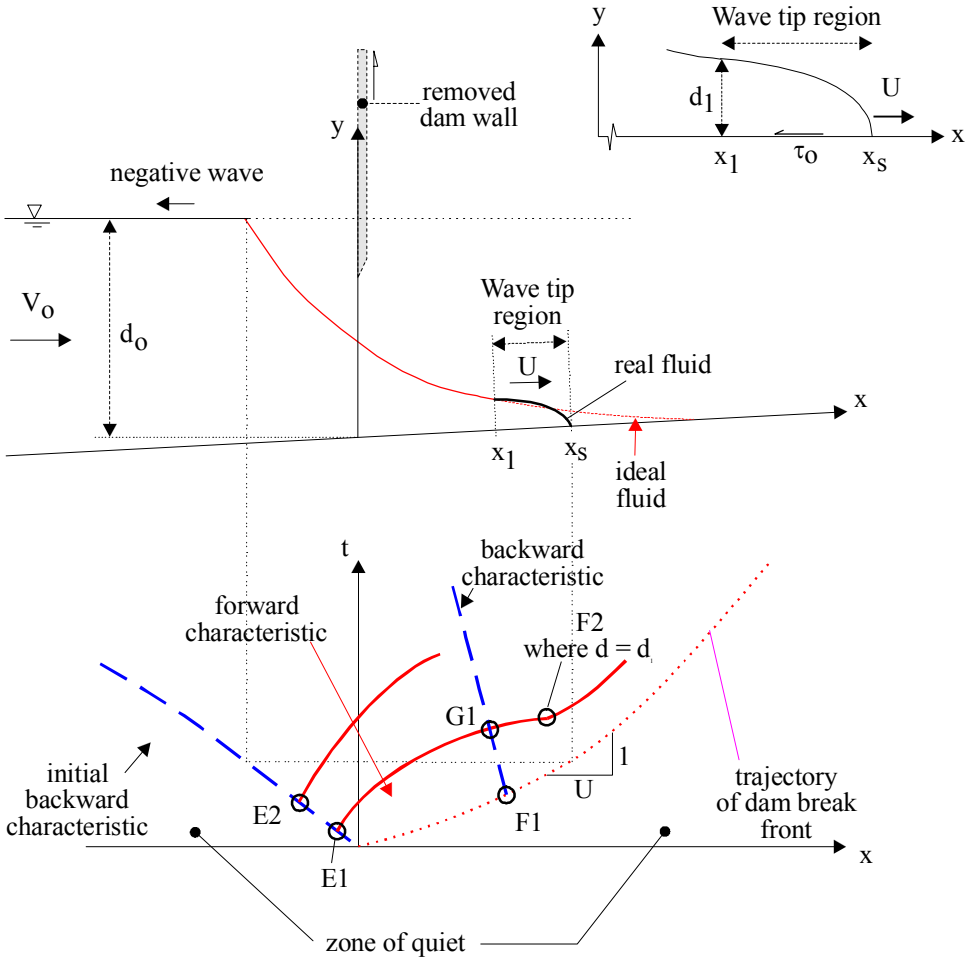

4.5 DAM BREAK IN A DRY, UPWARD SLOPING CHANNEL WITH BED FRICTION AND INITIAL FLOW MOTION

Considering a dam break wave surging over a dry river bed with some boundary friction, the above solution may be extended when the flow velocity behind the dam is initially V_o as sketched in Figure 4-10. Prior to dam break, it is assumed that the translation of both dam and reservoir is frictionless. After dam break, the flow is assumed to be an ideal fluid flow region behind a friction dominated wave tip region. Further it is assumed that the translation of the undisturbed reservoir remains frictionless for $t > 0$.

The dam break wave occurs in a sloping, prismatic, wide rectangular channel with a semi-infinite reservoir. The sudden dam removal takes place at $t = 0$ when the dam wall is located at $x = 0$ (Fig. 4-10). The dam break is approximated by an ideal fluid flow solution for $x \leq x_1$ and a diffusive wave model for $x_1 \leq x \leq x_s$. The transition between the ideal dam break wave profile and the wave tip is located at point F2 where $x = x_1$, $d = d_1$ and $V = V_1$.

The instantaneous dam break creates a negative wave propagating upstream into a fluid at rest with known water depth. In the (x, t) plane, the initial negative wave characteristic has a slope $dt/dx = -1/(C-V_o)$ with $C = C_o$ for $t = 0$ (Fig. 4-10). For a flat slope, the initial backward characteristic propagates upstream with a celerity $(\sqrt{g*d_o}-V_o)$ in first approximation.

Forward characteristics can be drawn issuing from the initial backward characteristic for $t > 0$: Between the points E1 and F2 (Fig. 4-10), the flow properties satisfy the ideal dam break wave properties :

$$\frac{C}{\sqrt{g * d_o}} = \frac{1}{3} * \left(2 + \frac{V_o}{\sqrt{g * d_o}} + \frac{1}{2} * S_o * \sqrt{\frac{g}{d_o}} * t - \frac{x}{t * \sqrt{g * d_o}} \right)$$

$$\text{for } \frac{V_o}{\sqrt{g * d_o}} - 1 \leq \frac{x}{t * \sqrt{g*d_o}} \leq \frac{x_1}{t * \sqrt{g*d_o}} \quad (4\text{-}57)$$

$$\frac{V}{\sqrt{g * d_o}} = \frac{2}{3} * \left(1 + \frac{1}{2} * \frac{V_o}{\sqrt{g * d_o}} + S_o * \sqrt{\frac{g}{d_o}} * t + \frac{x}{t * \sqrt{g * d_o}} \right)$$

$$\text{for } \frac{V_o}{\sqrt{g * d_o}} - 1 \leq \frac{x}{t * \sqrt{g*d_o}} \leq \frac{x_1}{t * \sqrt{g*d_o}} \quad (4\text{-}58)$$

For $x_1 \leq x \leq x_s$ (i.e. wave tip region), it is assumed that the velocity of water does not vary rapidly and equals the wave front celerity U. The flow properties in the wave tip region may be estimated using the diffusion wave equation taking into account flow resistance and bed slope :

$$\frac{\partial d}{\partial x} + \frac{f}{8} * \frac{U^2}{g*d} - S_o = 0 \qquad \text{Wave tip region (4-36)}$$

assuming $V = U$ (paragraph 4.4). The above equation was solved analytically in paragraph 4.4.1. A truncated Taylor series of the solution is :

$$d \approx \sqrt{\frac{f}{4 * g} * U^2 * (x_s - x)} \qquad \text{Wave front (4-38)}$$

assuming a constant Darcy friction factor, neglecting the effect of the bed slope in the wave tip region, and where x_s is the wave front location.

The free-surface profile and velocity must be continue at point F2. Hence the flow properties at the point F2 (x_1, V_1, d_1) must satisfy :

$$\sqrt{\frac{d_1}{d_o}} = \frac{1}{3} * \left(2 + \frac{V_o}{\sqrt{g * d_o}} + \frac{1}{2} * S_o * \sqrt{\frac{g}{d_o}} * t - \frac{x_1}{t * \sqrt{g * d_o}} \right) \quad (4\text{-}59)$$

$$\frac{V_1}{\sqrt{g * d_o}} = \frac{2}{3} * \left(1 + \frac{1}{2} * \frac{V_o}{\sqrt{g * d_o}} + S_o * \sqrt{\frac{g}{d_o}} * t + \frac{x_1}{t * \sqrt{g * d_o}} \right) \quad (4\text{-}60)$$

$$U = V_1 \quad (4\text{-}61)$$

$$\frac{d_1}{d_o} = \sqrt{\frac{f}{4} * \frac{U^2}{g * d_o} * \frac{x_S - x_1}{d_o}} \quad (4\text{-}62)$$

The conservation of mass must be satisfied. The mass of fluid in the wave tip region (i.e. $x_1 \le x \le x_S$) must be equal to the mass of fluid in the wave tip of the ideal fluid flow profile (i.e. for $x_1 \le x \le (2*(\sqrt{g*d_o}+V_o+g*S_o/4*t)*t)$) :

$$\int_{x_1}^{x_S} \sqrt{\frac{f}{4 * g} * U^2 * (x_S - x)} * dx =$$

$$\int_{x_1}^{2*(\sqrt{g*d_o} + V_o/2 + g*S_o/4*t)*t} \frac{1}{9 * g} * \left(2 * \sqrt{g * d_o} + V_o + \frac{1}{2} * g * S_o * t - \frac{x}{t} \right)^2 * dx \quad (4\text{-}63)$$

The continuity equation is a polynomial equation in terms of the wave front location x_S, wave front celerity $U = dx_S/dt$ and location x_1 of the point F2 :

$$\frac{2}{3} * \sqrt{\frac{f}{4} * \frac{U^2}{g * d_o}} * \left(\frac{x_S - x_1}{\sqrt{g * d_o} * t} \right)^{3/2} =$$

$$\frac{1}{27} * \sqrt[4]{\frac{d_o}{g}} * \frac{1}{\sqrt{t}} * \left(2 + \frac{V_o}{\sqrt{g * d_o}} + \frac{1}{2} * S_o * \sqrt{\frac{g}{d_o}} * t - \frac{x_1}{\sqrt{g * d_o} * t} \right)^3 \quad (4\text{-}64)$$

Equations (4-59) and (4-60) may be rewritten to express in dimensionless form d_1 and x_1 as functions of U :

$$\frac{d_1}{d_o} = \left(1 + \frac{1}{2} * \frac{V_o}{\sqrt{g * d_o}} + \frac{1}{2} * S_o * \sqrt{\frac{g}{d_o}} * t - \frac{1}{2} * \frac{U}{\sqrt{g * d_o}} \right)^2 \quad (4\text{-}59b)$$

$$\frac{x_1}{t * \sqrt{g * d_o}} = \frac{3}{2} * \frac{U}{\sqrt{g * d_o}} - \frac{1}{2} * \frac{V_o}{\sqrt{g * d_o}} - S_o * \sqrt{\frac{g}{d_o}} * t - 1 \quad (4\text{-}60b)$$

The wave tip region has a parabolic free-surface profile (Eq. (4-38)). The water depth at point F2 satisfies:

$$\frac{d_1}{d_o} = \sqrt{\frac{f}{4} * \frac{U^2}{g * d_o} * \frac{x_S - x_1}{d_o}} \quad (4\text{-}62)$$

and the dimensionless length of the wave tip region is :

$$\frac{x_S - x_1}{d_o} = \frac{4}{f} * \frac{1}{\frac{U^2}{g * d_o}} * \left(1 + \frac{1}{2} * \frac{V_o}{\sqrt{g * d_o}} + \frac{1}{2} * \sqrt{\frac{g}{d_o}} * S_o * t - \frac{1}{2} * \frac{U}{\sqrt{g*d_o}} \right)^4$$

(4-52)

Using Equation (4-60b) and replacing into the continuity equation (Eq. (4-64)), the exact solution of the dam break wave in terms of the wave front celerity is :

$$\frac{8}{3} * \frac{1}{f} * \frac{\left(1 + \frac{1}{2} * \frac{V_o}{\sqrt{g * d_o}} + \frac{1}{2} * \sqrt{\frac{g}{d_o}} * S_o * t - \frac{1}{2} * \frac{U}{\sqrt{g * d_o}}\right)^3}{\frac{U^2}{g * d_o}} = \sqrt{\frac{g}{d_o}} * t \qquad (4\text{-}65)$$

while the wave front location equals:

$$\frac{x_S}{d_o} = \left(\frac{3}{2} * \frac{U}{\sqrt{g * d_o}} - \frac{1}{2} * \frac{V_o}{\sqrt{g * d_o}} - \sqrt{\frac{g}{d_o}} * S_o * t - 1\right) * \sqrt{\frac{g}{d_o}} * t + \frac{4}{f} * \frac{1}{\frac{U^2}{g * d_o}} * \left(1 + \frac{1}{2} * \frac{V_o}{\sqrt{g * d_o}} + \frac{1}{2} * \sqrt{\frac{g}{d_o}} * S_o * t - \frac{1}{2} * \frac{U}{\sqrt{g*d_o}}\right)^4 \qquad (4\text{-}66)$$

and the free-surface profile is :

$$\frac{d}{d_o} = 1 \qquad \text{for } \frac{x}{t * \sqrt{g*d_o}} \le \frac{V_o}{\sqrt{g * d_o}} - 1 \qquad (4\text{-}67a)$$

$$\frac{d}{d_o} = \frac{1}{9} * \left(2 + \frac{V_o}{\sqrt{g * d_o}} + \frac{1}{2} * \sqrt{\frac{g}{d_o}} * S_o * t - \frac{x}{\sqrt{g * d_o} * t}\right)^2 \qquad \text{for } \frac{V_o}{\sqrt{g * d_o}} - 1 \le \frac{x}{t * \sqrt{g*d_o}} \le \frac{x_1}{t * \sqrt{g*d_o}} \qquad (4\text{-}67b)$$

$$\frac{d}{d_o} = \sqrt{\frac{f}{4 * g} * U^2 * (x_S - x)} \qquad \text{for } \frac{x_1}{t * \sqrt{g*d_o}} \le \frac{x}{t * \sqrt{g*d_o}} \le \frac{x_S}{t * \sqrt{g*d_o}} \qquad (4\text{-}67c)$$

$$\frac{d}{d_o} = 0 \qquad \text{for } \frac{x}{t * \sqrt{g*d_o}} \le \frac{x_S}{t * \sqrt{g*d_o}} \qquad (4\text{-}67d)$$

The location of point F2 is given from Equation (4-60b).

Equation (4-65) provides an explicit relationship between the dimensionless wave front celerity $U/\sqrt{g*d_o}$ and dimensionless time $t*\sqrt{g/d_o}$. Note that the solution in terms of the wave front celerity is non-linear with the dimensionless time present on both sides of Equation (4-65). Equation (4-66) yields the dimensionless wave front location x_S/d_o as a function of the dimensionless wave front celerity $U/\sqrt{g*d_o}$ and dimensionless time $t*\sqrt{g/d_o}$. Equations (4-67) and (4-60b) give the entire dimensionless free-surface profile $d/d_o = F(x/(t*\sqrt{g*d_o}))$.

Some limited analytical results are summarised in Figure 4-11 for one bed slope and several initial flow conditions. Figure 4-11A presents the dimensionless wave front location for three initial flow conditions (V_o/C_o = 0, 0.2 & 1), while Figure 4-11B shows the dimensionless wave front celerity. Figure 4-11C illustrates the wave front shape at a given time. For small initial flow velocities ($V_o/C_o << 1$), the above solution tends to that developed in paragraph 4.4.

Discussion

Note that for $V_o = C_o$, the initial backward characteristic becomes the vertical axis in the characteristic diagram.

The results are based upon a series of crude approximations. In particular, it is assumed that the wave tip region is primarily affected by bed friction while the ideal-fluid flow motion behind is mostly affected by inertial effects and the gravity force component. Further the development assumes small times t and a flat bed slope. In particular, it implies $C = C_o$ on the initial backward characteristic, and straight backward characteristics in the ideal fluid flow region.

The present development is valid for turbulent flow motion assuming that of a constant Darcy friction factor.

Fig. 4-11 - Flow properties for a dam break wave in a dry, sloping upward, rectangular channel with boundary friction and with zero initial velocity (diffusive wave solution) assuming f = 0.03

(A) Dimensionless wave front location

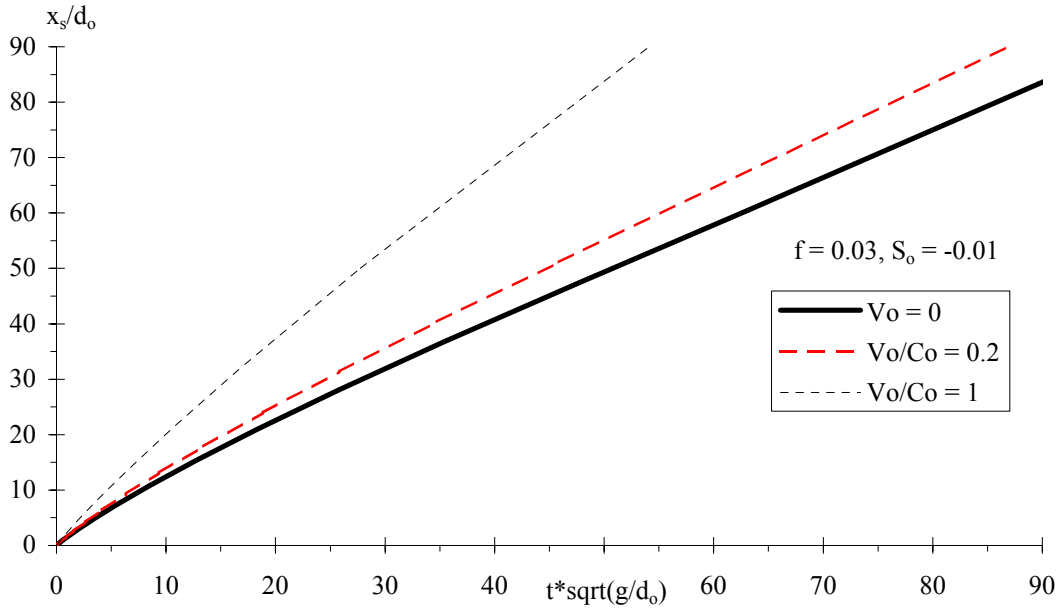

(B) Dimensionless wave front celerity

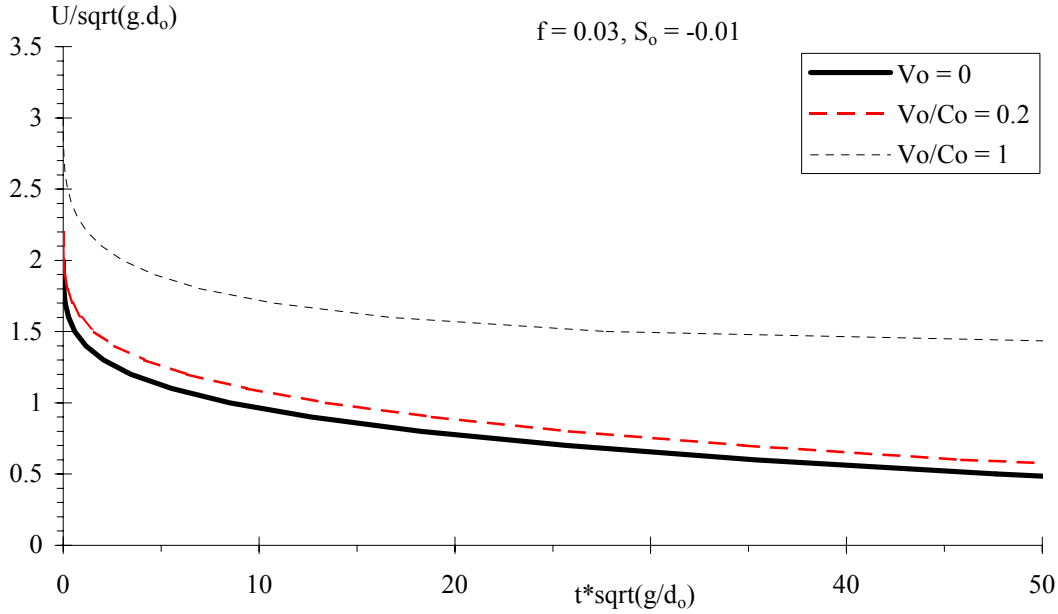

(C) Free-surface profile for $t^*\sqrt{g/d_o} = 2.25$ - Detail of the wave tip region

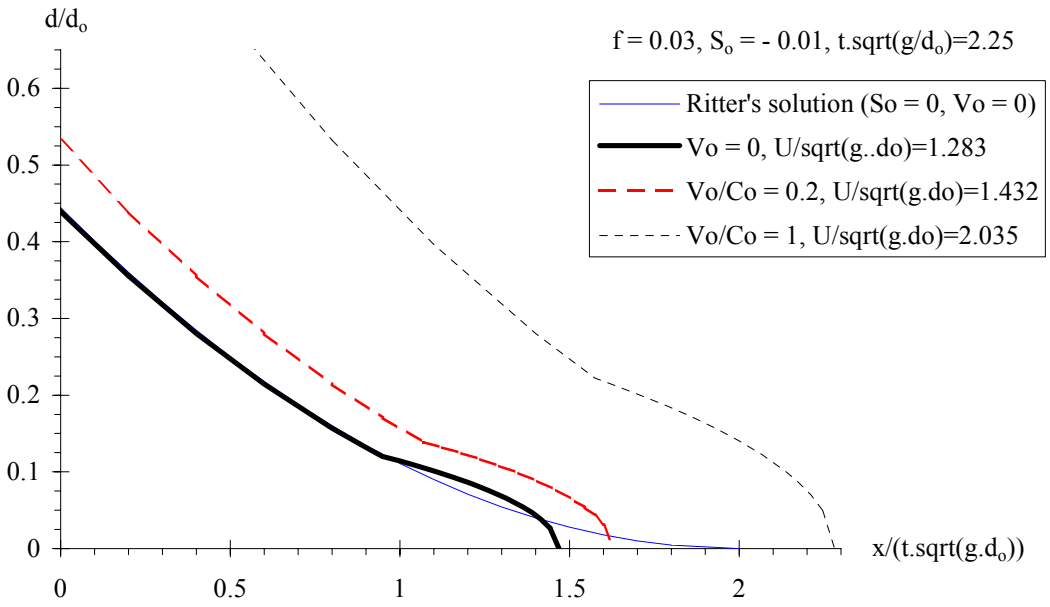

4.6 DISCUSSION

In this study (Section 4), new analytical solutions of turbulent dam break wave with bed friction are presented. For each theoretical development, the dam break wave flow is analysed as a wave tip region where flow resistance is dominant, followed by an ideal-fluid flow region where inertial effects and gravity effects are dominant. The analytical results were validated by successful comparisons between turbulent flow motion data in large-size facilities (App. B) and theoretical results in terms of wave front location, wave front celerity and instantaneous free-surface profiles (paragraph 4.2). The latter comparison is considered to be the most accurate for the estimation of the flow resistance. Indeed instantaneous free-surface measurements give a Lagrangian description of the flow that is most accurate in the initial stages of the dam break when the flow properties (depth and velocity) change very rapidly with time. Further the integration of the Saint-Venant equations yields the exact expression of the instantaneous free-surface profile assuming a constant flow resistance coefficient. The best data fit between instantaneous wave profiles and analytical expressions gives the average friction factor at a given time t. (It was found that the flow resistance coefficient was basically independent of the time (Table 4-3).) Overall this approach is regarded as the best validation technique of a dam break wave model.

The present theoretical solutions are based upon a few key assumptions. These include (a) the assumption V(x,t) = U(t) only in the wave tip region, (a) some discontinuity of $\partial d/\partial x$, $\partial V/\partial x$ and τ_o at the transition between the wave tip region and the ideal fluid flow region (i.e. $x = x_1$), and (c) the assumption of constant Darcy-Weisbach friction factor in the wave tip region.

A number of experimental data set tend to support the first approximation (a) : e.g., ESTRADE (1967), LAUBER (1997), CHANSON (2004d). These data suggested little longitudinal variations in velocity in the wave tip region: "*close to the positive wave front, the* [longitudinal] *velocity is essentially constant*" (LAUBER 1997). Further the comparisons between the present 'diffusive wave theory' and experimental results were successful for a fairly wide range of experimental data obtained independently and including instantaneous free-surface profiles, wave front celerity, and wave front locations. These comparisons constitute a solid validation of the proposed theory. More WHITHAM (1955) and DRESSLER (1952) produced two very different analytical solutions which gave nearly identical results. WHITHAM's theory included a discontinuity in terms of $\partial d/\partial x$, $\partial V/\partial x$

and τ_o at the transition between ideal flow region and wave tip region identical to the present approach. DRESSLER developed a theory that did not have such a discontinuity. Yet all theories gave very-close results, suggesting that the discontinuity in terms of $\partial d/\partial x$, $\partial V/\partial x$ and τ_o has little effect on the final solution in terms of wave front celerity and thickness, and instantaneous free-surface profiles.
It is however the writer's opinion that the strongest approximation is the assumption of constant friction factor f in the wave tip region (assumption (c)). This is a gross assumption that is probably untrue. In the wave tip region, the flow depth varies from zero to the wave tip thickness d_1. For a given equivalent bed roughness height (k_S), the Moody diagram shows that the flow resistance cannot be assumed constant (HENDERSON 1966, MONTES 1998). The wave tip ($x = x_S$) is a flow singularity in terms of flow resistance that is not accounted for within assumption (c).

The present developments (section 4) exhibit several main advantages over existing methods. First the theoretical results for real-fluid flows yield simple explicit analytical expressions that compares well with experimental data and more advanced theoretical solutions. In the next section (Section 5), the equations are applied to three flow situations: a dam break, the swash zone, and a tsunami runup. It will be shown that the theoretical results may be applied to a wider range of applications that the simple dam break problem.

Second the proposed development is a simple pedagogical application of the Saint-Venant equations and method of characteristics, linking together the simple wave equations yielding RITTER's solution, with a diffusive wave equation for the wave tip region. Both the simple wave and diffusive wave equations constitute relatively simple lecture materials that may be introduced in advanced undergraduate subjects (e.g. CHANSON 2004b) ([4]). The proposed development therefore provides a means to introduce realistic solutions of the dam break wave with bed friction (paragraphs 4.2 and 4.3) to undergraduate engineering and applied mathematics students.

Third, these explicit analytical solutions may be used to validate numerical solutions of the method of characteristics applied to the dam break wave problem. Numerical modelling is commonly used for real-fluid flow in natural system, when the Saint-Venant equations cannot be solved analytically (e.g. CUNGE 1975, CUNGE et al. 1980). It is however essential that the numerical scheme be validated with analytical solutions. This is important in dam break wave calculations where the wave tip is a flow singularity with zero water depth. Further most numerical models must be calibrated in terms of flow resistance. Some comparison between numerical results, analytical solutions and experimental results under controlled flow conditions may assist in the accurate selection of flow resistance coefficient.

Fourth the development were applied to a wider range of flow situations. For example, the effects of bed slope are included, although limited to relatively flat gradients and the initial flow motion may be taken into account. This yields to a wide range of practical applications which may encompass advancing flood waters in ephemeral streams, water runup downstream of wave breaking on beach slope and (e.g. Section 5).

Fifth the simplicity of the equations may allow the extension of the method to laminar flows (Section 5) and non-Newtonian fluids. For example, CHANSON et al. (2004) applied successfully the mathematical treatment of HUNT (1982,1984) (section 3.4) to dam break wave of non-Newtonian thixotropic fluids. Relevant applications include mud flows, self-flowing concrete and

[4]At the University of Queensland, this lecture material is taught as part of the undergraduate subject CIVL4120 Advanced open channel flow and design, offered as an advanced elective to civil and environmental engineering students in fourth year.

debris flows in civil engineering, but also the flow of some industrial paint, liquid dairy products, pasty sewage sludges and some wastewater treatment residues.

5. LAMINAR FLOW SOLUTIONS OF THE DAM BREAK PROBLEM

5.1 BASIC EQUATIONS

A dam break wave is the flow resulting from a sudden release of a mass of fluid in a channel. In unsteady open channel flows, the velocities and water depths change with time and longitudinal position. For one-dimensional applications, the continuity and momentum equations yield the Saint-Venant equations. The application of the Saint-Venant equations is limited by some basic assumptions : (1) the flow is one dimensional; (2) the streamline curvature is very small and the pressure distributions are hydrostatic; (3) the flow resistance are the same as for a steady uniform flow for the same depth and velocity; (4) the bed slope is small enough to satisfy : $\cos\theta \approx 1$ and $\sin\theta \approx \tan\theta \approx \theta$; (5) the water density is a constant; and (6) the channel has fixed boundaries, and air entrainment and sediment motion are neglected. With these hypotheses, the unsteady flow can be characterised at any point and any time by two variables: e.g., V and d where V is the flow velocity and d is the water depth (e.g. LIGGETT 1994, MONTES 1998, CHANSON 2004a,b). The unsteady flow properties are described by a system of two partial differential equations :

$$\frac{\partial d}{\partial t} + \frac{A}{B} * \frac{\partial V}{\partial x} + V * \frac{\partial d}{\partial x} + \frac{V}{B} * \left(\frac{\partial A}{\partial x}\right)_{d=constant} = 0 \qquad (5\text{-}1)$$

$$\frac{\partial V}{\partial t} + V * \frac{\partial V}{\partial x} + g * \frac{\partial d}{\partial x} + g * (S_f - S_o) = 0 \qquad (5\text{-}2)$$

where t is the tine, x is the streamwise co-ordinate, A is the cross-section area, B is the free-surface width, S_o is the bed slope ($S_o = \sin\theta$), θ is the angle between the bed and the horizontal, with $\theta > 0$ for a downward slope, and S_f is the friction slope. The friction slope is defined as : $S_f = f/2*V^2/(g*D_H)$ where D_H is the hydraulic diameter and the Darcy friction factor f is a non-linear function of both relative roughness and flow Reynolds number. Equation (5-1) is the continuity equation and Equation (5-2) is the dynamic equation.

Herein the dam break flow is analysed as an ideal-fluid flow region behind a flow resistance-dominated tip zone (Fig. 5-1). DEBIANE (2000) used a a similar conceptual approach, but his mathematical development differs from the present simplified solution. The transition between the ideal dam break wave profile and the wave tip region is located at $x = x_1$ where the water depth is $d = d_1$ as shown in Figure 5-1.

In the ideal fluid flow region, the basic equations yield the characteristic system of equations :

$$\frac{D}{Dt}(V + 2 * C) = 0 \qquad \text{forward characteristic} \quad (5\text{-}3a)$$

$$\frac{D}{Dt}(V - 2 * C) = 0 \qquad \text{backward characteristic} \quad (5\text{-}3b)$$

along :

$$\frac{dx}{dt} = V + C \qquad \text{forward characteristic C1} \quad (5\text{-}4a)$$

$$\frac{dx}{dt} = V - C \qquad \text{backward characteristic C2} \quad (5\text{-}4b)$$

Equations (5-3) and (5-4) are the characteristic equations of a simple wave problem (CHANSON 2004a,b).

In the wave tip region ($x_1 \leq x \leq x_s$, Fig. 5-1), flow resistance is dominant, and the acceleration and inertial terms are small. The flow velocity does not vary rapidly in the forward tip zone and experimental data showed that it is about the wave front celerity U (HUNT 1994). The dynamic

wave equation (Eq. (5-2)) may be reduced into a diffusive wave equation. For a horizontal channel, it yields :

$$\frac{\partial d}{\partial x} + \frac{f}{8} * \frac{U^2}{g * d} = 0 \qquad \text{Wave tip region (5-5)}$$

assuming a constant velocity U for $x_1 \leq x \leq x_S$. Next to the leading edge of the wave, the slope of the free-surface becomes important to counterbalance the flow resistance. For laminar flows, the Darcy friction factor in steady flows equals :

$$f = \frac{64}{Re}$$

where Re is the flow Reynolds number defined in terms of the hydraulic diameter D_H (LIGGETT 1994, MONTES 1998, CHANSON 2004a). Several researchers argued that the flow resistance may differ in unsteady dam break wave flows (e.g. AGUIRRE-PE et al. 1995, DEBIANE 2000). Therefore it is assumed that the flow resistance satisfies :

$$f = \alpha * \frac{64}{Re} \qquad (5\text{-}6)$$

where α is a correction factor. For a wide channel (i.e. $D_H \approx 4*d$), Equation (5-6) may be rewritten in the wave tip region as :

$$f = \frac{16 * \alpha * \mu}{\rho * U * d} \qquad (5\text{-}6B)$$

where ρ and μ is the density and dynamic viscosity of the fluid respectively. The diffusive wave equations may rewritten as :

$$\frac{\partial d}{\partial x} + \frac{2 * \alpha * \mu * U}{\rho * g * d^2} = 0 \qquad \text{Laminar flow motion (5-5B)}$$

The integration of the diffusive wave equation (Eq. (5-5)) yields the shape of wave tip region for a laminar flow motion :

$$d = \sqrt[3]{6 * \alpha * \frac{\mu * U}{\rho * g} * (x_S - x)} \qquad \text{Wave front profile (laminar flow) (5-7)}$$

assuming that the flow resistance correction coefficient α is a constant independent of x. Equation (5-7) is compared with some experimental data in Figure 5-2.

5.2 DETAILED SOLUTION FOR A HORIZONTAL CHANNEL WITH ZERO INITIAL MOTION

Considering a laminar dam break wave in a horizontal channel with zero initial flow motion, the instantaneous dam break creates a negative wave propagating upstream into a still fluid with known water depth d_o. In the (x, t) plane, the initial negative wave characteristic has a slope $dt/dx = -1/C_o$ where $C_o = \sqrt{g*d_o}$. Note that the initial backward characteristic is a straight line, but the other backward characteristics are not because the problem is not a simple wave since $S_f > 0$. Forward characteristics can be drawn issuing from the initial backward characteristic for $t > 0$ (Fig. 5-1). Between the points E1 and F2, the flow properties satisfy the ideal dam break wave properties:

Fig. 5-1 - Sketch of dam break wave in a horizontal dry channel with bottom friction

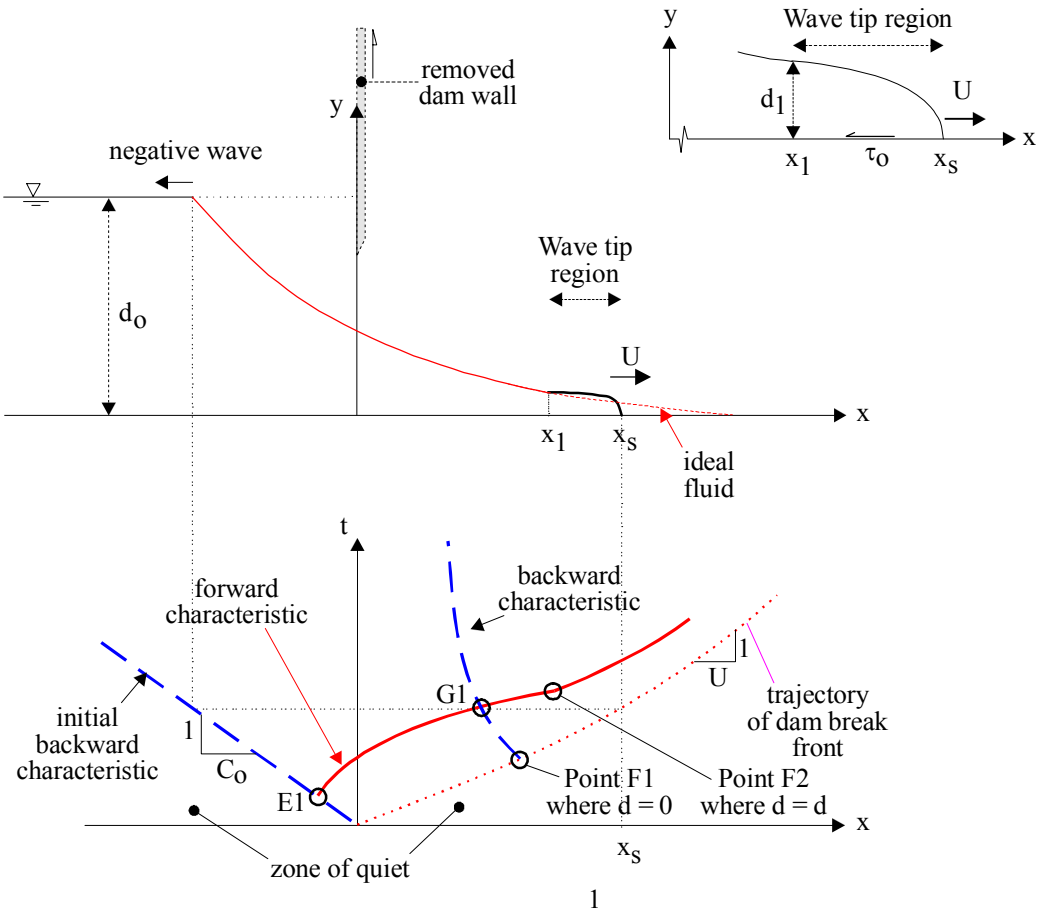

1

Fig. 5-2 - Laminar dam break wave front data: horizontal channel (test Glus.6), glucose-syrup solution, ρ = 1406 kg/m^3, μ = 12 Pa.s, d_o = 0.055 m, t = 421 s (DEBIANE 2000) - Comparison with Equation (5-7) assuming α = 1 and $U/\sqrt{g*d_o}$ = 0.0064

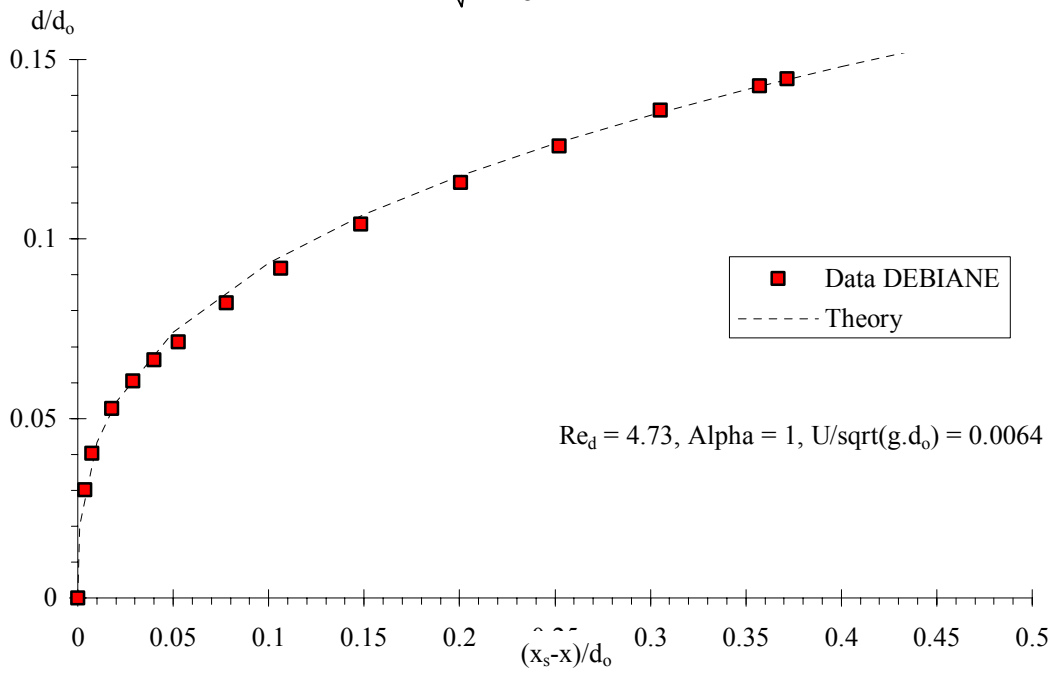

$$\sqrt{\frac{d}{d_o}} = \frac{1}{3} * \left(2 - \frac{x}{t * \sqrt{g * d_o}}\right) \qquad -1 \le \frac{x}{t * \sqrt{g * d_o}} \le \frac{x_1}{t * \sqrt{g * d_o}} \quad (5\text{-}8)$$

$$\frac{V}{\sqrt{g * d_o}} = \frac{2}{3} * \left(1 + \frac{x}{t * \sqrt{g * d_o}}\right) \qquad -1 \le \frac{x}{t * \sqrt{g * d_o}} \le \frac{x_1}{t * \sqrt{g * d_o}} \quad (5\text{-}9)$$

where d and V are the flow depth and velocity respectively at a distance x from the dam, and t is the time from the instantaneous dam removal.

For $x_1 \le x \le x_S$ (i.e. wave tip region), it is assumed that the velocity of water does not vary rapidly and that it equals the wave front celerity U. The flow properties in the wave tip region may be estimated using the diffusive wave equation taking into account flow resistance (Eq. (5-5)) assuming V = U. The integration of the diffusive wave equation yields the wave front profile:

$$\frac{d}{d_o} = \sqrt[3]{6 * \alpha * \frac{\mu}{\rho * \sqrt{g * {d_o}^3}} * \frac{U}{\sqrt{g * d_o}} * \frac{x_S - x}{d_o}}$$

$$\frac{x_1}{t * \sqrt{g * d_o}} \le \frac{x}{t * \sqrt{g * d_o}} \le \frac{x_S}{t * \sqrt{g * d_o}} \quad (5\text{-}7B)$$

assuming that Equation (5-6B) holds for $x_1 \le x \le x_S$.

Since the free-surface and velocity must be continue at the point F2, its flow properties (x_1, V_1, d_1) must satisfy :

$$\sqrt{\frac{d_1}{d_o}} = \frac{1}{3} * \left(2 - \frac{x_1}{\sqrt{g * d_o} * t}\right) \quad (5\text{-}10)$$

$$\frac{V_1}{\sqrt{g * d_o}} = \frac{2}{3} * \left(1 + \frac{x_1}{\sqrt{g * d_o} * t}\right) \quad (5\text{-}11)$$

$$\frac{U}{\sqrt{g * d_o}} = \frac{V_1}{\sqrt{g * d_o}} \quad (5\text{-}12)$$

$$\frac{d_1}{d_o} = \sqrt[3]{6 * \alpha * \frac{\mu * U}{\rho * g * {d_o}^2} * \frac{x_S - x_1}{d_o}} \quad (5\text{-}13)$$

The conservation of mass must be further satisfied. Specifically the mass of fluid in the wave tip region (i.e. $x_1 \le x \le x_S$) must equal the mass of fluid in the ideal fluid flow profile for $x_1 \le x \le 2*\sqrt{g*d_o}*t$. It yields :

$$\int_{x_1}^{x_S} \sqrt[3]{6 * \alpha * \frac{\mu * U}{\rho * g} * (x_S - x)} * dx = \int_{x_1}^{2*\sqrt{g*d_o}*t} \frac{1}{9 * g} * \left(2 * \sqrt{g * d_o} - \frac{x}{t}\right)^2 * dx \quad (5\text{-}14)$$

Note that the continuity equation becomes a differential equation in terms of the wave front location x_S and celerity $U = dx_S/dt$. It must be stressed that the development is limited. The Saint-Venant equations, hence the diffusive wave equation, are not valid near the wave leading edge where the free-surface curvature is not small and where the flow resistance becomes very significant.

The above equations may be transformed to express d_1 and x_1 as functions of U:

$$\frac{d_1}{d_o} = \left(1 - \frac{1}{2} * \frac{U}{\sqrt{g * d_o}}\right)^2 \tag{5-15}$$

$$\frac{x_1}{\sqrt{g * d_o} * t} = \left(\frac{3}{2} * \frac{U}{\sqrt{g * d_o}} - 1\right) \tag{5-16}$$

The continuity equation (Eq. (5-14)) yields a polynomial equation in terms of the wave front location x_S, wave celerity $U = dx_S/dt$ and location x_1 of the point F2 :

$$\frac{3}{4} * \sqrt[3]{6 * \alpha * \frac{\mu * U}{\rho * g * {d_o}^2}} * \left(\frac{x_S - x_1}{d_o}\right)^{4/3} = \frac{1}{27} * \sqrt{\frac{g}{d_o}} * t * \left(2 - \frac{x_1}{\sqrt{g * d_o} * t}\right)^3 \tag{5-17}$$

Since the wave tip region has a cubic-root free-surface profile, the water depth at point F2 satisfies:

$$\frac{d_1}{d_o} = \sqrt[3]{6 * \alpha * \frac{\mu * U}{\rho * g * {d_o}^2} * \frac{x_S - x_1}{d_o}} \tag{5-13}$$

and hence the wave tip region length is:

$$\frac{x_S - x_1}{d_o} = \frac{1}{6 * \alpha} * \frac{\rho * g * {d_o}^2}{\mu * U} * \left(1 - \frac{1}{2} * \frac{U}{\sqrt{g * d_o}}\right)^6 \tag{5-18}$$

By replacing into the continuity equation, the exact solution in terms of the wave front celerity is :

$$\frac{1}{8 * \alpha} * \frac{\rho * \sqrt{g * {d_o}^3}}{\mu} * \frac{\left(1 - \frac{1}{2} * \frac{U}{\sqrt{g * d_o}}\right)^5}{\frac{U}{\sqrt{g * d_o}}} = \sqrt{\frac{g}{d_o}} * t \tag{5-19}$$

while the wave front location equals:

$$\frac{x_S}{d_o} = \left(\frac{3}{2} * \frac{U}{\sqrt{g * d_o}} - 1\right) * \sqrt{\frac{g}{d_o}} * t + \frac{1}{6 * \alpha} * \frac{\frac{\rho * \sqrt{g * {d_o}^3}}{\mu}}{\frac{U}{\sqrt{g * d_o}}} * \left(1 - \frac{1}{2} * \frac{U}{\sqrt{g * d_o}}\right)^6 \tag{5-20}$$

and the free-surface profile satisfies :

$$\frac{d}{d_o} = 1 \qquad \frac{x}{d_o} \le -\sqrt{\frac{g}{d_o}} * t \tag{5-21a}$$

$$\frac{d}{d_o} = \frac{1}{9} * \left(2 - \frac{x}{t * \sqrt{g * d_o}}\right)^2$$

$$-\sqrt{\frac{g}{d_o}} * t \le \frac{x}{d_o} \le \left(\frac{3}{2} * \frac{U}{\sqrt{g * d_o}} - 1\right) * \sqrt{\frac{g}{d_o}} * t \tag{5-21b}$$

$$\frac{d}{d_o} = \sqrt[3]{6 * \alpha * \frac{\mu}{\rho * \sqrt{g * {d_o}^3}} * \frac{U}{\sqrt{g * d_o}} * \frac{x_S - x}{d_o}} \qquad \left(\frac{3}{2} * \frac{U}{\sqrt{g * d_o}} - 1\right) * \sqrt{\frac{g}{d_o}} * t \leq \frac{x}{d_o} \leq \frac{x_S}{d_o} \quad (5\text{-}21c)$$

$$\frac{d}{d_o} = 0 \qquad \frac{x_S}{d_o} \leq \frac{x}{d_o} \quad (5\text{-}21d)$$

The location of point F2 is given by :

$$\frac{x_1}{\sqrt{g * d_o} * t} = \left(\frac{3}{2} * \frac{U}{\sqrt{g * d_o}} - 1\right) \quad (5\text{-}16)$$

In the above development, the term :

$$Re_d = \frac{\rho * \sqrt{g * {d_o}^3}}{\mu}$$

is analogous to a Reynolds number. It is called herein the dam reservoir flow Reynolds number and it is a function of fluid properties and initial flow conditions only. Typical analytical results are summarised in Figure 5-3.

Fig. 5-3 - Dimensionless wave front location, celerity and free-surface profile solutions for laminar dam break wave (horizontal channel, zero initial motion)

(A) Dimensionless relationship between wave front celerity and time assuming $\alpha = 1$

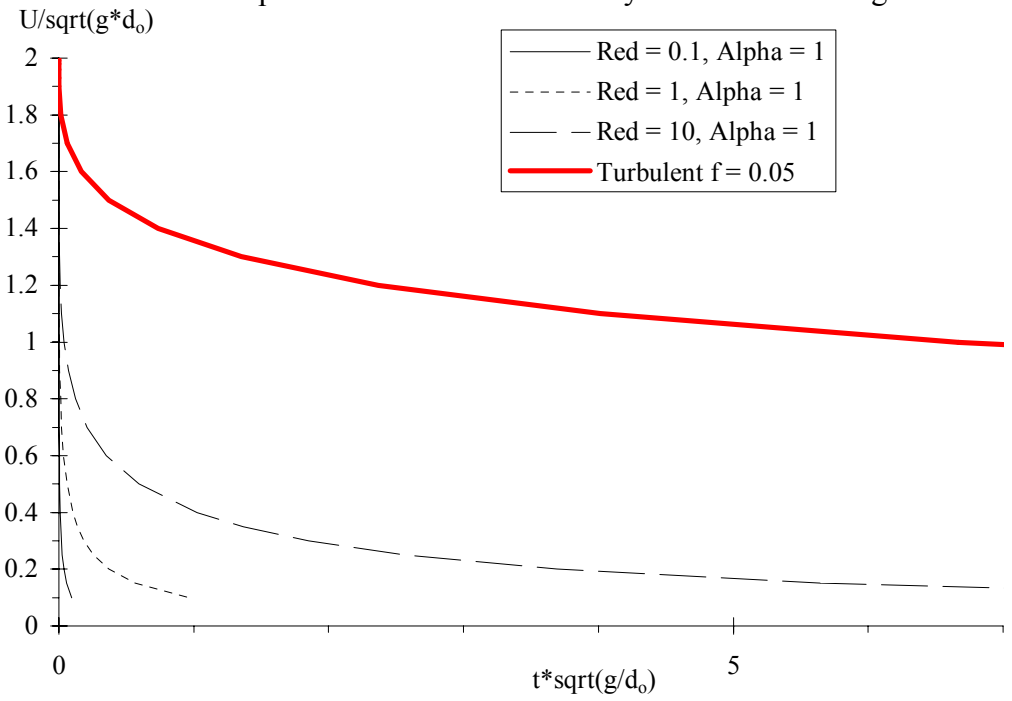

(B) Instantaneous dimensionless free-surface profile for $Re_d = 10$ and $\alpha = 1$ and 100

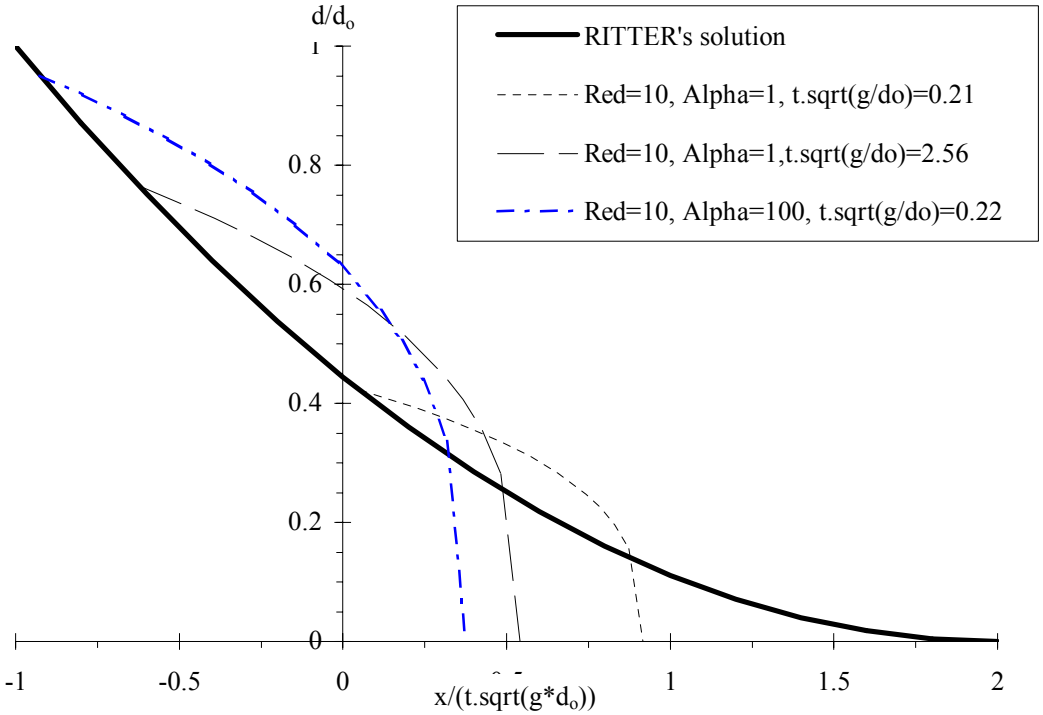

Table 5-1 - Asymptotic solutions of dam break wave on dry horizontal channel with boundary friction (horizontal channel with zero initial motion)

Reference (1)	Asymptotic solution (2)	Remarks (3)
<u>Small time t</u>		
DRESSLER (1952)	$\frac{U}{\sqrt{g*d_o}} = 2 - 3.59 * \frac{f}{8} * \sqrt{\frac{g}{d_o}} * t$	Turbulent flow motion.
WHITHAM (1955)	$\frac{U}{\sqrt{g*d_o}} = 2 - 3.452 * \frac{f}{8} * \sqrt{\frac{g}{d_o}} * t$	Turbulent flow motion.
Laminar flow motion (diffusive wave model)	$\frac{U}{\sqrt{g*d_o}} = 2 - \sqrt[5]{16 * \alpha * \frac{\mu}{\rho * \sqrt{g * d_o^3}} * \sqrt{\frac{g}{d_o}} * t}$	$\frac{U}{\sqrt{g*d_o}} > 1.2$ to 1.5
Turbulent flow motion (diffusive wave model)	$\frac{U}{\sqrt{g*d_o}} = 2 - \sqrt[3]{12 * f * \sqrt{\frac{g}{d_o}} * t}$	$\frac{U}{\sqrt{g*d_o}} > 1.2$ to 1.5
<u>Large time t</u>		
Laminar flow motion (diffusive wave model)	$\frac{U}{\sqrt{g*d_o}} = \frac{1}{8 * \alpha} * \frac{\rho * \sqrt{g * d_o^3}}{\frac{\mu}{\sqrt{\frac{g}{d_o}} * t}}$	$\frac{U}{\sqrt{g*d_o}} < 0.3$ to 0.4
Turbulent flow motion (diffusive wave model)	$\frac{U}{\sqrt{g*d_o}} = \sqrt{\frac{8}{3} * \frac{1}{f * \sqrt{\frac{g}{d_o}} * t}}$	$\frac{U}{\sqrt{g*d_o}} < 0.3$ to 0.4

Discussion

Asymptotic approximations for small and large times t are summarised in Table 5-1. These are compared with turbulent flow solutions and with well-known solutions for turbulent flows.

Overall the present method yields an explicit expression of the wave front celerity, wave front location and wave tip region characteristics. Equation (5-19) provides a direct relationship between the dimensionless wave front celerity $U/\sqrt{g*d_o}$ and dimensionless time $t*\sqrt{g/d_o}$. Equation (5-20) yields the dimensionless wave front location x_s/d_o as a function of the dimensionless wave front celerity $U/\sqrt{g*d_o}$. Equations (5-21) and (5-16) give the entire dimensionless free-surface profile $d/d_o = F(x/(t*\sqrt{g*d_o}))$. This simple system of linear equations provides a means to assess easily the effect of the flow resistance on the dam break wave propagation of real fluids.

In the wave tip region, the dimensionless boundary shear stress may be expressed as :

$$f = \frac{\tau_o}{\frac{f}{8} * \rho * U^2} = 16 * \alpha * \frac{\frac{U}{\sqrt{g * d_o}}}{\frac{\rho * \sqrt{g * d_o^3}}{\mu}} * \frac{d_o}{d} \qquad (5\text{-}6B)$$

The boundary shear stress increases with increasing distance towards the wave tip. At the wave front ($x = x_s$, $d = 0$), the boundary shear stress becomes infinite. Figure 5-4 illustrates an example assuming $\alpha = 1$.

Fig. 5-4 - Dimensionless distribution of boundary shear stress in laminar flow motion - Comparison with the laminar flow profile ($Re_d = 10$, $\alpha = 1$, $t*\sqrt{g/d_o} = 0.35$)

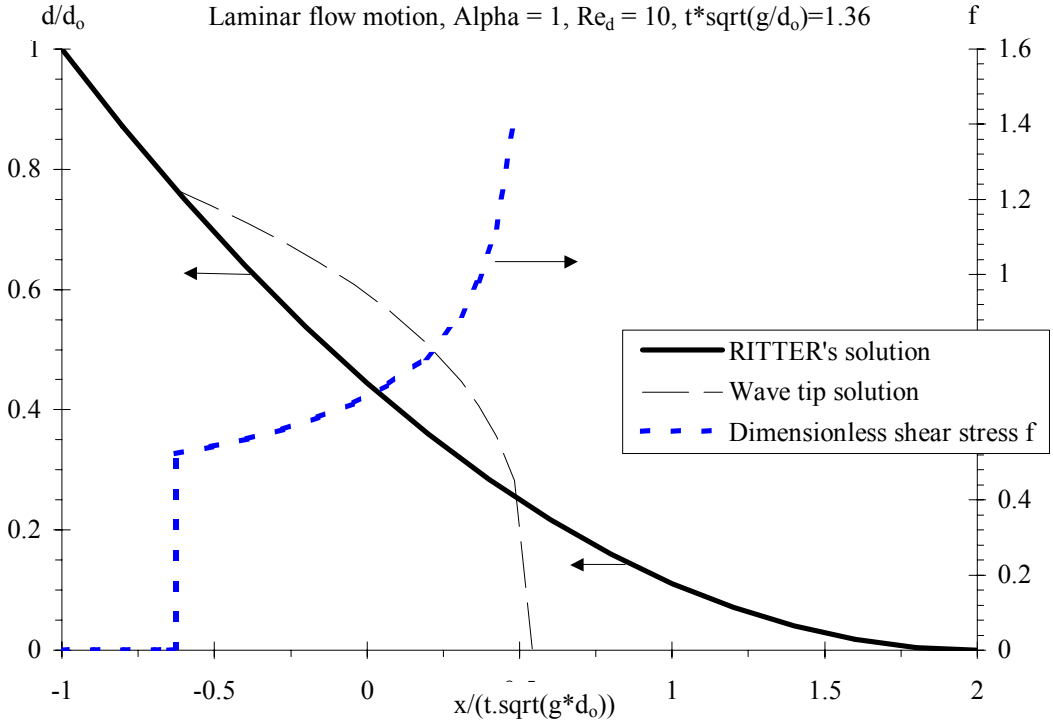

Comparison with experimental data

The theory was compared qualitatively with the viscous flow data of DEBIANE (2000) and with the analytical solution of HUNT (1994) for viscous dam break wave down a sloping channel.

DEBIANE (2000) presented an unique data set for laminar dam break wave in horizontal channel. He conducted basic experiments in a 3.0 m long, 0.3 m wide horizontal channel with an upstream reservoir length ranging from 0.11 to 0.60 m (App. B). The study was conducted with glucose-

syrup solutions of dynamic viscosities between 12 to 170 Pa.s. During the early stages of the dam break, the dam break wave flow was similar to the flow conditions for an infinitely large reservoir and only this data set is considered herein. Figure 5-5 presents some comparison between the data of DEBIANE (2000) and the present theory. Figure 5-5A shows the dimensionless wave front location as function of the dimensionless time. DEBIANE's data are compared with RITTER's (1892) solution (thick solid line) and with Equation (5-20) for $\alpha = 1$ (i.e. $f = 64/Re$) and $\alpha = 100$ (i.e. $f = 6400/Re$). Figure 5-5B illustrates an instantaneous free-surface profile. Overall the analytical development are qualitatively in agreement with the experimental trends.
In his thesis, however, DEBIANE (2000) acknowledged a number of experimental shortcomings (DEBIANE 2000, pp. 161-163). His results showed systematically that the dam break front celerity was much smaller than theoretical predictions. His data were about 7 times lower than both RITTER's solution and DEBIANE's theoretical solution for laminar flows. This problem is best illustrated in Figure 5-5A in terms of wave front locations. DEBIANE indicated that, during his experiments, the gate opening was relatively slow (0.25 s typically) and could not be considered as an instantaneous dam break, as demonstrated by the experimental work of ESTRADE (1967). Further, for very viscous solutions, some fluid was affected by the gate opening motion. Some fluid attached to the gate while other portions were projected away from the flume. DEBIANE indicated further problems with sidewall effects for the most viscous solutions ($\mu = 170$ Pa.s) as well as some fluid crystallisation next to the walls at the shock front (DEBIANE 2000, p. 163).

Fig. 5-5 - Comparison between theory and experimental data by DEBIANE (2000)
(A) Dimensionless wave front location for Re_d =4.73 - Comparison between RITTER's solution, Equation (5-20) and DEBIANE's data

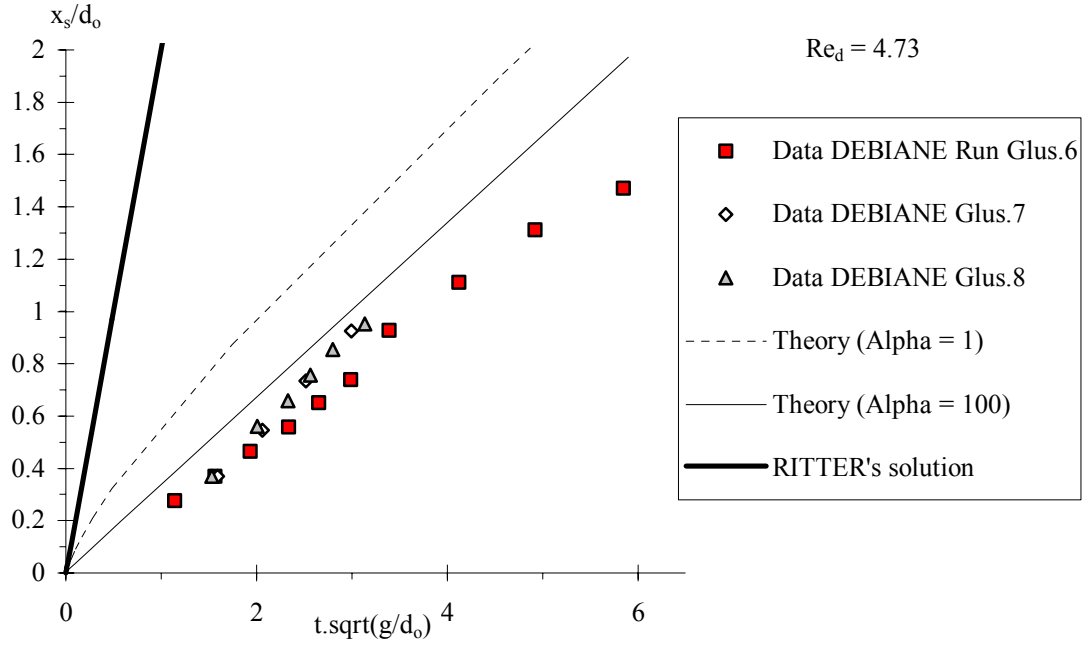

(B) Instantaneous free-surface profile for Re_d = 0.671 - Comparison between DEBIANE's data ($t^*\sqrt{g/d_o}$ = 114) and Equation (5-21) (for $t^*\sqrt{g/d_o}$ = 9.1, α = 1, 10 and 100)

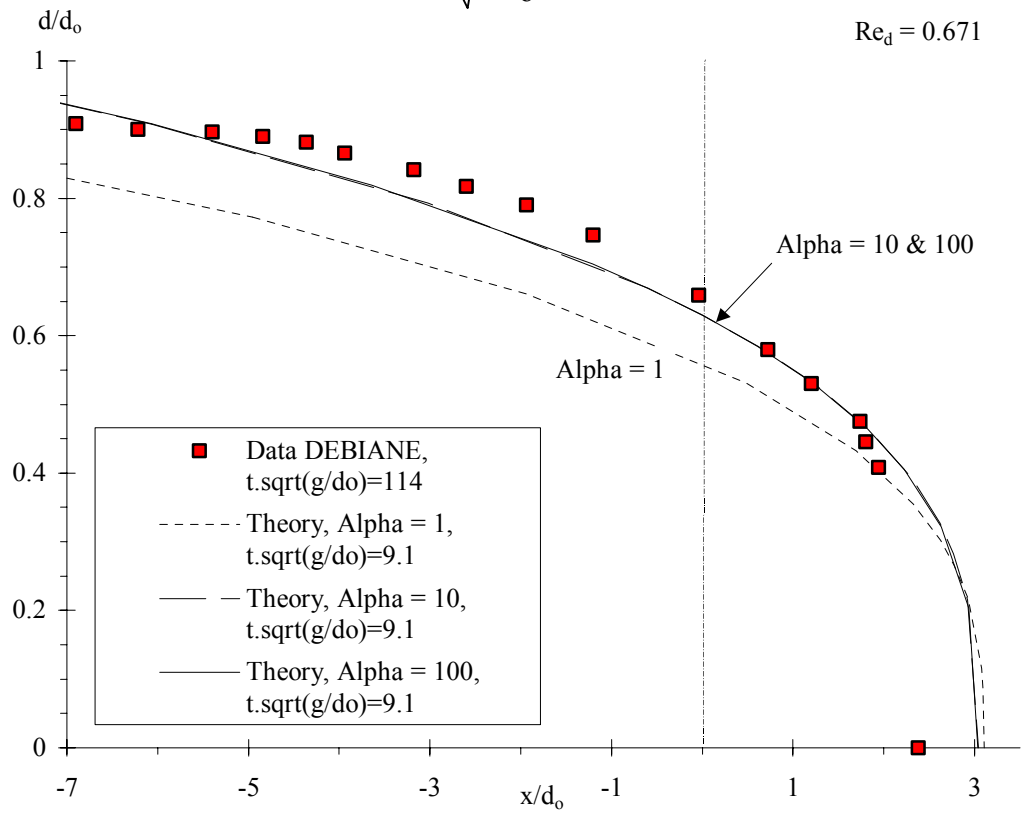

5.3 DETAILED SOLUTION FOR A HORIZONTAL CHANNEL WITH SOME INITIAL MOTION

The laminar dam break wave in a horizontal channel may be extended if the flow velocity behind the dam is V_o for $t < 0$ as sketched in Figure 4-5. It is assumed that the translation of both dam and reservoir at the speed V_o is frictionless prior to dam removal, and that the translation of the undisturbed reservoir remains frictionless for $t \geq 0$. The dam break is idealised by a vertical wall that is suddenly removed at $t = 0$ when the dam wall is located at $x = 0$.

The instantaneous dam break creates a negative wave propagating upstream ([1]) into the reservoir with a known water depth d_o. In the (x, t) plane, the initial negative wave characteristic has a slope $dt/dx = -1/(C_o - V_o)$ where $C_o = \sqrt{g*d_o}$ assuming a rectangular channel. Forward characteristics can be drawn issuing from the initial backward characteristic for $t > 0$. In the ideal fluid region, the flow properties satisfy the ideal dam break wave properties :

$$\sqrt{\frac{d}{d_o}} = \frac{1}{3} * \left(2 + \frac{V_o}{\sqrt{g * d_o}} - \frac{x}{t * \sqrt{g * d_o}} \right)$$

$$\text{for } -1 + \frac{V_o}{\sqrt{g * d_o}} \leq \frac{x}{t * \sqrt{g * d_o}} \leq \frac{x_1}{t * \sqrt{g * d_o}} \quad (5\text{-}22)$$

[1]The negative wave propagates upstream if $V_o < C_o$. For $V_o > C_o$, the leading edge of the initial negative characteristic may propagate downstream.

$$\frac{V}{\sqrt{g * d_o}} = \frac{2}{3} * \left(1 + \frac{1}{2} * \frac{V_o}{\sqrt{g * d_o}} + \frac{x}{t * \sqrt{g * d_o}}\right)$$

$$\text{for } -1 + \frac{V_o}{\sqrt{g * d_o}} \leq \frac{x}{t * \sqrt{g * d_o}} \leq \frac{x_1}{t * \sqrt{g * d_o}} \quad (5\text{-}23)$$

In the wave tip region (i.e. $x_1 \leq x \leq x_s$), the flow properties are calculated using the diffusive wave equation (Eq. (5-5)). Since the flow depth and velocity must be continue at the point F2, the flow properties at point F2 (x_1, V_1, d_1) and at wave front (x_s, U) are deduced from :

$$\sqrt{\frac{d_1}{d_o}} = \frac{1}{3} * \left(2 + \frac{V_o}{\sqrt{g * d_o}} - \frac{x_1}{\sqrt{g * d_o} * t}\right) \quad (5\text{-}24)$$

$$\frac{V_1}{\sqrt{g*d_o}} = \frac{2}{3} * \left(1 + \frac{1}{2} * \frac{V_o}{\sqrt{g * d_o}} + \frac{x_1}{\sqrt{g * d_o} * t}\right) \quad (5\text{-}25)$$

$$\frac{U}{\sqrt{g * d_o}} = \frac{V_1}{\sqrt{g * d_o}} \quad (5\text{-}26)$$

$$\frac{d_1}{d_o} = \sqrt[3]{6 * \alpha * \frac{\mu}{\rho * \sqrt{g * {d_o}^3}} * \frac{U}{\sqrt{g * d_o}} * \frac{x_s - x_1}{d_o}} \quad (5\text{-}27)$$

The conservation of mass must be further satisfied. The mass of fluid in the wave tip region (i.e. $x_1 \leq x \leq x_s$) equals the mass of fluid in the ideal fluid flow profile for $x_1 \leq x \leq (2*\sqrt{g*d_o}+V_o)*t$:

$$\int_{x_1}^{x_s} \sqrt[3]{6 * \alpha * \frac{\mu * U}{\rho * g} * (x_s - x)} * dx =$$

$$\int_{x_1}^{(2*\sqrt{g*d_o}+V_o)*t} \frac{1}{9 * g} * \left(V_o + 2 * \sqrt{g * d_o} - \frac{x}{t}\right)^2 * dx \quad (5\text{-}28)$$

The above equations may be transformed to express d_1 and x_1 as functions of U:

$$\frac{d_1}{d_o} = \left(1 + \frac{1}{2} * \frac{V_o}{\sqrt{g * d_o}} - \frac{1}{2} * \frac{U}{\sqrt{g * d_o}}\right)^2 \quad (5\text{-}29)$$

$$\frac{x_1}{\sqrt{g * d_o} * t} = \frac{3}{2} * \frac{U}{\sqrt{g * d_o}} - \frac{1}{2} * \frac{V_o}{\sqrt{g * d_o}} - 1 \quad (5\text{-}30)$$

The continuity equation becomes an equation in terms of the wave front location x_s and celerity U :

$$\frac{3}{4} * \sqrt[3]{6 * \alpha * \frac{\mu * U}{\rho * g * {d_o}^2}} * \left(\frac{x_s - x_1}{d_o}\right)^{4/3} = \frac{1}{27} * \sqrt{\frac{g}{d_o}} * t * \left(2 + \frac{V_o}{\sqrt{g * d_o}} - \frac{x_1}{\sqrt{g * d_o} * t}\right)^3 \quad (5\text{-}31)$$

The wave tip region has a parabolic free-surface profile (Eq. (5-7B)). The water depth at point F2 Equation (5-27). Hence the wave tip region length satisfies :

$$\frac{x_S - x_1}{d_o} = \frac{1}{6 * \alpha} * \frac{\rho * \sqrt{g * d_o^3}}{\frac{\mu}{\frac{U}{\sqrt{g * d_o}}}} * \left(1 + \frac{1}{2} * \frac{V_o}{\sqrt{g * d_o}} - \frac{1}{2} * \frac{U}{\sqrt{g*d_o}}\right)^6 \qquad (5\text{-}32)$$

The exact solution in terms of the wave front celerity is :

$$\frac{1}{8 * \alpha} * \frac{\rho * \sqrt{g * d_o^3}}{\mu} * \frac{\left(1 + \frac{1}{2} * \frac{V_o}{\sqrt{g * d_o}} - \frac{1}{2} * \frac{U}{\sqrt{g * d_o}}\right)^5}{\frac{U}{\sqrt{g * d_o}}} = \sqrt{\frac{g}{d_o}} * t \qquad (5\text{-}33)$$

while the wave front location equals:

$$\frac{x_S}{d_o} = \left(\frac{3}{2} * \frac{U}{\sqrt{g * d_o}} - \frac{1}{2} * \frac{V_o}{\sqrt{g * d_o}} - 1\right) * \sqrt{\frac{g}{d_o}} * t + \frac{1}{6 * \alpha} * \frac{\rho * \sqrt{g * d_o^3}}{\frac{\mu}{\frac{U}{\sqrt{g * d_o}}}} * \left(1 + \frac{1}{2} * \frac{V_o}{\sqrt{g*d_o}} - \frac{1}{2} * \frac{U}{\sqrt{g*d_o}}\right)^6 \qquad (5\text{-}34)$$

and the free-surface profile satisfies :

$$\frac{d}{d_o} = 1 \qquad \text{for } \frac{x}{d_o} \le \frac{V_o - \sqrt{g*d_o}}{d_o} * t \qquad (5\text{-}35a)$$

$$\frac{d}{d_o} = \frac{1}{9} * \left(2 + \frac{V_o}{\sqrt{g*d_o}} - \frac{x}{t * \sqrt{g * d_o}}\right)^2$$

$$\text{for } \frac{V_o - \sqrt{g*d_o}}{d_o} * t \le \frac{x}{d_o} \le \left(\frac{3}{2} * \frac{U}{\sqrt{g * d_o}} - \frac{1}{2} * \frac{V_o}{\sqrt{g * d_o}} - 1\right) * \sqrt{\frac{g}{d_o}} * t \qquad (5\text{-}35b)$$

$$\frac{d}{d_o} = \sqrt[3]{6 * \alpha * \frac{\mu}{\rho * \sqrt{g * d_o^3}} * \frac{U}{\sqrt{g * d_o}} * \frac{x_S - x}{d_o}}$$

$$\text{for } \left(\frac{3}{2} * \frac{U}{\sqrt{g * d_o}} - \frac{1}{2} * \frac{V_o}{\sqrt{g * d_o}} - 1\right) * \sqrt{\frac{g}{d_o}} * t \le \frac{x}{d_o} \le \frac{x_S}{d_o} \qquad (5\text{-}35c)$$

$$\frac{d}{d_o} = 0 \qquad \text{for } \frac{x_S}{d_o} \le \frac{x}{d_o} \qquad (5\text{-}35d)$$

The location x_1 of point F2 is deduced from Equations (5-32) and (5-34). Note that the results yield the results obtained in paragraph 5.2 for $V_o = 0$ (i.e. $Fr_o = 0$).

5.4 DETAILED SOLUTION FOR A MILD-SLOPE CHANNEL WITH SOME INITIAL MOTION

Using the same technique developed in Section 4 for turbulent dam break wave, the above problem may be extended to a mild-slope channel. Prior to dam break, it is assumed that the translation of both dam and reservoir is frictionless. After dam break, the flow is assumed to be an ideal fluid flow region behind a friction dominated wave tip region, while the translation of the undisturbed reservoir remains frictionless for $t > 0$. The sudden dam removal takes place at $t = 0$ when the dam wall is located at $x = 0$.

The instantaneous dam break creates a negative wave propagating upstream into a fluid at rest with known water depth. In the (x, t) plane, the initial negative wave characteristic has a slope $dt/dx = -1/(C-V_o)$ with $C = C_o$ for $t = 0$. For a flat slope, the initial backward characteristic propagates upstream with a celerity $(\sqrt{g*d_o}-V_o)$ in first approximation.

Forward characteristics can be drawn issuing from the initial backward characteristic for $t > 0$: In the ideal fluid flow region, the flow properties satisfy :

$$\frac{C}{\sqrt{g * d_o}} = \frac{1}{3} * \left(2 + \frac{V_o}{\sqrt{g * d_o}} + \frac{1}{2} * S_o * \sqrt{\frac{g}{d_o}} * t - \frac{x}{t * \sqrt{g * d_o}} \right)$$

$$\text{for } \frac{V_o}{\sqrt{g * d_o}} - 1 \le \frac{x}{t * \sqrt{g*d_o}} \le \frac{x_1}{t * \sqrt{g*d_o}} \quad (5\text{-}36)$$

$$\frac{V}{\sqrt{g * d_o}} = \frac{2}{3} * \left(1 + \frac{1}{2} * \frac{V_o}{\sqrt{g * d_o}} + S_o * \sqrt{\frac{g}{d_o}} * t + \frac{x}{t * \sqrt{g * d_o}} \right)$$

$$\text{for } \frac{V_o}{\sqrt{g * d_o}} - 1 \le \frac{x}{t * \sqrt{g*d_o}} \le \frac{x_1}{t * \sqrt{g*d_o}} \quad (5\text{-}37)$$

where $S_o = \sin\theta$ and S_o is positive for a downward slope.

In the wave tip region, the flow properties in the wave tip region may be estimated using the diffusion wave equation taking into account flow resistance and bed slope :

$$\frac{\partial d}{\partial x} + \frac{f}{8} * \frac{U^2}{g * d} - S_o = 0 \qquad \text{Wave tip region} \quad (5\text{-}38)$$

where the Darcy friction factor in steady laminar flows equals :

$$f = \frac{64 * \alpha}{Re} \quad (5\text{-}6)$$

with Re being the flow Reynolds number. Equation (5-38) may be solved analytically. A truncated Taylor series of the solution is :

$$\frac{d}{d_o} = \sqrt[3]{6 * \alpha * \frac{\frac{U}{\sqrt{g * d_o}}}{\frac{\rho * \sqrt{g * d_o^3}}{\mu}} * \frac{x_S - x}{d_o}} \qquad \text{Wave front profile} \quad (5\text{-}7B)$$

assuming that Equation (5-6) holds in unsteady flows and for a wide channel, neglecting the effect of the bed slope in the wave tip region, and where x_S is the wave front location.

The free-surface profile and velocity must be continue at point F2. Hence the flow properties at the point F2 (x_1, V_1, d_1) must satisfy :

$$\sqrt{\frac{d_1}{d_o}} = \frac{1}{3} * \left(2 + \frac{V_o}{\sqrt{g * d_o}} + \frac{1}{2} * S_o * \sqrt{\frac{g}{d_o}} * t - \frac{x_1}{t * \sqrt{g * d_o}} \right) \quad (5\text{-}39)$$

$$\frac{V_1}{\sqrt{g * d_o}} = \frac{2}{3} * \left(1 + \frac{1}{2} * \frac{V_o}{\sqrt{g * d_o}} + S_o * \sqrt{\frac{g}{d_o}} * t + \frac{x_1}{t * \sqrt{g * d_o}}\right) \quad (5\text{-}40)$$

$$U = V_1 \quad (5\text{-}41)$$

$$\frac{d_1}{d_o} = \sqrt[3]{6 * \alpha * \frac{\frac{U}{\sqrt{g * d_o}}}{\frac{\rho * \sqrt{g * d_o^3}}{\mu}} * \frac{x_S - x_1}{d_o}} \quad (5\text{-}42)$$

The conservation of mass must be satisfied. The mass of fluid in the wave tip region (i.e. $x_1 \le x \le x_S$) must be equal to the mass of fluid in the wave tip of the ideal fluid flow profile (i.e. for $x_1 \le x \le (2*(\sqrt{g*d_o}+V_o+g*S_o/4*t)*t)$) :

$$\int_{x_1}^{x_S} \sqrt[3]{6 * \alpha * \frac{\mu * U}{\rho * g} * (x_S - x)} * dx =$$

$$\int_{x_1}^{2*(\sqrt{g*d_o} + V_o/2 + g*S_o/4*t)*t} \frac{1}{9 * g} * \left(2 * \sqrt{g * d_o} + V_o + \frac{1}{2} * g * S_o * t - \frac{x}{t}\right)^2 * dx \quad (5\text{-}43)$$

The integration of the continuity equation gives :

$$\frac{3}{4} * \sqrt[3]{6 * \alpha * \frac{\mu * U}{\rho * g * d_o^2}} * \left(\frac{x_S - x_1}{d_o}\right)^{4/3} =$$

$$\frac{1}{27} * \sqrt{\frac{g}{d_o}} t * \left(2 + \frac{V_o}{\sqrt{g * d_o}} + \frac{1}{2} * S_o * \sqrt{\frac{g}{d_o}} * t - \frac{x_1}{\sqrt{g * d_o} * t}\right)^3 \quad (5\text{-}44)$$

Equations (5-39) and (5-40) may be rewritten to express, in dimensionless form, d_1 and x_1 as functions of U :

$$\frac{d_1}{d_o} = \left(1 + \frac{1}{2} * \frac{V_o}{\sqrt{g * d_o}} + \frac{1}{2} * S_o * \sqrt{\frac{g}{d_o}} * t - \frac{1}{2} * \frac{U}{\sqrt{g * d_o}}\right)^2 \quad (5\text{-}39b)$$

$$\frac{x_1}{t * \sqrt{g * d_o}} = \frac{3}{2} * \frac{U}{\sqrt{g * d_o}} - \frac{1}{2} * \frac{V_o}{\sqrt{g * d_o}} - S_o * \sqrt{\frac{g}{d_o}} * t - 1 \quad (5\text{-}40b)$$

The wave tip region has a cubic root free-surface profile. Hence the water depth at point F2 satisfies:

$$\frac{d_1}{d_o} = \sqrt[3]{6 * \alpha * \frac{\frac{U}{\sqrt{g * d_o}}}{\frac{\rho * \sqrt{g * d_o^3}}{\mu}} * \frac{x_S - x_1}{d_o}} \quad (5\text{-}42)$$

and the dimensionless length of the wave tip region is :

$$\frac{x_S - x_1}{d_o} = \frac{1}{6 * \alpha} * \frac{\frac{\rho * \sqrt{g * d_o^3}}{\mu}}{\frac{U}{\sqrt{g * d_o}}} * \left(1 + \frac{1}{2} * \frac{V_o}{\sqrt{g * d_o}} + \frac{1}{2} * \sqrt{\frac{g}{d_o}} * S_o * t - \frac{1}{2} * \frac{U}{\sqrt{g*d_o}}\right)^6 \quad (5\text{-}43)$$

Using Equation (5-40b) and replacing into the continuity equation (Eq. (5-43)), the exact solution of the dam break wave in terms of the wave front celerity is :

$$\frac{1}{8 * \alpha} * \frac{\rho * \sqrt{g * d_o^3}}{\mu} * \frac{\left(1 + \frac{1}{2} * \frac{V_o}{\sqrt{g * d_o}} + \frac{1}{2} * \sqrt{\frac{g}{d_o}} * S_o * t - \frac{1}{2} * \frac{U}{\sqrt{g * d_o}}\right)^5}{\frac{U}{\sqrt{g * d_o}}} = \sqrt{\frac{g}{d_o}} * t \quad (5\text{-}44)$$

while the wave front location equals:

$$\frac{x_S}{d_o} = \left(\frac{3}{2} * \frac{U}{\sqrt{g * d_o}} - \frac{1}{2} * \frac{V_o}{\sqrt{g * d_o}} - \sqrt{\frac{g}{d_o}} * S_o * t - 1\right) * \sqrt{\frac{g}{d_o}} * t + \frac{4}{f} * \frac{1}{\frac{U^2}{g * d_o}} * \left(1 + \frac{1}{2} * \frac{V_o}{\sqrt{g * d_o}} + \frac{1}{2} * \sqrt{\frac{g}{d_o}} * S_o * t - \frac{1}{2} * \frac{U}{\sqrt{g*d_o}}\right)^4 \quad (5\text{-}45)$$

and the free-surface profile is :

$$\frac{d}{d_o} = 1 \qquad \text{for } \frac{x}{t * \sqrt{g*d_o}} \le \frac{V_o}{\sqrt{g * d_o}} - 1 \quad (5\text{-}46a)$$

$$\frac{d}{d_o} = \frac{1}{9} * \left(2 + \frac{V_o}{\sqrt{g * d_o}} + \frac{1}{2} * \sqrt{\frac{g}{d_o}} * S_o * t - \frac{x}{\sqrt{g * d_o} * t}\right)^2 \qquad \text{for } \frac{V_o}{\sqrt{g * d_o}} - 1 \le \frac{x}{t * \sqrt{g*d_o}} \le \frac{x_1}{t * \sqrt{g*d_o}} \quad (5\text{-}46b)$$

$$\frac{d}{d_o} = \sqrt[3]{6 * \alpha * \frac{\frac{U}{\sqrt{g * d_o}}}{\frac{\rho * \sqrt{g * d_o^3}}{\mu}} * \frac{x_S - x}{d_o}} \qquad \text{for } \frac{x_1}{t * \sqrt{g*d_o}} \le \frac{x}{t * \sqrt{g*d_o}} \le \frac{x_S}{t * \sqrt{g*d_o}} \quad (5\text{-}46c)$$

$$\frac{d}{d_o} = 0 \qquad \text{for } \frac{x}{t * \sqrt{g*d_o}} \le \frac{x_S}{t * \sqrt{g*d_o}} \quad (5\text{-}46d)$$

The location of point F2 is given from Equation (5-40b).

Equation (5-44) provides an explicit relationship between the dimensionless wave front celerity $U/\sqrt{g*d_o}$ and dimensionless time $t*\sqrt{g/d_o}$. The solution in terms of the wave front celerity is non-linear with the dimensionless time present on both sides of Equation (5-44). Equation (5-45) yields

the dimensionless wave front location x_s/d_o as a function of the dimensionless wave front celerity $U/\sqrt{g*d_o}$ and dimensionless time $t*\sqrt{g/d_o}$. Equation (5-46) gives the entire dimensionless free-surface profile $d/d_o = F(x/(t*\sqrt{g*d_o}))$.

Discussion

The results are based upon a series of basic approximations. In particular, it is assumed that the wave tip region is primarily affected by bed friction while the ideal-fluid flow motion behind is mostly affected by inertial effects and the gravity force component. Further the development assumes small times t and a flat bed slope. In particular, it implies $C = C_o$ on the initial backward characteristic, and straight backward characteristics in the ideal fluid flow region.

6. NUMERICAL APPLICATIONS

6.1 PRESENTATION

Simple applications of the above developments are presented below for turbulent flow motion. The first one is an instantaneous dam break wave in a narrow, quasi-two-dimensional valley. The second application is a swash zone situation with wave runup on a mild beach slope. The last example is related to a tsunami runup on a flat coastline. In each case, the basic flow conditions are defined. For all investigated conditions, analytical calculations were conducted for both ideal- and real-fluid flows and quantitative results are presented. A comparison between different assumptions (e.g. ideal- versus real-fluid flow) is presented and the results are discussed.

Fig. 6-1 - Example of instantaneous dam break: the St Francis dam, USA (Courtesy of Santa Clarita Valley Historical Society) - Looking upstream at the dam wall ruins

6.2 DAM BREAK APPLICATION

Considering a 65 m high concrete dam (e.g. Fig. 6-1), calculate the dam break wave characteristics for an instantaneous break. Consider all test cases listed in Table 6-1 assuming :

d_o =	65	m	
d_3 =	0	m	Dry bed
	2	m	Initial water depth
V_o =	0	m/s	
S_o =	0		Horizontal
	+0.01		Downward bed slope
f =	0		Frictionless flow
	0.03		Real fluid flow (smooth bed)
	0.1		Real fluid flow (rough bed)

Analytical results are presented in Table 6-2, in terms of the dimensionless dam break wave celerity $U/\sqrt{g*d_o}$, dimensionless wave front celerity U (in m/s) and wave front location x_s (in m) at three different times. For example, the first series result [2.0 / 50 / 326] means : $U/\sqrt{g*d_o}$ = 2.0, U = 50 m/s and x_s = 326 m.

Table 6-1 - Dam break wave application : test cases

Case (1)	Flow conditions (2)	Remarks (3)
Case 1	Ideal fluid flow on dry, horizontal bed	RITTER's solution (paragraph 2.2).
Case 3	Ideal fluid flow over still water (horizontal bed)	Paragraph 3.2.
Case 5	Ideal fluid flow on dry, sloping downward bed	Paragraph 3.4.
Case 6	Real-fluid flow (diffusive wave model) on dry, horizontal bed	Paragraph 4.2.
Case 6a	Smooth downstream channel	
Case 6b	Rough downstream channel	
Case 8	Real-fluid flow (diffusive wave model) on dry, sloping downward bed with initial flow motion	Paragraph 4.4.
Case 8a	Smooth downstream channel	
Case 8b	Rough downstream channel	

Table 6-2 - Dam break wave application : analytical results [$U/\sqrt{g*d_o}$ / U (in m/s) / x_s (in m)]

Case (1)	$t*\sqrt{g/d_o} = 2.5$ t = 6.4 s (2)	$t*\sqrt{g/d_o} = 6.3$ t = 16.1 s (3)	$t*\sqrt{g/d_o} = 25.0$ t = 64.5 s (4)	Remarks (5)
Case 1	2 / 50 / 326	2 / 50 / 814	2 / 50 / 3256	$f = 0$, $S_o = 0$
Case 3	0.2 / 4.9 / 32	0.2 / 4.9 / 79	0.2 / 4.9 / 317	$d_3 = 2$ m, $S_o = 0$
Case 5	2.0 / 51 / 328	2.1 / 52 / 827	2.2 / 57 / 3460	$f = 0$, $S_o = +0.01$
Case 6a	1.28 / 32 / 236	1.11 / 28 / 544	0.84 / 21 / 1833	$f = 0.03$, $S_o = 0$
Case 6b	1.06 / 27 / 210	0.87 / 22 / 472	0.60 / 15 / 1547	$f = 0.1$, $S_o = 0$
Case 8a	1.30 / 33 / 239	1.15 / 29 / 551	0.97 / 24 / 1891	$f = 0.03$, $S_o = +0.01$
Case 8b	1.07 / 27 / 211	0.91 / 23 / 456	0.70 / 18 / 1566	$f = 0.1$, $S_o = +0.01$

Note : Result presentation =$U/\sqrt{g*d_o}$ / U (in m/s) / x_s (in m).

Discussion

Ideal fluid flow calculations (Cases 1, 3 and 5) indicate very-different results in presence of downstream still waters (Cases 3). Such a trend was observed experimentally (e.g. BAZIN 1865b, ESTRADE 1967, CHANSON et al. 2002), and it is caused by the presence of a positive surge at the leading edge of the shock.

Real fluid flow calculations (Cases 6 and 8) demonstrated the strong influence of the bed resistance and the relatively negligible influence of the bed slope (for a mild gradient $S_o = +0.01$) at relatively small times ($t < 65$ s). The results predict that the wave front location at 1 minute after dam break is 1.8 km and 1.55 km downstream of the dam site for Cases 6a and 6b respectively, corresponding to $f = 0.03$ and 0.1.

Cases 8a and 8b are possibly the most realistic situations. They yield a wave front celerity U of about 24 and 18 m/s respectively and a characteristic wave front thickness d_1 of 27 and 39 m respectively at $t = 65$ s.

6.3 SWASH ZONE APPLICATION

The above developments may be applied to the study of sediment motion in the swash zone. For breaking waves on a sloping beach, the resulting swash is somehow similar to a dam break wave running over dry, sloping bed or over retreating waters (Fig. 6-2). Calculate the wave runup

characteristics for an instantaneous dam break considering each test case listed in Table 6-3 and assuming :

d_o =	0.5	m	
d_3 =	0	m	Dry bed
	0.010	m	Initial water depth
V_o =	0	m/s	
	2		
V_3 =	0	m	Still water
	+1	m	Water rundown (retreating water)
S_o =	0		Horizontal
	-0.01		Downward bed slope
f =	0		Frictionless flow
	0.03		Real fluid flow (sand)

The above calculations were applied to the swash zone example, assuming a dam break wave in a rectangular channel, with and without friction, with and without initial downstream water level. Results are presented in Table 6-4 in terms of the dimensionless dam break wave celerity $U/\sqrt{g*d_o}$, dimensionless wave front celerity U (in m/s) and wave front location x_s (in m) at three dimensionless times.

Table 6-3 - Swash zone application : test cases

Case (1)	Flow conditions (2)	Remarks (3)
Case 1	Ideal fluid flow on dry, horizontal bed	RITTER's solution (paragraph 2.2).
Case 2	Ideal fluid flow on dry, frictionless bed with initial flow motion	Paragraph 3.3.
Case 3	Ideal fluid flow over still water (horizontal bed)	Paragraph 3.2.
Case 4a	Ideal fluid flow over still water (horizontal bed) with initial flow motion ($d_3 > 0$, $V_3 = 0$)	Paragraph 3.2.
Case 4b	Ideal fluid flow over still water (horizontal bed) with initial flow motion ($d_3 > 0$, $V_3 > 0$)	Paragraph 3.2.
Case 5	Ideal fluid flow on dry, sloping upward bed	Paragraph 3.4.
Case 6	Real-fluid flow (diffusive wave model) on dry, horizontal bed	Paragraph 4.2.
Case 7	Real-fluid flow (diffusive wave model) on dry, horizontal bed with initial flow motion	Paragraph 4.3.
Case 8	Real-fluid flow (diffusive wave model) on dry, sloping upward bed	Paragraph 4.4.
Case 9	Real-fluid flow (diffusive wave model) on dry, sloping upward bed slope with initial flow motion	Paragraph 4.5.

Discussion

In the ideal fluid flow calculations, the most realistic results are Cases 4a and 4b. Case 4b corresponds to a wave surging on the beach against some water rundown. Although Case 4 (paragraph 3.2) assume a horizontal channel, the results may be relevant for a gentle slope. In Table 6-4, note the strong effect that the presence of downstream water has on the wave front celerity.

Real-fluid flow calculations emphasise the significance of the initial flow conditions. It is expected that Case 9 would be most representative. It predicts that the wave runup would reach 8.5 and 19 m from breaking point in 2 and 5 seconds respectively.

Table 6-4 - Swash zone application : analytical results [$U/\sqrt{g*d_o}$ / U (in m/s) / x_s (in m)]

Case	$t*\sqrt{g/d_o} = 2.2$ t = 0.5 s	$t*\sqrt{g/d_o} = 8.9$ t = 2.0 s	$t*\sqrt{g/d_o} = 22.1$ t = 5.0 s	Remarks
(1)	(2)	(3)	(4)	(5)
Case 1	2 / 4.4 / 2.2	2 / 4.4 / 8.9	2 / 4.4 / 22.1	$f = 0$, $S_o = 0$, $V_o = 0$
Case 2	2.9 / 6.4 / 3.2	2.9 / 6.4 / 12.9	2.9 / 6.4 / 32.1	$f = 0$, $S_o = 0$, $V_o > 0$
Case 3	0.2 / 0.4 / 0.2	0.2 / 0.4 / 0.7	0.2 / 0.4 / 1.8	$f = 0$, $S_o = 0$, $V_o = 0$
Case 4a	0.26 / 0.6 / 0.3	0.26 / 0.6 / 1.1	0.26 / 0.6 / 2.8	$d_3 > 0$, $V_o > 0$, $V_3 = 0$
Case 4b	0.24 / 0.5 / 0.3	0.24 / 0.5 / 1.1	0.24 / 0.5 / 2.7	$d_3 > 0$, $V_o > 0$, $V_3 > 0$
Case 5	2.0 / 4.4 / 2.2	1.9 / 4.2 / 8.7	1.8 / 3.9 / 20.9	$f = 0$, $S_o = -0.01$, $V_o = 0$
Case 6	1.30 / 2.9 / 1.6	1.05 / 2.3 / 5.7	0.86 / 1.9 / 12.7	$f = 0.03$, $S_o = 0$, $V_o = 0$
Case 7	2.2 / 1.98 / 4.4	1.62 / 3.6 / 8.6	1.36 / 3.0 / 19.3	$f = 0.03$, $S_o = 0$, $V_o > 0$
Case 8	1.29 / 2.8 / 1.6	0.99 / 2.2 / 5.6	0.74 / 1.6 / 12.3	$f = 0.03$, $S_o = -0.01$, $V_o = 0$
Case 9	1.97 / 4.4 / 2.4	1.57 / 3.5 / 8.5	1.23 / 2.7 / 18.9	$f = 0.03$, $S_o = -0.01$, $V_o > 0$

Note : Result presentation =$U/\sqrt{g*d_o}$ / U (in m/s) / x_s (in m).

Fig. 6-2 - Swash zone processes on the Enshu coast of Japan
(A) Wave breaking and swash zone at Terasawa beach (Japan) on 23 Nov. 2001 around 12:00 noon (high tide)

(B) Wave runup at Terasawa beach (Japan) on 23 Nov. 2001 around 12:00 noon (high tide) - Same location at Fig. 6-2A - The surfer use a flatboard to "surf" the surging waters

6.4 TSUNAMI RUNUP APPLICATION

6.4.1 Introduction

A tsunami wave is a long-period wave generated by ocean bottom motion during an earthquake typically. The wave length is typically about 200 to 350 km and the tsunami behaves as a shallow water wave, even in deep sea. The main characteristics ([1]) of a tsunami wave are :

Wave celerity

$$C = \sqrt{\frac{g * l}{2 * \pi} * \tanh\left(\frac{2 * \pi * d}{l}\right)} \approx \sqrt{g * d} \quad \text{m/s}$$

Wave group celerity

$$C_g = \frac{C}{2} * \left(1 + \frac{4*\pi*\frac{d}{l}}{\sinh\left(4*\pi*\frac{d}{l}\right)} \right) \approx C \quad \text{m/s}$$

Wave energy spectral density

$$E = \frac{1}{2} * \rho * g * a^2 \quad \text{J/m}^2$$

Average energy flux

$$W = E * C_g = \frac{1}{4} * \rho * g * C * a^2 * \left(1 + \frac{4*\pi*\frac{d}{l}}{\sinh\left(4*\pi*\frac{d}{l}\right)} \right) \quad \text{J/m/s}$$

Momentum per unit area

$$\phi = \frac{E}{C} \approx \frac{1}{2} * \rho * \sqrt{g} * \frac{a^2}{\sqrt{d}} \quad \text{Pa.s}$$

Average momentum flux

$$\phi_F = \phi * C_g = \frac{1}{4} * \rho * g * a^2 * \left(1 + \frac{4*\pi*\frac{d}{l}}{\sinh\left(4*\pi*\frac{d}{l}\right)} \right) \quad \text{N/m}$$

[1]This paragraph is based upon CHANSON et al. (2000).

where a is the wave amplitude, d is the still water depth, l is the wave length, ρ is the water density, g is the gravity acceleration, and sinh and tanh are the hyperbolic sine and tangent functions respectively. Note that, for long-period waves, the wave group celerity, average energy flux and average momentum flux may be simplified since:

$$\left(1 + \frac{4 * \pi * \frac{d}{l}}{\sinh\left(4 * \pi * \frac{d}{l}\right)} \right) \approx 2 \qquad (6\text{-}1)$$

Although the wave amplitude is moderate in the middle of the ocean (e.g. 0.2 to 1 m), the tsunami wave speed decreases near the shoreline with decreasing water depths. For a constant energy flux, the wave height increases accordingly until wave breaking occurs ([2]). The arrival of a tsunami wave at the shore may be characterised either by a very-slow rise in water level or by a surging bore. In the former situation no wave breaking take place and the horizontal runup is a slow and gradual flooding of the land. In the latter case, wave breaking may occur before the tsunami reaches the coastline and the wave front becomes a turbulent surge (e.g. Fig. 6-3).

Several researchers developed an analogy between the wave breaking process of long-period waves, including tsunami waves, and solitary waves (e.g. SYNOLAKIS 1987, MONTES 1998 ([3])). Theoretical calculations suggest that solitary waves break for $H_{max}/d = 0.8$ to 0.85 while experimental observations give $H_{max}/d > 0.75$ where H_{max} is the maximum wave height at breaking ([4]) and d is the still water depth.

Considering a tsunami wave surging over the shoreline, the initial velocity head of the surging waters may be approximated as:

$$\frac{V_o^2}{2 * g} \approx \frac{H_{max}}{2} + \frac{C^2}{2 * g} \qquad (6\text{-}2)$$

where C is the velocity of the solitary wave. Assuming a constant energy flux, the wave height H_{max} must satisfies approximately :

$$\frac{1}{4} * \rho * g * C * H_{max}^2 = \frac{1}{4} * \rho * g * C_{dw} * a_{dw}^2 \qquad (6\text{-}3)$$

where C_{dw} and a_{dw} are the deep-water wave celerity and wave amplitude respectively, and assuming that the wave group velocity equals the solitary wave velocity. MONTES (1998, pp. 461-462) reviewed experimental data and computational results which are altogether best correlated by:

$$\frac{C}{\sqrt{g*d}} = 0.9983 * \left(1 + \frac{H_{max}}{d}\right)^{0.4688} \qquad (6\text{-}4)$$

where d is the still water depth and H_{max} is the solitary wave height at breaking measured above still water level. A solitary wave is characterised by a net transport of water in the wave direction. The momentum flux per meter width of the surging wave is about :

$$\rho * q * V_o \approx \rho * V * C * H_{max} \qquad \text{momentum flux per meter width} \quad (6\text{-}5)$$

---

[2]For short oscillatory waves (i.e. deep water waves), breaking takes place for $H_{max}/d = 0.35$ to 0.4 or $H_{max}/l > 1/24$ to 1/14 where H_{max} is the maximum wave height, d is the water depth and l is the wave length (PONDS and PICKARD 1983).

[3]"*Solitary waves are believed to model some important aspects of the coastal effects of tsunamis well.*" (SYNOLAKIS 1987, p. 523). "*Most oscillatory waves take the characteristics of solitary waves when shoaling.* [...] *As the* [wave] *period increased, the solitary wave analogy was approached*" (MONTES 1998, p. 463).

[4]being measured above the still water level for a solitary wave.

while the initial surging water depth d_o above the mean still water level may be derived from continuity :

$$V_o * d_o = H_{max} * C \qquad (6\text{-}6)$$

6.4.2 Application

Considering a tsunami wave (0.25 m high) generated in deep water (4,000 m), solitary wave calculations indicate that the wave breaking occurs near the shore for a water depth d = 6.25 m, with a maximum wave height of 4.4 m and a wave celerity at breaking C = 7.8 m/s. Calculate the surge runup characteristics on the coastline for several cases (Table 6-5) assuming :

d_o =	6.25	m	
d_3 =	0	m	Dry bed
	0.5	m	Initial water depth
V_o =	0	m/s	
	7.8		
S_o =	0		Horizontal
	-0.01		Upward bed slope
f =	0		Frictionless
	0.05		Real fluid flow

Analytical results are presented in Table 6-6, in terms of the dimensionless dam break wave celerity $U/\sqrt{g*d_o}$, dimensionless wave front celerity U (in m/s) and wave front location x_s (in m) for three times.

Table 6-5 - Tsunami runup application : test cases

Case (1)	Flow conditions (2)	Remarks (3)
Case 1	Ideal fluid flow on dry, horizontal bed	RITTER's solution (paragraph 2.2).
Case 2	Ideal fluid flow on dry, frictionless bed with initial flow motion	Paragraph 3.3.
Case 3	Ideal fluid flow over still water (horizontal bed)	Paragraph 3.2.
Case 4	Ideal fluid flow over still water (horizontal bed) with initial flow motion	Paragraph 3.2.
Case 5	Ideal fluid flow on dry, sloping upward bed	Paragraph 3.4.
Case 6	Real-fluid flow (diffusive wave model) on dry, horizontal bed	Paragraph 4.2.
Case 7	Real-fluid flow (diffusive wave model) on dry, horizontal bed with initial flow motion	Paragraph 4.3.
Case 8	Real-fluid flow (diffusive wave model) on dry, sloping upward bed slope	Paragraph 4.4.
Case 9	Real-fluid flow (diffusive wave model) on dry, sloping upward bed slope with initial flow motion	Paragraph 4.5.

Table 6-6 - Tsunami runup application : analytical results [$U/\sqrt{g*d_o}$ / U (in m/s) / x_s (in m)]

Case	$t*\sqrt{g/d_o}$ = 2.5 t = 2.0 s	$t*\sqrt{g/d_o}$ = 12.5 t = 10.0 s	$t*\sqrt{g/d_o}$ = 25.0 t = 20.0 s	Remarks
(1)	(2)	(3)	(4)	(5)
Case 1	2.1 / 15.7 / 31.3	2.0 / 15.7 / 156	2.0 / 15.7 / 313	
Case 2	3.0 / 23.5 / 47	3.0 / 23.5 / 234	3.0 / 23.5 / 469	
Case 3	0.3 / 2.2 / 4.5	0.3 / 2.2 / 22.4	0.3 / 2.2 / 45	Small bore height: d_2-d_3 = 0.01 m.
Case 4	0.5 / 3.6 / 7.3	0.5 / 3.6 / 36.3	0.5 / 3.6 / 72	Bore height: d_2-d_3 = 0.44 m. Undular bore.
Case 5	2.0 / 15.5 / 31	1.9 / 14.7 / 152	1.7 / 13.7 / 293	Maximum runup : ~ 200 m. Maximum height: ~ 12 m
Case 6	1.19 / 9.3 / 21.8	0.92 / 7.2 / 80	0.73 / 5.8 / 164	
Case 7	1.89 / 15 / 34	1.5 / 11.7 / 129	1.22 / 9.6 / 260	
Case 8	1.17 / 9.2 / 22	0.85 / 6.6 / 79	0.62 / 4.9 / 161	
Case 9	1.9 / 15 / 33	1.42 / 11.1 / 128	1.1 / 8.6 / 255	

Note : Result presentation =$U/\sqrt{g*d_o}$ / U (in m/s) / x_s (in m).

Discussion

First ideal fluid flow calculations (Cases 1 to 5) yield different results when the coastline is covered by a layer of still water (Cases 3 and 4) (see paragraph 6.4.4). This was observed experimentally by several researchers (e.g. BAZIN 1865b, ESTRADE 1967, CHANSON et al. 2002). For a dry coastline, the results show a major influence of the initial translation velocity of the reservoir V_o.

Real fluid flow calculations (Cases 6 to 9) demonstrate the strong effect of bed resistance on wave propagation, even for short times t, in all situations. For example, Cases 1 and 5 (V_o = 0, S_o = 0), Cases 2 and 6 (V_o = 7.8 m/s, S_o = 0) and Cases 5 and 8 (V_o = 0, S_o = -0.01). Although the effects of bed slope are ignored in Cases 4 and 7, the calculations showed that these are relatively negligible for small to moderate times t.

Overall, Case 9 is possibly the most realistic test case for a tsunami wave runup on a flat, dry coastline as illustrated in Figure 6-3, while Case 4 could be most representative of a tsunami wave runup in shallow waters (see paragraph 6.4.4). Present results (Case 9) yield a wave front celerity U = 11 m/s and a wave front location x_s = 130 m at about 10 seconds after the "instantaneous dam break" on dry land. These results, in terms of both wave front location and celerity, are comparable with video observations of tsunami runup at Patong Beach, Phuket Island on 26 Dec. 2004 (e.g. Fig. 6-3B). Figure 6-3B shows a video-frame taken about 10 seconds after tsunami wave breaking. Figure 6-3B is a single-frame from a video taken on 26 December 2004 at Patong Beach, Phuket (Thailand). Figure 6-3C shows a still photograph from about the same observation point, looking at the devastation one or two days later.

In presence of still water (Case 4), for comparison, the positive surge celerity is only (!) 3.6 m/s, but a positive surge is a self-perpetuating process that can travel very-long distances, provided that the channel (i.e. coastline) shape does not change (e.g. HENDERSON 1966, CHANSON 2004a).

Note that the calculations are highly dependent upon the initial flow conditions. These were deduced from a few key assumptions.

Figure 6-3 - Images of tsunami wave runup on 26 December 2004 in Thailand
(A) Tsunami wave breaking before runup (Channel 9 TV News, Australia on 01/01/05 at 18:00) - View from a 2nd or 3rd floor, looking down at the 6-m high breaking wave coming straight at the building

(B) Tsunami wave runup on dry land about 9-10 seconds after wave breaking at Patong Beach (ABC TV News, Australia on 27/12/05 at 19:00) - View from a building balcony, looking down at the wave runup (flow from right to left) - The wave front leading edge is highlighted by its 'white waters'

(C) View from the sun terrace of the Novotel, Patong Beach (Courtesy of Phil BLISS) - Photograph taken after the tsunami disaster

6.4.3 Tsunami surge front

After wave breaking in shallow waters, the tsunami waters may surge on dry or inundated coastal plains, in a manner somehow similar to a dam break wave. Such tsunami surges were witnessed in Indonesia (Western Aceh, Banda Aceh) and Thailand (Khao Lak, Patong) on 26 Dec. 2004 (Fig. 6-4 and App. A) (CHANSON 2005). Figure 6-4 shows an advancing surge front in a street of Banda Aceh. While the exact location is unknown, it is believed to be about 1.5 to 3 km inland. In the 100 m long street stretch, the surge advanced with an average celerity U of about 1.5 to 1.6 m/s. However the advance was neither two-dimensional nor smooth. The surge appeared to progress section by section, in a somewhat disorganised manner. Although this behaviour might be induced by flow turbulence, it might also be related to the fluid rheology.

The time variations of water depth were estimated at four different locations of the street,. The data are shown in Figure 6-5 with the (bottom) horizontal axis being a time being measured from when the surge front reached the location, and the (left) vertical axis is the flow depth in metres. The data were compared with the present theoretical development for a horizontal channel. Assuming a 1 m high tsunami wave generated in deep water (1,000 m depth), solitary wave calculations predict wave breaking near the shore with a maximum wave height of 10.5 m and a wave celerity at breaking of V_o = 12 m/s (SYNOLAKIS 1997, MONTES 1988, CHANSON et al. 2000).

Dam break wave calculations were conducted for comparable conditions, assuming d_o = 10.5 m, V_o = 0 and 12 m/s, x = 2 km, and a flow resistance coefficient f = 0.5. Note that, for a reservoir height d_o = 10. 5 m, corresponding to the maximum wave height, the calculations yield a water depth at the end of the process of $4/9*d_o$ = 4.7 m that is close to maximum flooding heights in Banda Aceh (TSUJI 2005; BORRERO 2005, *Person. Comm.*, CHANSON 2005). Four cases were considered: ideal- and real-flows, with and without initial motion. The predictive results are summarised in Table 6-7.

Real fluid flow calculations highlighted the strong effect of bed resistance on wave propagation. The quantitative results in terms of surge front celerity were comparable with observations for the surge shown in Figure 6-4 and 6-5. Field observations were further compared with Equations (4-15) to (4-18) for the above conditions (d_o = 10.5 m, x = 2000 m). Results are presented in Figure 6-5 for the case $V_o = 0$, as d/d_o versus $x/(t*\sqrt{g*d_o})$. Both calculations (dotted line) and observed data (grey triangles) are presented in dimensionless terms corresponding to the top horizontal and right vertical axes. Figure 6-5 shows a surprisingly good agreement between data and theory in terms of the wave front shape. Despite simplistic approximations, the calculations are based upon physically-based principles, and the resulting method provides a simple tool to predict rapidly tsunami surge in emergency situations.

Fig. 6-4 - Advancing mud and debris surge in Banda Aceh (26 December 2004 tsunami) - Looking upstream for four different times: (A) t = 8.48 s (B) t = 13.12 s (C) t = 16.0 s (D) t = 39.0 s

Table 6-7 - Tsunami surge application: analytical results at x = 2000 m for d_o =10.5 m (V_o = 0 & 12 m/s), S_o = 0 - Comparison between ideal- and real-fluid flow calculations

Flow property at x = 2000 m d_o =10.5 m, S_o = 0 (1)	Case A Ideal fluid V_o = 0 (2)	Case B Ideal fluid V_o = 12 m/s (3)	Case C Real fluid V_o = 0 (4)	Case D Real fluid V_o = 12 m/s (5)
Surge arrival time since breaking (s) =	99	62	340	200
U (m/s) =	20.3	32.3	1.2	2.9

Fig. 6-5 - Time-variations of the water depth for the surge shown in Figure 6-4 (Banda Aceh, 26 Dec. 2004) and dimensionless comparison with Equation (4-17)

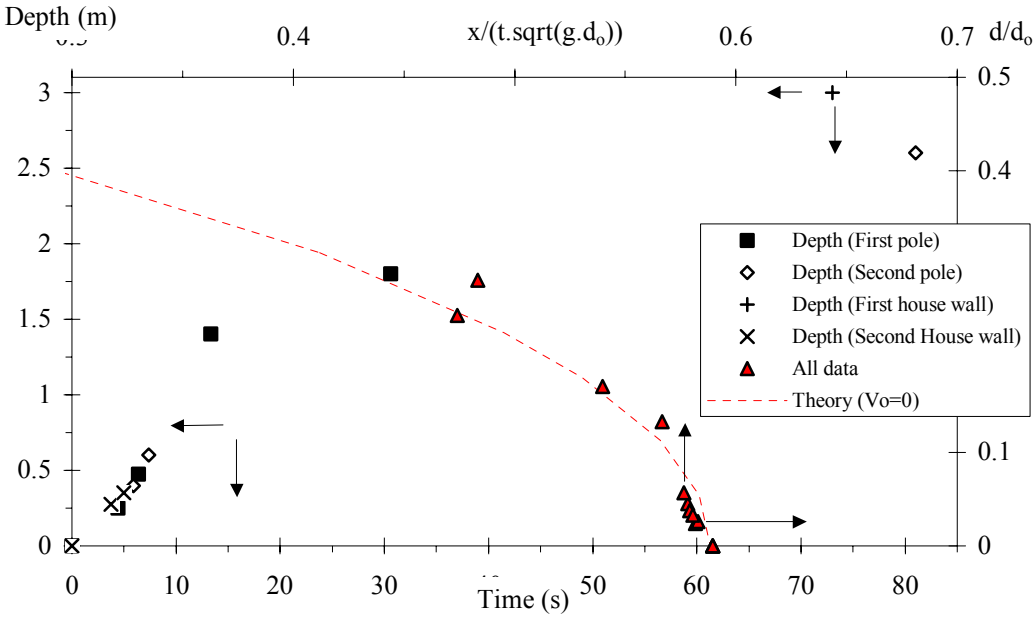

6.4.4 Discussion

After breaking, a tsunami surge propagating in shallow-water regions is led by a positive surge. In shallow rivers, the process is somehow similar to a tidal bore and the bore may propagate far upstream. A tsunami-induced river bore was observed in Hawaii in 1946, in Japan in 1983 and 2003, and in 2005 in Thailand, Malaysia and Sri Lanka (SHUTO 1985, YEH 1991, CHANSON 2005) (Fig. 6-6). Figure 6-6 shows an aerial view of an undular bore, induced by the 2003 Tokachi-oki tsunami, propagating upstream in a Japanese river.

In rivers and shallow-water bays, the propagation of the positive surge is associated with sediment scour, strong mixing and suspended sediment advection upstream. These features are well-known to tidal bore processes (e.g. DONNELLY and CHANSON 2002).

Although the above approach is very simplistic and relies upon basic assumptions, it is derived from basic principles and physically-based equations that were successfully validated with a wide range of physical data in large size facilities. The resulting set of equations provides a simple tool to predict tsunami surge and dam break wave propagation. Such calculations can be performed in real-time and provides very rapid information that may be vital in emergency situations.

Figure 6-6 -Tsunami-induced bore during the 2003 Tokachi-oki tsunami in Japan (Courtesy of Professor SHUTO, with assistance of Prof. Kenji SATAKE) - Bore propagation from top right to bottom left - The bore propagates upstream toward the bridge

7. SUMMARY AND CONCLUSION

Most dams and reservoirs are designed for an optimum use at the most economical cost. A safety analysis must be conducted, and the optimum design is the one that minimises the real total cost : i.e. the cost of construction + maintenance cost + cost of safety. The cost of a failure is not always measurable : damage to properties is assessable, damage to the environment is real and has often a political value, but the loss of life is a matter of suffering. It is a human tragedy that has a very strong political impact, in particular in developed countries. In the past, a significant number of dams failed (e.g Fig. 7-1).

The present work is focused on simple solutions of dam break wave problems using the Saint-Venant equations and the method of characteristics for both laminar and turbulent flow motion. Analytical solutions are developed for an instantaneous dam break with a semi-infinite reservoir in a wide rectangular channel. After a review of well-known solutions, some simple ideal-fluid flow solutions are detailed. These include ideal dam break wave flow on horizontal and sloping channels, with or without initial flow motion. The effect of the presence of water in the downstream channel is discussed. This type of ideal dam break wave solutions is typically taught in advanced undergraduate subjects (e.g. HENDERSON 1966, CHANSON 2004).

Section 4 presents new analytical solutions of dam break wave of real fluids with turbulent flow motion. It encompasses dam break wave in horizontal channels with bed friction, dam break wave with initial flow motion, and dam break waves in flat-slope channels. In the theoretical developments, the dam break wave flow is analysed as a wave tip region where flow resistance is dominant, followed by an ideal-fluid flow region where inertial effects and gravity effects are dominant. The analytical results were validated by successful comparisons between several experimental data sets obtained in large-size facilities (App. B) and theoretical results, in terms of instantaneous free-surface profiles, wave front location and wave front celerity. The former comparison with instantaneous free-surface data is considered to be the most accurate technique to estimate the flow resistance and the best validation technique. Section 5 presents new analytical solutions of dam break wave with laminar flow motion. The dam break wave flow is analysed as a wave tip region where viscous flow resistance is dominant, followed by an ideal-fluid flow region where inertial effects and gravity effects are dominant. The analytical results were validated qualitatively by comparisons between experimental and theoretical results.

In the last section, the analytical results are applied to three flow situations: a dam break, the swash zone, and a tsunami runup. Detailed comparison was conducted between ideal- and real-fluid flow calculations. It was shown that the theoretical results may be applied successfully to a wider range of applications that the simple dam break problem.

It is the writer's strong opinion that the present developments provide several main advantages over existing methods. First the theoretical results for real-fluid flows yield simple explicit analytical expressions that compare well with experimental data and more advanced theoretical solutions. Second the proposed development is a simple pedagogical application of the Saint-Venant equations and method of characteristics, linking together the simple wave equations yielding RITTER's solution, with a diffusive wave equation for the wave tip region. Third, these explicit analytical solutions provide simple tools to validate numerical solutions of the method of characteristics applied to the dam break wave problem. Fourth the development were applied to a wide range of flow situations, and includes the effects of bed slope and initial flow motion. This yields to a wide range of practical applications (e.g. Section 6). Fifth the simplicity of the equations may allow the extension of the method to more complex fluids (e.g. non-Newtonian fluids). CHANSON et al. (2004) proved the concept by applying successfully the mathematical treatment of HUNT (1982,1984) to dam break wave of non-Newtonian thixotropic fluids.

However it is acknowledged that the present approach is limited to semi-infinite reservoir, rectangular channel and quasi-instantaneous dam break. The latter approximation is often reasonable for concrete dam failure (e.g. Fig. 6-1) and plunging breaking waves, but it is not

applicable to many other applications including embankment breach (e.g. COLEMAN et al. 2002, CHANSON 2004b,e).

Fig. 7-1 - Examples of instantaneous dam break catastrophes
(A) St Francis dam, USA (Courtesy of Santa Clarita Valley Historical Society) - Large wall section lying just at the foot and downstream of the remnant monolith (Fig. 1-1A) - Looking from the right bank - Note people examining the wreckage on the bottom right of the photograph

(B) Malpasset dam in the late 1990s, looking from the top of the dam on the right abutment (Courtesy of Didier TOULOUZE) - More than 300 people died in the catastrophe

ACKNOWLEDGMENTS

The writer thank Dr A. HOGG (University of Bristol) and Dr T. BALDOCK (University of Queensland) for their review of the report and valuable comments. He further acknowledge valuable discussions with Dr Andrew HOGG, as well as with others. He acknowledges the assistance of many people who provided him with valuable, relevant informations.

REFERENCES

AGUIRRE-PE, J., PLACHCO, F.P., and QUISCA, S. (1995). "Tests and Numerical One-Dimensional Modelling of a High-Viscosity Fluid Dam-Break Wave." *Jl of Hyd. Res.*, IAHR, Vol. 33, No. 1, pp. 17-26.

BARRÉ de SAINT-VENANT, A.J.C. (1871a). "Théorie et Equations Générales du Mouvement Non Permanent des Eaux Courantes." *Comptes Rendus des séances de l'Académie des Sciences*, Paris, France, Séance 17 July 1871, Vol. 73, pp. 147-154 (in French).

BARRÉ de SAINT-VENANT, A.J.C. (1871b). "Théorie du Mouvement Non Permanent des Eaux, avec Application aux Crues de Rivières et à l'Introduction des Marées dans leur Lit." *Comptes Rendus des séances de l'Académie des Sciences*, Paris, France, Vol. 73, No. 4, pp. 237-240 (in French).

BASCOM, W. (1980). "Waves and Beaches. The Dynamics of the Ocean Surface." *Anchor Press*, New York, USA, revised edition, 366 pages.

BAZIN, H. (1865a). "Recherches Expérimentales sur l'Ecoulement de l'Eau dans les Canaux Découverts." ('Experimental Research on Water Flow in Open Channels.') *Mémoires présentés par divers savants à l'Académie des Sciences*, Paris, France, Vol. 19, pp. 1-494 (in French).

BAZIN, H. (1865b). "Recherches Expérimentales sur la Propagation des Ondes." ('Experimental Research on Wave Propagation.') *Mémoires présentés par divers savants à l'Académie des Sciences*, Paris, France, Vol. 19, pp. 495-644 (in French).

BRYANT, E. (1991). "Natural Hazards." *Cambridge University Press*, Cambridge, UK, 294 pages.

BUTCHER, G.W., BEETHAM, R.D., MILLAR, P.J., and TANAKA, H. (1994). "The Hokkaido-Nansei-Oki Earthquake. Final Report of the NZNSEE Reconnaissance Team." *Bulletin of the New Zealand Society for Earthquake Engineering*, Vol. 27, No. 1, p. 2.

CAVAILLE, Y. (1965). "Contribution à l'Etude de l'Ecoulement Variable Accompagnant la Vidange Brusque d'une Retenue." ('Contribution to the Study of Unsteady Flow Following a Dam Break.') *Publ. Scient. et Techn. du Ministère de l'Air*, No. 410, Paris, France, 165 pages (in French).

CHANSON, H. (2004a). "The Hydraulics of Open Channel Flows : An Introduction." *Butterworth-Heinemann*, Oxford, UK, 2nd edition, 630 pages (ISBN 0 7506 5978 5). {http://www.uq.edu.au/~e2hchans/reprints/book3_2.htm}

CHANSON, H. (2004b). "Environmental Hydraulics of Open Channel Flows." *Elsevier Butterworth-Heinemann*, Oxford, UK, 483 pages (ISBN 0 7506 6165 8). {http://www.uq.edu.au/~e2hchans/reprints/book7.htm}

CHANSON, H. (2004c). "Unsteady Air-Water Flow Measurements in Sudden Open Channel Flows." *Experiments in Fluids*, Vol. 37, No. 6, pp. 899-909 (ISSN 0723-4864). {http://www.uq.edu.au/~e2hchans/reprints/expfl_04.pdf}

CHANSON, H. (2004d). "Dam Break Wave Propagation on Abrupt Drops: an Experimental Study." *Proc. 15th Australasian Fluid Mech. Conf.*, AFMC, Sydney, Australia, M. BEHNIA, W. LIN & G.D. McBAIN Ed., Paper AFMC00014, 4 pages (CD-ROM) (ISBN 1-864-87695-6). {http://www.uq.edu.au/~e2hchans/reprints/afmc0014.pdf}

CHANSON, H. (2004e). "Overtopping Breaching of Noncohesive Homogeneous Embankments. Discussion." *Jl of Hyd. Engrg.*, ASCE, Vol. 130, No. 4, pp. 371-374 (ISSN 0733-9429). {http://www.uq.edu.au/~e2hchans/reprints/dis_col.pdf}

CHANSON, H. (2005). "Le Tsunami du 26 Décembre 2004: un Phénomène Hydraulique d'Ampleur Internationale. Premier Constats." ('The 26 December 2004 Tsunami: a Hydraulic Engineering Phenomenon of International Significance. First Comments') *Jl La Houille Blanche*, No. 2, pp. 25-32 (ISSN 0018-6368) (in French).

CHANSON, H., AOKI, S., and MARUYAMA, M. (2000). "Experimental Investigations of Wave Runup Downstream of Nappe Impact. Applications to Flood Wave Resulting from Dam Overtopping and Tsunami Wave Runup." *Coastal/Ocean Engineering Report*, No. COE00-2, Dept. of Architecture and Civil Eng., Toyohashi University of Technology, Japan, 38 pages.

CHANSON, H., AOKI, S., and MARUYAMA, M. (2002). "An Experimental Study of Tsunami Runup on Dry and Wet Horizontal Coastlines." *International Journal of the Tsunami Society*, Science of Tsunami Hazards., Vol. 20, No. 5, pp. 278-293 (ISSN 8755-6839). {http://www.uq.edu.au/~e2hchans/reprints/sth_02.pdf}

CHANSON, H., COUSSOT, P., JARNY, S., and TOQUER, L. (2004). "A Study of Dam Break Wave of Thixotropic Fluid: Bentonite Surges down an Inclined Plane." *Report No. CH54/04*, Dept. of Civil Engineering, The University of Queensland, Brisbane, Australia, June, 90 pages (ISBN 1864997710). {http://www.uq.edu.au/~e2hchans/reprints/ch5404.zip}

CLAGUE, J.J., and BOBROWSKY, P.T. (1999). "The Geological Signature of Great Earthquakes off Canada's West Coat." *Geoscience Canada*, Vol. 26, No. 1, pp. 1-15.

COLEMAN, S.E., ANDREWS, D.P., WEBBY, M.G. (2002). "Overtopping Breaching of Noncohesive Homogeneous Embankments." *Jl of Hyd. Engrg.*, ASCE, Vol. 128, No. 9, pp. 829-838. Discusion: 2004, Vol. 130, No. 4, pp. 371-374. Closure: 2004, Vol. 130, No. 4, pp. 374-376.

COMOLET, R. (1976) "Mécanique Expérimentale des Fluides." ('Experimental Fluid Mechanics') *Masson editor*, Paris, France. (in French)

CUNGE, J.A. (1975). "Numerical Methods of Solution of the Unsteady Flow Equations." in "Unsteady Flow in Open Channels." *WRP Publ.*, Fort Collins, USA, K. MAHMOOD and V. YEVDJEVICH Ed., Vol. 2, pp. 539-586.

CUNGE, J.A., HOLLY Jr, F.M., and VERWEY, A. (1980). "Practical Aspects of Computational River Hydraulics." *Pitman*, Boston, USA, 420 pages.

DARCY, H.P.G., and BAZIN, H. (1865). "Recherches Hydrauliques." ('Hydraulic Research.') *Imprimerie Impériales*, Paris, France, Parties 1ère et 2ème (in French).

DAVIES, T.R.H. (1988). "Debris Flow Surges - A Laboratory Investigation." *Mitteilungen der Versuchsanstalt fur Wasserbau, Hydrologie und Glaziologie*, No. 96, ETH-Zurich, Switzerland, 122 pages.

DEBIANE, K. (2000). "Hydraulique des Ecoulements Laminaires à Surface Libre dans une Canal pour des Milieux Visqueux ou Viscoplastiques: Régimes Uniformes, Graduellement Varié, et Rupture de Barrage." ('Hydraulics of Laminar Free-Surface Flow in Channel for Viscous or Viscoplastic Models: Uniform Regime, Gradually-Varied Flow, and Dam-Break Problem.') *Ph.D. thesis*, University of Grenoble I, Rheology Laboratory INPG-UJF-CNRS, France, 273 pages (in French).

DONNELLY, C., and CHANSON, H. (2002). "Environmental impact of a Tidal Bore on Tropical Rivers." *Proc. 5th Intl River Management Symp.*, Brisbane, Australia, Sept., 3-6, 9 pages (PDF file http://www.uq.edu.au/~e2hchans/reprints/riv02_1.pdf).

DRESSLER, R.F. (1952). "Hydraulic Resistance Effect upon the Dam-Break Functions." *Jl of Research, Natl. Bureau of Standards*, Vol. 49, No. 3, pp. 217-225.

DRESSLER, R. (1954). "Comparison of Theories and Experiments for the Hydraulic Dam-Break Wave." *Proc. Intl Assoc. of Scientific Hydrology Assemblée Générale*, Rome, Italy, Vol. 3, No. 38, pp. 319-328.

ESCANDE, L., NOUGARO, J., CASTEX, L., and BARTHET, H. (1961). "Influence de Quelques Paramètres sur une Onde de Crue Subite à l'Aval d'un Barrage." ('The Influence of certain Parameters on a Sudden Flood Wave Downstream from a Dam.') *Jl La Houille Blanche*, No. 5, pp. 565-575.

ESTRADE, J. (1967). "Contribution à l'Etude de la Suppression d'un Barrage. Phase Initiale de l'Ecoulement." ('Contribution to the Study of Dam Break. Initial Stages of the Wave.') *Bulletin de la Direction des Etudes et Recherches*, Series A, Nucléaire, Hydraulique et Thermique, EDF Chatou, France, No. 1, pp. 3-128.

ESTRADE, J., and MARTINOT-LAGARDE, A. (1964). "Ecoulement Consécutif à la Suppression d'un Barrage dans un Canal Horizontal de Section Rectangulaire." ('Dam Break Wave Flow in a Horizontal Rectangular Canal.') *Comptes-Rendus de l'Académie des Sciences de Paris*, Vol. 259, 21 December, Group 2, pp. 4502-4505.

FAURE, J., and NAHAS, N. (1961). "Etude Numérique et Expérimentale d'Intumescences à Forte Courbure du Front." ('A Numerical and Experimental Study of Steep-Fronted Solitary Waves.') *Jl La Houille Blanche*, No. 5, pp. 576-586. Discussion: No. 5, p. 587.

FUJIMA, K., and SHUTO, N. (1990). "Formulation of Frictions Laws for Long Waves on a Smooth Dry Bed." *Coastal Engineering in Japan*, Vol. 33, No. 1, pp. 25-47.

HEBENSTREIT, G. (1997). "Perspectives on Tsunami Hazard Reduction. Observations, Theory and Planning." *Kluwer Academic*, Dordrecht, the Netherlands, 218 pages. (also *Proc. 17th Intl Tsunami Symp.*, AGU, Boulder CO, USA, July 1995.)

HECK, N.H. (1936). "Earthquakes." *Princeton University Press*.

HENDERSON, F.M. (1966). "Open Channel Flow." *MacMillan Company*, New York, USA.

HOGG, A.J., and PRITCHARD, D. (2004). "The Effects of Hydraulic Resistance on Dam-break and Other Shallow Inertial Flows." *Jl Fluid Mech.*, Vol. 501, pp. 179-212.

HUNT, B. (1982). "Asymptotic Solution for Dam-Break Problems." *Jl of Hyd. Div.*, Proceedings, ASCE, Vol. 108, No. HY1, pp. 115-126.

HUNT, B. (1984). "Perturbation Solution for Dam Break Floods." *Jl of Hyd. Engrg.*, ASCE, Vol. 110, No. 8, pp. 1058-1071.

HUNT, B. (1988). "An Asymptotic Solution for Dam Break Floods in Sloping Channels." in "Civil Engineering Practice", *Technomic Publ.*, Editors P.N. CHEREMISINOFF, N.P. CHEREMISINOFF and S.L. CHENG, Lancaster Pen., USA, Lancaster, USA, Vol. 2, Section 1, Chapter 1, pp. 3-11.

HUNT, B. (1994). "Newtonian Fluid Mechanics Treatment of Debris Flows and Avalanches." *Jl of Hyd. Engrg.*, ASCE, Vol. 120, No. 12, pp. 1350-1363.

IDEL'CIK, I.E. (1969). "Mémento des Pertes de Charge." ('Handbook of Hydraulic Resistance.') *Eyrolles Editor*, Collection de la direction des études et recherches d'Electricité de France, Paris, France.

IDELCHIK, I.E. (1986). "Handbook of Hydraulic Resistance." *Hemisphere Publ.*, 2nd rev. and augm. ed., New York, USA.

IDELCHIK, I.E. (1994). "Handbook of Hydraulic Resistance." *CRC Press*, 3rd edition, Boca Raton, USA, 790 pages.

JENSEN, A., PEDERSEN, G.K., and WOOD, D.J. (2003). "An Experimental Study of Wave Run-up on a Steep Beach." *Jl of Fluid Mech.*, Vol. 486, pp. 166-188.

KOMAR, P.D. (1998). "Beach Processes and Sedimentation." Prentice Hall, Upper Saddle River NJ, USA, 2nd edition, 544 pages.

LAUBER, G. (1997). "Experimente zur Talsperrenbruchwelle im glatten geneigten Rechteckkanal." ('Dam Break Wave Experiments in Rectangular Channels.') *Ph.D. thesis*, VAW-ETH, Zürich, Switzerland (in German). (also *Mitteilungen der Versuchsanstalt fur Wasserbau, Hydrologie und Glaziologie*, ETH-Zurich, Switzerland, No. 152).

LEAL, J.G.A.B., FERREIRA, R.M.L., FRANCO, A.B., and CARDOSO, A.H. (2001). "Dam-Break Waves over Movable Bed Channels. Experimental Study." *Proc. 29th IAHR Congress*, Beijing, China, Theme C, Tsinghua University Press, Beijing, G. LI Ed., pp. 232-239.

LEVIN, L. (1952). "Mouvement Non Permanent sur les Cours d'Eau à la Suite de Rupture de Barrage." ('Unsteady Flow Motion Induced by a Dam Break.') *Revue Générale de l'Hydraulique*, Vol. 18, pp. 297-315.

LIGGETT, J.A. (1994). "Fluid Mechanics." *McGraw-Hill*, New York, USA.

MANO, A. (1994). "Boundary Layer Developed near Surging Front." *Coastal Engineering in Japan*, Vol. 37, No. 1, pp. 23-39.

MARTINOT-LAGARDE, A., and ESTRADE, J. (1966). "Sur la Détermination du Champ des Vitesses à Deux Dimensions dans un Canal Horizontal peu après la Suppression Instantatanée d'un Barrage." ('Calculation of the two-Dimensional Velocity Field in a Horizontal Channel shortly after a Sudden Dam Break.') *Comptes-Rendus Académie des Sciences de Paris*, France, Vol. 262, Series A, 17 Jan., pp. 188-191.

MONTES, J.S. (1998). "Hydraulics of Open Channel Flow." *ASCE Press*, New-York, USA, 697 pages.

MURCK, B.W., SKINNER, B.J., and PORTER, S.C. (1997). "Dangerous Earth. An Introduction to Geologic Hazards." *John Wiley*, New York, USA, 300 pages.
NSOM, B., DEBIANE, K., and PIAU, J.M. (2000). "Bed Slope Effect on the Dam Break Problem." *Jl of Hyd. Res.*, IAHR, Vol. 38, No. 6, pp. 459-464.
PEREGRINE, D.H., and WILLIAMS, S.M. (2001). "Swash Overtopping a Truncated Plane Beach." *Jl of Fluid Mech.*, Vol. 440, pp. 391-399.
POHLE, F.V. (1952). "Motion of water due to Breaking of a Dam and Related Problems." *Circular*, National Bureau of Standards, Dept of Commerce, Vol. 521, No. 8, pp. 47-53.
POND, S., and PICKARD, G.L. (1983). "Introductory Dynamical Oceanography." *Butterworth Heinemann*, Oxford, UK, 2nd edition, 329 pages.
RITTER, A. (1892). "Die Fortpflanzung der Wasserwellen." *Vereine Deutscher Ingenieure Zeitswchrift*, Vol. 36, No. 2, 33, 13 Aug., pp. 947-954 (in German).
SARRE (1998?). "Calculating the Threat of a Tsunami." *Australian Academy of Science Nova Internet paper* {Internet address : http://www.science.org.au/nova/045/045key.htm}.
SCHLICHTING, H. (1979). "Boundary Layer Theory." *McGraw-Hill*, New York, USA, 7th edition.
SCHLICHTING, H., and GERSTEN, K. (2000). "Boundary Layer Theory." *Springer Verlag*, Berlin, Germany, 8th edition., 707 pages.
SCHOKLITSCH, A. (1917). Über Dambruchwellen." *Sitzungberichten der Königliche Akademie der Wissenschaften, Vienna*, Vol. 126, Part IIa, pp. 1489-1514.
SHUTO, N. (1985). "The Nihonkai-Chubu Earthquake Tsunami on the North Akita Coast." *Coastal Eng. in Japan*, Vol. 20, pp. 250-264.
STANSBY, P.K., CHEGINI, A., and BARNES, T.C.D. (1998). "The Initial Stages of Dam-Break Flow." *Jl of Fluid Mech.*, Vol. 374, pp. 407-424.
STOKER, J.J. (1957). "Water Waves. The Mathematical Theory with Applications." *Interscience Publishers*, New York, USA, 567 pages.
SYNOLAKIS, C.E. (1987). "The Run-up of Solitary Waves." *Jl of Fluid Mech.*, Vol. 195, pp. 523-545.
TSUJI, Y. (2005). "Distribution of the Tsunami Heights of the 2004 Sumatra Tsunami in Banda Aceh measured by the Tsunami Survey Team." *Internet Resource* {http://www.eri.u-tokyo.ac.jp/namegaya/sumatera/surveylog/eindex.htm}.
WANG, Z.Y. (2002). "Initiation and Mechanism of Two Phase Debris Flow." *Proc. Conf. on Flood Defence'2002*, Ed. WU et al., Science Press, New York, pp. 1637-1648.
WHITHAM, G.B. (1955). "The Effects of Hydraulic Resistance in the Dam-Break Problem." *Proc. Roy. Soc. of London*, Ser. A, Vol. 227, pp. 399-407.
WOOD, D.J., PEDERSEN, G.K., and JENSEN, A. (2003). "Modelling of Run-up of Steep Non-Breaking Waves." *Ocean Eng.*, Vol. 30, pp. 625-644.
YEH, H.H. (1991). "Tsunami Bore Runup." *Natural Hazards*, Vol. 4, pp. 209-220.
YEH, H., LIU, P., and SYNOLAKIS, C. (1996). "Long-wave Runup Models." *World Scientific*, Singapore, 403 pages. (also *Proc. 2nd Intl Workshop on Long-Wave Runup Models*, Friday Harbour WAS, USA, Sept. 1995.)

INTERNET REFERENCES

Dale Dyke reservoir catastroph	{http://www.shef.ac.uk/misc/personal/cs1ma/flood/photogal/picflud1.html}
Habra dams and their stories	{http://peraltap.club.fr/P15-barrage.htm}
Photographs of the Malpasset dam and St Francis dam sites	{http://www.uq.edu.au/~e2hchans/photo.html - Failures}
Malpasset dam (in Structurae)	{http://www.structurae.net/structures/data/index.cfm?ID=s0000335}
Teton dam failure	{http://www.geol.ucsb.edu/faculty/sylvester/Teton Dam/welcome_dam.html} {http://www.usbr.gov/pn/about/Teton.html}

Vajont dam (in Structurae)	{http://www.structurae.net/structures/data/index.cfm?ID=s0001119}
Tsunami information & photographs	{http://www.uq.edu.au/~e2hchans/photo.html - Tsunami}
NOOA Compilation of report, data and information on the 26 Dec. 2004 tsunami	{http://www.pmel.noaa.gov/tsunami/sumatra20041226.html}
The December 26, 2004 Earthquake Tsunami Disaster of Indian Ocean, by the Research Group on The December 26, 2004 Earthquake Tsunami Disaster of Indian Ocean	{http://www.drs.dpri.kyoto-u.ac.jp/sumatra/index-e.html}

BIBLIOGRAPHIC REFERENCE OF THE REPORT CH55/05

The Hydraulic Model research report series CH is a refereed publication published by the Department of Civil Engineering at the University of Queensland, Brisbane, Australia.

The bibliographic reference of the present report is :

CHANSON, H. (2005). "Applications of the Saint-Venant Equations and Method of Characteristics to the Dam Break Wave Problem." *Report No. CH55/05*, Dept. of Civil Engineering, The University of Queensland, Brisbane, Australia, May, 135 pages (ISBN 1864997966).

The Report CH55/05 is available, in the present form, as a series of .PDF files on the Internet at the following address :

http://www.uq.edu.au/~e2hchans/reprints/ch5505.zip

The .zip file contains the following files :

00_damb.pdf	Cover pages
01_damb.pdf	Title page, abstract, table of contents, list of symbols, contributors' biography
1_damb.pdf 4_damb.pdf 5_damb.pdf 6_damb.pdf	Chap. 1. Introduction Chap. 2. A bibliographic review Chap. 3. Ideal-fluid flow solutions of the dam break problem Chap. 4. Real-fluid flow solutions of the dam break problem (turbulent flow motion) Chap. 5. Laminar flow solutions of the dam break problem Chap. 6. Applications Chap. 7. Summary and conclusion Acknowledgments
a_damb.pdf	Appendices. App. A - Major tsunami catastrophes App. B - Basic experiments of dam break wave App. C. Laminar dam break motion in a dry horizontal channel with bed friction (diffusive wave model) App. D. App. D. Fully-Rough turbulent Dam break motion in a dry horizontal channel with bed friction (diffusive wave model)
referenc.pdf	References Internet references Bibliographic reference of the Report CH55/05

HYDRAULIC MODEL RESEARCH REPORT CH

The Hydraulic Model Report CH series is published by the Department of Civil Engineering at the University of Queensland. Orders of any of the Hydraulic Model Reports should be addressed to the Departmental Secretary.

Departmental Secretary, Dept. of Civil Engineering, The University of Queensland
Brisbane 4072, Australia
Tel.: (61 7) 33 65 41 63 Fax : (61 7) 33 65 45 99
Url: http://www.uq.edu.au/civeng/ Email: civeng@uq.edu.au

Report CH	Unit price	Quantity	Total price
CHANSON, H. (2005). "Applications of the Saint-Venant Equations and Method of Characteristics to the Dam Break Wave Problem." Report No. CH55/05, Dept. of Civil Engineering, The University of Queensland, Brisbane, Australia, May (ISBN 1864997966).	AUD$60.00		
CHANSON, H., COUSSOT, P., JARNY, S., and TOQUER, L. (2004). "A Study of Dam Break Wave of Thixotropic Fluid: Bentonite Surges down an Inclined plane." *Report No. CH54/04*, Dept. of Civil Engineering, The University of Queensland, Brisbane, Australia, June, 90 pages (ISBN 1864997710).	AUD$60.00		
CHANSON, H. (2003). "A Hydraulic, Environmental and Ecological Assessment of a Sub-tropical Stream in Eastern Australia: Eprapah Creek, Victoria Point QLD on 4 April 2003." *Report No. CH52/03*, Dept. of Civil Engineering, The University of Queensland, Brisbane, Australia, June, 189 pages (ISBN 1864997044).	AUD$90.00		
CHANSON, H. (2003). "Sudden Flood Release down a Stepped Cascade. Unsteady Air-Water Flow Measurements. Applications to Wave Run-up, Flash Flood and Dam Break Wave." *Report CH51/03*, Dept of Civil Eng., Univ. of Queensland, Brisbane, Australia, 142 pages (ISBN 1864996552).	AUD$60.00		
CHANSON, H,. (2002). "An Experimental Study of Roman Dropshaft Operation : Hydraulics, Two-Phase Flow, Acoustics." *Report CH50/02*, Dept of Civil Eng., Univ. of Queensland, Brisbane, Australia, 99 pages (ISBN 1864996544).	AUD$60.00		
CHANSON, H., and BRATTBERG, T. (1997). "Experimental Investigations of Air Bubble Entrainment in Developing Shear Layers." *Report CH48/97*, Dept. of Civil Engineering, University of Queensland, Australia, Oct., 309 pages (ISBN 0 86776 748 0).	AUD$90.00		
CHANSON, H. (1996). "Some Hydraulic Aspects during Overflow above Inflatable Flexible Membrane Dam." *Report CH47/96*, Dept. of Civil Engineering, University of Queensland, Australia, May, 60 pages (ISBN 0 86776 644 1).	AUD$60.00		
CHANSON, H. (1995). "Flow Characteristics of Undular Hydraulic Jumps. Comparison with Near-Critical Flows." *Report CH45/95*, Dept. of Civil Engineering, University of Queensland, Australia, June, 202 pages (ISBN 0 86776 612 3).	AUD$60.00		
CHANSON, H. (1995). "Air Bubble Entrainment in Free-surface Turbulent Flows. Experimental Investigations." *Report CH46/95*, Dept. of Civil Engineering, University of Queensland, Australia, June, 368 pages (ISBN 0 86776 611 5).	AUD$80.00		
CHANSON, H. (1994). "Hydraulic Design of Stepped Channels and Spillways." *Report CH43/94*, Dept. of Civil Engineering, University of Queensland, Australia, Feb., 169 pages (ISBN 0 86776 560 7).	AUD$60.00		
POSTAGE & HANDLING (per report)	AUD$10.00		
GRAND TOTAL			

OTHER HYDRAULIC RESEARCH REPORTS

Report CH	Unit price	Quantity	Total price
TOOMBES, L. (2002). "Experimental Study of Air-Water Flow Properties on Low-Gradient Stepped Cascades." *Ph.D. thesis*, Dept of Civil Engineering, The University of Queensland.	AUD$120.00		
CHANSON, H. (1988). "A Study of Air Entrainment and Aeration Devices on a Spillway Model." *Ph.D. thesis*, University of Canterbury, New Zealand.	AUD$60.00		
POSTAGE & HANDLING (per report)	AUD$10.00		
GRAND TOTAL			

PAYMENT INFORMATION

1- VISA Card

Name on the card :	
Visa card number :	
Expiry date :	
Amount :	AUD$ .....

2- Cheque/remittance payable to : THE UNIVERSITY OF QUEENSLAND and crossed "Not Negotiable".

N.B. For overseas buyers, cheque payable in Australian Dollars drawn on an office in Australia of a bank operating in Australia, payable to: THE UNIVERSITY OF QUEENSLAND and crossed "Not Negotiable".

APPENDIX A - MAJOR TSUNAMI CATASTROPHES

A tsunami ([1]) is a long-period wave generated by ocean bottom motion during an earthquake. Occasionally it might be caused by another earth movement (e.g. underwater landslide, volcanic activity) ([2]). The wave length is typically about 200 to 350 km and the tsunami behaves as a shallow water wave, even in deep sea. Although the wave amplitude is moderate in the middle of the ocean (e.g. 0.5 to 1 m), the tsunami wave slows down and the wave height increases near the shoreline, with periods ranging between 20 minutes and several hours typically. The wave runup height might reach several metres above the natural sea level (Table A-1, column 4).

Table A-1 summarises major tsunami disasters, associated with well in excess of 350,000 losses of life. Photographs of the 26 December 2004 tsunami disaster are presented in Figure A-1, and well-documented studies include TSUJI (2005) and CHANSON (2005).

Fig. A-1 - Photographs of the 26 December 2004 tsunami disaster
(A) Car floating after tsunami waves near Madras, India (Courtesy of AFP/Podhigai TV via LCI)
(B) People along a beach littered with debris, coastal areas in Colombo, Sri Lanka on Sunday 26 Dec. 004 (Courtesy of AP Photo/Eranga Jayawardena)

(C) Town's main road after a tsunami wave hit the southern Sri Lanka town of Galle - Photograph taken on Monday 27 Dec. 2004 (Courtesy of AP Photo/Elizabeth Dalziel)
(D) Group of Buddhist monks and villagers along railroad tracks at Telwatte, about 100 km South of Colombo, Sri Lanka on Tuesday 28 Dec. 2004 - The "Queen of the Sea" train was beaten off its tracks, leaving more than 1,000 dead or missing (Courtesy of AP Photo/Eranga Jayawardena)

[1]Japanese word meaning "harbour wave". A tsunami is also called seismic sea wave. It is sometimes incorrectly termed "tidal wave" but the process is not related to the tides.
[2]A related case is the impulse wave generated by rockfalls, landslides, ice falls, glacier breakup or snow avalanches in lakes and man-made reservoirs. Some impulse waves might be induced by earthquake-generated falls.

(E) Houses being flooded by the tsunami flood wave (flow from top left to bottom right) in Sri Lanka (Courtesy AP Photo/Dita Alangkara)
(F) Damage at a beach in Phuket, Thailand on 26 Dec. 2004 (Courtesy of Reuters)


(G) Damaged boats in Victoria port in the Seychelles - Photograph taken on 27 Dec. 2004 (Courtesy of REUTERS/George Thande)
(H) Photograph of St Pierre beach, Reunion island on 26 Dec. 2004 - The tsunami runup traces are clearly visible on the beach slope (Courtesy of Axou)


(I) Tsunami waves wash through houses at Maddampegama, about 60 km South of Colombo, Sri Lanka, on 26 Dec. 2004 (Courtesy AP Photo/Gemunu Amarasinghe)
(J) Tsunami waves wash through houses at Maddampegama, about 60 km South of Colombo, Sri Lanka, on 26 Dec. 2004 (Courtesy of AP Photo/Gemunu Amarasinghe)


(K) Aerial image showing villagers stand next to a road destroyed by tsunami waves at Telwatte, about 100 km South of Colombo, Sri Lanka, on 29 Dec. 2004 (Courtesy AP Photo/Vincent Thian)
(L) Aerial view of the bodies of victims, in the city of Banda Aceh, Indonesia on 27 Dec. 2004 (Courtesy REUTERS/Beawiharta)


(M) Tsunami waters surging through a tourist resort (Seagull Andaman Resort) at Khao Lak, Thailand on 26 Dec. 2004 (Courtesy of John M. THOMPSON)
(N) Massive destruction at Khao Lak, Thailand, on 27 Dec. 2005 (Courtesy of John M. THOMPSON)


(O) Impact of the tsunami on North-West Aceh, Indonesia: Lhoknga, located about 60-70 km South of Banda Aceh

(O1) Satellite photographs, DLR / IKONOS data from Centre for Remote Imaging, Sensing and Processing (Credit "Space Imaging/CRISP-Singapore") - Left : Before (10 Jan. 2003); Right: After (29 Dec. 2004); The red circles are the barge and cement factory seen in the next Figures

(O2) Photographs of the coastline after the tsunami

(Left) Barge and tugboat, with the jetty and a sunk boat in the background (Courtesy of Dr. Jose BORRERO, University of Southern California Tsunami research group)

(Right) Cement factory (Courtesy of Dr. Jose BORRERO, University of Southern California Tsunami research group)

(O3) Looking South at the devastated coastline, with the cement factory and barge in the background, photograph taken on 4 Jan. 2005 (Courtesy U.S. Navy photo by Photographer's Mate 3rd Class Tyler J. CLEMENTS Ref. 050104-N-6817C-23)

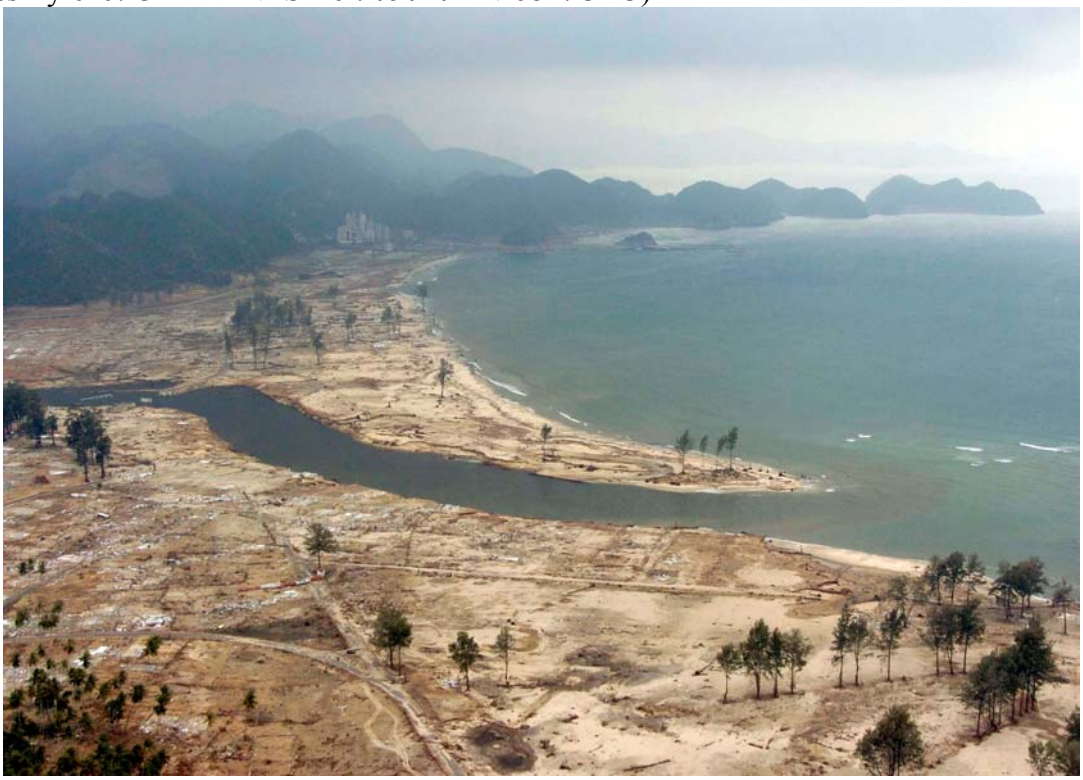

(O4) Lhoknga, North-West Aceh, Indonesia
(Left) Overturned and damaged cargo ship at the harbor near cement factory on 28 Jan. 2005 (Courtesy of Dr V. GUSIAKOV)
(Right) Traces of tsunami run-up on the surface of small coastal hill on 28 Jan. 2005 (Courtesy of Dr V. GUSIAKOV) - All vegetation and soil are removed by 20-25m waves

Table A-1 - Major tsunami catastrophes

Location [Ref.]	Date	Loss of life	Maximum runup height m	Runup soil / conditions	Remarks
(1)	(2)	(3)	(4)	(5)	(6)
MEDITERRANEAN AREA					
Amnisos, Crete [1,6,9]	BC 1500?		40		Volcanic eruption on Santorini island. Marked the end of Minoan civilisation.
Istanbul/Galata, Turkey [6]	14 Sept. 1509				Overtopped the walls of Constantinople
Gargano, Italy [3]	30 July 1637	> 5,000		Lakes	Runup over Lakes Lesina and Varano.
Messina, Italy (?) [7]	1908	several thousands	10		
Amorgos island, Greece	9 July 1956		25		Quake magnitude 7.7
ATLANTIC OCEAN					
Lisbon, Portugal [5,6,9]	1 Nov. 1755	~ 60,000	5 to 10	Coast	Terrible disaster during day time. Many people killed, attracted by the retreating sea prior to the bore.
Burin peninsula, Newfoundland, Canada [6]	18 Nov. 1929		15		Grand Banks earthquake
PACIFIC OCEAN					
CANADA					
West Coast of Canada [8]	27 Jan. 1700		20		Earthquake at the Cascadia subduction zone, West Coast, Canada.
Port Alberni, British Columbia, Canada [8]	28 Mar. 1964		4.3	Cliff and rocks	"Great Alaska Earthquake" at Prince William Sound (27/3/61). 1st wave arrived at 12:20am. 3 waves, the last being the largest. (Period ~ 1.5 to 2 hours.) Runup velocity = 50 km/h.
CHILE					
Valdivia, Chile [6]	16 Dec. 1575				2 Spanish gallions wrecked.
Concepcion, Chile [6]	25 Mar. 1751				Disaster at Juan Fernandez island.
Arica, Peru [Peru-Chile] (today North Chile) [1,10]	13 Aug. 1868		21		Carried USS Wateree and Peruvian warship America inland.
Chile [7]	1922				Seiche over the Pacific Ocean for several days.
Chile [1]	23 May 1960	909 dead + 834 missing	> 10		
INDONESIA					
Celebes, Makassar [6]	29 Dec. 1820		24		
Sunda Strait, Java-Sumatra, Indonesia [6,9]	27 Aug. 1883	> 36,000	40		Explosion of Krakatoa volcano.
Indonesia [9]	2 Dec. 1992	137	26		
SE Java, Indonesia [2]	3 June 1994	> 250	5	Coastline	3 successive waves, largest runup being the 3rd wave.
JAPAN					
Pacific coast, Japan [8]	27 Jan. 1700		3		Earthquake at the Cascadia subduction zone, West Coast, Canada.
Sanriku coast, Honshu, NE Japan, Japan [6,9]	15 June 1896	> 26,000	30		Destroyed most of Yoshihama and Kamaishi towns.
Miyagi prefecture, Honshu, Japan [3,9]	3 Mar. 1933	3064	27.8		
Wakayama prefecture, Japan [3]	7 Dec. 1944	998			
Hokkaido, Japan [3]	4 Mar. 1952	33			
Japan [1,3]	23 May 1960	> 142			Earthquake near Chile coastline, travelling about 22 hours to Japan.
Akita and Aomori prefectures, Japan [3]	26 May 1983	104			

Table A-1 - Major tsunami catastrophes

Location [Ref.]	Date	Loss of life	Maximum runup height m	Runup soil / conditions	Remarks
(1)	(2)	(3)	(4)	(5)	(6)
JAPAN					
Okushiri island, SW Hokkaido, Japan [3]	12 July 1993	> 120	30.5	Coast and cliffs	
NICARAGUA					
Nicaragua[9]	2 Sept. 1992	~170	10		
PNG					
Sissano Lagoon, Papua New Guinea [1]	17 Jul. 1998	> 3,000		Lagoon	
RUSSIA					
Kamchatka, Russia [10]	1737		64		
TAIWAN					
Chaitung, Pingtung county Taiwan	1781				
Yunlin County, Taiwan	1845	10,000			
Keelung, Taiwan	18 Dec. 1867	50,000			Magnitude 7.0.
USA (incl. Alaska and Hawaii)					
Scotch Cap, Alaska [6]	1 Apr. 1946	5	32	Coast/cliff	Destroying concrete lighthouse (2:40am).
Hilo, Hawaii [9]	1 Apr. 1946	90	18		Earthquake near Unimak island, Alaska.
Laie point, Oahu, Hawaii [10]	9 Mar. 1957	54			Earthquake in Aleutian islands. Slow water rise.
Hilo, Hawaii [10]	21 May 1960	61			
Prince Williams Sound, Alaska [8]	27 Mar. 1964				"Great Alaska Earthquake".
California, USA [9]	28 May 1964	119			Earthquake in Alaska.
INDIAN OCEAN					
Sumatra 26 Dec. 2004	26 Dec. 2004				Magnitude 9.0.
India		> 10,700			
Indonesia		> 220,000	> 35		Epicentre beside Aceh province.
Malaysia		> 70			
Maldives		> 80	> 4		
Myanmar		> 55			
Somalia		> 295			
Sri Lanka		> 30,900	> 10		
Thailand		> 5,400	> 10		

References : [1] SARRE (1998?); [2] HEBENSTREIT (1996); [3] BUTCHER et al. (1994); [4] YEH et al. (1996); [5] KOMAR (1998); [6] BASCOM (1980); [7] HECK (1936); [8] CLAGUE and BOBROWSKY (1999); [9] MURCK et al. (1997); [10] BRYANT (1991); CHANSON et al. (2000), TSUJI (2005); CHANSON (2005); Present study.

APPENDIX B - BASIC EXPERIMENTS OF DAM BREAK WAVE

B.1 PRESENTATION

Physical modelling of dam break wave is relatively limited. In particular, few experiments were conducted in relatively large size facilities under controlled flow conditions (Table B-1).

In retrospect, the experiments of SCHOKLITSCH (1917) were well ahead of their time, and demonstrated that Armin von SCHOKLITSCH (1888–1968) had a solid understanding of both physical modelling and dam break processes.

Table B-1 - Characteristics of dam break wave experiments in dry rectangular channels

Reference	Bed slope θ deg.	Channel characteristics	Reservoir characteristics	Remarks
(1)	(2)	(3)	(4)	(5)
Water flows				
SCHOKLITSCH	0	(1) L = 26 m, B = 0.6 m	(1) d_o up to 0.25 m	
(1917)	0	(2) L = 150 m, B = 1.3 m	(2) d_o up to 1 m	
DRESSLER (1954)	0	L = 65 m, B = 0.225 m (a) Painted timber (b) Coarse sand paper (c) Strips (slats) h=0.00635 m, l = 0.0254 m	d_o = 0.055, 0.11 and 0.22 m	
FAURE and NAHAS (1961)	0.0069	L = 40.6 m, B = 0.25 m 2 types of roughness	d_o = 0.23 m	S_o = 1.2 E-4.
CAVAILLE (1965)	0	L = 40 m, B = 0.25 m Glass walls and steel invert. (a) Smooth invert. (b) Rough invert (cylindrical elements ∅ = 20 mm in zigzag, l = 28 mm, h= 8 mm)	L_{res} = 18 m, rectangular reservoir (a) d_o = 0.115, 0.23 m (b) d_o = 0.23 m	
ESTRADE (1967)	0	(1) L = 23.65 m, B = 0.50 m (1a) Smooth invert (1b) Rough invert (rough cement)	(1) d_o = 0.20 & 0.40 m, L_{res} = 13.65 m, rectangular reservoir	Also ESTRADE & MARTINOT-LAGARDE (1964)
	0	(2) L = 23.65 m, B = 0.25 m (2a) Smooth invert (2b) Rough invert (cylindrical elements ∅ = 20 mm in zigzag, l = 28 mm, h= 6 mm)	(2) d_o = 0.30 m, L_{res} = 0.70 m, rectangular reservoir	
LAUBER (1997)	0	L = 2 m, B = 0.5 m PVC invert	$0.15 \le d_o \le 0.6$ m, $L_{res} < 3.6$ m, rectangular reservoir	
	5.7, 26.5	L = 14 m, B = 0.5 m PVC invert	d_o = 0.3 m, $L_{res} < 3.6$ m, trapezoidal reservoir	Vertical gate.
CHANSON et al. (2000)	0	L = 15 m, B = 0.8 m Smooth paint invert	Reservoir volume: 0.9 to 1 m^3, q(t=0) = 0.15 to 0.17 m^2/s	Free-jet discharging vertically at one end of channel
Viscous fluid flows				
DEBIANE (2000)	0	L = 3 m, B = 0.3 m	d_o = 0.055 & 0.054 m, $0.11 \le L_{res} \le 0.60$ m, rectangular reservoir	Glucose syrup-water solutions ($12 \le \mu \le 170$ Pa.s, $1413 \le \rho \le 1443$ kg/m^3).
	3, 6, 10, 12	L = 3 m, B = 0.3 m	Triangular reservoir, gate normal to invert	Glucose syrup-water solutions.

Thixotropic fluid flows CHANSON et al. (2004)	15	L = 2 m, B = 0.34 m Sand paper invert.	d_o = 0.047 to 0.08 m, $L_{res} \leq$ 0.755 m, triangular reservoir with vertical gate	Bentonite suspensions. Mass concentrations: 0.10 to 0.20 ($1064 \leq \rho \leq 1115$ kg/m^3).

Notes : B : channel width; d_o : reservoir height; h : (strip/element) roughness height; L : total channel length; L_{res} : upstream reservoir length; l : longitudinal spacing between (strip) roughness element.

B.2 BASIC RESULTS IN TERMS OF FREE-SURFACE PROFILES

Fig. B.1 - Dimensionless instantaneous free-surface profiles in a 26 m long channel (SCHOKLITSCH 1917)
(A) d_o =0.074 m, t = 3.75 s

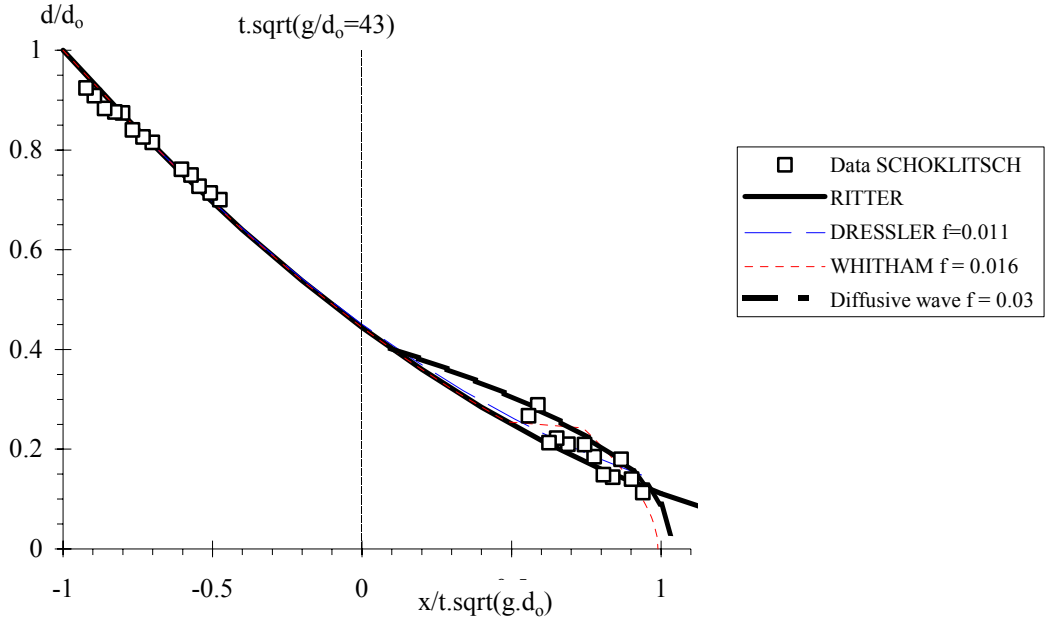

(B) d_o =0.074 m, t = 9.4 s

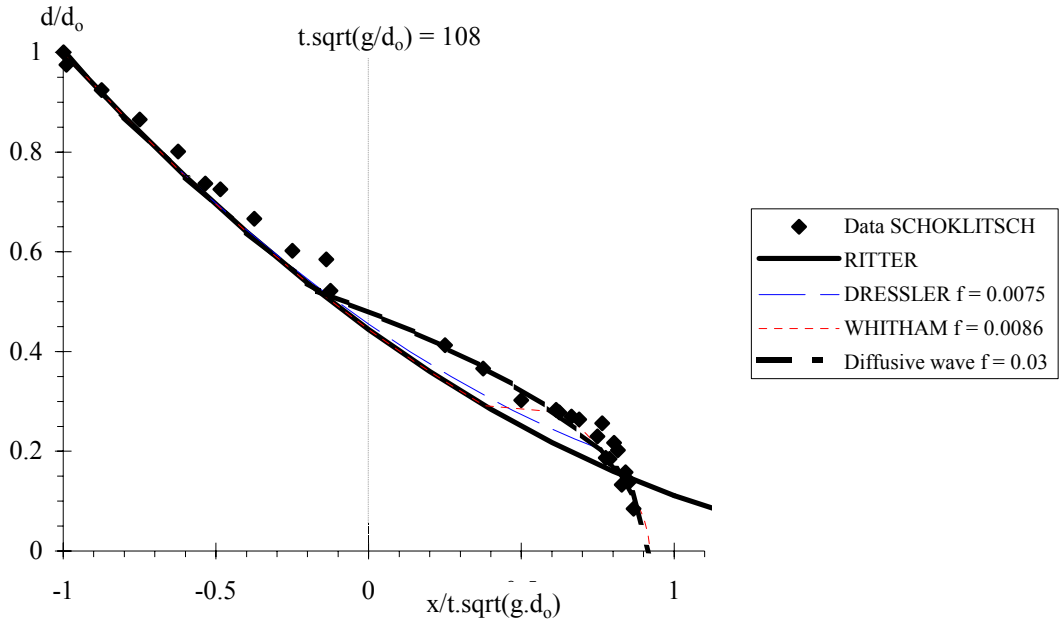

Fig. B.2 - Dimensionless instantaneous free-surface profiles in a 65 m long channel (DRESSLER 1954)

(A) Smooth painted invert - d_o = 0.22 m, $\sqrt{g/d_o}$*t = 42 & 66

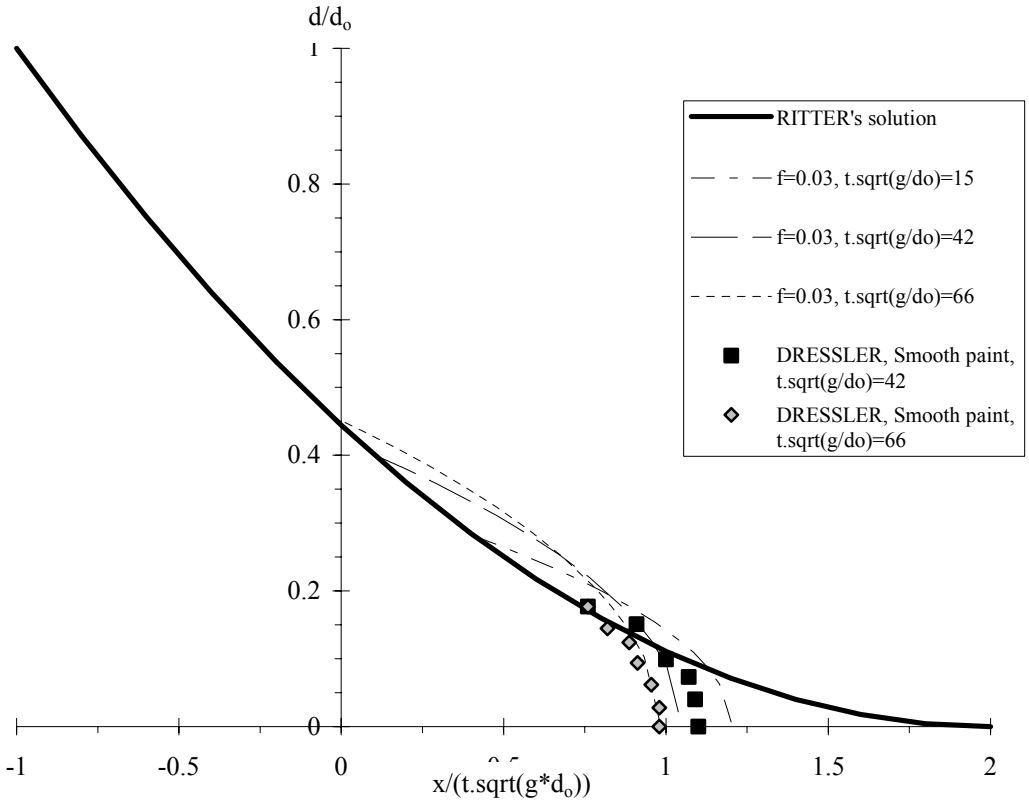

(B) Sand paper invert - d_o = 0.11 m, $\sqrt{g/d_o}$*t = 14 & 44

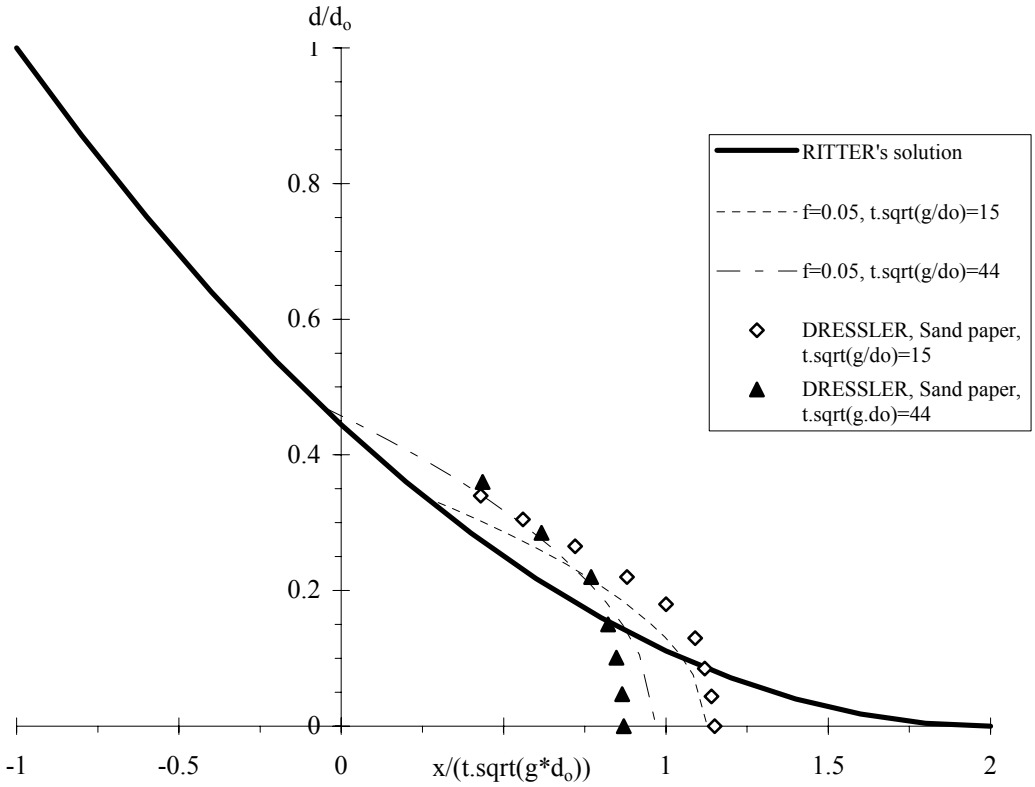

(C) Slat invert (strip roughness) - d_o = 0.22 m, $\sqrt{g/d_o}$*t = 13 & 64

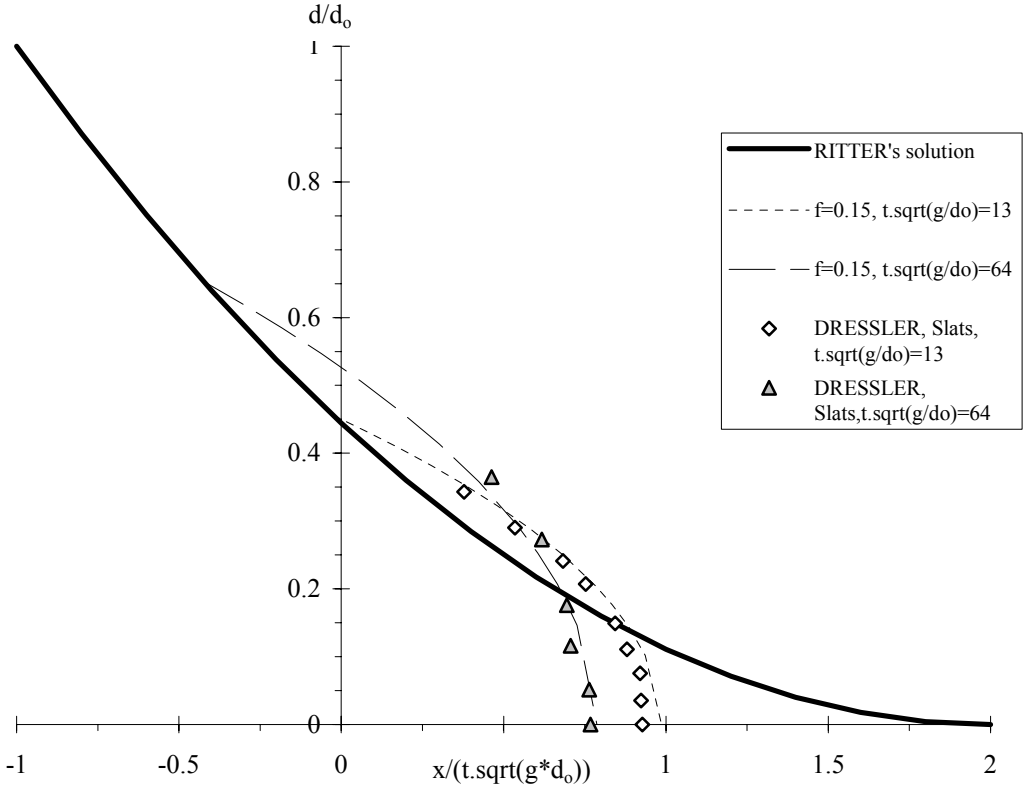

Fig. B.3 - Dimensionless instantaneous free-surface profiles in a 40 m long channel (CAVAILLE 1965)

(A) Smooth invert - d_o = 0.23 m, $\sqrt{g/d_o}$*t = 21.5, 52.2, 56.8, 83.6

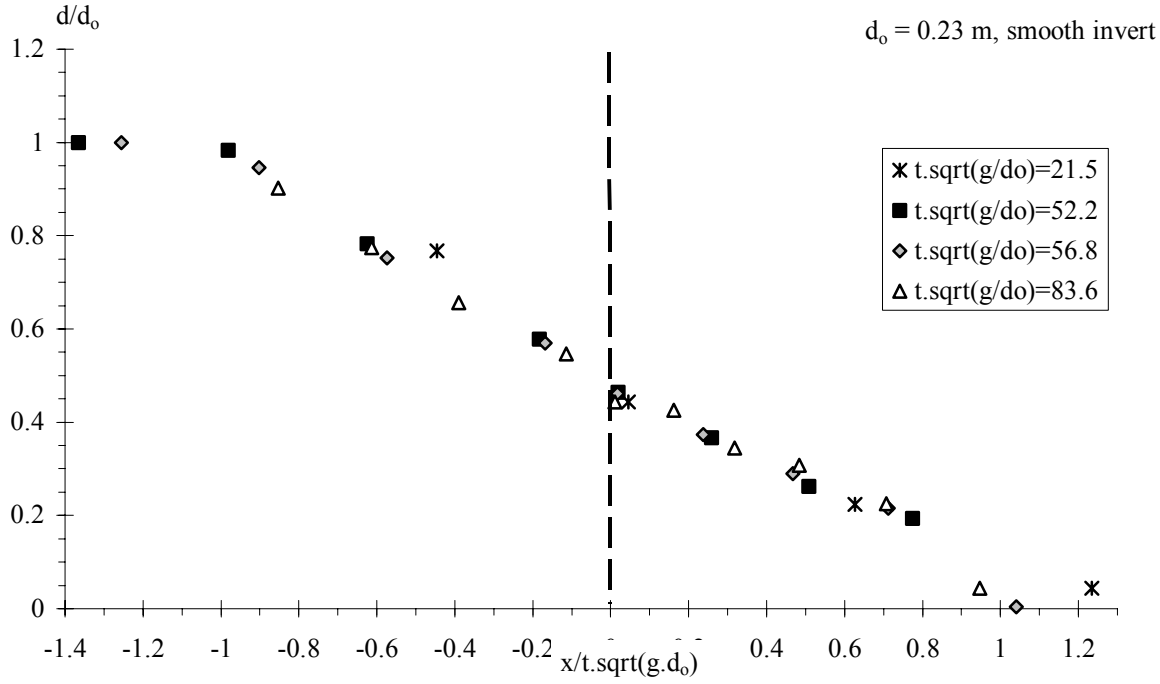

(B) Rough invert - d_o = 0.23 m, $\sqrt{g/d_o}$*t = 32.0, 55.6, 59.0, 136.5

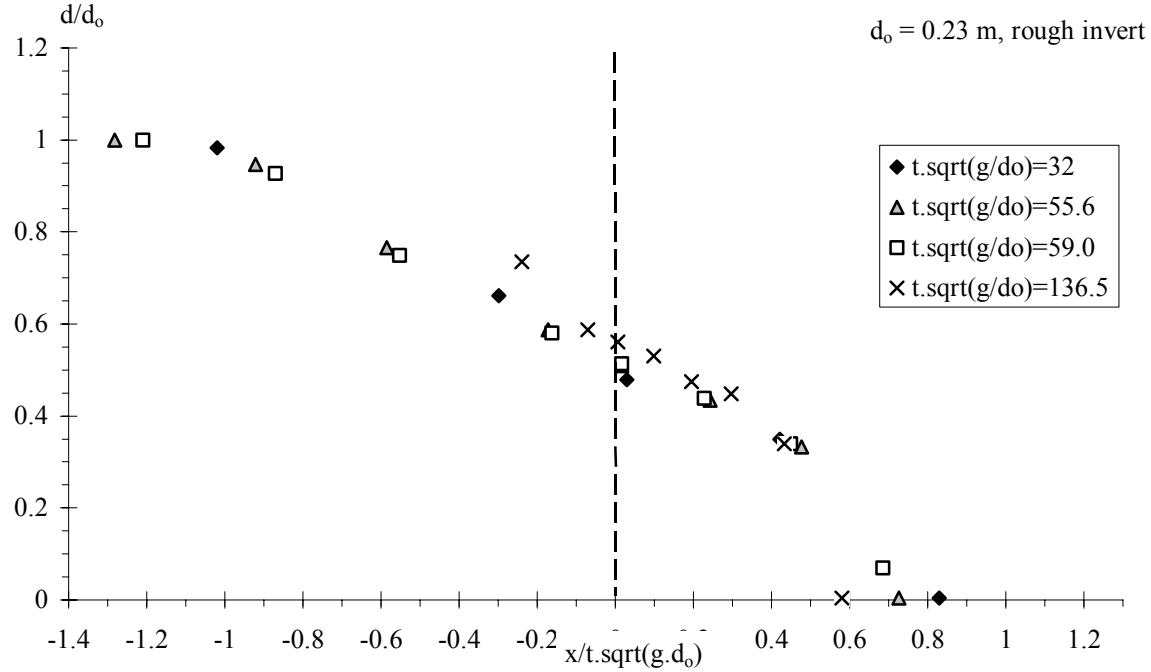

Fig. B.4 - Dimensionless free-surface profiles in a 40.6 m long channel (FAURE and NAHAS 1961) - d_O = 0.23 m, x = 3.1 & 6.1 m

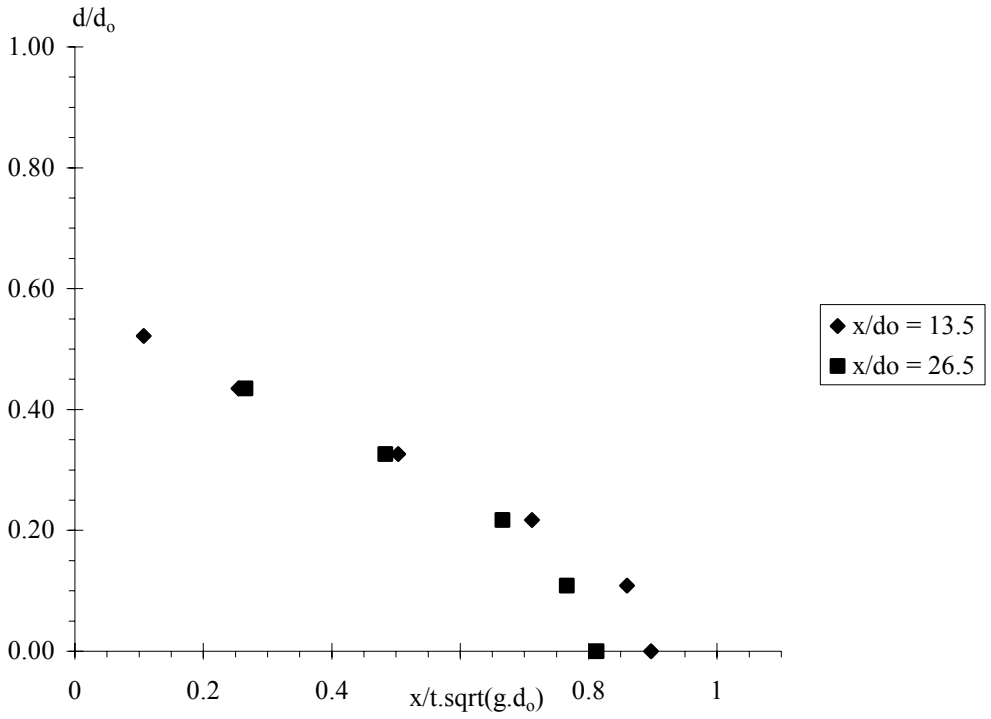

APPENDIX C - LAMINAR DAM BREAK MOTION IN A DRY HORIZONTAL CHANNEL WITH BED FRICTION (DIFFUSIVE WAVE MODEL)

C.1 PRESENTATION

A dam break wave is the flow resulting from a sudden release of a mass of fluid in a channel. In unsteady open channel flows, the velocities and water depths change with time and longitudinal position. For one-dimensional applications, the continuity and momentum equations yield the Saint-Venant equations. The application of the Saint-Venant equations is limited by some basic assumptions : (1) the flow is one dimensional; (2) the streamline curvature is very small and the pressure distributions are hydrostatic; (3) the flow resistance are the same as for a steady uniform flow for the same depth and velocity; (4) the bed slope is small enough to satisfy : $\cos\theta \approx 1$ and $\sin\theta \approx \tan\theta \approx \theta$; (5) the water density is a constant; and (6) the channel has fixed boundaries, and air entrainment and sediment motion are neglected. With these hypotheses, the unsteady flow can be characterised at any point and any time by two variables: e.g., V and d where V is the flow velocity and d is the water depth (e.g. LIGGETT 1994, MONTES 1998, CHANSON 2004a,b). The unsteady flow properties are described by a system of two partial differential equations :

Fig. C-1 - Sketch of dam break wave in a horizontal dry channel with bottom friction

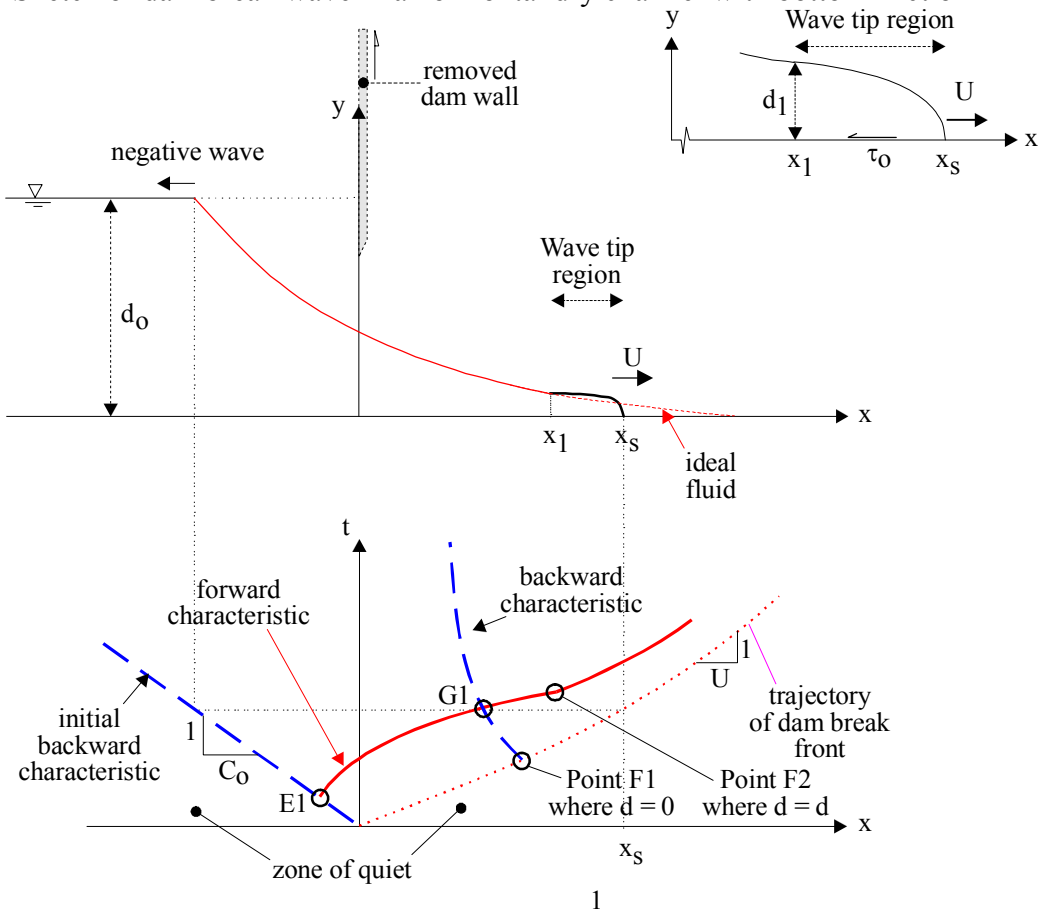

1

$$\frac{\partial d}{\partial t} + \frac{A}{B} * \frac{\partial V}{\partial x} + V * \frac{\partial d}{\partial x} + \frac{V}{B} * \left(\frac{\partial A}{\partial x}\right)_{d=constant} = 0 \qquad (C\text{-}1)$$

$$\frac{\partial V}{\partial t} + V * \frac{\partial V}{\partial x} + g * \frac{\partial d}{\partial x} + g * (S_f - S_o) = 0 \qquad (C\text{-}2)$$

where t is the tine, x is the streamwise co-ordinate, A is the cross-section area, B is the free-surface width, S_o is the bed slope ($S_o = \sin\theta$), θ is the angle between the bed and the horizontal, with $\theta > 0$

for a downward slope, and S_f is the friction slope. The friction slope is defined as : $S_f = f/2*V^2/(g*D_H)$ where D_H is the hydraulic diameter and the Darcy friction factor f is a non-linear function of both relative roughness and flow Reynolds number. Equation (C-1) is the continuity equation and Equation (C-2) is the dynamic equation.

C.2 BASIC ANALYSIS

The dam break flow is analysed as an ideal-fluid flow region behind a flow resistance-dominated tip zone (Fig. C-1) ([3]). The transition between the ideal dam break wave profile and the wave tip region is located at $x = x_1$ where the water depth is $d = d_1$ as shown in Figure C-1.
In the ideal fluid flow region, the basic equations yield the characteristic system of equations :

$$\frac{D}{Dt}(V + 2 * C) = 0 \qquad \text{forward characteristic (C-3a)}$$

$$\frac{D}{Dt}(V - 2 * C) = 0 \qquad \text{backward characteristic (C-3b)}$$

along :

$$\frac{d x}{dt} = V + C \qquad \text{forward characteristic C1 (C-4a)}$$

$$\frac{d x}{dt} = V - C \qquad \text{backward characteristic C2 (C-4b)}$$

Equations (C-3) and (C-4) are the characteristic equations of a simple wave problem (CHANSON 2004a,b).
In the wave tip region ($x_1 \leq x \leq x_S$, Fig. C-1), flow resistance is dominant, and the acceleration and inertial terms are small. The flow velocity does not vary rapidly in the forward tip zone and experimental data showed that it is about the wave front celerity U (HUNT 1994). The dynamic wave equation (Eq. (C-2)) may be reduced into a diffusive wave equation :

$$\frac{\partial d}{\partial x} + \frac{f}{8} * \frac{U^2}{g * d} = 0 \qquad \text{Wave tip region (C-5)}$$

assuming a constant velocity U for $x_1 \leq x \leq x_S$. Next to the leading edge of the wave, the slope of the free-surface becomes important to counterbalance the flow resistance.
For laminar flows, the Darcy friction factor in steady flows equals:

$$f = \frac{64}{Re}$$

where Re is the flow Reynolds number (LIGGETT 1994, MONTES 1998, CHANSON 2004a). In unsteady dam break flows, the flow resistance is assumed to follow a similar expression

$$f = \alpha * \frac{64}{Re} \qquad \text{(C-6)}$$

where α is a correction coefficient. For a wide channel, Equation (C-6) may be rewritten in the wave tip region as :

$$f = \frac{16 * \alpha * \mu}{\rho * U * d} \qquad \text{(C-6B)}$$

where ρ and μ is the density and dynamic viscosity of the fluid respectively. The diffusive wave equations may transformed as :

---

[3]DEBIANE (2000) used a similar conceptual model, but his mathematical treatment and solutions differed.

$$\frac{\partial d}{\partial x} + \frac{2 * \alpha * \mu * U}{\rho * g * d^2} = 0 \qquad \text{Wave tip region (laminar flow motion) (C-5B)}$$

The integration of the diffusive wave equation (Eq. (C-5B)) yields the shape of wave tip region for a laminar flow motion :

$$d = \sqrt[3]{6 * \alpha * \frac{\mu * U}{\rho * g} * (x_S - x)} \qquad \text{Wave front profile (laminar flow) (C-7)}$$

assuming that the flow resistance correction coefficient α is a constant independent of x. Equation (C-7) is compared with experimental data in Figure C-2.

Fig. C-2 - Laminar dam break wave front data: horizontal channel (test Glus.6), glucose-syrup solution, ρ = 1406 kg/m^3, μ = 12 Pa.s, d_o = 0.055 m, t = 421 s (DEBIANE 200) - Comparison with Equation (C-7) assuming α = 1 and $U/\sqrt{g*d_o}$ = 0.0064

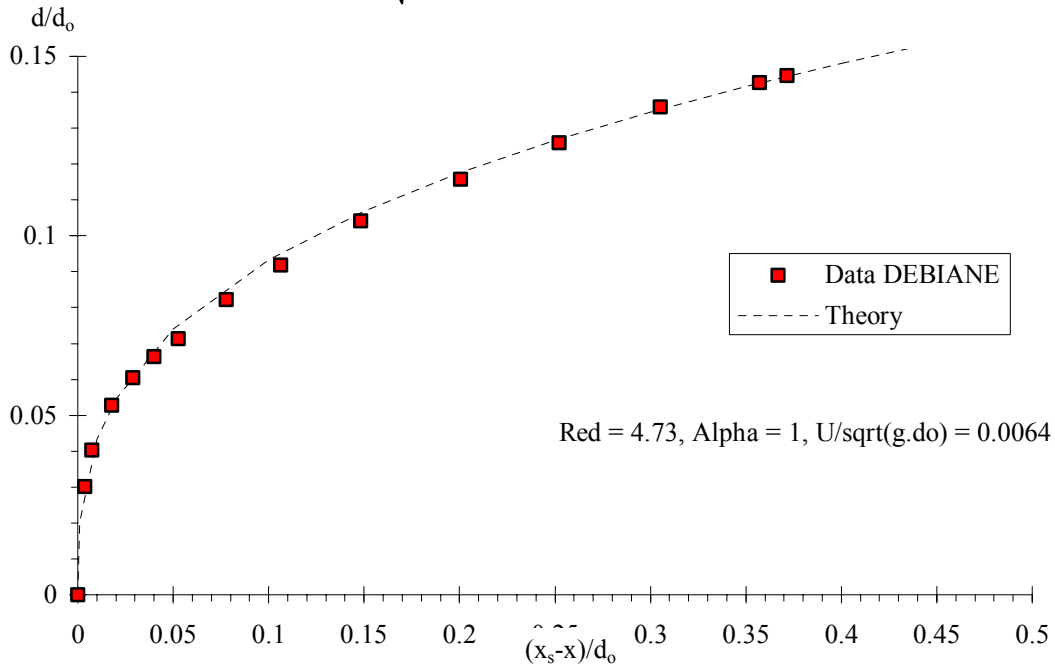

C.3 DETAILED SOLUTION

The instantaneous dam break creates a negative wave propagating upstream into a still fluid with known water depth d_o. In the (x, t) plane, the initial negative wave characteristic has a slope dt/dx = $-1/C_o$ where $C_o = \sqrt{g*d_o}$. Note that the initial backward characteristic is a straight line, but the other backward characteristics are not because the problem is not a simple wave since $S_f > 0$.. Forward characteristics can be drawn issuing from the initial backward characteristic for t > 0 (Fig. C-1). Between the points E1 and F2, the flow properties satisfy the ideal dam break wave properties:

$$\sqrt{\frac{d}{d_o}} = \frac{1}{3} * \left(2 - \frac{x}{t * \sqrt{g * d_o}}\right) \qquad -1 \le \frac{x}{t * \sqrt{g * d_o}} \le \frac{x_1}{t * \sqrt{g * d_o}} \quad \text{(C-8)}$$

$$\frac{V}{\sqrt{g * d_o}} = \frac{2}{3} * \left(1 + \frac{x}{t * \sqrt{g * d_o}}\right) \qquad -1 \le \frac{x}{t * \sqrt{g * d_o}} \le \frac{x_1}{t * \sqrt{g * d_o}} \quad \text{(C-9)}$$

where d and V are the flow depth and velocity respectively at a distance x from the dam, and t is the time from the instantaneous dam removal.

For $x_1 \le x \le x_S$ (i.e. wave tip region), it is assumed that the velocity of water does not vary rapidly and that it equals the wave front celerity U. The flow properties in the wave tip region may be estimated using the diffusive wave equation taking into account flow resistance (Eq. (C-5)) assuming V = U. The integration of the diffusive wave equation yields the wave front profile:

$$\frac{d}{d_o} = \sqrt[3]{6 * \alpha * \frac{\mu * U}{\rho * g * d_o^2} * \frac{x_S - x}{d_o}}$$

$$\frac{x_1}{t * \sqrt{g * d_o}} \le \frac{x}{t * \sqrt{g * d_o}} \le \frac{x_S}{t * \sqrt{g * d_o}} \quad \text{(C-7B)}$$

assuming that Equation (C-6B) holds for $x_1 \le x \le x_S$.
Since the free-surface and velocity must be continue at the point F2, its flow properties (x_1, V_1, d_1) must satisfy :

$$\sqrt{\frac{d_1}{d_o}} = \frac{1}{3} * \left(2 - \frac{x_1}{\sqrt{g * d_o} * t}\right) \quad \text{(C-10)}$$

$$\frac{V_1}{\sqrt{g*d_o}} = \frac{2}{3} * \left(1 + \frac{x_1}{\sqrt{g * d_o} * t}\right) \quad \text{(C-11)}$$

$$\frac{U}{\sqrt{g * d_o}} = \frac{V_1}{\sqrt{g * d_o}} \quad \text{(C-12)}$$

$$\frac{d_1}{d_o} = \sqrt[3]{6 * \alpha * \frac{\mu * U}{\rho * g * d_o^2} * \frac{x_S - x_1}{d_o}} \quad \text{(C-13)}$$

The conservation of mass must be further satisfied. Specifically the mass of fluid in the wave tip region (i.e. $x_1 \le x \le x_S$) must equal the mass of fluid in the ideal fluid flow profile for $x_1 \le x \le 2*\sqrt{g*d_o}*t$. It yields :

$$\int_{x_1}^{x_S} \sqrt[3]{6 * \alpha * \frac{\mu * U}{\rho * g} * (x_S - x)} * dx = \int_{x_1}^{2*\sqrt{g*d_o}*t} \frac{1}{9 * g} * \left(2 * \sqrt{g * d_o} - \frac{x}{t}\right)^2 * dx \quad \text{(C-14)}$$

Note that the continuity equation becomes a differential equation in terms of the wave front location x_S and celerity $U = dx_S/dt$. It must be stressed that the development is limited. The Saint-Venant equations, hence the diffusive wave equation, are not valid near the wave leading edge where the free-surface curvature is not small and where the flow resistance becomes very significant.
The above equations may be transformed to express d_1 and x_1 as functions of U:

$$\frac{d_1}{d_o} = \left(1 - \frac{1}{2} * \frac{U}{\sqrt{g * d_o}}\right)^2 \quad \text{(C-15)}$$

$$\frac{x_1}{\sqrt{g * d_o} * t} = \left(\frac{3}{2} * \frac{U}{\sqrt{g * d_o}} - 1\right) \quad \text{(C-16)}$$

The continuity equation (Eq. (C-14)) yields a polynomial equation in terms of the wave front location x_S, wave celerity $U = dx_S/dt$ and location x_1 of the point F2 :

$$\frac{3}{4} * \sqrt[3]{6 * \alpha * \frac{\mu * U}{\rho * g * {d_o}^2}} * \left(\frac{x_S - x_1}{d_o}\right)^{4/3} = \frac{1}{27} * \sqrt{\frac{g}{d_o}} * t * \left(2 - \frac{x_1}{\sqrt{g * d_o} * t}\right)^3 \quad \text{(C-17)}$$

assuming that the flow resistance correction coefficient α is a constant independent of x. Since the wave tip region has a cubic-root free-surface profile, the water depth at point F2 satisfies:

$$\frac{d1}{d_o} = \sqrt[3]{6 * \alpha * \frac{\mu * U}{\rho * g * {d_o}^2} * \frac{x_S - x_1}{d_o}} \quad \text{(C-13)}$$

and hence the wave tip region length is:

$$\frac{x_S - x_1}{d_o} = \frac{1}{6 * \alpha} * \frac{\rho * g * {d_o}^2}{\mu * U} * \left(1 - \frac{1}{2} * \frac{U}{\sqrt{g * d_o}}\right)^6 \quad \text{(C-18)}$$

By replacing into the continuity equation, the exact solution in terms of the wave front celerity is :

$$\frac{1}{8 * \alpha} * \frac{\rho * \sqrt{g * {d_o}^3}}{\mu} * \frac{\left(1 - \frac{1}{2} * \frac{U}{\sqrt{g * d_o}}\right)^5}{\frac{U}{\sqrt{g * d_o}}} = \sqrt{\frac{g}{d_o}} * t \quad \text{(C-19)}$$

while the wave front location equals:

$$\frac{x_S}{d_o} = \left(\frac{3}{2} * \frac{U}{\sqrt{g * d_o}} - 1\right) * \sqrt{\frac{g}{d_o}} * t + \frac{1}{6 * \alpha} * \frac{\frac{\rho * \sqrt{g * {d_o}^3}}{\mu}}{\frac{U}{\sqrt{g * d_o}}} * \left(1 - \frac{1}{2} * \frac{U}{\sqrt{g * d_o}}\right)^6 \quad \text{(C-20)}$$

and the free-surface profile satisfies :

$$\frac{d}{d_o} = 1 \qquad \frac{x}{d_o} \le -\sqrt{\frac{g}{d_o}} * t \quad \text{(C-21a)}$$

$$\frac{d}{d_o} = \frac{1}{9} * \left(2 - \frac{x}{t * \sqrt{g * d_o}}\right)^2 \qquad -\sqrt{\frac{g}{d_o}} * t \le \frac{x}{d_o} \le \left(\frac{3}{2} * \frac{U}{\sqrt{g * d_o}} - 1\right) * \sqrt{\frac{g}{d_o}} * t \quad \text{(C-21b)}$$

$$\frac{d}{d_o} = \sqrt[3]{6 * \alpha * \frac{\mu * U}{\rho * g * {d_o}^2} * \frac{x_S - x}{d_o}} \qquad \left(\frac{3}{2} * \frac{U}{\sqrt{g * d_o}} - 1\right) * \sqrt{\frac{g}{d_o}} * t \le \frac{x}{d_o} \le \frac{x_S}{d_o} \quad \text{(C-21c)}$$

$$\frac{d}{d_o} = 0 \qquad \frac{x_S}{d_o} \le \frac{x}{d_o} \quad \text{(C-21d)}$$

The location of point F2 is given by :

$$\frac{x_1}{\sqrt{g * d_o} * t} = \left(\frac{3}{2} * \frac{U}{\sqrt{g * d_o}} - 1\right) \qquad \text{(C-16)}$$

In the above development, the term :

$$Re_d = \frac{\rho * \sqrt{g * d_o^3}}{\mu}$$

is analogous to a Reynolds number. It is called herein the dam reservoir flow Reynolds number and is a function of fluid properties and initial flow conditions only. Typical analytical results are summarised in Figure C-3.

The theory was compared qualitatively with the viscous flow data of DEBIANE (2000) (see below) and with the analytical solution of HUNT (1994) for viscous dam break wave down a sloping channel.

Fig. C-3 - Dimensionless wave front location, celerity and free-surface profile solutions for laminar dam break wave

(A) Dimensionless relationship between wave front celerity and time assuming $\alpha = 1$

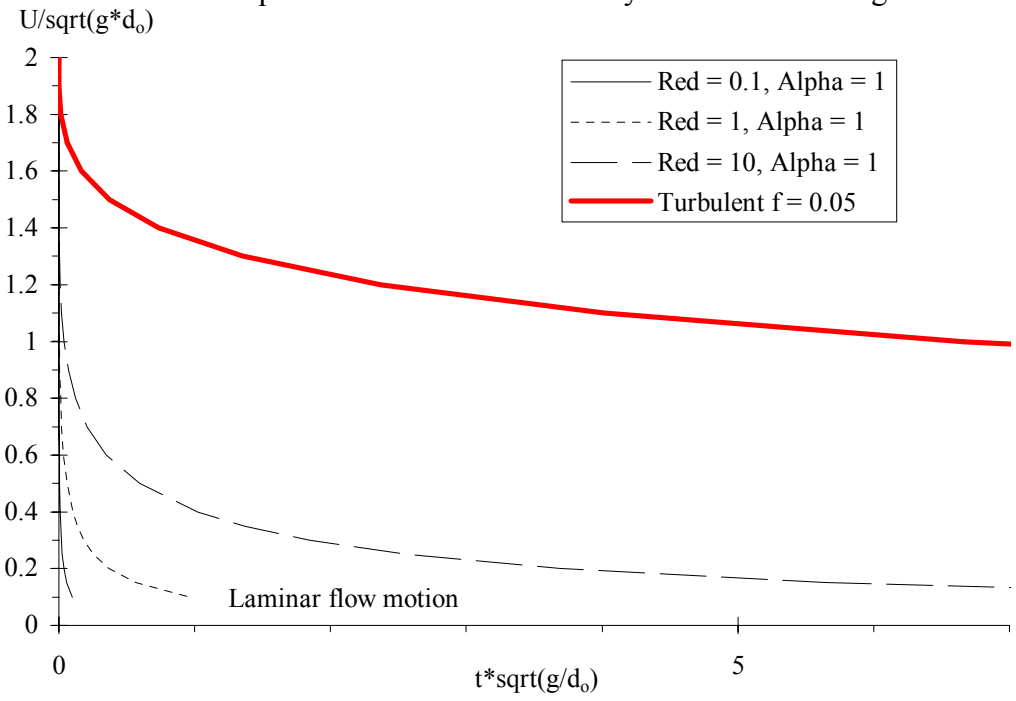

(B) Instantaneous dimensionless free-surface profile for $Re_d = 10$ and $\alpha = 1$ and 100

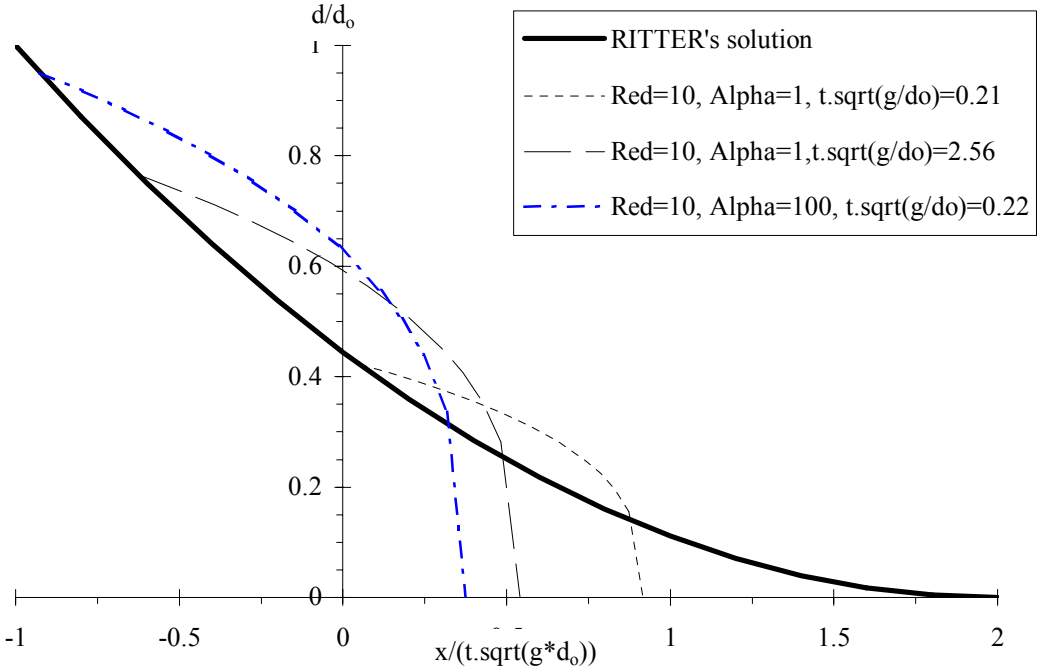

Table C-1 - Asymptotic solutions of dam break wave on dry horizontal channel with boundary friction

Reference (1)	Asymptotic solution (2)	Remarks (3)
<u>Small time t</u>		
DRESSLER (1952)	$\frac{U}{\sqrt{g*d_o}} = 2 - 3.59 * \frac{f}{8} * \sqrt{\frac{g}{d_o}} * t$	Turbulent flow motion.
WHITHAM (1955)	$\frac{U}{\sqrt{g*d_o}} = 2 - 3.452 * \frac{f}{8} * \sqrt{\frac{g}{d_o}} * t$	Turbulent flow motion.
Laminar flow motion (diffusive wave model)	$\frac{U}{\sqrt{g*d_o}} = 2 - \sqrt[5]{16 * \alpha * \frac{\mu}{\rho * \sqrt{g * d_o^3}} * \sqrt{\frac{g}{d_o}} * t}$	$\frac{U}{\sqrt{g*d_o}} > 1.2$ to 1.5
Turbulent flow motion (diffusive wave model)	$\frac{U}{\sqrt{g*d_o}} = 2 - \sqrt[3]{12 * f * \sqrt{\frac{g}{d_o}} * t}$	$\frac{U}{\sqrt{g*d_o}} > 1.2$ to 1.5
<u>Large time t</u>		
Laminar flow motion (diffusive wave model)	$\frac{U}{\sqrt{g*d_o}} = \frac{1}{8 * \alpha} * \frac{\rho * \sqrt{g * d_o^3}}{\frac{\mu}{\sqrt{\frac{g}{d_o}} * t}}$	$\frac{U}{\sqrt{g*d_o}} < 0.3$ to 0.4
Turbulent flow motion (diffusive wave model)	$\frac{U}{\sqrt{g*d_o}} = \sqrt{\frac{8}{3} * \frac{1}{f * \sqrt{\frac{g}{d_o}} * t}}$	$\frac{U}{\sqrt{g*d_o}} < 0.3$ to 0.4

C.4 COMPARISON WITH EXPERIMENTAL DATA

DEBIANE (2000) presented an unique data set for laminar dam break wave in horizontal channel, the only set known to the writer. DEBIANE conducted basic experiments in a 3.0 m long, 0.3 m wide horizontal channel with an upstream reservoir length ranging from 0.11 to 0.60 m (App. B). The study was conducted with glucose-syrup solutions with dynamic viscosities between 12 to 170 Pa.s. During the initial stages of the dam break, the dam break wave flow was similar to the flow conditions for an infinitely large reservoir and only this data set is considered herein.

Figure C-4 presents some comparison between the data of DEBIANE (2000) and the present theory. Figure C-4A shows the dimensionless wave front location as function of the dimensionless time. DEBIANE's data are compared with RITTER's (1892) solution (thick solid line) and with Equation (C-20) for $\alpha = 1$ (i.e. $f = 64/Re$) and $\alpha = 100$ (i.e. $f = 6400/Re$). Figure C-4B illustrates an instantaneous free-surface profile. Overall the analytical development are qualitatively in agreement with the experimental trends.

Experimental problems experienced by DEBIANE (2000)

In his thesis, however, DEBIANE (2000) acknowledged a number of experimental issues (DEBIANE 2000, pp. 161-163). His results showed systematically that the dam break front celerity was much smaller than theoretical predictions. His data were about 7 times lower than both RITTER's solution and DEBIANE's theoretical solution for laminar flows. This problem is best illustrated in Figure C-4A in terms of wave front locations.

DEBIANE indicated that, during his experiments, the gate opening was relatively slow (0.25 s typically) and could not be considered as an instantaneous dam break, as demonstrated by the experimental work of ESTRADE (1967). Further, for very viscous solutions, some fluid was affected by the gate opening motion. Some fluid attached to the gate while other were projected away from the flume. DEBIANE indicated further problems with sidewall effects for the most viscous solutions ($\mu = 170$ Pa.s) as well as some fluid crystallisation next to the walls at the shock front (DEBIANE 2000, p. 163).

Fig. C-4 - Comparison between theory and experimental data by DEBIANE (2000)
(A) Dimensionless wave front location for Re_d =4.73 - Comparison between RITTER's solution, Equation (C-20) and DEBIANE's data

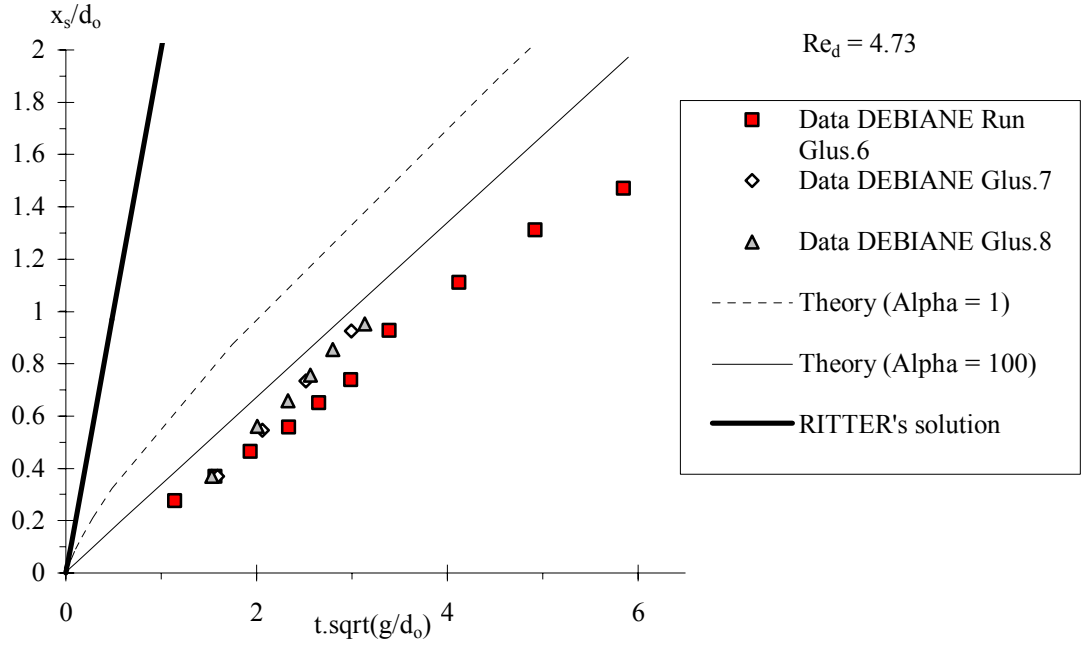

(B) Instantaneous free-surface profile for Re_d = 0.671 - Comparison between DEBIANE's data ($t^*\sqrt{g/d_o}$ = 114) and Equation (C-21) (for $t^*\sqrt{g/d_o}$ = 9.1, α = 1, 10 and 100)

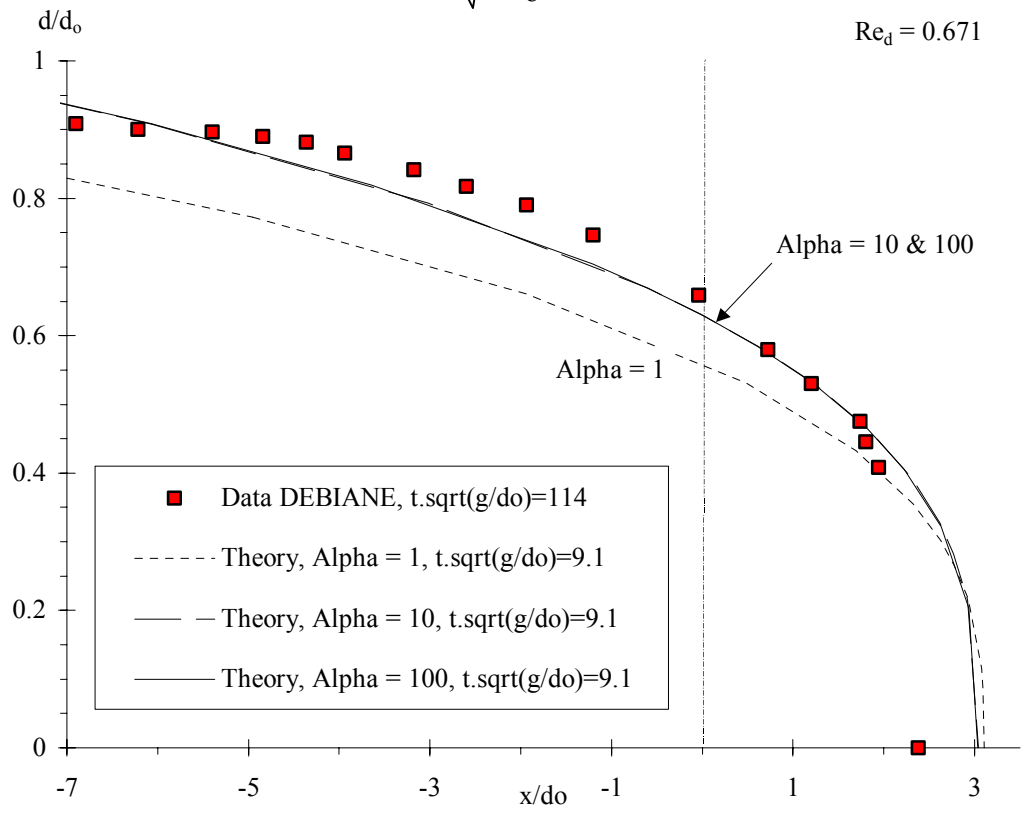

C.5 DISCUSSION

The diffusive wave approximation is limited to a semi-infinite reservoir, and it assumes that Equation (C-6) holds in highly unsteady flows and in the next to the wave tip where streamline curvature is important. A further limitation is the use of the Saint-Venant equations and their underlying assumptions. For example, the Saint-Venant equations are not valid during the initial instants following dam break.

Asymptotic approximations for small and large times t are summarised in Table C-1. These are compared with turbulent flow solutions and with well-known solutions for turbulent flows.

The present method yields an explicit expression of the wave front celerity, wave front location and wave tip region characteristics. Equation (C-19) provides a direct relationship between the dimensionless wave front celerity $U/\sqrt{g^*d_o}$ and dimensionless time $t^*\sqrt{g/d_o}$. Equation (C-20) yields the dimensionless wave front location x_s/d_o as a function of the dimensionless wave front celerity $U/\sqrt{g^*d_o}$. Equations (C-21) and (C-16) give the entire dimensionless free-surface profile $d/d_o = F(x/(t^*\sqrt{g^*d_o}))$. This simple system of linear equations provides a means to assess easily the effect of the flow resistance on the dam break wave propagation of real fluids.

The main advantages of the present development are four-fold. It is a simple explicit method that compares well with experiments and theoretical solutions. Further it a simple pedagogical application linking together the simple wave equations, yielding RITTER's solution, with a diffusive wave equation for the wave tip region. More this explicit solution may be used to validate simple numerical solutions of the method of characteristics applied to the dam break wave problem. Lastly the development may be extended simply for mid channel slopes and to account for initial flow motion, using the same approach as for turbulent flows.

APPENDIX D - FULLY-ROUGH TURBULENT DAM BREAK MOTION IN A DRY HORIZONTAL CHANNEL WITH BED FRICTION (DIFFUSIVE WAVE MODEL)

D.1 PRESENTATION

A dam break wave is the flow resulting from a sudden release of a mass of fluid in a channel. In unsteady open channel flows, the velocities and water depths change with time and longitudinal position. For one-dimensional applications, the continuity and momentum equations yield the Saint-Venant equations. The application of the Saint-Venant equations is limited by some basic assumptions : (1) the flow is one dimensional; (2) the streamline curvature is very small and the pressure distributions are hydrostatic; (3) the flow resistance are the same as for a steady uniform flow for the same depth and velocity; (4) the bed slope is small enough to satisfy : $\cos\theta \approx 1$ and $\sin\theta \approx \tan\theta \approx \theta$; (5) the water density is a constant; and (6) the channel has fixed boundaries, and air entrainment and sediment motion are neglected. With these hypotheses, the unsteady flow can be characterised at any point and any time by two variables: e.g., V and d where V is the flow velocity and d is the water depth (e.g. LIGGETT 1994, MONTES 1998, CHANSON 2004a,b). The unsteady flow properties are described by a system of two partial differential equations :

Fig. D-1 - Sketch of dam break wave in a horizontal dry channel with bottom friction

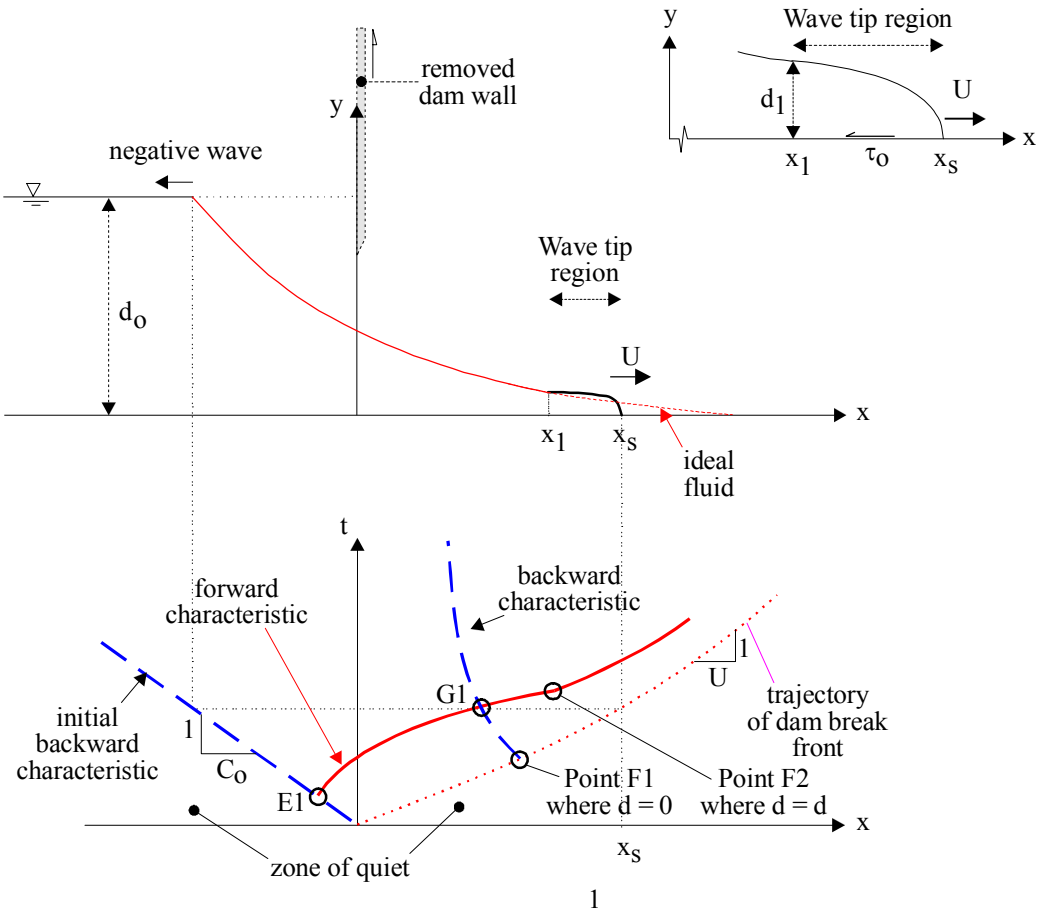

1

$$\frac{\partial d}{\partial t} + \frac{A}{B} * \frac{\partial V}{\partial x} + V * \frac{\partial d}{\partial x} + \frac{V}{B} * \left(\frac{\partial A}{\partial x}\right)_{d=constant} = 0 \qquad (D\text{-}1)$$

$$\frac{\partial V}{\partial t} + V * \frac{\partial V}{\partial x} + g * \frac{\partial d}{\partial x} + g * (S_f - S_o) = 0 \qquad (D\text{-}2)$$

where t is the tine, x is the streamwise co-ordinate, A is the cross-section area, B is the free-surface width, S_o is the bed slope ($S_o = \sin\theta$), θ is the angle between the bed and the horizontal, with $\theta > 0$ for a downward slope, and S_f is the friction slope. The friction slope is defined as : $S_f = f/2*V^2/(g*D_H)$ where D_H is the hydraulic diameter and the Darcy friction factor f is a non-linear function of both relative roughness and flow Reynolds number. Equation (1) is the continuity equation and Equation (2) is the dynamic equation.

D.2 BASIC ANALYSIS

The dam break flow is analysed as an ideal-fluid flow region behind a flow resistance-dominated tip zone (Fig. C-1). Herein the transition between the ideal dam break wave profile and the wave tip region is located at $x = x_1$ where the water depth is $d = d_1$ as shown in Figure C-1.

In the ideal fluid flow region, the basic equations yield the characteristic system of equations :

$$\frac{D}{Dt}(V + 2 * C) = 0 \qquad \text{forward characteristic (D-3a)}$$

$$\frac{D}{Dt}(V - 2 * C) = 0 \qquad \text{backward characteristic (D-3b)}$$

along :

$$\frac{d x}{dt} = V + C \qquad \text{forward characteristic C1 (D-4a)}$$

$$\frac{d x}{dt} = V - C \qquad \text{backward characteristic C2 (D-4b)}$$

Equations (D-3) and (D-4) are the characteristic equations of a simple wave problem (CHANSON 2004a,b).

In the wave tip region ($x_1 \leq x \leq x_S$, Fig. D-1), flow resistance is dominant, and the acceleration and inertial terms are small. The flow velocity does not vary rapidly in the forward tip zone and experimental data showed that it is about the wave front celerity U (DRESSLER 1952,1954, ESTRADE 1967, LAUBER 1997). The dynamic wave equation (Eq. (D-2)) may be reduced into a diffusive wave equation :

$$\frac{\partial d}{\partial x} + \frac{f}{8} * \frac{U^2}{g * d} = 0 \qquad \text{Wave tip region (D-5)}$$

assuming a constant velocity U for $x_1 \leq x \leq x_S$. Next to the leading edge of the wave, the slope of the free-surface becomes important to counterbalance the flow resistance.

For turbulent flows, the flow resistance may be approximated by the Altsul formula :

$$f = 0.1 * \left(1.46 * \frac{k_S}{D_H} + \frac{100}{Re}\right)^{1/4} \qquad \text{(D-6)}$$

where k_S is the equivalent sand roughness height, D_H is the hydraulic diameter and Re is the flow Reynolds number (IDELCHIK 1969,1986,1994, CHANSON 2004a). The Altsul is a slightly less-accurate formula which can be used to initialise the calculation with the Colebrook-White formula. In fully-rough turbulent flows, it becomes :

$$f = 0.11 * \left(\frac{k_S}{D_H}\right)^{1/4} \qquad \text{fully-rough turbulent flow (D-7)}$$

Assuming that Equation (D-7) holds in unsteady flows, and for a wide channel (i.e. $D_H \approx 4*d$), it may be rewritten in the wave tip region as :

$$f = 0.0778 * \left(\frac{k_s}{d}\right)^{1/4} \qquad \text{(D-7B)}$$

where d is the water depth. The diffusive wave equations may transformed as :

$$\frac{\partial d}{\partial x} + \frac{0.0778 * k_s^{1/4}}{8} * \frac{U^2}{g * d^{5/4}} = 0 \quad \text{Wave tip region (fully-rough turbulent motion)} \quad \text{(D-5B)}$$

The integration of the diffusive wave equation (Eq. (D-5)) yields the shape of wave tip region for a fully-rough turbulent motion :

$$d = \left(\frac{9}{4} * \frac{0.0778 * k_s^{1/4}}{8} * \frac{U^2}{g} * (x_s - x)\right)^{4/9}$$

Wave front profile (fully-rough turbulent motion) (D-8)

assuming a constant invert equivalent sans roughness height k_s.

D.3 DETAILED SOLUTION

The instantaneous dam break creates a negative wave propagating upstream into a still fluid with known water depth d_o. In the (x, t) plane, the initial negative wave characteristic has a slope dt/dx = $-1/C_o$ where $C_o = \sqrt{g*d_o}$. Note that the initial backward characteristic is a straight line, but the other backward characteristics are not because the problem is not a simple wave since $S_f > 0$.. Forward characteristics can be drawn issuing from the initial backward characteristic for t > 0 (Fig. D-1). Between the points E1 and F2, the flow properties satisfy the ideal dam break wave properties:

$$\sqrt{\frac{d}{d_o}} = \frac{1}{3} * \left(2 - \frac{x}{t * \sqrt{g * d_o}}\right) \qquad -1 \le \frac{x}{t * \sqrt{g * d_o}} \le \frac{x_1}{t * \sqrt{g * d_o}} \quad \text{(D-9)}$$

$$\frac{V}{\sqrt{g * d_o}} = \frac{2}{3} * \left(1 + \frac{x}{t * \sqrt{g * d_o}}\right) \qquad -1 \le \frac{x}{t * \sqrt{g * d_o}} \le \frac{x_1}{t * \sqrt{g * d_o}} \quad \text{(D-10)}$$

where d and V are the flow depth and velocity respectively at a distance x from the dam, and t is the time from the instantaneous dam removal.

For $x_1 \le x \le x_s$ (i.e. wave tip region), it is assumed that the velocity of water does not vary rapidly and that it equals the wave front celerity U. The flow properties in the wave tip region may be estimated using the diffusive wave equation taking into account flow resistance (Eq. (D-5)) assuming V = U. The integration of the diffusive wave equation yields the wave front profile:

$$\frac{d}{d_o} = \left(\frac{9}{4} * \frac{0.0778 * \left(\frac{k_s}{d_o}\right)^{1/4}}{8} * \frac{U^2}{g * d_o} * \frac{(x_s - x)}{d_o}\right)^{4/9}$$

$$\frac{x_1}{t * \sqrt{g * d_o}} \le \frac{x}{t * \sqrt{g * d_o}} \le \frac{x_s}{t * \sqrt{g * d_o}} \quad \text{(D-8B)}$$

assuming that Equation (D-7B) holds for $x_1 \le x \le x_s$.

Since the free-surface and velocity must be continue at the point F2, its flow properties (x_1, V_1, d_1) must satisfy :

$$\sqrt{\frac{d_1}{d_o}} = \frac{1}{3} * \left(2 - \frac{x_1}{\sqrt{g * d_o} * t}\right) \qquad \text{(D-11)}$$

$$\frac{V_1}{\sqrt{g*d_o}} = \frac{2}{3} * \left(1 + \frac{x_1}{\sqrt{g * d_o} * t}\right) \tag{D-12}$$

$$\frac{U}{\sqrt{g * d_o}} = \frac{V_1}{\sqrt{g * d_o}} \tag{D-13}$$

$$\frac{d_1}{d_o} = \left(\frac{9}{4} * \frac{0.0778 * \left(\frac{k_S}{d_o}\right)^{1/4}}{8} * \frac{U^2}{g * d_o} * \frac{(x_S - x_1)}{d_o}\right)^{4/9} \tag{D-14}$$

The conservation of mass must be further satisfied. Specifically the mass of fluid in the wave tip region (i.e. $x_1 \leq x \leq x_S$) must equal the mass of fluid in the ideal fluid flow profile for $x_1 \leq x \leq 2*\sqrt{g*d_o}*t$. It yields :

$$\int_{x_1}^{x_S} \left(\frac{9}{4} * \frac{0.0778 * k_S^{1/4}}{8} * \frac{U^2}{g} * (x_S - x)\right)^{4/9} * dx = \int_{x_1}^{2*\sqrt{g*d_o}*t} \frac{1}{9 * g} * \left(2 * \sqrt{g * d_o} - \frac{x}{t}\right)^2 * dx \tag{D-15}$$

Note that the continuity equation becomes a differential equation in terms of the wave front location x_S and celerity $U = dx_S/dt$. It must be stressed that the development is limited. The Saint-Venant equations, hence the diffusive wave equation, are not valid near the wave leading edge where the free-surface curvature is not small and where the flow resistance becomes very significant.
The above equations may be transformed to express d_1 and x_1 as functions of U:

$$\frac{d_1}{d_o} = \left(1 - \frac{1}{2} * \frac{U}{\sqrt{g * d_o}}\right)^2 \tag{D-16}$$

$$\frac{x_1}{\sqrt{g * d_o} * t} = \left(\frac{3}{2} * \frac{U}{\sqrt{g * d_o}} - 1\right) \tag{D-17}$$

The continuity equation (Eq. (D-15)) yields a polynomial equation in terms of the wave front location x_S, wave celerity $U = dx_S/dt$ and location x_1 of the point F2 :

$$\frac{9}{13} * \left(\frac{9}{4} * \frac{0.0778 * \left(\frac{k_S}{d_o}\right)^{1/4}}{8} * \frac{U^2}{g * d_o}\right)^{4/9} * \left(\frac{x_S - x_1}{d_o}\right)^{13/9} = \frac{1}{27} * \sqrt{\frac{g}{d_o}} * t * \left(2 - \frac{x_1}{\sqrt{g * d_o} * t}\right)^3 \tag{D-18}$$

The water depth at point F2 satisfies:

$$\frac{d_1}{d_o} = \left(\frac{9}{4} * \frac{0.0778 * \left(\frac{k_S}{d_o}\right)^{1/4}}{8} * \frac{U^2}{g * d_o} * \frac{(x_S - x_1)}{d_o}\right)^{4/9} \tag{D-14}$$

while Equations (D11) to (D13) yield :

$$2 - \frac{x_1}{\sqrt{g * d_o} * t} = 3 - \left(1 + \frac{x_1}{\sqrt{g * d_o} * t}\right) = 3 * \left(1 - \frac{1}{2} * \frac{U}{\sqrt{g * d_o}}\right) \quad \text{(D-19)}$$

Hence the dimensionless wave tip length is:

$$\frac{x_S - x_1}{d_o} = \frac{4}{9} * \frac{8}{0.0778 * \left(\frac{k_S}{d_o}\right)^{1/4}} * \frac{g * d_o}{U^2} * \left(1 - \frac{1}{2} * \frac{U}{\sqrt{g*d_o}}\right)^{9/2} \quad \text{(D-20)}$$

By replacing into the continuity equation, the exact solution in terms of the wave front celerity is :

$$\frac{4}{13} * \frac{\left(1 - \frac{1}{2} * \frac{U}{\sqrt{g * d_o}}\right)^{7/2}}{\frac{0.0778 * \left(\frac{k_S}{d_o}\right)^{1/4}}{8} * \frac{U^2}{g * d_o}} = \sqrt{\frac{g}{d_o}} * t \quad \text{(D21)}$$

while the wave front location equals:

$$\frac{x_S}{d_o} = \left(\frac{3}{2} * \frac{U}{\sqrt{g * d_o}} - 1\right) * \sqrt{\frac{g}{d_o}} * t + \frac{4}{9} * \frac{8}{0.0778 * \left(\frac{k_S}{d_o}\right)^{1/4}} * \frac{g * d_o}{U^2} * \left(1 - \frac{1}{2} * \frac{U}{\sqrt{g*d_o}}\right)^{9/2} \quad \text{(D22)}$$

and the free-surface profile satisfies :

$$\frac{d}{d_o} = 1 \qquad \frac{x}{d_o} \le -\sqrt{\frac{g}{d_o}} * t \quad \text{(D-23a)}$$

$$\frac{d}{d_o} = \frac{1}{9} * \left(2 - \frac{x}{t * \sqrt{g * d_o}}\right)^2 \qquad -\sqrt{\frac{g}{d_o}} * t \le \frac{x}{d_o} \le \left(\frac{3}{2} * \frac{U}{\sqrt{g * d_o}} - 1\right) * \sqrt{\frac{g}{d_o}} * t \quad \text{(D-23b)}$$

$$\frac{d}{d_o} = \left(\frac{9}{4} * \frac{0.0778 * \left(\frac{k_S}{d_o}\right)^{1/4}}{8} * \frac{U^2}{g * d_o} * \frac{(x_S - x)}{d_o}\right)^{4/9} \qquad \left(\frac{3}{2} * \frac{U}{\sqrt{g * d_o}} - 1\right) * \sqrt{\frac{g}{d_o}} * t \le \frac{x}{d_o} \le \frac{x_S}{d_o} \quad \text{(D-23c)}$$

$$\frac{d}{d_o} = 0 \qquad \frac{x_S}{d_o} \le \frac{x}{d_o} \quad \text{(D-23d)}$$

Fig. D-2 - Dimensionless wave front location, celerity and free-surface profile solutions for fully-rough turbulent dam break wave

(A) Dimensionless relationship between wave front celerity and time for k_S/d_o = 0.001 and 0.01 - Comparison with analytical solution for f = 0.05

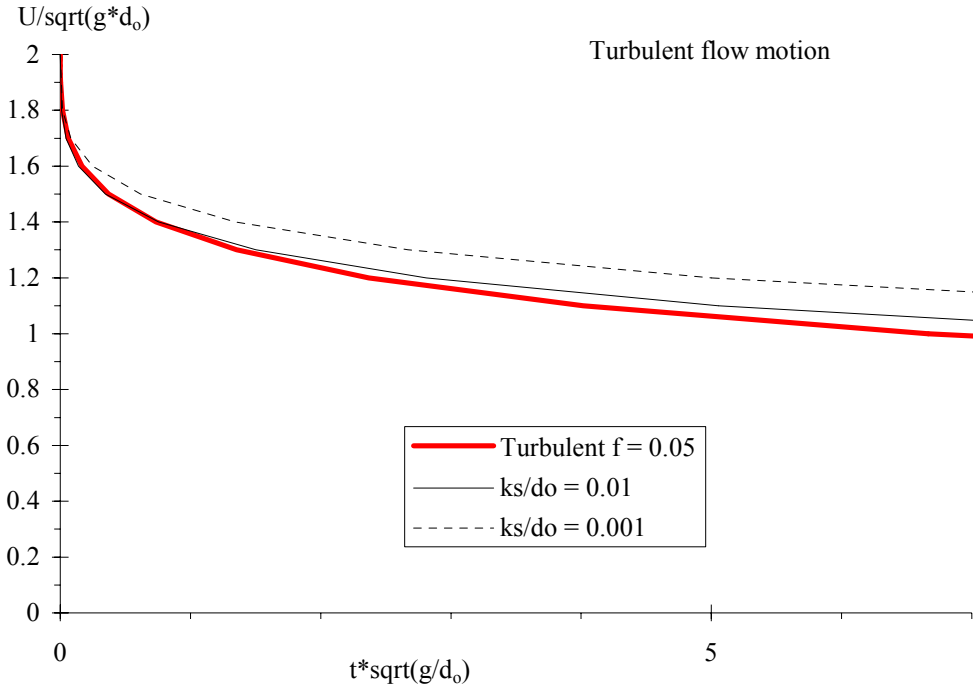

(B) Instantaneous dimensionless free-surface profile for k_S/d_o = 0.091 and $t^*\sqrt{g/d_o}$ = 15 and 44 - Comparison with DRESSLER's (1954) data (sand paper) and the analytical solution assuming f = 0.05

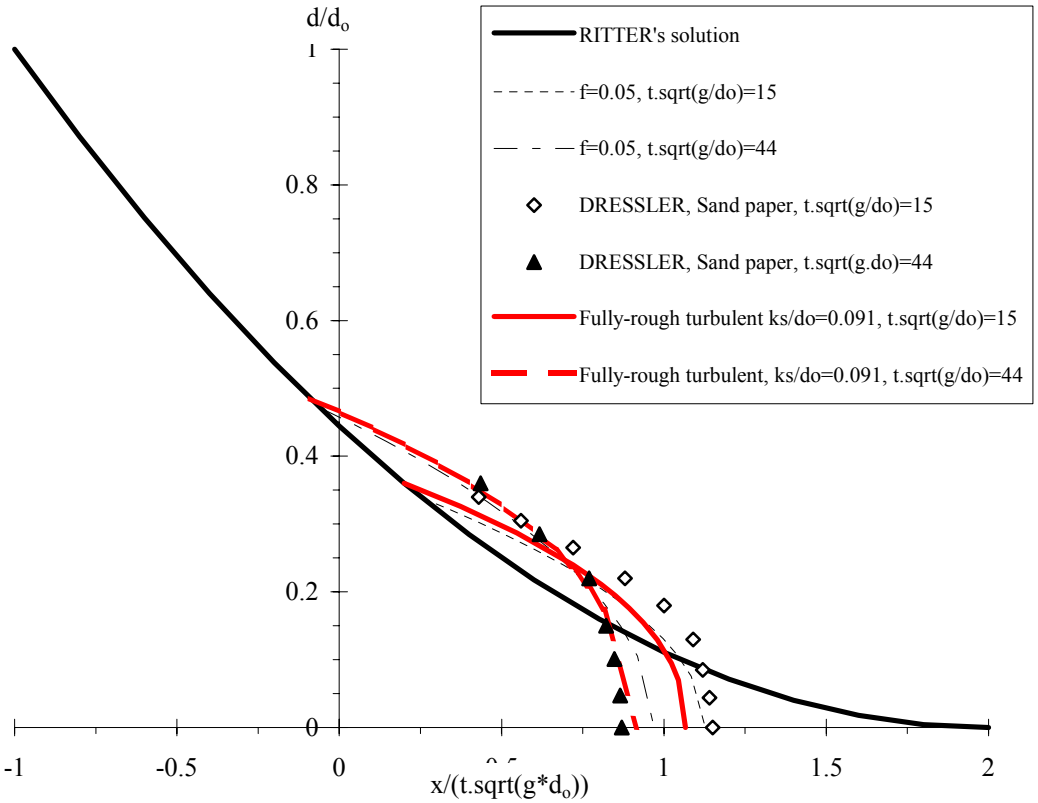

Table D-1 - Asymptotic solutions of dam break wave on dry horizontal channel with boundary friction

Reference (1)	Asymptotic solution (2)	Remarks (3)
<u>Small time t</u>		
Laminar flow motion (diffusive wave model)	$\frac{U}{\sqrt{g*d_o}} = 2 - \sqrt[5]{16 * \frac{\mu}{\rho * \sqrt{g * d_o^3}} * \sqrt{\frac{g}{d_o}} * t}$	$\frac{U}{\sqrt{g*d_o}} > 1.2$ to 1.5
Turbulent flow motion (diffusive wave model)		
constant Darcy-Weisbach friction factor f	$\frac{U}{\sqrt{g*d_o}} = 2 - \sqrt[3]{12 * f * \sqrt{\frac{g}{d_o}} * t}$	$\frac{U}{\sqrt{g*d_o}} > 1.2$ to 1.5
fully-rough turbulent flow	$\frac{U}{\sqrt{g*d_o}} = 2 - \left(13 * \sqrt{2} * 0.0778 * \left(\frac{k_S}{d_o}\right)^{1/4} * \sqrt{\frac{g}{d_o}} * t\right)^{2/7}$	$\frac{U}{\sqrt{g*d_o}} > 1.2$ to 1.5
<u>Large time t</u>		
Laminar flow motion (diffusive wave model)	$\frac{U}{\sqrt{g*d_o}} = \frac{1}{8} * \frac{\frac{\rho * \sqrt{g * d_o^3}}{\mu}}{\sqrt{\frac{g}{d_o}} * t}$	$\frac{U}{\sqrt{g*d_o}} < 0.3$ to 0.4
Turbulent flow motion (diffusive wave model)		
constant Darcy-Weisbach friction factor f	$\frac{U}{\sqrt{g*d_o}} = \sqrt{\frac{8}{3} * \frac{1}{f * \sqrt{\frac{g}{d_o}} * t}}$	$\frac{U}{\sqrt{g*d_o}} < 0.3$ to 0.4
fully-rough turbulent flow	$\frac{U}{\sqrt{g*d_o}} = \sqrt{\frac{4}{13} * \frac{1}{\frac{0.0778 * \left(\frac{k_S}{d_o}\right)^{1/4}}{8} * \sqrt{\frac{g}{d_o}} * t}}$	$\frac{U}{\sqrt{g*d_o}} < 0.3$ to 0.4

The location of point F2 is given by :

$$\frac{x_1}{\sqrt{g * d_o} * t} = \left(\frac{3}{2} * \frac{U}{\sqrt{g * d_o}} - 1\right) \qquad \text{(D-17)}$$

Typical analytical results are summarised in Figure D-2. They are compared qualitatively with the analytical results. derived assumed a constant Darcy-Weisbach friction factor in the wave tip region (CHANSON 2005). Figure D-2B shows also a comparison with some experimental data by DRESSLER (1954).

D.4 DISCUSSION

Asymptotic approximations for small and large times t are summarised in Table D-1. These are compared with turbulent flow solutions and with well-known solutions for turbulent flows.

The present method yields an explicit expression of the wave front celerity, wave front location and wave tip region characteristics. Equation (D-21) provides a direct relationship between the dimensionless wave front celerity $U/\sqrt{g*d_o}$ and dimensionless time $t*\sqrt{g/d_o}$. Equation (D-22) yields the dimensionless wave front location x_s/d_o as a function of the dimensionless wave front celerity $U/\sqrt{g*d_o}$. Equations (D-23) and (D-17) give the entire dimensionless free-surface profile $d/d_o = F(x/(t*\sqrt{g*d_o}))$. This simple system of linear equations provides a means to assess easily the effect of the flow resistance on the dam break wave propagation of real fluids.

The main advantages of the present development are four-fold. It is a simple explicit method that compares well with experiments and theoretical solutions. Further it a simple pedagogical application linking together the simple wave equations, yielding RITTER's solution, with a diffusive wave equation for the wave tip region. More this explicit solution may be used to validate simple numerical solutions of the method of characteristics applied to the dam break wave problem. Lastly the development may be extended simply for mid channel slopes and to account for initial flow motion, using the same approach as for turbulent flows.